

**PREPARATION OF ALUMINOSILICATE BASED
CERAMICS, β -SPODUMENE AND CORDIERITE
USING ZEOLITES AS PRECURSORS AND
THEIR CHARACTERISATION FOR
MICROELECTRONIC AND OTHER APPLICATIONS**

A THESIS
SUBMITTED TO
THE UNIVERSITY OF PUNE
FOR THE DEGREE OF
DOCTOR OF PHILOSOPHY
(IN CHEMISTRY)



BY

K. SELVARAJ

CATALYSIS DIVISION
NATIONAL CHEMICAL LABORATORY
PUNE - 411 008 (INDIA)

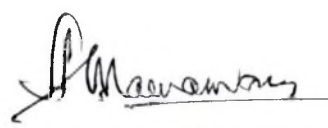
 MARCH 2000 

Certificate

Certified that the work incorporated in the thesis, "Preparation of aluminosilicate based ceramics, β -spodumene and cordierite using zeolites as precursors and their characterisation for microelectronic and other applications" submitted by Mr. K. Selvaraj, for the degree of Doctor of Philosophy, was carried out by the candidate under our supervision in the catalysis division of National Chemical Laboratory, Pune, India. Materials obtained from other sources have been duly acknowledged in the thesis.



Dr. (Mrs). VEDA RAMASWAMY
Research Co-guide



Dr. A. V. RAMASWAMY
Research Guide

Date : 31.03.2000

Place : Pune



Acknowledgement

A research fellowship offered by the Council of Scientific and Industrial Research (CSIR) to me made my dream, to work in a challenging research field like ceramics from zeolites, to come true. I would like to gratefully acknowledge the financial support by CSIR, New Delhi.

'Curiosity is the base of any research' is the lesson taught to me by Dr. A. V. Ramaswamy, my research guide, who has given me a freedom to work on a very new thrust area of research, which is totally away from the regular research activities of our group. He has been a constant source of inspiration and a great moral support to me throughout the period of my research. Whenever I faced dark and tough time in my research progress, there was always a hold for me, my co-guide Dr. (Mrs.) Veda Ramaswamy, to get my courage back. The valuable guidance from both of my guides in every means has molded me to a proper shape to live better on earth. I am greatly indebted to them. I am grateful to Dr. S. K. Date, who is almost my third research guide and who has been suggesting many ideas to refine my research work. I am thankful to Dr. S. Sivasanker, who has been so caring, helping and guiding me during my research. I thank all the scientific and supporting staff members of catalysis division for all their help during the course of this work.

A major part of the ceramic characterisation was done in other laboratories, as NCL could not support completely due to lack of instrumental facilities. I am grateful to all those helped me to carry out many characterisation techniques in their laboratories and helped me in interpreting the acquired data. Prof. A. Narayanasamy, Dr. Ramamurthy and Mr. Chinnasamy of Department of Nuclear Physics, Madras University helped me in AC Impedance characterisation. I am thankful to Dr. K.G.K. Warriar, Head, Structural Ceramics Unit, RRL-Trivandrum who allowed me to visit his unit and to do the shrinkage measurements on my ceramic products. I thank Prof. A. Umarji, IISc, Bangalore for his help in carrying out the dilatometric studies in his instrument. I am thankful to Dr. B.V. Mohan and the ceramic technology institute wing of BHEL, Bangalore for providing commercial cordierite samples for comparison. I am very much indebted to Dr. J. S. Gnanaraj and Prof. R. N. Karekar, Department of Physics, University of Pune for allowing me to use

the LCR bridge facility for the dielectric measurements and for valuable discussions on dielectric and impedance properties. I am very much obliged to Mr. Marimuthu and Mr. Rambabu of CMET – Pune for their help in TMA and SEM analyses respectively. I thank the Zeolyst Corporation and IPCL-Thane unit for providing the zeolite powder in large quantities.

I am very thankful to Dr. K. Vijayamohan, Physical Chemistry Division of NCL, who taught me the basics of AC circuits and impedance and helped me in interpreting the impedance results. I thank Dr. S. Ganapathy, Dr. P. R. Rajamohan and Mr. K. Damodaran of NMR facility, NCL for their great support for NMR characterisations and interpretation of the results. I thank Dr. S. B. Deshpande, Dr. H. S. Potdhar and Dr. P.N. Santhosh of Physical Chemistry Division for their support during the ceramic fabrication processes.

I am thankful to Dr. M. P. Kulkarni, Dr. B. R. K. Murthy and my labmates for their kind cooperation. It is very difficult for me to individually mention the names of all my friends in NCL and outside. However, I thank all of them who have made my stay in Pune memorable and comfortable, in particular Dr. K. Saravanan, who helped me during the tough time of my stay in NCL. I am very grateful to Dr. (Ms.) S. Krishnamurthy who has been of a great support during the making and formatting of my thesis and helped in data processing programs.

I am finally thankful to Dr. Paul Ratnasamy, the Director, NCL for suggesting this interesting research problem and for allowing me to carry out this work in this renowned institute, NCL.

It is just impossible for me to put in words the support and care that I got from my parents Capt. and Mrs. Kaliaperumal and my sisters Rani and Kumari who were so patient with me to complete this work. Without their love, care and blessings, it is very difficult to imagine a dissertation like this. I am grateful to them forever.

March, 2000
Pune – 8

Selvaraj K

ABBREVIATIONS USED

ρ	-Density	N_x	-Number of (ion) Exchanges
AAS	-Atomic Absorption Spectroscopy	PVA	-PolyVinyl Alcohol
AC	-Alternating Current	R	-Resistance
AMORPH	-Amorphous Phase	R&D	-Research and Development
AS	-AluminoSilicate	RT	-Room Temperature
BET	-Brunauer-Emmett-Teller (model)	SEM	-Scanning Electron Microscope
bn.	-Billion	Si/Al	-Silicon to Aluminium Ratio
C	-Capacitance	Soln.,	-Solution
CA	-Chemical Abstract	SS	-Solid Solutions
CMC	-Ceramic Matrix Composites	TEC	-Thermal Expansion Coefficient
Conc.	-Concentration	TG/DTA	-ThermoGravimetry and Differential Thermal Analysis
CVD	-Chemical Vapour Deposition	TGA	-ThermoGravimetric Analysis
DEC	-Dielectric Constant	TMA	-ThermoMechanical Analysis
Dr.	-Derivative	Wt. %	-Weight percentage
DTA	-Differential Thermal Analysis	XRD	-X – Ray Diffraction
E_a	-Energy of Activation	XRF	-X – Ray Fluorescence Spectroscopy
EDAX	-Energy Dispersive X-ray Analysis		
FID	-Free Induction Decay		
GR	-Guaranteed Reagent		
HQ	-High Quartz		
HT	-High Temperature		
IC	-Integrated Circuit		
IR	-Infra Red		
IS	-Impedance Spectroscopy		
IZA	-International Zeolite Association		
JCPDS	-Joint Committee on Powder Diffraction Standards		
k	-Dielectric Constant		
K	-Kelvin		
LAS	-Lithium Aluminosilicate		
LCR	-Inductance-Capacitance-Resistance (bridge)		
LVDT	-Linearly Variable Differential Transducer		
M	-Metal		
M	-Molar		
M\$	-Million dollars		
m. p.	-Melting Point		
M^+	-Cation M		
MAS	-Magnesium Aluminosilicate		
MEP	-MicroElectronic Packaging		
Min.	-Minute		
Mpa	-Mega Pascal		
MW	-Molecular Weight		
Na-P	-Na- from zeolite P		
Na-X	-Na- from zeolite X		
Na-Y	-Na- from zeolite Y		
NMR	-Nuclear Magnetic Resonance		

CONTENTS

CHAPTER 1 - INTRODUCTION

1.1. Materials science	1
1.1.1. Introduction.....	1
1.1.2. Ceramic science and its evolution.....	2
1.1.3. Contemporary ceramic science	2
1.2. Classification of ceramics	3
1.2.1. Classification.....	3
1.2.2. Advanced ceramics.....	4
1.3. Process involved in advanced ceramic processing	4
1.3.1. Introduction.....	4
1.3.2. Ceramic fabrication processes.....	4
1.3.3. Gas phase reactions.....	5
1.3.3.a. <i>Chemical vapour deposition</i>	5
1.3.3.b. <i>Directed metal oxidation</i>	6
1.3.3.c. <i>Reaction bonding</i>	6
1.3.4. Liquid precursor methods.....	6
1.3.4.a. <i>Sol-gel process</i>	6
1.3.4.b. <i>Polymer pyrolysis</i>	8
1.3.5. Solid powder fabrication.....	8
1.3.5.a. <i>Melt casting</i>	8
1.3.5.b. <i>Firing compacted powders</i>	9
1.3.5.c. <i>Comparison between various methods of ceramics fabrication</i>	10
1.4. Application of advanced ceramics	11
1.4.1. Structural applications.....	11
1.4.2. Electronic applications.....	12
1.4.2.a. <i>Introduction</i>	12
1.4.2.b. <i>Various branches of electronic ceramic applications</i>	12
1.4.2.c. <i>MEP and its developments</i>	13
1.4.2.d. <i>Hurdles in MEP materials</i>	13
1.4.2.e. <i>The demand based synthesis pathway</i>	15
1.5. Synthesis of powders	17
1.5.1. Introduction.....	17
1.5.2. Classifications of the synthesis methods.....	17
1.5.2.a. <i>Mechanical methods</i>	17

1.5.2.a.1. <i>Comminution</i>	17
1.5.2.a.2. <i>Jet mills</i>	17
1.5.2.a.3. <i>Ball mills</i>	18
1.5.2.a.4. <i>Mechanosynthesis</i>	18
1.5.2.b. <i>Chemical methods</i>	18
1.5.2.b.1. <i>Solid state reactions</i>	18
1.5.2.b.2. <i>Liquid solutions</i>	18
1.5.2.b.3. <i>Precipitation</i>	19
1.5.2.b.4. <i>Hydrothermal preparation</i>	19
1.5.2.b.5. <i>Evaporation of liquid</i>	19
1.5.2.b.6. <i>Sol-gel process</i>	20
1.5.2.b.7. <i>The Pechini and glycine nitrate (citrate) method</i>	20
1.5.2.b.8. <i>Nonaqueous liquid reaction</i>	20
1.5.2.b.9. <i>Vapour phase reactions</i>	20
1.5.3. <i>Conclusions</i>	22
1.6. The research problem	22
1.6.1. <i>Introduction</i>	22
1.6.2. <i>Preferred application criteria</i>	22
1.6.2.a. <i>Dielectric properties</i>	22
1.6.2.b. <i>Thermal conductivity</i>	23
1.6.2.c. <i>Thermal expansion</i>	23
1.6.2.d. <i>Hermiticity</i>	23
1.6.2.e. <i>Low temperature processability</i>	23
1.6.3. <i>Conventional materials and their suitability</i>	24
1.6.3.a. <i>Beryllia</i>	24
1.6.3.b. <i>Silicon carbide</i>	24
1.6.3.c. <i>Aluminum nitride</i>	24
1.7. Zeolites	25
1.7.1. <i>Introduction</i>	25
1.7.2. <i>Classification and nomenclature</i>	26
1.7.3. <i>Synthesis of zeolites</i>	27
1.7.4. <i>Properties of zeolites</i>	27
1.7.5. <i>Characterisations</i>	28
1.7.6. <i>Catalytic properties</i>	29
1.7.7. <i>Zeolites as advanced materials</i>	29
1.7.8. <i>Zeolites as raw materials for MEP</i>	29
1.8. Objective of this work	30
1.9. Scope of the thesis	31
References	33

CHAPTER 2 - METHODOLOGY – PREPARATION PROCEDURES AND CHARACTERISATION TECHNIQUES

2.1. Preparation procedures	36
2.1.1. Introduction.....	36
2.1.2. Preparation of precursors.....	36
2.1.2.a. <i>Ion exchange</i>	36
2.1.2.b. <i>Post ion exchange treatment</i>	38
2.1.3. Forming and consolidation processes	38
2.1.3.a. <i>Binding the powder</i>	38
2.1.3.b. <i>Consolidation of powder</i>	39
2.1.4. Sintering	39
2.1.5. Sintering in different atmospheres.....	39
2.2. Materials used	40
2.2.1. Precursor bases.....	40
2.2.2. Exchanging ion sources.....	41
2.2.3. Binder material.....	41
2.3. Characterisation techniques	42
2.3.1. Introduction.....	42
2.3.2. Chemical analysis by AAS and XRF.....	42
2.3.3. X-ray diffraction.....	42
2.3.4. Thermogravimetry	43
2.3.5. Scanning electron microscopy.....	44
2.3.6. Solid state MAS & static NMR.....	44
2.3.6.a. <i>²⁹Si and ²⁷Al magic angle spinning (MAS) NMR</i>	45
2.3.6.b. <i>⁷Li static and quad-echo NMR</i>	45
2.3.7. Dielectric constant measurements.....	45
2.3.8. Impedance spectroscopy.....	46
2.3.8.a. <i>Introduction</i>	46
2.3.8.b. <i>Theory</i>	47
2.3.8.c. <i>Experimental</i>	48
2.3.9. Thermal shrinkage and expansion studies by TMA.....	49
2.3.9.a. <i>Thermal shrinkage studies</i>	49
2.3.9.b. <i>Thermal expansion studies</i>	50
2.3.10. Apparent density and linear and volumetric shrinkage of ceramics	50
2.3.10.a. <i>Apparent density measurements</i>	50
2.3.10.b. <i>Linear and volumetric shrinkage measurements</i>	51
References	52

CHAPTER 3 - THE β - SPODUMENE (LAS systems)

PART A. GENERAL STUDIES

3.1. Ceramic preparation and characterisation	53
3.1.1. Introduction.....	53
3.1.1.a. <i>The importance of $\text{Li}_2\text{O}-\text{Al}_2\text{O}_3-\text{SiO}_2$ (LAS) systems</i>	53
3.1.1.b. <i>The ore spodumene and its β phase – A mineralogical background</i>	54
3.2. Experimental	54
3.2.1. Plan of work.....	54
3.2.2. Preparation of β -spodumene.....	55
3.2.2.a. <i>The LAS precursor powder preparation</i>	55
3.2.2.b. <i>Powder characterisation</i>	55
3.2.3. Sintering at various temperatures.....	56
3.2.4. Characterisation of ceramics.....	56
3.3. Results and discussion	56
3.3.1. Thermal properties.....	56
3.3.2. Phase transformations by X-ray diffraction	57
3.3.3. Scanning electron microscopy.....	60
3.3.4. Powder X-ray diffraction studies	61
3.3.5. Stoichiometry- bulk compositional analysis by EDX.....	65
3.3.6. Dielectric constant.....	66
3.3.7. Density calculations.....	67
3.3.8. Shrinkage studies on green samples	68
3.3.9. Thermal expansion studies on sintered samples by dilatometry....	69
3.3.10. NMR studies on LASY3 system.....	71
3.3.10.a. <i>^{29}Si nuclear magnetic resonance studies</i>	73
3.3.10.b. <i>^{27}Al nuclear magnetic resonance studies</i>	75
3.3.10.c. <i>^7Li nuclear magnetic resonance studies</i>	77
3.3.10.d. <i>Quantitative NMR study on Li content</i>	79
3.3.10.e. <i>Summary of multinuclear NMR studies on sintering of LASY</i>	80

PART B. INFLUENCE OF PRECURSOR STOICHIOMETRY ON LAS SYSTEM

3.4. Introduction	81
3.4.1. Effect of cation concentration and Si/Al ratio in precursor.....	82
3.4.1.a. <i>Plan of work</i>	82
3.4.1.b. <i>Experimental</i>	82
3.4.1.b.1. <i>Sample preparation</i>	82
3.4.1.b.2. <i>Consolidation and sintering</i>	83

3.4.1.b.3. Characterisation.....	83
3.4.1.c. X-ray based phase study.....	83
3.4.1.c.1. Effect of cation concentration on phase transformation..	83
3.4.1.d. Density based study.....	86
3.4.1.d.1. Effect of cation concentration on density.....	86
3.4.1.d.2. Effect of Si/Al ratio on density.....	88
3.4.1.e. Shrinkage based study.....	89
3.4.1.e.1. Influence of cation concentration on shrinkage	90
3.4.1.e.2. Influence of Si/Al ratio on shrinkage	90
3.4.2. Effect of sintering atmosphere.....	91
3.4.2.a. Plan of work.....	91
3.4.2.b. Experimental.....	91
3.4.2.c. Results and discussion.....	91
3.4.3. Probable phase transformation mechanism.....	94
3.5. Conclusions.....	96
References.....	98

CHAPTER 4 – THE CORDIERITE (MAS systems)

PART A. GENERAL STUDIES

4.1. Ceramic preparation and characterisation.....	100
4.1.1. Introduction.....	100
4.1.1.a. The importance of MgO-Al ₂ O ₃ -SiO ₂ (MAS) systems.....	100
4.1.1.b. The cordierite and its other phases – A mineralogical background.....	102
4.2. Experimental.....	102
4.2.1. Plan of work.....	102
4.2.2. Preparation of cordierite.....	103
4.2.2.a. The MAS precursor powder preparation.....	103
4.2.2.b. Powder characterisation.....	103
4.2.3. Consolidation and sintering	104
4.2.3.a. Nomenclature of samples.....	104
4.2.4. Ceramic characterisation.....	105
4.3. Results and discussion.....	105
4.3.1. Thermal properties.....	105
4.3.2. Phase transformations by X-ray diffraction.....	106
4.3.3. Scanning electron microscopy (SEM).....	107
4.3.4. XRD based crystal studies	109
4.3.5. Dielectric characterisation.....	110
4.3.6. Density calculation.....	111

4.3.7. Shrinkage studies on green samples by TMA.....	111
4.3.8. Thermal expansion studies on sintered samples by dilatometry	112
4.3.9. AC impedance spectroscopy studies on MAS ceramics.....	114
4.3.9.a. <i>Introduction</i>	114
4.3.9.b. <i>Plan of work</i>	115
4.3.9.c. <i>Effect of temperature on AC impedance</i>	115
4.3.9.d. <i>Studies on the electrical conductivity mechanism</i>	118
4.3.9.e. <i>Studies on activation energies</i>	120
4.3.9.f. <i>Conclusions</i>	123

**PART B. INFLUENCE OF PRECURSOR STOICHIOMETRY
ON MAS SYSTEM**

4.4. Introduction	124
4.4.1. Effect of cation concentration and Si/Al ratio.....	124
4.4.1.a. <i>Plan of work</i>	124
4.4.1.b. <i>Experimental</i>	125
4.4.1.b.1. <i>Sample preparation</i>	125
4.4.1.b.2. <i>Consolidation and sintering</i>	126
4.4.1.b.3. <i>Characterisation</i>	126
4.4.1.c. <i>X-Ray based phase study</i>	127
4.4.1.c.1. <i>Effect of cation concentration on phase transformation</i> ...	127
4.4.1.c.2. <i>Effect of Si/Al ratio</i>	131
4.4.1.d. <i>Density based study</i>	132
4.4.1.d.1. <i>Effect of cation concentration on density</i>	132
4.4.1.d.2. <i>Effect of Si/Al ratio on density</i>	133
4.4.1.e. <i>Shrinkage based study</i>	134
4.4.1.e.1. <i>Effect of cation concentration on shrinkage</i>	134
4.4.1.e.2. <i>Effect of Si/Al ratio on shrinkage</i>	135
4.4.2. Effect of sintering atmosphere.....	136
4.4.2.a. <i>Plan of work</i>	136
4.4.2.b. <i>Experimental</i>	136
4.4.2.c. <i>Results and discussion</i>	136
4.5. Conclusions	139
References	141

CHAPTER 5 – COMPREHENSIVE SUMMARY AND FUTURE SCOPE

5.1. Introduction.....	142
5.2. The dissertation work.....	142
5.3. Realisation.....	143
5.4. Limitation.....	147
5.5. Update of the field.....	147
5.6. Future scope.....	148
References.....	150

APPENDIX.....	i
----------------------	----------

LIST OF PUBLICATIONS

LIST OF PAPERS PRESENTED IN SYMPOSIA

INTRODUCTION

Chapter

1

1. 1. MATERIALS SCIENCE

1. 1. 1. INTRODUCTION

The past three decades have witnessed a phenomenal development in the global scenario of materials research. It was the rapid and revolutionary development that the concept of semiconductors in the electronics industry, beginning in the early 1960s, which gave materials science its first major impetus. Having discovered that non-metallic materials such as silicon could be made to conduct electricity in ways that metals could not, scientists and engineers devised ways of fashioning thousands of tiny integrated circuits on a small chip of silicon. This then made it possible to miniaturize the components of electronic devices such as computers. Figure 1.1. shows a the relative dimension of a F-100 processor chip. Multidimensional directions opened up new avenues in the area of new materials to achieve this.



Figure 1. 1. Integrated circuit, an F-100 microprocessor, only 0.6 cm square and small enough to pass through the eye of a needle (from ref. 2)

In the late 1980s, materials science research was given renewed emphasis with the discovery of ceramics that display superconductivity at higher temperatures than metals. If the temperature at which these new materials become superconductive can be raised sufficiently, new applications, including magnetic levitation trains and superfast computers may be possible. Although the latest developments in materials science have tended to focus on electrical properties, mechanical properties are also of major and enduring importance. Materials are anything from which products can be made. Materials science is the study of the properties, structure and processing of materials. Properties of materials are the characteristics of materials that determine their suitability for specific applications.

Starting from clay, metals, alloys, ceramics, polymers, to composite materials and glasses, there are varieties of materials of interest in the modern materials research. However, ***the present work is going to deal only about the ceramic materials that are prepared using an unconventional route for improved applications.*** This chapter would discuss about the ceramics science and its evolution to a versatile field of importance on today's R&D. Also, it will recapitulate various processes involved in ceramics processing. It is more meaningful to understand the distinction of the special route, which was followed in this work. As this is an applied materials

work, it is needed to know the major applications of these advanced ceramics, especially the microelectronic packaging substrate application, as the materials of our interest are very useful in these areas. It is very interesting to view the conventional materials and the speciality of alternative materials. A preliminary idea about the ceramic science and its evolution will help to understand the issue better.

1. 1. 2. CERAMIC SCIENCE AND ITS EVOLUTION

Wood and stone are few of the very early materials human could make use of, for diversified purpose from simple tools and weapons to buildings and sculptures. Among the earliest materials to be put to use by human beings were ceramics, in the form of the clays used in pottery. Archaeologists date early civilizations by the pottery associated with them. Ceramics is one of the oldest technologies, with a history of about 10,000 years behind it. In fact, it is from the pottery that he left behind him that we learnt much of what we know of prehistoric man. The survival of pottery over many years illustrates one of the greatest advantages that they have, the better durability over other materials. Nevertheless, those survived are mostly not the whole pieces but only fragments. This illustrates the brittleness of the material. Though these twin characters are still there today and expected to be in future too, there are studies as on today for making these materials ductile¹. Ceramics (Greek *keramos*, "potter's clay"), originally the art of making pottery, now a general term for the science of manufacturing articles prepared from pliable, earthy materials that are made rigid by high-temperature treatment. Ceramic materials are non-metallic, inorganic compounds, primarily oxides, but also carbides, nitrides, borides, and silicides. Ceramics includes the manufacture of earthenware, porcelain, bricks, and some kinds of tile and stoneware. Ceramic products are used not only for artistic objects and tableware, but also for such utilitarian items as sewer pipe and building walls².

The engineering properties of a polycrystalline ceramic are controlled by the *microstructure*, which in turn depends on the processing method used to fabricate the body. It is often stated that material science is a field at the interface of the physical sciences (physics, chemistry and mathematics) and the engineering (such as electrical, mechanical and civil). In this point of view the understanding of the fundamental issues about the production of such microstructure with desired properties is a must. The approach of this research work presented in this thesis has been based on this intention. Because, the process needs more understanding, when the fabrication methods involve new modification.

1. 1. 3. CONTEMPORARY CERAMIC SCIENCE

Along with the ceramic materials, polymers and their composites are having a great deal of interest as well as applications. In the materials point of view, the whole of modern information and communication technology depends on semiconductors. These may be elements, such as silicon, or compounds, such as gallium arsenide, that have just enough electrical conductivity to make them useful for controlling and amplifying electrical signals. Silicon is universally used for digital switching devices such as those that are used in computers. For more difficult jobs, such as converting electrical signals to light or vice versa, semiconducting compounds are used, and it is possible to tailor the properties of components by growing alternating layers of different materials.

Desirable properties of more than one material can be combined in *composites*. Glass-fibre-reinforced composites (fibreglass) are widely used to give high strength and stiffness without the fragility usually associated with glass. Many composites use carbon or polymer fibres in an epoxy *matrix* (the matrix is the material in which fibres or particles are embedded). Advanced composites are being developed that consist of ceramic fibres and different ceramic or metal matrix materials.

Wide ranges of properties of different materials that are challenging today's ceramic science are being studied for a spectrum of applications. Density, stiffness, strength, ductility, toughness and creep-resistance are some of the very vital mechanical properties that are studied on ceramic materials. Electrical conductivity, semiconducting properties, dielectric properties, piezoelectric properties, electro-optic properties, magnetic properties are the other electronic related properties. Corrosion resistance, colour and biocompatibility are some of the chemical properties that make the ceramics to be eligible to be used in the respective applications. Atoms and molecules arrange together in every material to give rise to the microstructural properties. The crystal structure plays a key role in giving a material its mechanical, electrical, and, to some extent, chemical properties. But here, in this thesis, we deal only with those properties that are required for electronic and structural applications within the limit of availability of the facilities.

Iron oxide particles are the active component in a variety of magnetic recording media, such as recording tape and the computer diskette. Ceramic insulators with a wide range of electrical properties have increasingly replaced conventional manufacturing materials. The electrical properties of a recently discovered family of copper-oxide-based ceramics allow them to become superconductive at temperatures much higher than those at which metals display this phenomenon. In space technology, ceramic materials and cermets (strong, highly heat-resistant alloys, typically made by mixing, pressing, and then baking an oxide or carbide with a powdered metal) are used to make aircraft and rocket nose cones and the heat-shield tiles on the space shuttle.

1. 2. CLASSIFICATION OF CERAMICS

1. 2. 1. CLASSIFICATION

For a long time, ceramics were mainly used for plumbing or for cooking or eating utensils, but relatively strong *engineering ceramics* have now been developed with good mechanical properties, and others, called *electroceramics*, are essential for a wide range of electrical and electronic devices. These recent ceramics are generally called as *advanced ceramics*. *Advanced Ceramics* mark that they are relatively highly pure with more or less carefully controlled composition and are more readily understood than the *traditional ceramics*. The latter are made from naturally occurring, and therefore impure and inconsistent raw materials. Even so, the special ceramics pose many problems understanding of which might give much more complex and advantageous materials.

On the basis of their chemistry they can be divided into many groups. Familiar silicates like kaolinite ($\text{Al}_2\text{Si}_2\text{O}_3(\text{OH})_4$) and mullite ($\text{Al}_6\text{Si}_2\text{O}_{13}$), simple oxides like alumina (Al_2O_3) and zirconia (ZrO_2), complex oxides other than silicates like barium titanate (BaTiO_3), and the superconducting material $\text{YBa}_2\text{Cu}_3\text{O}_{6+\delta}$ ($0 \leq \delta \leq 1$) are a few of

them. In addition, there are non-oxides such as silicon carbide (SiC) and boron carbide (B₄C), nitrides such as silicon nitride (Si₃N₄) and boron nitride (BN) borides such as titanium diboride (TiB₂), silicides such as molybdenum disilicide (MoSi₂) and halides like lithium fluoride (LiF). There are compounds based on nitride-oxide or oxynitride systems (e.g., β'-sialons). On the basis of their applications they again fall into various classifications. Adiabatic engine components, heat exchangers and cutting tools are few of the applications and come under the classification called *structural ceramics*.

Electroceramics are those used as insulators, substrates, capacitors, semiconductors, magnetic ferrites, piezoelectric materials and superconductors. A new field opened up exclusively on electronic industry with materials called as *electronic ceramics* that are used in integrated packaging. This thesis describes the preparation of one such material and its characterisation for electronic application in microelectronic packaging. Structurally, all materials are either *crystalline* or *amorphous* (also referred to as *glassy*). Actually crystalline ceramics are polycrystalline – they are made up of large number of small crystals, or grains separated by grain boundaries. The very first property, which affects the property of a ceramic, is at atomic scale i.e., the nature of bonding and the crystal structure. The second is at microstructure level i.e., the nature, quantity of the structural elements or the phases. Depending on this, ceramics may be *dense*, *glassy* or *porous*. Recently, the combination of crystalline as well as amorphous phases within a material called as *solid solution* is of growing interest.

1. 2. 2. ADVANCED CERAMICS

The intrinsic properties of a ceramic are dependent on the structure at atomic level, which are not susceptible to significant change by modification of the microstructure and properties like melting point, thermal expansion coefficient and elastic modulus. But in contrast many of the critical properties to the engineering applications are strongly dependent on the microstructure. Intrinsically, ceramics usually have high melting points and are therefore generally described as highly refractory. They are also usually hard and brittle.

1. 3. PROCESS INVOLVED IN ADVANCED CERAMIC PROCESSING

1. 3. 1. INTRODUCTION

In traditional ceramic processing, the raw material was mostly a plastic mixture of natural clay with water, which on thermal treatment agglomerates into a cohesive, useful product. There are two main processes involved in this procedure. One is to find or prepare the fine particles, shape them, and then stick them back together by heating. The second is to melt the material to form a liquid and then shape it during cooling and solidification; this is most widely practiced in forming glasses. This section will review various methods, which are reported in the literature.

1. 3. 2. CERAMIC FABRICATION PROCESSES

The basic ceramics fabrication process involves selection of suitable starting material, making it into a desired solid shape and then heating at high temperature to get a condensed ceramic solid. The types of raw materials

found in nature are controlled mainly by the abundance of the elements and their geochemical characteristics. Since oxygen, aluminium and silicon together account for 90% of the elements in the earth crust, mostly silicates and aluminosilicates are the basic raw materials in traditional ceramic manufacturing. Although most traditional ceramics formulations are based on the use of natural mineral materials which are inexpensive and readily available, an increasing fraction of specialised ceramic ware depends on the availability of chemically processed materials. This may or may not directly start from mined products in which the particle size characteristics and chemical purity are closely controlled. The chemically processed materials give rise to new compositions that in turn convert to new phases after heating, with exciting new properties. The hunt for the new processed materials opened up new research in various natural and synthetic raw materials. The new methods can be basically divided into three groups depending up on the nature of the raw materials such as gas- phase reactions, liquid precursor method and solid powder fabrication. It would be more useful to have glimpses of these techniques. ***This work is on a novel preparation of the raw materials using zeolites as precursors for the ceramic fabrication.*** However, the ceramic fabrication from the precursors follows the very widely used, "sintering of the compacted solid powders" method. The uniqueness of the preparation using zeolites may be well understood if one has an overview about the other existing techniques for both raw materials and the ceramic fabrications.

1. 3. 3. GAS PHASE REACTIONS

Any gaseous starting material may have reactions between the gas and gas, gas and liquid and the gas and solid. The most important gas to gas reaction is *Chemical Vapour deposition* (CVD)³ where the reaction occurs between the gaseous species. The fabrication process involving the gas liquid reactions has been shown to offer some promise only recently and is referred to as *directed metal oxidation*. Reaction between a gas and a solid referred to as *reaction bonding*, has been used mainly for the production of Si₃N₄ and SiC.

1. 3. 3. a. Chemical vapour deposition

CVD is a well-established technique for the production of thin films, thick films and even monolithic bodies. A variety of chemical compositions, consisting of nonoxides as well as oxide compositions, can be fabricated by CVD. Few important reactions used for fabrication of ceramics are given in Table 1.1. along with the temperature and their applications⁴.

Table 1.1 Some important CVD reactions for ceramics fabrications

Reaction	Temperature (K)	Application
$\text{TiCl}_4 + \text{O}_2 \rightarrow \text{TiO}_2 + 2\text{Cl}_2$	1200-1500	Films for electronic devices
$3\text{SiCl}_4 + 4\text{NH}_3 \rightarrow \text{Si}_3\text{N}_4 + 12\text{HCl}$	1200-1800	Films for semiconductor devices
$\text{W}(\text{CO})_6 \rightarrow \text{WC} + \text{CO}_2 + 4\text{CO}$	600-1100	Coatings

CVD method provides a distinct advantage of fairly low fabrication temperatures for ceramics and composites with high melting points that are difficult to prepare by other routes or need very high fabrication temperatures.

However, the major disadvantage is that the material deposition rate by CVD is too low ($\approx 1-100 \mu\text{m/h}$). Another disadvantage usually encountered during the monolithic fabrication is that they form microstructure consisting of large, columnar grains, which leads to fairly low intergranular strength. So these problems limit CVD for the thin film and coating works.

1. 3. 3. b. Directed metal oxidation

Usually the reaction between a gas and liquid becomes difficult because of the formation of the solid protective coat in the interface and thereby stopping the reaction. However, a novel method involving a directed oxidation of a molten metal by a gas has been used by the Lanxide Corporation for the production of porous and dense materials as well as composites⁵.

1. 3. 3. c. Reaction bonding

Reactions between a gas and a solid are well known for the production of SiN_4 and SiC . For example, the production of SiN_4 involves first the shaping of silicon powder (by slip casting, die pressing or injection mold) then preheating at 1200°C . After machining into the desired shape, it is heated, usually in nitrogen atmosphere at temperatures around $1200-1400^\circ\text{C}$, where the reaction bonding occurs to produce 'reaction bonded silicon nitride' (RBSN). The advantage is that RBSN bodies with a high degree of dimensional accuracy and with complex shapes can be prepared readily without the need for expensive machining after firing as these bodies shrink (porosity $\approx 20\%$) very less. However, they are less strong than the dense Si_3N_4 prepared by other routes (e.g., hot pressing).

1. 3. 4. LIQUID PRECURSOR METHODS

The process of transforming a solid material from a liquid is another way and is often referred to as liquid precursor method. One of such method, that has attracted interest since the mid-1970s is the *sol-gel process*⁶. Another process that attracted a fair degree of interest for the past two decades is the *polymer pyrolysis*⁷, in which nonoxides (mainly Si_3N_4 and SiC) are produced by the pyrolysis of suitable polymers.

1. 3. 4. a. Sol-gel process

A solution of metal compounds or a suspension of very fine particles in a liquid (referred to as *sol*) is converted into a semirigid mass (the *gel*). Two different sol-gel processes can be distinguished, depending on whether a sol or a solution is used. Figure 1.2. gives a schematic flow chart of this process.

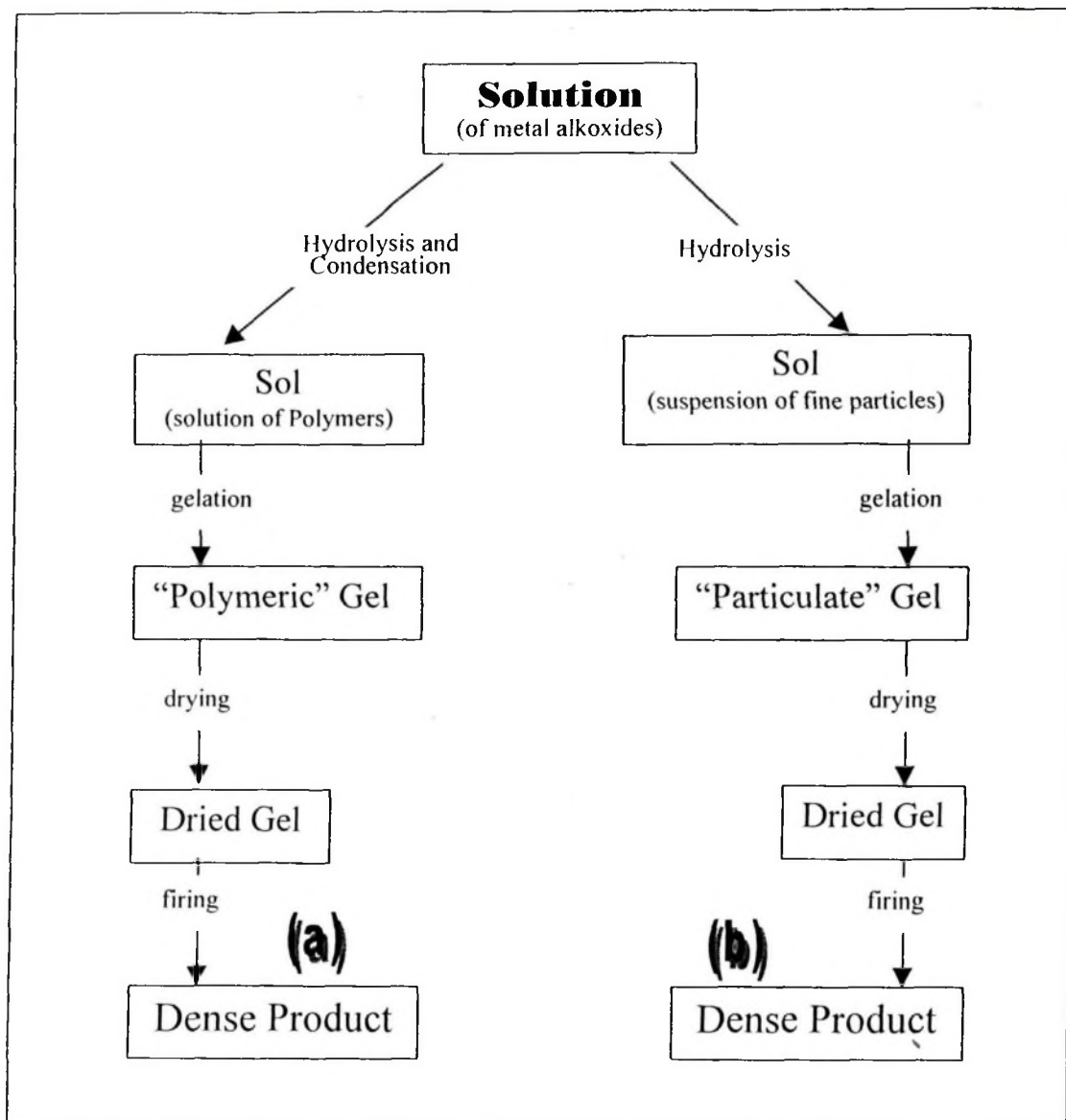
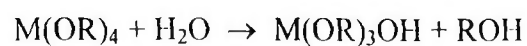


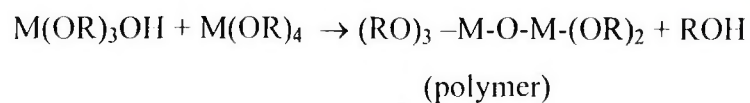
Figure 1.2. Flow chart for Sol-Gel preparation using (a) a solution and (b) a suspension

Metal alkoxides have a general formula $M(OR)_x$, where M is the metal and R is the alkyl group. The hydrolysis and condensation are done (usually around 50-90°C and) with suitable concentration of the reactants and pH. For a tetravalent metal, the reactions may be expressed as follows.

Hydrolysis:



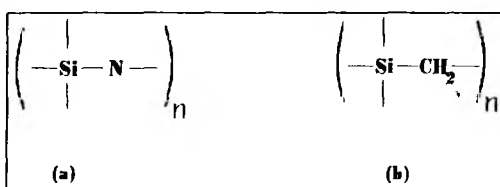
Condensation:



As a fabrication route the sol-gel process has a number of advantages. Due to the ease of purification of liquids (as the starting materials for the process), materials with high purity can be produced. The homogeneity through this route is in molecular level. This leads to highly pure and dense product. Another advantage is the lower densification temperature. However, the disadvantages are also real. The starting materials (eg., metal alkoxides) can be fairly expensive. There are common problems like cracking, warping and considerable shrinkage during the conventional drying. The enormous amount of shrinkage during the drying and firing process (volumetric shrinkage of more than 90 %) is a big problem for works like monolithic preparations.

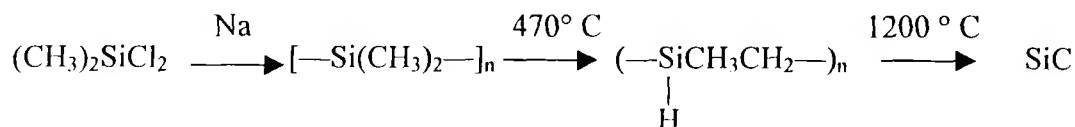
1. 3. 4. b. Polymer pyrolysis

Polymer pyrolysis is another route similar to sol-gel but the difference is that polymerisation occurs inside the liquid solutions and the product is formed after pyrolysis of the polymerised material unlike the formation of the



gel containing metal-oxygen bonds in sol-gel route. This is mostly applicable to Si_3N_4 and SiC . Si_3N_4 may be produced by the pyrolysis of polysilazanes (a), in which the Si has a direct bonding with nitrogen in the polymer backbone itself. The polycarbosilanes (b) are having the CH_2 -Si bonds in the polymer

backbones, and so even Si_3N_4 can be prepared from polycarbosilanes after suitable nitridation. Usually this polymer is used for the production of SiC . The steps involved are as follows,



The product formation through this technique is anywhere from 20 to 80 % after pyrolysis of the polymer depending on the chemistry of the polymer. So, the inherent nature of major mass loss and considerable shrinkage makes this process extremely unfit for monolithic preparations. However, this route is good for making films and fibers (commercially for SiC fiber)⁸.

1. 3. 5. SOLID POWDER FABRICATION

The basic process is to fabricate ceramic by heating finely divided solid matter (powder). There are two major classifications viz., (i) *melt casting* and (ii) *firing compacted powders* but they have the origins from ancient civilisations.

1. 3. 5. a. Melt casting

There are not many developments in the recent years in the conventional *melt casting* technique. Scholes and group have described the various processes involved elsewhere⁸. New developments have come in this technique for special applications like making precursors for bismuth type superconducting materials. The casting

involves pouring the material melt into a mold segmentally. The casting process effectively reduces the size of its expensive Pt crucible for melting the material⁹. Melt casting involves melting a batch of powdered raw materials,

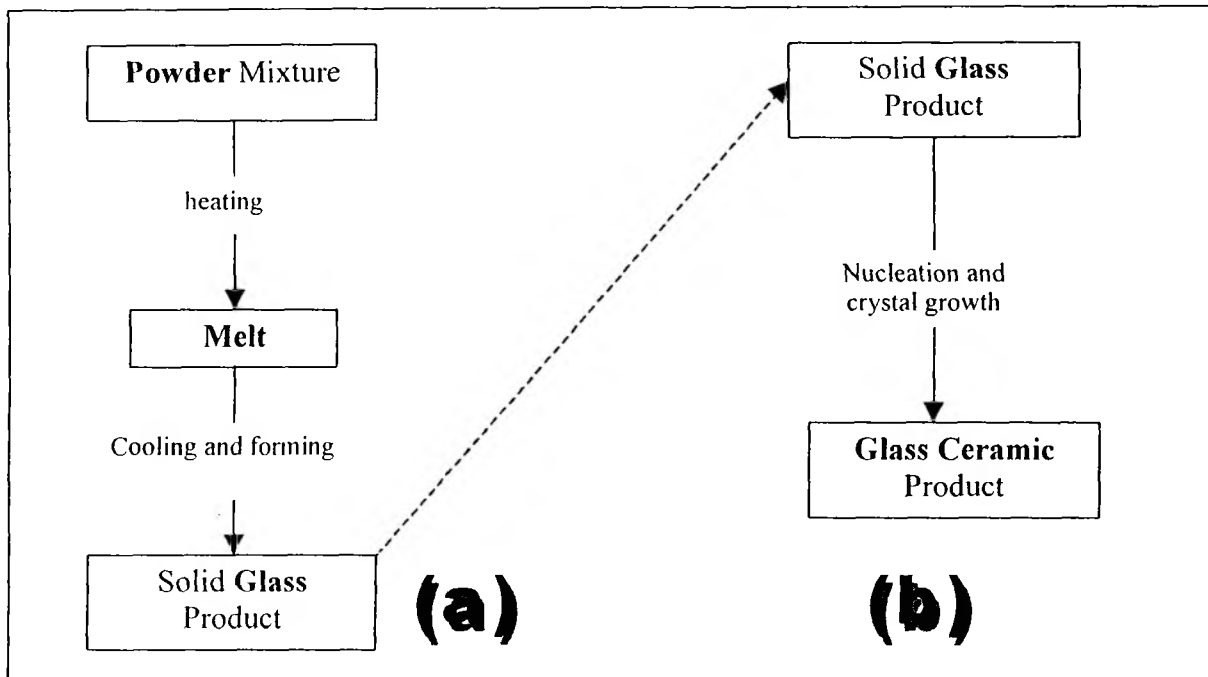


Figure. 1.3. Flow chart for production of (a) glasses and (b) glass ceramics by melt casting

followed by cooling and forming to produce a finished body (Figure. 1.3.). The mechanism includes solidification of the melt accompanied by the rapid nucleation and growth of crystals (grains). The major draw back of this technique is the uncontrolled crystal growth, which leads to a low strength for the product. Many ceramics either have high melting points (eg., ZrO_2 , m.p. $\approx 2600^\circ C$) or many times the precursors decompose before they reach the melting point (e.g., Si_3N_4). This limits this technique for the fabrication of glasses.

Another alteration to this is the *glass ceramic process*¹⁰. Raw materials are formed into glass (by melt casting) then heated in two steps, one for nucleation and the other for growth of crystals. The best example is the magnesium aluminosilicate system, *cordierite* ($2MgO \cdot 2Al_2O_3 \cdot 5SiO_2$) which is one of the two systems studied in the present work.

1.3.5.b. Firing compacted powders

This method is widely used for the production of polycrystalline materials, which involves compaction of the mass of fine particles (powders) into a porous, shaped, consolidated form and then heating to high temperature to form the dense product. Figure 1.4. shows the basic steps.

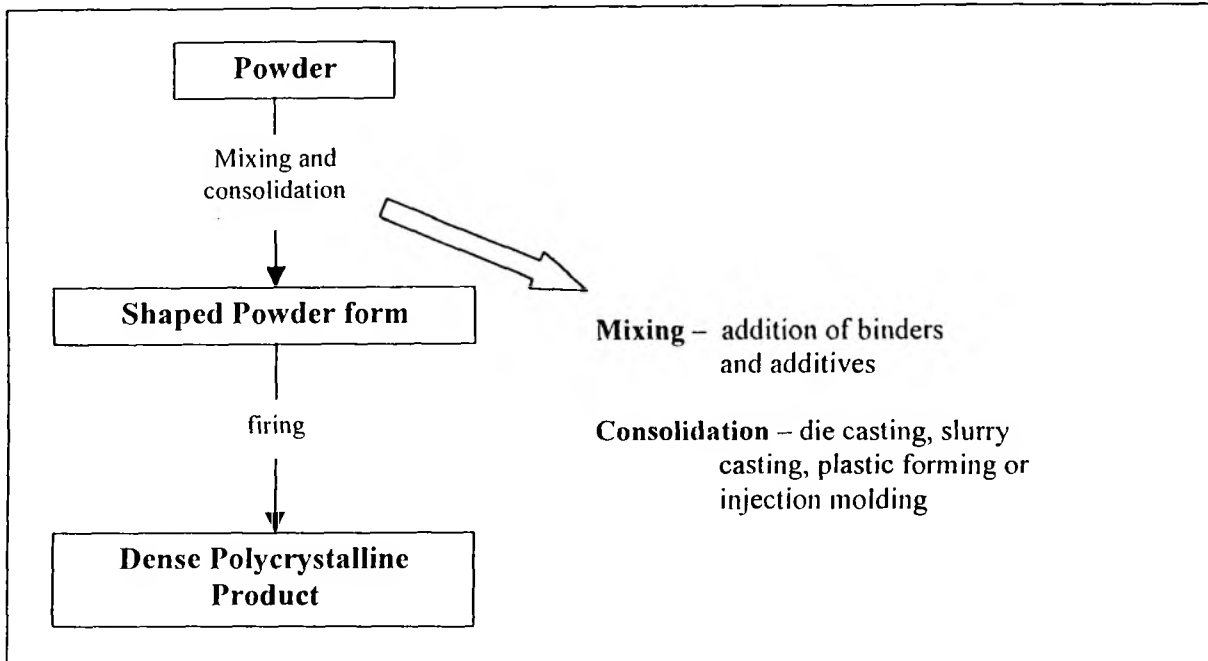


Figure.1.4. Flowchart for steps involved in production of polycrystalline ceramic by firing compacted powders

Being the most widely used method, this process of production of polycrystalline ceramics from powders has been a constant interest for many ceramic researchers for a long time, which yielded extensive studies and that can be reflected by the large volumes of reports¹¹⁻¹⁴. Excluding the preparation of precursors, for ceramic preparation, this work also adopts this same method.

1. 3. 5. c. Comparison between various methods of ceramics fabrication

After looking into different methods for ceramic fabrication, an overall summary of various methods is given in Table 1.2

*Table 1.2. Common ceramics fabrication methods**

Starting materials	Method	Product
Gases	Chemical vapour deposition	Films, Monoliths
Gas-Liquid	Directed metal oxidation	Monoliths
Gas-Solid	Reaction bonding	Monoliths
Liquids	Sol-gel process	Films, fibers
	Polymerisation	Films, fibers
Solids(powders)	Melt casting	Monoliths
	Sintering of powders	Films and monoliths

(* From *Ceramic Processing and Sintering*, M. N. Rahaman, Marcel Dekker, Inc., New York, 1995)

1. 4. APPLICATION OF ADVANCED CERAMICS

The ceramics have a wide variety of applications starting from household utensils to nuclear fuels depending on their nature. Various ceramic applications are discussed in literature¹⁵. Out of all these applications, the structural and electronic ones are the most fascinating area of recent research. Also, the ceramics prepared and analyzed in this current work have the main interest in these two applications. And hence, it must be appropriate to have an idea about the practicability of these applications and their demand worldwide.

1. 4. 1. Structural applications

High mechanical strength at high temperatures and attractive properties, including wear and corrosion resistance, stiffness and low density, are expected to promote the use of crystalline non-silicate ceramics in applications ranging from automobile engines to dental implants. These special ceramics are coming under *structural ceramics*. They are used to form monoliths, composites and coatings for engine components, cutting tools, wear components, heat exchangers and aerospace components. Demand for materials based on alumina, titania, carbides, nitrides, borides and other mineral fibers accounted for \$ 171 M in 1987 and should grow to \$ 2.65 bn by 2000 in US. Japan leads in the world's advanced structural ceramics business, and has commercialized many applications. The demand for structural ceramics in industrial applications and wear parts is expected to reach \$ 720 M by 2000. Cutting tools represent another massive end use and is expected to reach \$ 500 M by 2000¹⁶.

Catalytic converter is a device incorporated into the exhaust system of a motor car that reduces the quantities of pollutants in the exhaust gases. A catalytic converter contains small beads or monolithic honeycombs that are coated with metals such as palladium and platinum. When exhaust gases pass through the catalytic converter, these metals act as catalysts, encouraging chemical reactions, such as the oxidation of carbon monoxide and certain hydrocarbons, into less harmful carbon dioxide and water. Unleaded petrol must be used in cars that have catalytic converters; otherwise, the noble metals in the honeycombs will be poisoned by lead and will cease to function properly. All new cars in many countries including India are equipped with catalytic converters. Monolithic substrates for coating catalysts in auto-exhaust emission control devices are the recent areas of research in special application for ceramics¹⁷. As the exhaust gases are carrying temperature ranging from 200 to 800 °C in different places¹⁸ of the exhaust, the ceramic monolith should have very high thermal shock resistance and the thermal expansion coefficient should be very less. Monoliths should have very high melting points and high thermal conduction. While metal-based monoliths many times fail in these properties, ceramic monoliths are most suited¹⁹.

Structural ceramics are important in the aerospace applications. Advanced ceramics have been developed for use in structural engineering applications. Silicon nitride and silicon carbide are used to produce ceramic-matrix composites (CMC), which are more durable than monolithic ceramics. The National Aeronautics and Space Administration (NASA) is one of the major users of advanced ceramics, primarily for the heat resistant layers required to protect the spacecraft upon re-entry. Commercial production of continuous fiber reinforced CMCs is carried out by Textron Specialty Metals. The company is conducting research and development work on hot gas

filters that have a high strength, enhanced durability and are environmentally acceptable. Thermal protection used by the NASA include high-temperature reusable surface tiles, fibrous refractory composite tiles, low-temperature reusable surface tiles, advanced flexible reusable surface blankets and flexible reusable surface blankets. Total demand for CMCs in the US in 1990 was worth \$ 130.8 M. This is likely to grow by 14.6 % to \$ 509 M in 2000²⁰.

1. 4. 2. ELECTRONIC APPLICATIONS

1. 4. 2. a. Introduction

Electronics will be one of the most successful industries in the new millenium as the dependence of human life on it grows exponentially. The global electronics industry is in search of more reliable, alternative and cost effective raw materials. In the field of advanced ceramics, electronic ceramics are expected to constitute a major share of the advanced ceramic markets atleast till 2000 AD²¹. The industry analysis division of the US Department of commerce indicates markets worth \$1825 million for advanced ceramics in the year 1985 out of which about \$1700 million is for electronic ceramics. The predicted figure in 2000 AD is \$ 3485 million for electronic ceramics out of a total of \$ 5895. A report²², which forecasts the trend of utility of advanced ceramics, shows that the total ceramics applications, 79% are for electronic and 14 % are structural applications. Circuit miniaturization and cost reduction are the two aspects at which most of the developments in electronic ceramics are aimed²³. As described in Table 1.4, the ceramics have wide range of electronic applications.

1. 4. 2. b. Various branches of electronic ceramic applications

Dielectric resonators, varistors, multilayer capacitors, piezoelectric materials and semiconductor applications are the frontier areas in this. Dielectric and optical materials were reviewed by Subbarao et al²⁴. More applications are described elsewhere²⁵. The main R&D areas of interest for electronic packaging are the development of low dielectric constant ceramics with thermal expansion matching to that of silicon and a process capable of finer resolutions for printing the conducting patterns²⁶. The present work is more focussed on the microelectronic packaging (MEP) applications. Later part of this chapter describes various aspects of MEP technology.

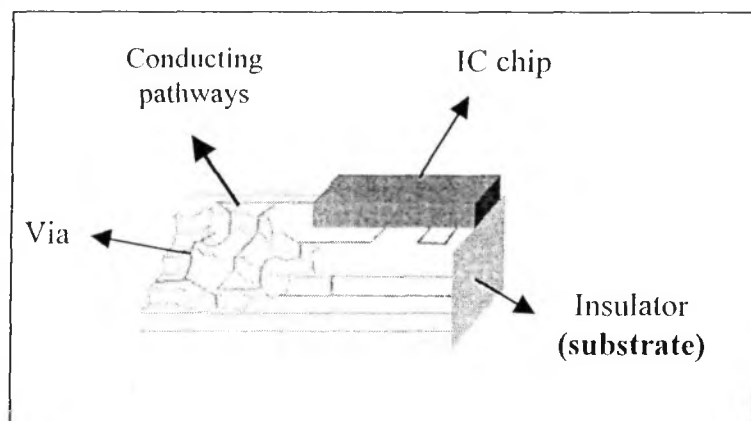


Figure 1.5. Schematic representation of a typical microelectronic packaging (MEP) substrate assembly

1. 4. 2. c. MEP and its developments

The continuing desire for faster and denser electronic microcircuits leads to the challenges in materials engineering on both the atomic and micrometer scale. The integrated circuitry (IC) on a silicon chip is the central component of all logic and memory functions on which today's computers and other electronic systems are based²⁷. Figure. 1.5. shows a schematic diagram of a multilayer microelectronic packaging which has been formed by screen printing insulating layers and conducting pathways into rigid substrate. The term *microelectronic packaging* refers to the assembly of functions that support, protect, provide power to and transmit signals from IC chip. The chip is bonded on the top of the multiple layer of insulating layers of ceramic-glass thick film paste that have been screen printed and sintered into a rigid *substrate* (like alumina). The Figure 1.5. shows a schematic representation of a multilayer microelectronic packaging.

Generally, the substrate materials can be divided into three major classes: Ceramic based, Polymer based and structures built on metal core. For high performance packages in which excellent thermal stability and impermeability are essential, ceramics-based packages are preferred. Several authors have described the evolution of ceramic package technology²⁸⁻³⁰. For example, IBM has developed various such ceramic modules in due course, viz., Solid Logic Technology (SLT) in 1964, Monolithic Systems Technology (MST) in 1970, Metallised ceramics (MC) in 1975, Multi-chip modules (MCM) in 1979 and Thermal conduction modules (TCM) in 1980³¹.

The general manufacturing process of ceramic packaging towards the use of co-fired multilayer structures consists of different steps such as production of ceramic by doctor bladed wafers, metallisation, lamination, and simultaneous sintering of the insulating layer and conducting components. Figure 1.6. shows a schematic representation of these processes. The most widely used substrate material is α -alumina. Table 1.6. illustrates the most wanted properties for a better substrate material. However, the merits and demerits of the existing substrate materials are discussed and analysed in the later part of this chapter.

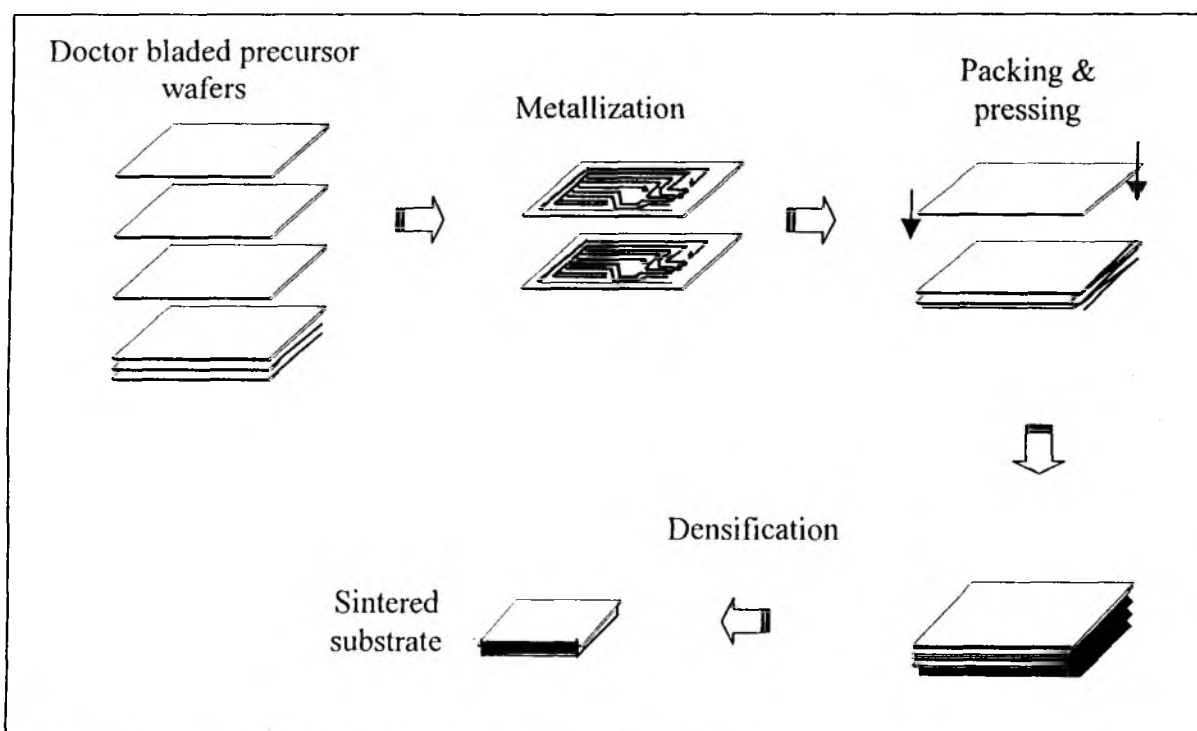
1. 4. 2. d. Hurdles in MEP materials

The technology for preparing microelectronic packaging is making a remarkable and rapid progress to meet existing needs for materials with more precision, high performance and with better cost effect. Though high purity aluminas ($\text{Al}_2\text{O}_3 = 96$ to 99.5%) are used for thin and thick film application widely, other materials like BeO, SiC and AlN are also used quite frequently. Different materials and their material properties are given in Table 1.3.

Table 1.3. Ceramics currently used in packaging and substrate applications.

Material	Dielectric constant	Thermal expansion ($10^{-6}/^{\circ}\text{C}$)	Thermal Conductivity (W/mK)	Strength (Mpa)
Alumina 96 %	10	7.1	21	280
Alumina 92 %	9.5	6.9	17	320
Alumina 90 %	8.5	7.0	17	280
Alumina 55% + glass 45%	7.5	4.2	4.2	300
SiC	40	3.4	33	280
BeO	7.0	8.0	25	170

MICROELECTRONIC PACKAGING TECHNOLOGY

*Figure. 1.6 Schematic illustration of various steps in MEP technology*

Aluminosilicate based ceramic substrate materials have fascinated the attention of the advanced ceramic society, as they have many advantages over the conventional materials like α -alumina, BeO, AlN etc³². These conventional substrates require very high sintering temperatures in addition to, some of them being toxic and result in inhomogeneous sintering³³. For example, α -alumina being a better dielectric material, requires a higher sintering temperature (above 1873 K) to form a good dense phase and the usage of expensive high refractory metals like W, Mo, for printing the conducting patterns on the substrates becomes inevitable. Many trials have been made to substitute the widely and traditionally used ceramics like α -alumina with aluminosilicate-based

ceramics like cordierite ($Mg_2Al_4Si_5O_{18}$), anorthite ($CaAl_2Si_2O_8$), mullite (Al_6SiO_{18}) and β -spodumene ($LiAlSi_2O_6$) which have appealing properties. For a better substrate material, one should have a low dielectric constant, thermal expansion match with that of silicon, high thermal conductivity, thermal shock resistance, good mechanical strength, and low temperature processability^{32,34}. Schwartz suggested a list of ceramic packaging materials that are currently in use (Table 1.3.) and those under consideration for the future (Table 1.4.)³⁵.

Table 1.4. Ceramics for future use in substrate and packaging

Material	Dielectric constant	Thermal expansion ($10^{-6}/^{\circ}C$)	Thermal conductivity (W/mK)	Strength (Mpa)
Aluminium nitride	8.8	4.6	84 – 240	360
Silicon nitride	6.0	32.	33	590
Glass-ceramics	4.5 - 6.5	2.5 - 6.5	0.84 – 2.1	241
Mullite	6.1	4.5	2.1	210

To pass through every step of the MEP, the raw material needs to possess some important properties. The preparation of the wafers or casted tapes needs a good powder property. Uniform particle sized powder gives a better strength and smoothness to the surface. The process of compaction and pressing needs a well-bonded powder with good binding capacity.

1. 4. 2. e. The demand based synthesis pathway

From consolidation to firing of the green body, the effect of characteristics of the powder is remarkable. As a result, the powder preparation is very important to produce the desired microstructure. Let us first define what are the desired properties for a ceramic body and then define what is important for the electronic (MEP) and the structural applications. Table 1.5. gives a list of such parameters and expected properties.

Table 1.5. Desirable powder characteristics for advanced ceramics

Powder characteristics	Desired property
Particle size	Fine ($< \sim 1. \mu m$)
Particle size distribution	Narrow
Particle shape	Spherical or equiaxial
State of agglomeration	No agglomeration or soft agglomeration
Chemical composition	High purity
Phase composition	Single phase

Advanced ceramics must meet very specific property requirements and therefore their chemical composition and microstructure must be well controlled. Careful attention must be paid to the quality of the starting powders. For advanced ceramics, the important powder characteristics are the particle size, particle size distribution, shape

state of agglomeration, chemical composition, and the phase composition. The structure and chemistry of the surface are also important. Each characteristic has its own influence on the ceramic processing. Table 1.5. shows the general desirable powder characteristics for advanced ceramics. However, they may change according to needs for a special application. In MEP the desired property requirements are listed in Table 1.6. However, none of the existing materials meets all the desired properties. Although Al_2O_3 is the most widely used material for fabrication of packages, BeO, SiC and AlN are also used quite frequently. Various alumina materials with different % of alumina are listed in the Table 1.3. AlN especially, has been increasing in popularity recently³⁶. Generally, for electronic packaging substrate application, the materials are expected to have properties as given below in Table 1.6.

Table 1.6. Property requirement for electronic packaging material

1. Low dielectric constant
2. Low dielectric loss
3. High dielectric strength
4. High electrical resistivity
5. High thermal conductivity
6. Thermal Expansion match with that of the chip materials (Si)
7. Good mechanical strength
8. Surface smoothness
9. Hermetic
10. Low temperature processability
11. Compatibility with copper metallisation
12. Stable
13. Nontoxic
14. Low cost

All trials have been made to get materials with the possession of most of these properties to be better candidates for these applications. However, the present work is about the preparation of solid powders using an unconventional route and their characterisation for packaging substrate applications. Hence, the various methods of preparation of the powders would help in understanding the uniqueness of this special route. Conventional oxide route syntheses have been still in interest for a long time even after the evolution of the new synthetic routes. Synthesis of high-temperature superconducting ceramics, Yttrium barium cuprate ($\text{YBa}_2\text{Cu}_3\text{O}_{7-x}$) and thallium barium calcium magnesium copper oxide ($\text{TlBa}_2\text{Ca}_3-x\text{Mg}_x\text{Cu}_4\text{O}_y$ ($x = 0-3$)) are good examples^{37,38}. Combustion is another method. Microwave combustion is relatively a newer process³⁹. It has the advantage of more synchronized crystallisation of fine structure. A report, authored by K. S. Mazdiyasi, reviews various aspects of the synthesis of single and mixed-phase oxide ceramic powders by thermal and hydrolytic decomposition of metal alkoxides⁴⁰. Sol-gel based preparation is considered to be one of the efficient ways of getting fine ceramics. More than 170 reviews appeared on this topic in a single year, 1998 alone. Many publications reveal the preferred choice of sol-gel technique for ceramic powder preparations⁴¹.

1. 5. SYNTHESIS OF POWDERS

1. 5. 1. *Introduction*

The advanced ceramics science and development are on the improvement in the characteristics of those materials. But these properties are more dependent on the way of the raw material preparations. Since every preparatory route has its own chemistry and kinetics which provide different nature for the powders. It is important to know and understand the various aspects of the synthesis route of powders.

1. 5. 2. *Classifications of the synthesis methods*

Many different methods are available for powder preparation from literature^{42,43}. Powder preparation methods can be broadly classified into two different classes.

1. mechanical methods
2. chemical methods

Mechanical methods are generally used for producing powders of the traditional ceramics from naturally occurring raw materials and are in a fairly mature area and the scope of new developments is somewhat small. However, recently for advanced ceramics powders, high-speed ball milling, one of the mechanical methods, has attracted the attention of many researchers. Chemical methods are generally used for preparing advanced ceramics from synthetic materials or from naturally occurring materials that have been treated chemically to a considerable degree. However, some chemical methods include grinding (which is a mechanical method) as a part of the process. In fact, the grinding process is to breakdown the agglomerated particles and to get a desired physical characteristic of the powder (for e.g., particle size and its distribution). An outline about each of these routes may be interesting to gain some idea about the various methods available for powder preparation.

1. 5. 2. a. *Mechanical methods*

1. 5. 2. a. 1. *Comminution*

This process involves operations like crushing, grinding and milling. For traditional clay-based ceramics, machines such as jaw, gyratory, and cone crushers are used. The most common way to achieve the size reduction is by milling. One or more of a variety of mills may be used, including high compression roller mills, jet mills (fluid energy mills) and ball mills⁴⁴. The material is pressed between two roller mill as like conventional roller mill but the contact pressure is considerably higher (in the range of 100 – 300 MPa). The stock of coarse particles is comminuted and compacted.

1. 5. 2. a. 2. *Jet mills*

Generally, the operation consists of interaction of one or more streams of high-speed gas bearing the stock of coarse particles with another high-speed stream. Comminution occurs due to collisions between the particles. An

inert gas like nitrogen or argon is used as the high-speed stream to reduce the possible oxidation of non-oxide materials. A recent review describes various aspects of the fluidized-bed jet milling of ceramics⁴⁵.

1. 5. 2. a. 3. Ball mills

Comminution roller mills and the jet mills are to achieve the comminution without grinding media. This method is to use balls or rods to make comminution by compression, impact, and shear (friction) between the grinding media and the particles. Rod milling is not suitable for fine powders whereas ball milling is. This provides powder size in the range from 10 μm to as small as a fraction of a micrometer. Ball milling is suitable for wet and dry milling. However, the rate of grinding depends on various factors^{46,47}.

1. 5. 2. a. 4. Mechanochemistry

Especially with prolonged milling or milling under vigorous conditions, both physical and chemical characteristics of the particles can undergo significant changes. Mechanochemistry is one of the best examples of such conditions. Grinding in fact enhances the chemical reactivity of the powder. Rupture of the bonds during the particle fracture results in surfaces with unsatisfied valences. This in addition with the high surface energy activates the powders to react with each other and their surroundings. First successful preparation was for Ni and Al alloys strengthened by oxide dispersions and later it was used for many other powders like oxides, carbides, nitrides, borides and silicides⁴⁸. A recent result of mechanochemistry of MoSi_2 from Mo and Si powders appear to rule out a true solid state reaction between the particles as the prominent mechanism⁴⁹.

1. 5. 2. b. Chemical methods

1. 5. 2. b. 1. Solid state reactions

Chemical decomposition reactions, in which a solid reactant is heated to produce a new solid plus a gas are commonly used to produce simple oxide powders from carbonates, hydroxides, nitrates, sulfates, acetates, oxalates, alkoxides and the other metal salts. For example,



These reactions, involving decomposition of solids or reaction between solids are referred to in the ceramic literature as *calcination*.

1. 5. 2. b. 2. Liquid Solutions

There are two general ways of producing a powdered material from a solution; (i) evaporation of the liquid and (ii) precipitation by adding a chemical reagent that reacts with the solution.

1. 5. 2. b. 3. Precipitation

Stober et al. carried out systematic study on various factors that affects the precipitation of fine SiO_2 particles by hydrolysis of silicon alkoxide in the presence of NH_3 .⁵⁰ The differences in the rates of hydrolysis have been the problem always if two or more components are present in the solution in the case of preparing a mixed oxide powder. The process is referred to as coprecipitation (sometimes as co-hydrolysis). A good example is the preparation of BaTiO_3 by the hydrolysis of the solution of barium isopropoxide, $\text{Ba}(\text{OC}_3\text{H}_7)_2$, and titanium tertiary amyloxyde, $\text{Ti}(\text{OC}_5\text{H}_{11})_4$, by Mazdiyasi and coworkers⁵¹.

1. 5. 2. b. 4. Hydrothermal preparation

Hydrothermal precipitation involves heating reactants – often metal salts, oxides, hydroxides or metal powders – as a solution or a suspension, usually in water, at elevated temperature and pressure. Temperature usually falls in the boiling point and the critical temperature (374 °C) of water and then pressure ranges upto ≈ 20 MPa. The process is carried out in a hardened steel autoclave, which can be heated to the desired temperature. Hydrothermal crystallisation⁵² is another method employed to make a highly crystalline material (e.g., 24 h at 300°C under 100 MPa) from a poorly ordered precursor material (e.g., amorphous ZrO_2). Large scale of commercial exploitation of this technique is being investigated for few decades. Production of zeolites is a classic example for this technique^{53,54}. However, this domain will be discussed later in this thesis, as the raw materials used in this work are basically prepared through this hydrothermal route.

1. 5. 2. b. 5. Evaporation of liquid

Evaporation of liquid involves supersaturation of the liquid and thereby causing nucleation and a growth of the crystal. If the process of super saturation is very rapid, a large number of nuclei are formed in a short time. This can be achieved by forming fine drops of the liquid, which gives very high surface area for the liquid so that the evaporation becomes more rapid. However, this has the disadvantage of probable partial crystallisation in case solutions of two salts are used.

Spray drying is one of these methods, in which a fluid atomiser is used to produce fine droplets into a drying chamber. With respect to how energy is given for production of droplets, there are varieties of atomisers⁵⁵. Spray drying has been found to be useful for the preparation of ferrite powders⁵⁶. The powder produced by spray drying can be sintered to almost theoretical density. But by using a higher temperature and reactive (e.g., oxidising) atmosphere in the chamber, the salts can be dried and decomposed directly in a single step⁵⁷. This process is referred to as *spray pyrolysis* (also called as spray roasting, spray reaction, and evaporative decomposition). In *Freeze Drying*, the solution is broken into fine drops into a chamber, which are then frozen into a cold bath of immiscible liquid such as hexane and dry ice or directly into liquid nitrogen. The cold droplets are then placed into a cooled chamber and then solvent is removed under vacuum by sublimation without any melting. Powders of Al_2O_3 produced from freeze dried slurries are found to consist of soft agglomerates that could be broken down easily⁵⁸.

1. 5. 2. b. 6. Sol-gel Process

The gel formed by hydrolysis, condensation and gelation of the initial solution (normally with a polymeric structure) is dried and ground to produce a powder. Because the mixing of the constituents in the gel formation is achieved at a molecular level, the powders have a high degree of chemical homogeneity. Controlled drying is not needed in the production of a powder. Liquid removal under supercritical (or hypercritical) conditions produces almost no shrinkage, so a dried powder with low strength is obtained. Some recent developments in aqueous sol-gel processing are described well by Atkinson et al⁵⁹. Another report by Ismail and coworkers reveals the preparation of mullite- cordierite composite powders by sol-gel method⁶⁰.

1. 5. 2. b. 7. The Pechini and glycine nitrate (Citrate) method

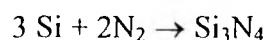
The Pechini method is a process developed by Pechini⁶¹, and is also referred to as Citrate gel process or amorphous citrate process. The metal ions from the starting materials such as carbonates, nitrates, and alkoxides are complexed in an aqueous solution with a-carboxylic acid such as citric acid. When heated with a polyhydroxy alcohol, such as ethylene glycol, polyesterification occurs and on removal of the excess liquid a transparent resin is formed. The resin is then heated to decompose the organic constituents, ground and finally calcined to produce the powder. Powders with high surface area can be produced by this method⁶². The glycine nitrate process is one of a general class of combustion methods for preparation of ceramic powders. A highly viscous mass formed by evaporation of a solution of metal nitrates and glycine is ignited to produce the powder⁶³.

1. 5. 2. b. 8. Nonaqueous liquid reaction

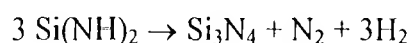
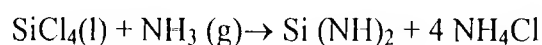
This process is mainly used for the production of Si₃N₄ powders. The reaction between liquid SiCl₄ and liquid NH₃ has been used even on an industrial scale by UBE Industries, Japan to produce Si₃N₄ powders. The product formed by the interfacial reaction between the two liquids were collected and washed with liquid NH₃ and calcined at 1000°C to produce amorphous Si₃N₄ powders.

1. 5. 2. b. 9. Vapour phase reactions

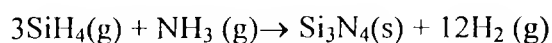
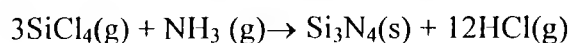
These are mainly used for the production of nonoxides and refractory oxides like Si₃N₄ and SiC powders. Gas to Solid reactions are studied and reported⁶⁴. Nitridation of Si has been reviewed by Moulson⁶⁵.



Mazdiyasi and Cooke^{66,67} showed that the reaction between liquid SiCl₄ and NH₃ gas in dry hexane at 0°C could be used to prepare a fine Si₃N₄ powder with very low levels of metallic impurities.



Reactions between gases are also reported. The typical reaction can be illustrated as follows,



However the advantages and disadvantages of all these techniques are given in Table 1.7., which gives the overall summary of the common powder preparation methods for ceramics.

Table 1.7. Common powder preparation methods for ceramics

Powder preparation method	Advantages	Disadvantages
Mechanical		
<u>Comminution</u>	Inexpensive, wide applicability	Limited purity, limited homogeneity, large particles
<u>Mechanochemical Synthesis</u>	Fine particle size, good for nonoxides, low temperature route	Limited purity, limited homogeneity
Ball mill	Suitable for wet & dry milling, fine particle size	Mill parameters affect the particle size
Jet mill	Rapid method, narrow particle size	Limited purity
Chemical		
<u>Solid state reactions</u>	Simple apparatus, inexpensive	Agglomerated powder, limited homogeneity for multi component powders
<u>Liquid solutions</u>		
Precipitation or coprecipitation : Solvent evaporation (spray drying, spray pyrolysis, freeze drying, sol-gel processing);	High purity, small particles, composition control, chemical homogeneity	Expensive, poor for nonoxides, powder agglomeration usually a problem
Combustion (Pechini method, glycine nitrate process)	High homogeneity, chemical surface area	Limited to few oxides
Non-aqueous liquid reactions.	High purity, small particles	Limited to nonoxide
<u>Vapour phase reactions</u>		
Gas-solid reaction	Inexpensive	Low purity, limited to nonoxides
Gas-liquid & gas-gas reaction	High purity, small particles	Expensive, limited to nonoxides

1. 5. 3. CONCLUSIONS

Various methods available in the literature for the preparation of ceramic powders were analyzed in this section to gain a preparatory idea about the ceramic preparations. The advantages and disadvantages of them were compared. This would help to understand a new route of ceramic preparation with a better perception.

1. 6. THE RESEARCH PROBLEM

1. 6. 1. INTRODUCTION

The present work is to study the preparation procedures and find out the properties of alternative ceramic materials as compared to conventionally used ones in microelectronic packaging. As mentioned earlier conventionally, alumina and BeO and SiC are a few of the most widely used materials in electronic packaging. But according to the property requirements as given in the Table 1.6., almost all these materials had many drawbacks. This section will discuss the importance of those properties, their actual relationships between them and the need and scope of this research work in brief.

1. 6. 2. PREFERRED APPLICATION CRITERIA

1. 6. 2. a. Dielectric properties

Any good packaging ceramic should have lower dielectric constant. In designing high-speed circuitry, there are two parameters of transmission line conductors of greatest importance, (1) velocity of propagation and (2) characteristic impedance⁶⁸. Both are influenced by the dielectric constant of the ceramic substrate. The time delay for signal propagation in a transmission line is given by,

$$t_d = \sqrt{k} \frac{l}{c}$$



where k is the dielectric constant of the medium; l is the distance the signal should travel; and c is the velocity of light⁶⁹. When the conductor is surrounded by a medium of lowest dielectric constant, the propagation is the highest. To have a control over the conductor line width and the dielectric thickness, the impedance of the line should be matched with the impedance of the device input. Both the dielectric constant and the dielectric loss are directly related to the four different frequency dependent polarisations namely electronic, ionic, orientation and space polarisations. Electronic component of the polarisation depends on the number of electrons constituting the atom. So, for low k materials, it is preferable to have ions with atomic number less than 18. Orbitals that are unoccupied but energetically available cause more polarisation because of change in atomic shape. So elements of d^0 electronic configurations, (e.g., Pb^{2+} , Ti^{4+} and Nb^{5+}) should be usually avoided. The contribution of other three frequency dependent polarisations are relatively less.

1. 6. 2. b. Thermal conductivity

Ceramic substrates can serve as heat sink and therefore they are preferred to plastic substrates for high-speed circuits. Conventional circuits are air or water cooled for the power density of up to 20 W/cm². In ceramics heat conduction is due to phonon transport. The frequency of the lattice vibrations is proportional to $\sqrt{s/m}$, where s is bond stiffness and m is the mass of the lattice atom or ion. The phonon velocity is proportional to E/ρ , E is the energy of the lattice vibrations and ρ is the density, which in turn proportional to the frequency of lattice vibrations. Thus it is preferred to have low atomic number, low atomic density and high degree of covalency for high thermal conductivity. Phonon waves are disrupted by defects and by grain boundaries. Thus the thermal conductivity of a polycrystalline material is always less than that of a single crystal and is higher for simple crystal structures. (eg., thermal conductivity of diamond is 2000 W/mK and that of polyimide is 0.2 W/mK)

1. 6. 2. c. Thermal Expansion

On operation, thermal cycling can cause cracks to form in the solder joints usually used for connecting the chip on to the substrate, if the thermal expansion is not comparable with the silicon chip. On fundamental level, usually thermal expansion can be directly related to covalency. The potential well in an energy diagram of a covalent bond will be more harmonic than that of an ionic bond. Taylor⁷⁰ has reported a study of the influence of structural factors on the thermal expansion on various forms of SiO₂.

1. 6. 2. d. Hermiticity

Other than these, the hermiticity is one of the important properties, which means the ability of the material to resist the admission of any foreign matter like moisture and adsorbent gases to penetrate into it. This penetration changes the dielectric properties of the materials. This can be partially correlated with the pores in the sintered ceramics.

1. 6. 2. e. Low temperature processability

The metal conductor or alloy used in metallisation on the thin wafers of the substrate for making the conducting patterns depends on the temperature range of sinterability of the material. For example, substrates like α -alumina sinter beyond 1600 ° C to get a good dense phase. In those cases, the metals used for metallisation have to be high temperature refractory metals like W, Mo or the alloys of them, which enhances the cost of the product considerably. To make use of inexpensive but better conductors like Cu, Au, and Pd/Ag, the processing temperature should be lower than the melting point of these low melting metals. So, a reduction in the sintering temperature of any new substrate is always a drive for the modern research and technology. More discussions on these properties and other desired properties will be made at appropriate places in the thesis later. Now it would be interesting to analyse how much the existing materials meet up to the demand of these properties.

1. 6. 3. CONVENTIONAL MATERIALS AND THEIR SUITABILITY

1. 6. 3. a. Beryllia (BeO) has been attractive for packaging due to its superior thermal conductivity, which is 8 to 10 times that of alumina at room temperature. But the major draw back of BeO is its high toxicity. Though the finished package is entirely safe to handle, in powder, BeO is highly toxic. This makes the handling of powder materials very risky.

1. 6. 3. b. Silicon Carbide (SiC) is the least used of the ceramics packaging materials. Its dielectric constant is nearly 4 to 5 times greater than that of alumina and also 20 to 100 times more expensive. But when this is hot pressed with 2 % of BeO, its thermal conductivity is slightly higher than BeO itself⁷¹. Its thermal expansion coefficient is almost a perfect match with silicon and has a good toughness. Another uniqueness about SiC is that it is a highly covalent (89%) material among all other electronic ceramics in use. This leads to high thermal conductivities and toughness.

1. 6. 3. c. Aluminum Nitride (AlN) has appeared only in recent times in the market and is generally superior to Al₂O₃ in all desired properties. Thermal conductivity is about four times that of 96% alumina and the mechanical flexibility is twice as high and so it is less likely to crack. The thermal expansion coefficient matches with that of silicon, and is also better than alumina. But AlN is relatively difficult to sinter; the most successful sintering aid has been found to be 0.5 to 15 wt. % Y₂O₃.

As a result, it is easily seen that every conventional material has got its own drawbacks. So there was a need for alternative materials. Aluminosilicate based ceramics like cordierite⁷² (Mg₂Al₄Si₅O₁₈), anorthite⁷³ (CaAl₂Si₂O₈) and mullite⁷⁴ (Al₆SiO₁₈) have attracted the attention in recent years as alternative substrate materials.

However, the conventional method of preparation of these materials through melting of appropriate oxides needs a high temperature, generally > 1400 °C, quenching the glass and then crystallisation through controlled heating. A recent review on the trend of modern ceramic research and development suggested that new methods of synthesizing the starting powders, improved precursor materials, clean room processing will be the future R&D direction in ceramic packaging³⁵. Aluminosilicate based ceramic substrate preparations have been tried using various conventional as well as synthetic chemical routes. For example, the preparation of cordierite was reported by using coprecipitation method⁷⁵. However, the sintering must be carried out at about 1420°C in order to obtain cordierite ceramic article with a density of 97% of its theoretical density.

The decomposition of modified zeolites has evolved as a route for the preparation of electronic ceramics and they have been found to possess excellent applications⁷⁶. A brief introduction about zeolite materials would be appropriate here to understand more about the process.

1. 7. ZEOLITES

1. 7. 1. INTRODUCTION

Zeolite is a combination of two Greek words, *zein* meaning "to boil" and *lithos* meaning "a stone", and is a large group of minerals composed of hydrated aluminium silicates of alkali metals and alkaline earth metals. The zeolites are named so due to their swelling and bubbling nature under moderately high temperature. The minerals range in hardness from 3 to 6 and have a relative density of 1.9 to 2.8. Zeolites are usually found naturally in veins and cavities of basic igneous rocks especially basalt. Among the more common are stilbite, chabazite, natrolite, and analcime, which are widely distributed. Zeolites are used for ion-exchanger in many areas including in nuclear waste treatments, drying agents and molecular sieves and as effective shape selective catalysts. By

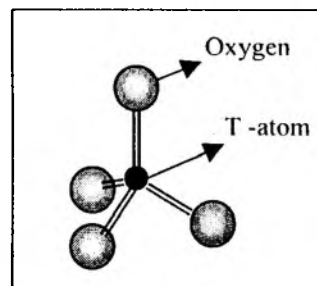
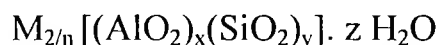


Figure 1.7. Schematic representation of a tetrahedron and T-atom (may be Si or Al)

definition, zeolites, a class of fascinating materials, are hydrated, crystalline, microporous aluminosilicates, which are comprised of a framework based on an indefinitely extending three-dimensional network of SiO_4 and AlO_4 tetrahedra, linked together through common oxygen atoms; each bridging oxygen is shared with adjacent tetrahedra. Each tetrahedron looks like the one shown schematically in Figure 1.7. The framework T atom (Si^{4+} and Al^{3+}) gives rise to a net negative charge balanced by non-framework cations. The crystallographic unit cell of the zeolites may be represented by the general formula⁵³,



where 'M' is the charge compensating cation with valency n, generally from group I or group II. Both inorganic (mono or divalent metal ions) as well as organic cations may be used to compensate the framework charge. 'z' represents the moles of water molecules, which are reversibly adsorbed, and the values of y/x can be from one to infinity since according to Loewenstein's rule, two aluminium atoms can not exist adjacent to each other.

Zeolites, as on today's world scenario, are almost the backbones of many industrial heterogeneous catalytic processes. As they are crystalline solids with regular, molecular-scale pores that incorporate catalytically active centers, exert unique catalytic influence due to their molecular sieving properties and solvent like character of their narrow pores. These catalysts provide a three dimensional media for reactions. Faujasite (please refer table) zeolites are used to effectively crack the high boiling petroleum fractions for the manufacture of gasoline and HZSM-5 to convert methanol into gasoline and in other petrochemical conversion processes including xylene isomerisation and toluene disproportionation⁷⁷.

1.7.2. CLASSIFICATION AND NOMENCLATURE

The nomenclature of zeolites was haphazard until the IUPAC commission published certain guidelines for their nomenclature⁷⁸. The IUPAC nomenclature is based on their framework density and number of T atoms per 1000 Å, irrespective of their composition, distribution of T-atoms, cell dimensions or symmetry parameters. A unique three letter code helps to simplify the nomenclature of the complicated frameworks structures (e.g., MFI stands for ZSM-5, MEL for ZSM-11 and AEL stands for AIPO₄-11 structures)

The zeolite structure is mainly comprised of a tetrahedral primary unit, TO₄, where T can be either Si or Al. Zeolites can be classified on the basis of morphological characteristics^{53,54,79,80}, crystal structure^{53,81}, chemical composition⁸² and effective pore diameter^{53,83}. Based on the morphology, zeolites are classified as fibrous, lamellar or materials with open framework structure. Structure classification of the zeolites has been proposed depending on differences in secondary building units and they are grouped as: analcime, natrolite, chabazite, phillipsite, heulandite, mordenite, faujasite, laumontite, pentasil and clathrate. The classification under chemical composition is exclusively based on the Si/Al ratio (SAR)⁸²; (a) low silica (SAR = 1.0 – 1.5), (b) medium silica (SAR = > 1.5 – 5.0), (c) high silica (SAR = > 5 to several thousand) and (d) Al-free pure silica molecular sieves. Zeolites are also classified with respect to their pore openings, defined as the number of T (or TO₄ T = Si or Al) units that shape the channels. There are four types of pore openings known to date in the microporous zeolites referred to as the 8-, 10-, 12-, and 14 rings openings called small-, medium-, large- and extralarge-pore zeolites respectively. A list of common zeolites classified according to their pore openings is presented in Table 1.8.

Table 1.8. Classification of zeolites according to the pore opening

8-membered ring (small pore)		10-membered ring (medium pore)		12-membered ring (large pore)		14-membered ring (extralarge pore)
	IZA code		IZA code		IZA code	
Linde A	LTA	ZSM-5	MFI	X	FAU	UTD-1*
Bikite	BIK	ZSM-11	MEL	Y	FAU	
Chabazite	CHA	ZSM-22	TON	EMC-2	EMT	
Edingtonite	EDI	ZSM-23	MTT	LTL		
Erionite	ERI	ZSM-35	FER	Beta	BEA	
Gismondine	GIS	ZSM-50/EU-1	EUO	ZSM-12	MTW	
ZK-5	KFI	ZSM-57	MFS	ZSM-18	MEI	
ZSM-39	MTN	NU-10	TON	NU-13	MTW	
ZSM-51	NON	NU-87	NES	SSZ-24	AFI	
Levynite	LEV	Theta-1	TON	Mordenite	MOR	
Melinoite	MER			Omega	MAZ	
Paulingite	PAU			ZSM-20	EMT/FAU	
Phillipsite	PHI					
Rho	RHO					

* UTD-1 (University of Texas at Dallas number – 1) is the only 14-membered ring synthetic zeolite

1. 7. 3. SYNTHESIS OF ZEOLITES

The pioneering work of Barrer on the synthesis and adsorption heralded the era of synthetic zeolites⁵⁴. The zeolite formation is a nucleation controlled-operation occurring from inhomogeneous hydrogels⁷⁸ in the temperature range of 348 to 523 K. Zeolites are synthesised hydrothermally by the combination of cations (both organic or/and inorganic), a source of silicon, a source of aluminum and water. Silicon sources normally used are sodium silicate, silica sol, silica gel, fumed silica and tetraethylorthosilicate (TEOS). Aluminium sources include sodium aluminate, aluminium sulphate and aluminium nitrate.

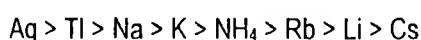
The major factors, which influence the structure of zeolites, are the hydrothermal synthesis time and temperature. The SAR (Si/Al ratio) determines the elemental framework composition of the crystalline zeolite product. Several other factors such as OH⁻ concentration, water concentration, cations and anions other than OH⁻ influence the synthesis of zeolites. Apart from them, there are some history dependent parameters such as aging period, stirring speed and time, and the order of mixing the components also may influence in some synthesis. The first step in synthesis is the dissolution (sometimes called as depolymerisation) of aluminium and silicon sources to form aluminate and silicate anions. These species are then condensed (polymerised) to form a gel. This gel is later cooked hydrothermally to form crystals of zeolites. Various aspects of the crystallisation of zeolites are described elsewhere⁸³. The guest species that occupy the channels and cavities account for the stabilisation of the crystals and the species are called the *templates*⁸⁴. But explaining the exact role played by the templates is rather very complex and not yet fully understood, although it is postulated that zeolite structures grow around the template thus stabilizing certain pore systems. Other than this structure directing effect, it may have roles such as gel modifier, buffer to maintain the pH of the gel, void filler to disperse water molecules⁸⁵. However, the present work does not include any zeolite synthesis but are modified to change in stoichiometry. So, it would be more useful to understand their properties and modifications that are possible in zeolite structures.

1. 7. 4. PROPERTIES OF ZEOLITES

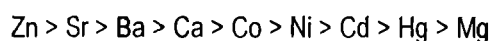
These materials are having properties such as adsorption, diffusion, molecular sieving, acid catalysis, shape selective catalysis, surfactant nature and solvent nature and many others as characteristics of their own due to their unique structural features. Ion exchange is the exceptional property of zeolites that is used in many industrial applications. For example, the elimination of radioactive ions from radioactive waste materials by clinoptilolite. However, our interest is to use this nature to alter the stoichiometry in the precursor powder for the ceramic preparation. Cation exchange behaviour of zeolites depends on

- (1) the nature of the cation species, the cation size, both anhydrous and hydrated, and cation charge
- (2) the temperature
- (3) the concentration of the cation species in the solution
- (4) the anion species associated with the cation in solution
- (5) the solvent (mostly it is water)
- (6) the structural characteristics of the zeolite

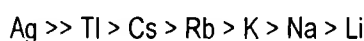
Ion exchange is accompanied by dramatic changes in the stability, adsorption behaviour and selectivity, catalytic activity and other important physical properties. The ultimate base exchange capacity of a zeolite depends on the chemical composition; a higher exchange capacity is observed with zeolites of low $\text{SiO}_2/\text{Al}_2\text{O}_3$ ratio. Zeolite A displays a double ion-sieve action. Only small cations can penetrate the single 6-rings into a β -cage. The order of decreasing selectivity for univalent ions in zeolite A is



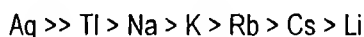
For divalent ions, the order of decreasing selectivity is



Zeolites X and Y are ideal materials for studying cation exchange phenomenon in zeolites. Differences in structures (cation positions, cation distribution, framework charge, Si/Al ordering) are evidenced in the differences observed in the cation exchange behavior of these zeolites. Below the level of 40% exchange, the selectivity for univalent ions was observed to be in the order,



At 50% exchange the selectivity series was found to be



The ion exchange capacity of a typical zeolite Y is lower than that of zeolite X due to the framework charge.

1. 7. 5. CHARACTERISATION

Powder X-ray diffraction is one of the prime tools extensively used for the characterization of zeolites. The crystallinity and phase purity are readily determined using this technique. However, the chemical composition can be determined by other spectroscopic techniques such as AAS, XRF, and EDAX. The thermal stability of zeolites varies depending on the chemical composition and the structure. This is often examined from the shape of the high temperature differential thermal analysis (DTA) exotherm. Various physico-chemical changes such as dehydration of adsorbed water, decomposition of occluded template material, the dehydroxylation and structure collapse can be analysed in combination with thermal gravimetric analysis (TGA). To understand the catalytic applications of zeolites, properties such as surface area, acidity, adsorption and diffusion may also be studied using various techniques. Selectivity in catalytic reaction products is another interesting inference during the characterization of a zeolite. However these techniques have no direct relevance to the present work.

1. 7. 6. CATALYTIC PROPERTIES

In the field of heterogeneous catalysis, zeolites are unique because of their selective nature. The term, 'shape-selective catalysis' was coined by Weisz and Frillette more than three decades ago⁸⁶. The molecular dimensional pore sizes of zeolites are the striking feature of the zeolites and related materials, which bring the comparison between different organic molecules and the zeolite pore leading to the concept of shape-selectivity. Shape selectivity consists of a combination of shape, size and configuration of reactants, transition states and products with dimensions, geometry and tortuosity of the channels and cages of zeolites. Csicsery⁸⁷ has categorised these selectivity effects as

1. Reactant selectivity
2. Product selectivity
3. Restricted transition state selectivity

1. 7. 7. ZEOLITES AS ADVANCED MATERIALS

In today's search for shorter, faster, more selective and efficient processes, the ability to engineer well defined spatial microarrangements of pure substances and composite materials is playing a pivotal role in creating new molecular level electronic, optical and magnetic devices. The host lattices and guest structures concept in nanometer architecture can be visualised in these microporous zeolite materials. A new frontier of solid state chemistry with great opportunities for innovative research and development is in the exploitation of zeolite materials. Against the traditional users of zeolites, within the last decade considerable effort has been directed at other uses of zeolites as advanced materials. For example, in the field of solar energy conversion technology a spatially well-organised molecular system is required that models photosynthetic mechanisms, thereby allowing redox reactions. Other potential applications include zeolite electrodes and electron relays, zeolite batteries, zeolite fast ion conductors, intrazeolite semiconductors, zeolite chemical sensors, zeolite imaging and data storage materials, zeolite lasers and displays, as well as zeolite composites to form perm selective membranes or thin films⁸⁸. Luminescence of zeolites themselves is another exploitable property of this class of materials, the range of which has been recently reviewed^{89,90}. However zeolites, like any other solid materials, have their limitations. Those specific to zeolites include pore plugging, poisoning, structural defects, the difficulties of growing large single crystals and interfacing a zeolite device with outside world. Many of these problems can although be solved, are deemed to be interesting research projects.

1. 7. 8. ZEOLITES AS RAW MATERIALS FOR MEP

Aluminosilicate based ceramics like, cordierite, mullite, β -spodumene, are attractive candidates for substrate applications in MEP as against the conventional materials. Preparation of these aluminosilicate based ceramics however becomes difficult using conventional methods. For example, conventional manner of preparing cordierite involves sintering at temperatures above 1250°C, and the resultant material does not have the desired high thermal conductivity⁹¹. Therefore, there is a need for a process to prepare cordierite at as low a temperature as possible and which has as high a thermal conductivity as possible⁹². Breck discloses that zeolites can be used to form cordierite by heating Mg exchanged X zeolite⁹³. The disclosed process involves heating the Mg-X zeolite at

1500°C to form a glass and then heating the glass above 1000°C to form cordierite. Thus, two steps are required to form cordierite. Another reference reveals the preparation of cordierite based ceramic article by heating Mg form of zeolites X, Y and A at a temperature above 900°C to about 1350°C⁹⁴. It also reveals that removal of sodium to very few ppm level enhances the reduction of dielectric constant and dielectric loss.

1. 8. OBJECTIVE OF THIS WORK

The zeolite-based route of preparing aluminosilicate type of ceramics opens up another area of modern ceramic research. The relative density and the phase purity are the two major problems always. Many times the formation of satellite phases such as polymorphs of silica and other metal oxides is possible depending on the chemical compositions⁹². Nevertheless, the above mentioned reports offer only preliminary details. When this work was started, on the basis of the literature survey carried out on this field, it was noticed that very limited reports were available. A survey in American Chemical Society's online-search conducted on 8th July 1995 covering a period from 1967 to then date with a search string of "micro" & "electronic" & "packaging" & "zeolite" showed only two references (CA No., 120:277842 and 112:243884). As the advantages over this novel route is tremendous compared to the conventional route of synthesis and fabrication, the scope over this work is also immense. Table 1.9. describes various advantages of this new route. Though the main thrust is to reduce the processing temperature and the thermal expansion match, they are well associated with the chemical and physical nature of the precursors. So, *the effect of various variables offered by zeolite precursors such as the effect of cation concentrations, effect of Si/Al ratio, effect of sintering atmosphere and so on are to be reevaluated.* However, these details are neither studied well enough nor available in open literature. *The present work is an attempt to gain such knowledge to overcome the hurdles in fabricating a best-suited candidate of zeolites based ceramic materials for MEP and other applications.* Table 1.9. summarises few of the marked points for comparison between the advantages of the zeolite route over the conventional route

Table no. 1.9. Advantages of zeolite route over other conventional methods.

Need for ZEOLITE route and advantages	
Problems with Conventional materials	Advantages of ceramics with zeolite route
High temperature to sinter (>1600 °C) Need of refractory metals (Pt, W etc.) Particle level Homogeneity Toxic powders (eg. BeO) Some are expensive (eg. SiC)	Low temp. sintering (< 1100° C) Possible usage of low cost metals Atomic level Homogeneity Non-toxic Relatively inexpensive Good Thermal Expansion Match(Si) Meets other needed properties

METAL OXIDE BASED

ZEOLITE BASED

1. 9. SCOPE OF THE THESIS

This thesis includes a novel preparation of electronic ceramics such as spodumene and cordierite using zeolites as precursors. It describes in detail how to modify the zeolite materials to get the required chemical composition using ion exchange with the desired cation source. It also illustrates the treatment of the powders like binding and the consolidation by die casting and then sintering into a range of temperatures to trace the various phenomena happening with the zeolite powder as a function of temperature and then ultimately to get the desired dense ceramic phase. It also studies the identification of the various impurity phases accompanied with different precursor powders prepared under various conditions to deduce a general correlation of ceramic fabrication with the precursor nature. The precursors' characterisation by various physico-chemical techniques like XRD, SEM, TG-DTA, NMR, EDAX, XRF, particle size analyser, etc., have been described. The studies on sintering processes of the precursors by XRD and NMR are also explained. The various ceramic characterisations of the final products have also been elucidated. The thesis is divided into five chapters.

The present chapter gives an introduction for materials science, ceramics, advanced ceramic powder preparation and processing and fabrication methods.

The second chapter gives detailed experimental procedures of various processes followed for the modification of the zeolite precursor powder. It also describes the instrumental and experimental specifications of various characterisation techniques used to analyse the samples.

The third chapter describes the preparation of lithium exchanged aluminosilicate (LAS) powder and fabrication into dense ceramic material (β -spodumene) and its characterisation using various techniques as mentioned above. The effects of different parameters like the concentration of Li^+ cation and Si/Al ratio are also discussed in the light of results obtained from various experiments. The dielectric and other structure related properties like density and shrinkage are discussed too. Impurity phases are identified and reported using XRD and solid state MAS NMR techniques.

The fourth chapter describes the preparation of magnesium aluminosilicate (MAS) using ion exchange and the fabrication of ceramics after the consolidation and sintering. It also discusses various characterisation of both the powders and the final ceramic products with several variation studies on the chemical stoichiometry of precursors. Another important study is the effect of atmosphere on phase transformation. Impurity phases formed with different sample powders are identified and reported using XRD and NMR. The dielectric and other structural studies are also explained. AC impedance spectroscopy has been used to study the nature of electrical conductivity in the ceramic materials.

The fifth chapter concludes the present investigation and summarises the important findings during the present work. The future scope of this research area is explained. An appendix has been furnished which includes the standard JCPDS powder XRD data along with the computer generated XRD lines for comparison.

Though this route has definite advantages with respect to chemical homogeneity and reduction in processing temperature, there is also some improvement in the product properties for electronic applications. These aspects are described in the fifth chapter along with few practical limitations.

Unlike conventional oxide route, the attainable stoichiometry of the precursor here is limited. The Si content is fixed for a given system, though the Si/Al ratio can be modified by de-alumination. Although, the cation concentration can be well adjusted as the exchange can be controlled by the concentration of the cation in the solution, the maximum degree of exchange is fixed for a given zeolite-cation pair. Though one can still fine tune the precursor stoichiometry and try for a better final phase purity, it is out of the scope this thesis. Rather the objective is to analyse the effect of various parameters in the precursor preparation and their reflections in the qualities of final ceramic product and to compare this route with the other conventional routes to have an idea about the relative ease of making it. The ceramics formed have better utilization in electronic packaging substrate applications. However, the ceramic characterisations carried out with the samples for this research work is not sufficient to launch this material for manufacturing. Lack of instruments in the laboratory for a complete characterisation for substrate application limits the extent of assurance for the unmediated operation of manufacturing for the mentioned application. However, the general and most desired properties are studied in detail within the reach of facilities.

"...I have only seen so far because I have been standing on the shoulders of other giants"

- Newton

REFERENCES

1. Ductile ceramic, News Brief, *American Ceramic Society Bulletin*, Vol 76, 12, p. 24 (1997)
2. Microsoft® Encarta® 98 Encyclopedia, *Microsoft Corporation* © 1993-1997 (1998)
3. Naslain, R; Langlais, F.; *Mater. Sci. Res.*, 20 (Tailoring Multiphase Compos. Ceram.), 145 (1986)
4. Evans, J. W.; De Jonghe, L.C.; *The production of inorganic materials*, Macmillan, New York (1991)
5. Newkirk, M.S.; Leshner H. D.; White, D.R.; Kennedy, C. R.; Urquhart, A. W.; Claar, T. D.; *Ceram. Eng. Sci. Proc.*, 8 (7-8), 879 (1987)
6. Brinker, C. J., Scherer, G. W.; *Sol-Gel Science*, Academic, New York, (1990)
7. Segal, D.; *Chemical Synthesis of Advanced Materials*, Cambridge Univ. Press., Cambridge, UK, (1989)
8. Yajima, S.; Okamura, K.; Hayashi, J.; Omori, M.; *J. Am. Ceram. Soc.*, 59 (7-8): 324 (1976)
9. Furukawa, K.; *Jpn. Kokai Tokkyo Koho JP patent JP 04089361 A2* (Mar 23, 1992)
10. McMillan, P.W.; *Glass Ceramics*, 2nd ed., Academic, London (1976)
11. Matijevic, E.; *Ultrastructure Processing of Ceramics, Glasses and Composites* (L.L. Hench and D. R. Ulrich, Eds.) Wiley, NY, pp 334-352 (1984)
12. Brook, R. J.; *Concise Encyclopedia of Advanced Ceramic Materials*, MIT Press, Cambridge, MA (1990)
13. Lange, F. F.; *J. Am. Ceram. Soc.*, 72(1), 3 (1989)
14. Chu, G. P. K.; *Ceramic Microstructures* (Fulrath, R. M. and Pask, G. A. Eds), Wiley, NY p. 828 (1968)
15. Rahman, M. N.; *Ceramic processing and sintering*, Marcel Dekker, Inc., NY (1995)
16. Advanced Structural Ceramics, *Business Communications Co. Inc.*, (BCC) USA, (1987)
17. Atmur, S. D.; Strasser, T. E.; *US Patent 5879640 A* (Mar 9, 1999)
18. Arapatsakos, C. L.; Sparis, P. D. and Botsaris, P. D. *Heat Technol.* (Pisa), 16(1), 83 (1998)
19. Gulati, S. T.; Zak, M. E.; Jones, L. F.; Rieck, J. S.; Russ, M.; Brady, M. J.; *Soc. Automot. Eng.*, [Spec. Publ.] SP, SP-1409 (Advanced Converter Technologies), 49, (1999)
20. TradeTech, CO, USA "Aerospace applications for structural ceramics", *Elements*, Vol 4, Iss 3 16 (1995)
21. Rah, H.; *Interceram*, 4:36, (1986)
22. World advanced ceramics: *Forecasts to 1995 and 2000*, Freedonia Group Inc, USA. (1991)
23. Subbarao, E. C.; *Advanced ceramics- II*, Indian Academy of Sciences pp 37 (1991)
24. Subbarao, E. C.; *Preparation and characterisation of materials* (eds) Honig, J.M.; Rao, C. N. R., Academic, NY (1981)
25. Niwa, K.; Hashimoto, K.; Goto, Y.; *NATO ASI Ser.*, Ser. 3, 58(Interfacial Science in Ceramic Joining), 417 (1998)
26. Schwartz, B.; *Am.Ceram.Soc. Bull.*, 63, 577 (1984)
27. Choudhary U.; Sleight A. W.; *Am. Rev. mater. Sci.*, 17, 323 (1987)
28. Schwartz. B.; Microelectronics packaging, *Electronic ceramics*, pp 12, Am. Ceram. Soc. Publication No.3. (1969)
29. Wilcox. D. L.; *Solid St. Technol.* 14(1), 40, (1971); 14 (2), 55 (1971)
30. Seraphin D.P.; Feinberg, I.; *IBM J. Res. Dev.* 25(5) 617 (1981)
31. Schwartz. B., J.; *Phys. Chem. Solids*, 45, 10, 1051 (1989)
32. Subramanium, M. A.; Corbin D.R.; Farlee R.D.; *Mat. Res. Bull.*, 21, 1525 (1986)

33. Selvaduray, G.; *Symp. Proc. ASM 4th Intl. Conf. On Electronic Materials and Processing*, Montreal, CA, Aug 19 (1991)
34. Subramaniam, M. A.; Corbin, D. R.; Chowdhary, U., *Advanced Ceramics*, 26, 239 (1989)
35. Schwartz, B.; *Am.Ceram.Soc. Bull.*, 65, 1032 (1986)
36. Kuwahara, M.; Funaki, M.; Hiraga, K., Jpn. Kokai Tokkyo Koho, *Japan patent JP 10265267 A2* (Oct 6, 1998)
37. Shishkov, N. V.; Kozlova, N. M.; Velichko, A. V.; Vakhlamova, I. A.; Shishkov, A. K.; Kozlenkova, N. I.; Orlova, L. P.; Mikulenok, V. V.; Khlebova, N. E.; *Vysokotemperaturn. Sverkhprovodimost, Moskva*, (4), 70 From: Ref. Zh., Khim (1990)
38. Gromov, V. V.; Ivanov, V. V.; Popov, I. B.; *Sverkhprovodimost: Fiz., Khim., Tekh.*, 3(8), 1685 (1990)
39. Clark, D. E.; Iftikhar, A.; Dalton, R. C.; *US Patent 89-351059* (May 14, 1990)
40. Mazdiyasi, K. S.; *Mater. Res. Soc. Symp. Proc.*, 32(Better Ceram. Chem.), 175 (1984)
41. Livage, J.; Beteille, F.; Roux, C.; Chatry, M.; Davidson, P.; *Acta Mater.*, 46 (3), 743 (1998)
42. Johnson, D.W.; *Am.Ceram Soc. Bull.*, 60 (2) : 221 (1981)
43. Johnson, D.W.; *Advances in Powder Technology* (G. Y. Chin, Ed.), American Society for Metals, OH, pp 27 (1982)
44. Polke, R.; Stadler, R.; *Concise Encyclopedia of Advanced Ceramic Materials* (R. J. Brook, Ed.), MIT Press, Cambridge, MA, pp 187 (1991)
45. Ghosh, B.; (Micron Powder Syst., Summit, NJ 07901, USA). *Ceram. Eng. Sci. Proc.*, 14(1-2), 264 (1993)
46. Beddow, J. K.; *Particulate Science and Technology*, Chemical Publishing Co., NY (1980)
47. Evans, J. W.; De Jonghe, L. C.; *The production of Inorganic Materials*, Macmillan, NY (1991)
48. Lin, I. J.; Nadiv, S.; *Mater.Sci. Eng.*, 39 : 93 (1979)
49. Patankar, S. N.; Xiao, S. Q.; Lewandowski, J. J.; Heur, A. H.; *J. Mater. Res.*, 8 (6) : 1311 (1993)
50. Stober, W.; Fink, A.; Bohn, E.; *J. Colloid Interf. Sci.*, 26:62 (1968)
51. Mazdiyasi, K. S.; Doloff R. T.; Smith, J. S., Jr.; *J. Am. Ceram. Soc.*, 52 (10) : 523 (1969)
52. Somiya, S.; *Concise Encyclopedia of Advanced Ceramic Materials* (R.J. Brook, Ed.) MIT Press, Cambridge, MA, pp 375 (1991)
53. Breck D. W.; *Zeolite Molecular Sieves*, John Wiley and Sons, New York (1974)
54. Barrer R. M.; *Hydrothermal Chemistry of Zeolites*, Academic Press, New York (1982)
55. Masters, K.; *Spray drying*, 4th ed., Wiley, NY (1985)
56. DeLau, J. G. M.; *Am. Ceram. Soc. Bull.*, 49 (6) 572 (1970)
57. Messing, G. L.; Zhang, S. C.; Jayanthi, G. V.; *J. Am. Ceram. Soc.*, 76; 2707 (1993)
58. Real, M. W.; *Proc. Br.Ceram. Soc.*, 38:59 (1986)
59. Atkinson, A.; Segal, D. L., J.; *Sol-Gel Sci. Technol.*, 13(1/2/3), 133 (1998)
60. Ismail, M. G. M. U.; Tsunatori, H.; Nakai, Z., J.; *Am. Ceram. Soc.*, 73, 537 (1990)
61. Pechini, M.; U. S. Patent 3,330,697 (1967)
62. Kakihana, M; Arima, M; Yoshimura, M; Ikeda, N; Sugitani, Y.; *J. Alloys Compd.*, 283(1-2), 102 (1999)
63. Chick, L. A.; Pederson, L. D.; Maupin, G. D.; Bates, J. L.; Thomas, L. E.; Exarhos, G.; *J. Mater. Lett.*, 10 (12):6 (1990)
64. Li, J; Tian, J.; *Gongneng Cailiao*, 29(5), 452 (1998)
65. Moulson, A. J.; *J. Mater. Sci.*, 14, 1017 (1979)
66. Mazdiyasi, K.S.; Cooke, C. M.; *J. Am. Ceram. Soc.*, 56, 628 (1973)

67. Mazdiyasi, K.S.; Cooke, C. M.; *U. S. Patent* 3, 959, 446 (1976)
68. Harper, C. A.; Staley, W. W.; *Electronic Packaging and Production*, pp 58 (1985)
69. Schwartz, B.; *Am. Ceram. Soc. Bull.*, 63: 577-81 (1984)
70. Taylor, D.; *Br. Ceram. Trans. J.*, 83:129-34 (1984)
71. Maeda, K.; *Advances in ceramics*, Yan, M.F.; Heuer, A. H.; Eds, Am. Ceram. Soc., Inc. Vol 7 p 260 (1983)
72. Genesse, C.; Chowdhry, U.; *Better Ceramics Through Chemistry II*, Brinker, C. J., Clark, D. E.; Ulrich, D. R.; Eds., (Mater. Res. Soc. Proc. 73 Pittsburgh, PA) pp 693 (1986)
73. Hayashi, K.; Fukui, M.; *Sci. Technol.*, 29, 58 (1980)
74. Mussler, B. H.; Shafer, M. W.; *Am. Ceram. Soc. Bull.*, 63, 5 (1984)
75. Moyer, J. R.; Prunier, A. R., Jr.; Hughes, N. N.; Winterton, R. C.; *Mater. Res. Soc. Symp. Proc.*, Vol 73, p117, (1986)
76. Subramaniam, M. A.; Corbin, D. R.; Farlee, R. D.; *Mat. Res. Bull.*, 21, 1525 (1986)
77. Weisz P. B.; *Proc. 7th Int. Cong. Catal.*, 1, 1 (1981)
78. Barrer R. M.; *Pure Appl. Chem.*, 51, 1091 (1979)
79. Meier, W. M.; Olson, D. H.; *Atlas of zeolite Structure Types*, London Butterworths, (1987)
80. Bragg, W. L.; *The atomic Structures of Minerals*, Cornell University Press, Ithaca, New York (1937)
81. Meier, W. M.; *Molecular Sieves*, Soc. of Chem. Ind., London, p10 (1968)
82. Flanigen, E. M.; *Proceedings of the 5th International Conference of Zeolites*, (L.V.C. Reeds, Eds.) Naples, Italy, June 2-6, p760 (1980)
83. Sand, L. B.; *Econ. Geol.* p191 (1967)
84. Flanigen, E. M.; *ACS Symp. Ser.*, 121, 119 (1973)
85. Szostak, R.; *Molecular Sieves, Principles of synthesis and Modification*, Van Nostrand Reinhold, NY (1989)
86. Weisz, P. B.; Frillette, V. J.; *J. Phys. Chem.*, 64, 382 (1960)
87. Csicsery, S. M.; *Zeolites*, 4, 202 (1984)
88. Ozin, G. A.; Kuperman A.; Stein, A.; *Angew. Chem. Int. Ed. Eng.*, 28(3), 359 (1989)
89. Stucky, G. D.; *Prog. Inorg. Chem.*, 40, 99 (1992)
90. Ozin, G. A.; *Adv. Mater.*, 4, 613 (1992)
91. Moyer, J. R.; Prunier, A. R., Jr.; Hughes, N. N.; Winterton, R. C.; *Mater. Res. Soc. Symp.*, 73, 117 (1986)
92. Bedard, R. L.; Flainigen, E. M.; *U. S. Patent* 4,980,323, (Dec. 25, 1990)
93. Breck, D. W.; *Zeolite Molecular Sieves*, John wiley & sons, NY, 493 (1974)
94. Chowdhry, U.; Corbin D. R.; Subramanian, M. A.; *U.S. Patent* No. 4 814 303 (Mar. 21, 1989)

METHODOLOGY – PREPARATION PROCEDURES AND CHARACTERISATION TECHNIQUES

Chapter



2.1. PREPARATION PROCEDURES

2.1.1 INTRODUCTION

This chapter describes the general methodology followed and the materials used for the current research.. The first part of this chapter includes the methods adopted for the preparation of samples, the second part, the materials used for the preparation. The third part describes the characterisation techniques used to analyse the sample and the general methods of calculations used to estimate the properties and demonstrate the advantages of the materials studied.

The basic aim of the current study is to synthesize ceramic materials and characterize them for specific applications. Though chapter 3 and chapter 4 will deal with two different ceramic systems, namely Lithium Aluminosilicates (LASs. for eg., β -spodumene) and Magnesium Aluminosilicates (MASs. for eg., cordierite), basically the methods adopted are almost the same, as far as the basic characterisation is concerned. However, just because of the curiosity to learn and analyse the ceramics using new and different characterisation methods as research tools for understanding purposes, few special techniques have been tried for each system individually. Few of them are not done for both the samples due to lack of facility and availability of the instrument of interest. Nevertheless, it is important to note that for ceramic materials prepared using zeolites as precursors these techniques are employed for the first time. So the third part of this chapter is mainly focused on few such uncommon characterisation techniques on these ceramic materials. It includes a brief introduction about the theory behind the technique, the instrumentation and then experimental condition of the machines at which the measurements were made.

2.1.2. PREPARATION OF PRECURSORS

2.1.2.a. *Ion exchange*

The section 1.7.d of the first chapter gives a general idea about the ion exchange property of the zeolites. This is one of the important properties of these materials that attracted many researchers and subsequently numerous reports have come out after substantial work in this area. Various models were predicted and theories were proposed¹. Breck compiles many such reports as a special chapter on the theory of ion exchange in his book². In the present work, ion exchange has been used to alter the chemical composition of the zeolite materials to get the desired composition for ceramic preparation. The cation to be exchanged, M^+ varies for each system, e.g., univalent Li^+ for LAS and the divalent Mg^{2+} in case of MAS systems. The ion exchange procedure usually involves refluxing the zeolite powder along with the ion solution of interest in a round-bottomed flask at a constant

temperature for a period of time with intermittent shaking. However, for laboratory preparations in higher scale this becomes somewhat difficult, as the transfer of solid slurry for filtration, for removal of exchanged ions is not easy. So, an ion exchange reactor was designed and the exchange was carried out advantageously. Figure 2.1.1 gives a schematic representation of the reactor used for the ion exchange process.

It is a double walled reactor, which has an outer jacket, fitted with an inlet-outlet setup to circulate hot water to maintain uniform heat throughout the time of ion exchange. The baffled inner wall gives a continuous swirl of the solid particle to suspend during the process and avoids settling of the particles during stirring. The detachable top makes the transfer of slurry easier after ion exchange for washing. Extra inlets on the top may be used for the constant and slow supply of fresh ion solution into the slurry.

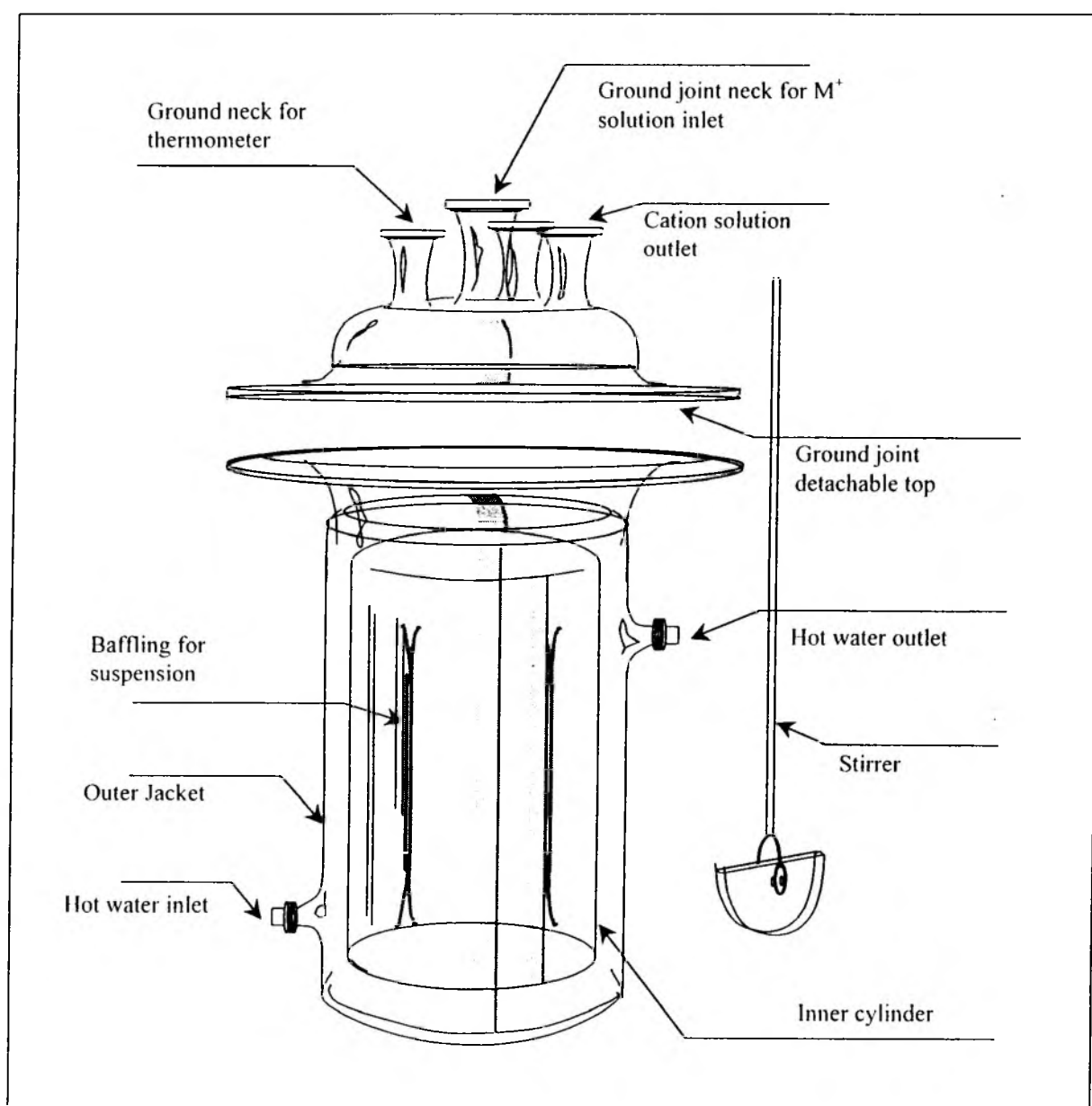


Figure 2.1.1. The reactor designed for ion exchange

For both LAS and MAS systems the cation sources used were the solutions of nitrate salts of Li and Mg respectively. The salts were diluted in distilled water to get different molar solutions as per need (from 0.01 M to 1 M). These solutions were introduced into the solid zeolite powder in the ion exchange reactor. The ratio of solid zeolite powder to the solution was maintained as 1:10. This exchange procedure was repeated for N_x (N_x is the number of exchanges and x varies from 1 - 3) times for few of the samples as per the need as mentioned in various places. Each exchange reaction was carried out for ~ 5 hours and then the slurry was removed for washing, drying at 120 °C and was reused for the next exchange. Figure 2.1.2. illustrates the process.

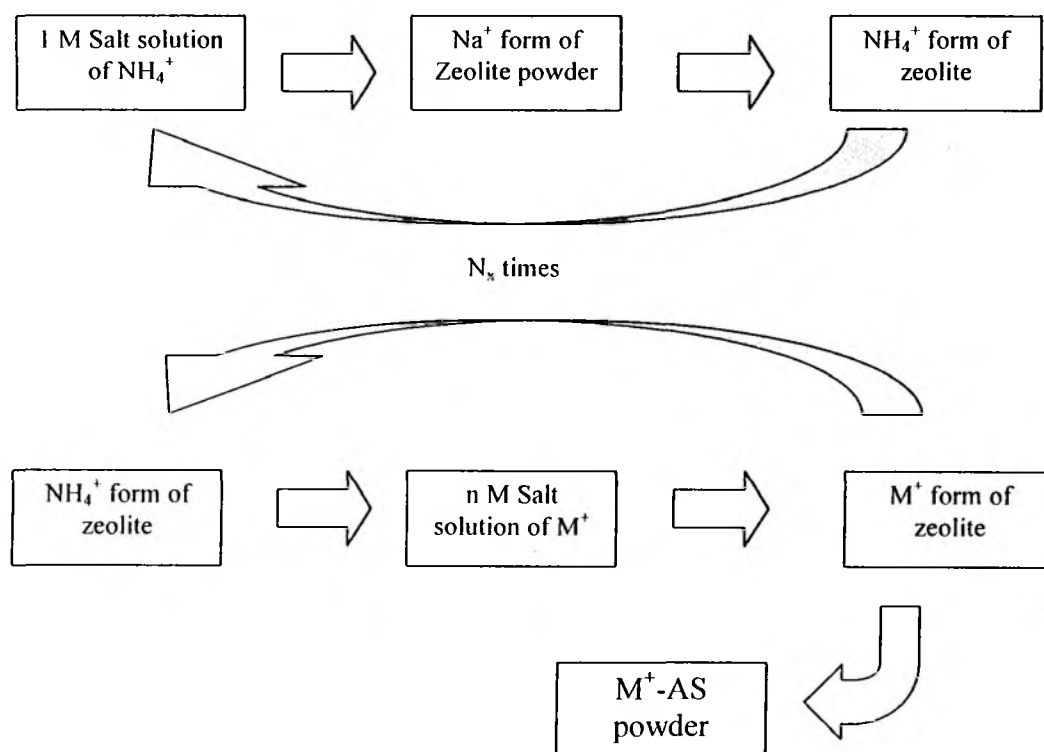


Figure 2.1.2. Scheme of procedure followed for ion exchanging the precursor material. "n" changes from 0.01 to 1 for different samples. M^+ can be Li^+ or Mg^{2+} and "x" changes from 1 - 3 for different samples of various M^+ samples as the case may be.

2.1.2.b Post ion exchange treatment

The powder was washed in hot distilled water for several times to ensure complete removal of cations from the zeolite network to the solution after exchange. The powder was then dried at 120 °C for over night and then calcined at 480 °C for 5 hours. The dry solid was crushed into fine powder and used for other studies and modifications.

2.1.3. FORMING AND CONSOLIDATION PROCESSES

2.1.3.a. Binding the powder

Binding of the powder before sintering is a very vital aspect and many researchers have suggested a choice for binders³. Onoda reviews the use of a series of binders (mostly organic) and their advantages⁴. In the present investigation, a low-medium viscosity grade and non-ionic binder, namely polyvinyl alcohol (PVA) was used

before consolidating the powder. 1 wt % binder was added to the solid powder. Using the following procedure, 10 wt % solution of PVA was prepared. 10 g PVA was added with 90 g of distilled water and stirred for complete dissolution at 70 - 80 °C. The heating was continued till the solution becomes clear. This solution was used for all the powders as binder. 10 g of this solution and 99 g of the powder was mixed thoroughly. The mixture was dried under IR lamp until air dry with intermittent grinding and mixing with a spatula. This powder was used for pelletisation.

2.1.3.b. Consolidation of powder (pelletisation)

The powder was pressed into pellets of desired dimensions. In this study two sizes of steel dies with inner diameters of 13 mm and 20 mm were used for specific characterisations. The pellets were made in a hydraulic press with an optimised pressure of 2.5 tons. The pellets were used for sintering studies. This pellet is called a "green pellet".

2.1.4. SINTERING

The green pellets were given heat treatments in sintered MgO boats. These boats can withstand temperatures up to 1600 °C. The pellets were heated at different temperatures as per the need at air atmosphere (except for the study on the effect of atmosphere on sintering). The sintering processes were done in a programmable furnace (NEBOURTHERM) at relatively low heating rates (eg., 4 °C per minute). All the cooling processes were natural. Figure 2.1.3. shows a typical program of heating. T1 is the temperature at which the binder gets away the system and T2 is the temperature at which the sample is sintered isothermally. The parameters t1, t2, t3 and t4 are the respective times taken (in minutes) for the individual processes since the starting of the program. However, the heating rates and programs have been given at appropriate places wherever necessary in the thesis. The sintered pellets are used as such or crushed into powder for different studies as required.

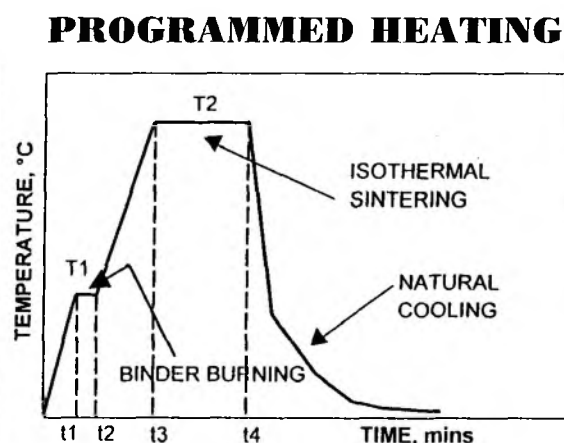


Figure 2.1.3. Typical heating program for sintering the precursor.

2.1.5. SINTERING IN DIFFERENT ATMOSPHERES

For special studies like the effect of reducing and oxidising atmospheres during sintering at high temperature, the furnace was attached to a continuous flow system of controlled gas. A mass flow controller controlled the gas flow from the cylinder and the gas was passed at a flow rate range of 20 cc/min. Before starting the heating process the furnace was purged with an inert gas (Argon - INOX grade) for 3 hours. The entire setup has been depicted in Figure 2.1.4. The study of sintering behaviour in different atmosphere is one of the research fields in which there are interesting reports⁵⁻⁷.

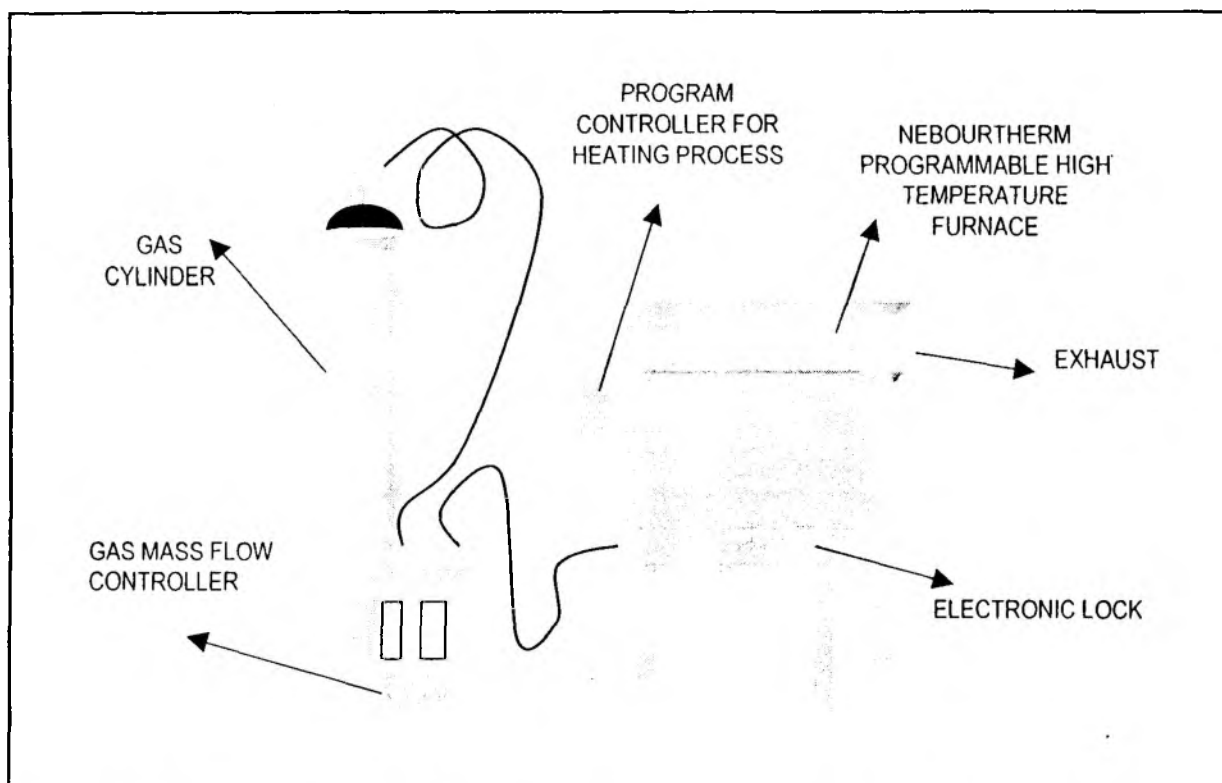


Figure 2.1.4. The reactor setup for high temperature solid-state reactions with different atmospheres

2.2. MATERIALS USED

All the chemicals used for preparation and reagents used for special operations on these materials are included here along with other details.

2.2.1 PRECURSOR BASES

All the zeolites used in this study were commercially available from different companies and their properties are listed below. The Na^+ form of the zeolites were converted into NH_4^+ form using the ion exchange method provided in the earlier section. The chemical compositions and surface areas were estimated in the laboratory and found matching with the reported value by the company. Chemical compositions were checked by XRF and the surface areas were estimated using N_2 sorption on OMNISORP adsorption unit on the basis of the BET model. Table 2.2.1 shows these details.

Table 2.2.1. Zeolites used and their properties

Material	From	Cation Form	Converted into form	Chemical Composition*		Surface Area, m ² /g
				SiO ₂ / Al ₂ O ₃	Na ₂ O %	
Zeolite A	CATAD, IPCL, INDIA	Na ⁺	NH ₄ ⁺	2.13	0.585	?
Zeolite Y	Zeolyst Corp., UK.	NH ₄ ⁺	NH ₄ ⁺	5.20	0.20	780
Zeolite P	CPP, NCL, INDIA.	Na ⁺	NH ₄ ⁺	2.82	0.07	?

* Chemical composition by XRF after converted into NH₄⁺ form.

2. 2. 2. EXCHANGING ION SOURCES

To convert the Na⁺ form of the zeolites to NH₄⁺ form and then to the M⁺ forms, the nitrate salts of the cations Li⁺ and Mg²⁺ were used as exchanging ion sources. The Table 2.2.2 provides details of the salts used.

Table 2.2.2. Details of ion sources used for ion exchanges

Source for ion	Salt	Chemical formula	From	Grade and Assay	
				Grade	Assay
Li ⁺	Lithium Nitrate	LiNO ₃ .3H ₂ O	Loba Chemie, INDIA	GR	98 %
Mg ²⁺	Magnesium Nitrate	Mg(NO ₃) ₂ .6H ₂ O	Loba Chemie, INDIA	GR	99 %
NH ₄ ⁺	Ammonium Nitrate	NH ₄ NO ₃	Loba Chemie, INDIA	GR	99.5 %

2. 2. 3. BINDER MATERIAL

The binder used for powder consolidation is PVA. The details including the molecular weight (MW) are given in Table 2.2.3.

Table 2.2.3. Details of the binder used in the process.

Binder	Full name	Chemical formula	From	Assay and MW	
				Assay	MW
PVA	Poly(vinyl alcohol)	[-CH ₂ CH(OH)-] _n	Aldrich Co., WI, USA	99+%	1,00,000

2.3. CHARACTERISATION TECHNIQUES

2.3.1 INTRODUCTION

This section will give a brief account of the various characterisation techniques used in this investigation. Though many of them are common techniques, few of them are not common. Brief outlines and the instrumental details are given for theoretical introduction e.g., Impedance spectroscopy and thermo-mechanical analysis. For other common techniques, the instrumentation details have been given.

2.3.2. CHEMICAL ANALYSIS BY AAS AND XRF

The chemical composition of the samples was analysed using X-ray fluorescence spectroscopy (XRF) and atomic absorption spectroscopy (AAS) with respect to the nature of the sample.

An exact amount of samples was taken in a platinum crucible with lid and ignited to get the dry weight of the sample. The sample was then cooled in a desiccator and weighed. The difference in weights gave the loss on ignition. The anhydrous weight of the sample was noted. The anhydrous sample was treated with hydrofluoric acid (40 wt.%) and evaporated on a hot plate to remove silicon in the form of SiF_6 . This treatment was repeated three times and the sample was again ignited, cooled in a desiccator and weighed. The loss in the weight of the sample was determined to get the content of silica. The residue was fused with potassium pyrosulphate and dissolved in water. It was then analysed by *CHEMITO 201* ATOMIC ABSORPTION SPECTROMETER in emission mode for the elements Na and Li. The Si content was determined by gravimetry. A known amount of samples were pressed into pellets of 20mm diameter. The pellets were dried under IR lamp and kept in a desiccator. They are directly introduced into XRF unit for elemental analysis by fluorescence spectroscopy. The concentration of Si and Al in terms of elemental weight percentages (wt. %) was determined and the Si/Al ratios were found out. The instrument used was a sequential X-Ray fluorescence spectrometer, *RIGAKU 3070E* with Rh target energized at 50 kV and 40 mA.

2.3.3. X-RAY DIFFRACTION

The high temperature solid state reactions include various transformations in physical nature and fine structure of the raw materials. X-ray diffraction is a common technique to follow the structural transformations and formation of crystal structure of the new phases⁸⁻⁹. Though this technique gives a qualitative account of the various crystalline phases present in the polycrystalline multi-component solid powder, the quantification of each phase and the amorphous impurities are still not yet established well. However, there are few reports on the latter¹⁰. And hence the present studies give a qualitative identification and a semi-quantitative analysis (by "search-match" software) of the phases at high temperatures.

Powder X-Ray diffraction pattern of the samples heated at various samples were recorded using *RIGAKU DMAX III VC* instrument equipped with a graphite crystal monochromator and NaI scintillation counter. Nickel filtered Cu K_{α} radiation ($\lambda=1.542 \text{ \AA}$) was used with Si as internal standard for those samples for which the lattice parameters were calculated. For other samples Si was used as external standard and then 2θ values and interplanar 'd' spacings were corrected accordingly and refined using least square fitting.

The XRD patterns of multiphase powder products after heating to various temperatures were subjected to an in-built Rigaku search-match software (*Casio* version) with the JCPDS standard file library facility. This facility offers a comparison of the unknown pattern with almost 40,000 JCPDS standard inorganic mineral files. The matching files were recorded and later to eliminate the repetition of similar structures, they were matched manually among the files listed in auto-search result. The best matching phases with respect to both 2θ and relative intensity values were reported with the semi-quantitative amount of each phase in it as calculated by the software. Research reports on similar work are available in literature¹¹.

2. 3. 4. THERMOGRAVIMETRY

As thermal treatment is the main force for crystallisation and phase transformation, the behaviour of precursors on heating reveals a lot of information about the possible phenomena involved in sintering. Thermogravimetry (TG) in combination with differential thermal analysis (DTA) has been a most successful technique to acquire information about this. Bruce reviews the latest developments in this technique¹². Recently, many reports have shown that this technique can be exploited in a better and efficient way in combination with other spectral techniques like FTIR, Mass Spectroscopy¹³⁻¹⁴. Usually, these are counted in terms of the weight losses and the energy variations. In the current investigation, the changes in precursor samples including the structure collapse and phase transfer processes at high temperatures were checked by recording TG/DTA plots using *SETARAM TG-DTA 92* instrument in air (in some cases, argon) atmosphere at a heating rate of 5°C or $10^{\circ}\text{C} / \text{min}$. The range of temperature studied using this instrument is from room temperature (RT) to 1000°C .

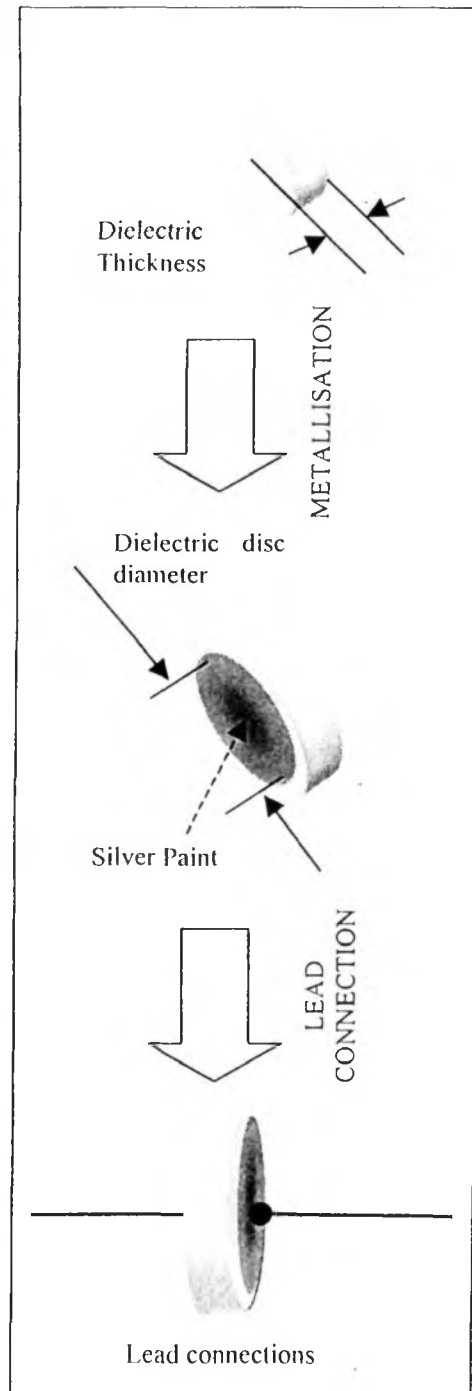


Figure 2.3.1. Electroding the disc for dielectric measurements.

2. 3. 5. SCANNING ELECTRON MICROSCOPY

Scanning Electron Microscopy (SEM) is a technique by which the changes in the solid samples due to the heat treatments can be visually seen. The new generation tool, high resolution SEM is therefore extremely useful as a rapid and versatile characterization technique, both during and after fabrication of ceramic materials. Using this, surface and cross-sectional views of mesoscopic systems can also be observed working in a range of accelerating voltages from 1 to 30 keV¹⁵. The sintered samples were analysed by scanning electron microscopy (SEM) to look at the morphological and particle size variations during the course of heating. The system used was JEOL JSM – 5200 instrument. The EDX analysis was carried out to determine the Si/Al ratio using the Kewax attachment to SEM. Few of the precursor samples were scanned for high resolution using SEM / EDX PHILIPS XL 30 HIGH RESOLUTION unit. The pictures were taken in different magnification with respect to the sample nature. The magnifications are given along with the micrograms.

2. 3. 6. SOLID STATE MAS & STATIC NMR

Recent reports show that solid state NMR is an effective technique to explore the dense solid ceramic matrices¹⁶⁻¹⁹. Exclusive NMR studies on the ceramic sintering aspects have also been carried out by MacKenzie and co-workers and others¹⁹⁻²². Although, NMR has not been used extensively in the area of zeolite based ceramic preparations, Colyer and his coworkers studied the structure collapse of zeolite sample by NMR²³. However, there were not many details on the secondary ceramic crystallisation. Matsumoto has studied the crystallisation of anorthite ceramic by NMR²⁴.

The present work includes studies of various sintered and green samples of MAS and LAS zeolite based systems by solid state nuclear magnetic resonance (NMR) for different probe nuclei, viz., ²⁹Si, ²⁷Al and ⁷Li. NMR offers a powerful tool in the characterization of precursor powder solids as well as sintered ceramics for studying the different forms of the nuclei present in them. Basically the interest was to follow up the HT sintering at various temperatures. However the precursor powders were also studied by NMR. It is important to note that such NMR studies on the zeolites based ceramic crystallisation of cordierite and β -spodumene materials are reported for the first time.

Though NMR is an effective tool for nuclei like ²⁷Al, ²⁹Si and ⁷Li, there are some inherent and undesired issues. Despite its low abundance (4.7 %) ²⁹Si offers less complications in spectral interpretations since the nuclear spin for ²⁹Si is half (1/2) and the magic angle spinning (MAS) at once guarantees a high resolution NMR spectrum. The MAS spectrum displays a narrower resonance, whose chemical shifts carry the signature about the chemical environment around the silicon.

On the other hand, despite the high natural abundance associated with ²⁷Al and ⁷Li (100 % and 92.58 % respectively), the line narrowing due to MAS is rather poor. This is attributed to the failure of MAS to narrow the spectral lines from integer-half quadrupolar nuclei to which ²⁷Al (I = 5/2) and ⁷Li (I = 3/2) belong. In spite of this drawback, MAS was sought to be used in the present study for ²⁷Al since we could identify the tetrahedral and octahedral Al under MAS. For ⁷Li, the experimental choice was limited to static samples since our MAS probe

was tunable only in the range of ^2H - ^{13}C (46.05 MHz to 75.43 MHz). A Quadecho experiment was tried to suppress the quadrupolar effect and to get well resolved ^7Li NMR spectra.

2. 3. 6. a. ^{29}Si and ^{27}Al Magic Angle Spinning (MAS) Nuclear Magnetic Resonance

The ^{29}Si and ^{27}Al MAS NMR spectra were recorded at 54.6 MHz and 78.2 MHz respectively using a *BRUKER MSL-300 FT NMR* spectrometer. The spectrometer is equipped with *ASPECT 3000* computer and a BC – 132 fast digitizer. A magic angle spinning probe housing a boron nitride stator with double-bearing design was used. ^{29}Si and ^{27}Al frequencies could be selectively tuned on the broad-banded X-nucleus channel. R.F pulses were generated in a broad band transmitter delivering 300 watts of pulsed power into the CP-MAS probe. The finely powdered samples were packed into a 7 mm zirconia rotor and spun at a speed of 2.4 kHz. The Free Induction Decays (FID) were collected using a 40° flip angle pulse and a 2 sec relaxation delay. 4000 to 5000 transients were added using a standard CYCLOPS pulse sequence to improve signal to noise ratio. The data were processed with 50 Hz line broadening prior to Fourier Transformation. The chemical shifts of ^{29}Si and ^{27}Al MAS NMR spectra were referred to TMS and $\text{Al}(\text{NO}_3)_3 \cdot 9\text{H}_2\text{O}$ (0.0 ppm) respectively.

2. 3. 6. b. ^7Li STATIC and QUAD-ECHO Nuclear Magnetic Resonance

The ^7Li NMR spectra were recorded in the static mode at the Larmor frequency of 116.59 MHz on the Bruker MSL-300 FT NMR spectrometer. In order to record ^7Li spectrum without severe baseline and intensity artifacts, a Bruker Wide-line probe was used. To achieve shorter 90° pulses, a 5 mm (i.d) radio frequency (r.f) coil made up of flattened 22 gauge copper wire was wound and this replaced the 10 mm r.f coil in the probe insert. By this way, 90° pulse of 3.2 μs could be achieved as against 5 μs generated by the 10 mm coil. For ^7Li NMR spectra, the time domain data were acquired either using a single pulse (QUADCYCL.PC) or a $90^\circ_x - \tau - 90^\circ_y$ (QUADECHO.PC) sequence. While employing single pulse sequence a pre-acquisition delay of 15 μs was used to minimize transients from probe ringing entering the analogue to digital converter. The probe ringing effects are, however eliminated when QUAD-ECHO sequence is used, since the second r.f pulse generates an echo at a time τ , which is conveniently chosen to be in the range of 20 to 40 μs , greater than the dead-time (c.a 10 to 15 μs .) of the receiver. By starting the data acquisition on top of the QUAD-ECHO, the full FID is digitized and this upon Fourier Transformation yields an undistorted ^7Li quadrupolar broadened NMR spectrum. Typically 800 and 1200 transients were signal averaged in the single pulse and quad-echo experiments, respectively.

2. 3. 7. DIELECTRIC CONSTANT MEASUREMENTS

The sintered pellets were lapped into regular discs of equal thickness throughout the disc. They were then electroded (metallised) with a uniform coating of conducting silver paint as circles of equal diameter on both sides. They were later cured at 450°C for 2 hours to ensure proper electroding. Figure 2.3.1. shows the electroding of the dielectric sample. The discs were mounted in a disc holder setup as illustrated in Figure 2.3.2. The contacts were adjusted to get a steady capacitance to avoid contact capacitance. The dielectric properties were measured at a frequency range of 20 Hz to 1 MHz with a measuring current of $I_m = 0.34 \mu\text{A}$. A *HP 4284 LCR BRIDGE* interfaced in parallel with a microprocessor controlled LCD display was used for analysis. The dielectric constants of the discs were calculated from the capacitance measured using the following relationship,

$$\epsilon_T = \frac{1/\epsilon_0 \cdot C_x \cdot t}{A}$$

where ' ϵ_T ' is the dielectric constant of the given disc and ' ϵ_0 ' is the permittivity of free space, ' C_x ' is the capacitance in pF, ' t ' is the dielectric thickness and ' A ' is the dielectric area of the disc as illustrated in Figure 2.3.1.

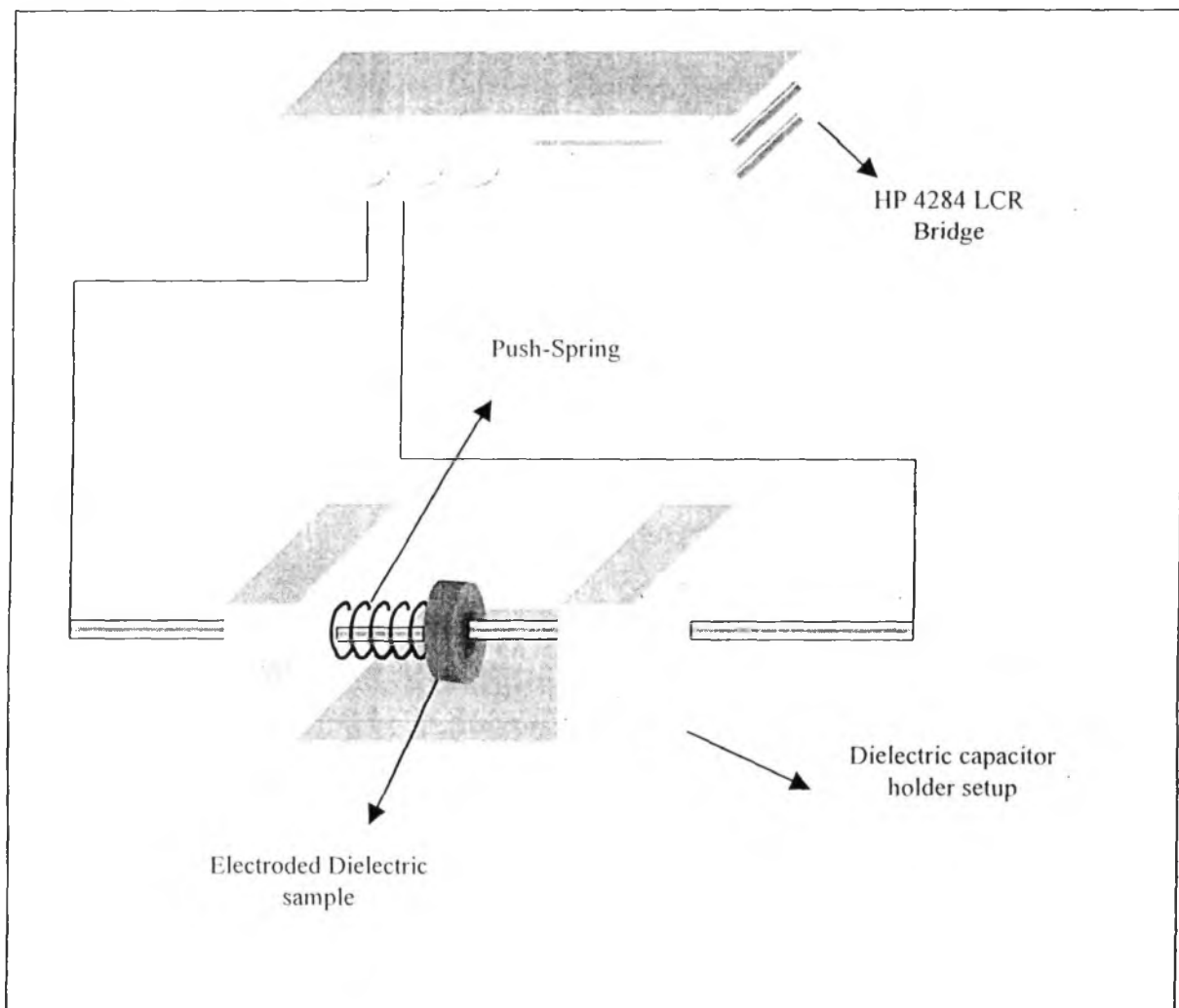


Figure 2.3.2. Measurement setup for Dielectric constant with HP LCR meter.

2.3.8. IMPEDANCE SPECTROSCOPY

2.3.8. a. Introduction

Impedance spectroscopy is one of the rapidly emerging techniques used to study the microstructural nature of the solid (as well as liquid) samples. Though the technique is relatively new, there are a number of reports in recent

years. In solid samples, the nature and order of the packing of crystals decide many of their properties especially the electronic properties. The knowledge about packing of crystals is very important to study. In many solid state sintering processes, the crystallite size increment is very common. In addition, the solid particles join together during the densification process. Many boundaries of the crystals and the crystal junctions are getting adjusted during this process. In electronic applications, this crystallite level approach is very important due to the fact that the each crystal resembles an individual component in a typical circuit. Many times they behave as resistors or capacitors or inductors or the combinations of all these in different permutations, when an electric current passes through. So the style of packing, nature of crystals and the crystal purity govern these phenomena. Each kind of packing can constitute each type of circuit. The impedance generated by each type of packing is characteristic and this is the basic principle behind this technique. However, if the material of interest has more than one phase, again it exponentially adds to further complications in interpretations of spectral data. But this spectroscopy offers an effective way of studying this aspect of matter.

The terms RESISTANCE and IMPEDANCE both imply an obstruction to current or electron flow. When dealing with a direct current (dc), only resistors provide this effect. However, for the case of an alternating current (ac), circuit elements such as capacitors and inductors can also influence electron flow. These elements can affect not only the magnitude of an ac waveform, but also its time-dependent characteristics or phase.

2. 3. 8. b. Theory

According to the Ohm's law, the resistance of any dc current (frequency = 0 Hz) is given by the equation $E = IR$ where E is the dc voltage (E, volts) and I is the resulting current (I, amps), R is the resistance (R, ohms). But for ac current (non-zero frequency) the resistance is $E = IZ$ and Z is the impedance, the ac equivalent of resistance and so $Z = E/I$. The vector representation of this relation which includes the real and imaginary part of a complex system, is

$$Z_{total} = \frac{E' + E''_j}{I' + I''_j}$$

which is nothing but the individual addition of real and imaginary impedance as

$$Z_{total} = Z' + Z''_j$$

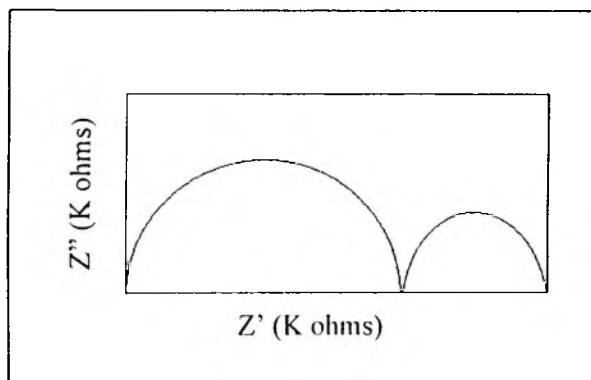


Figure. 2.3.3. A typical Impedance plot.

in which the real impedance Z' is compared with the "resistive" part (purely by resistance) of the total impedance and the imaginary impedance Z'' is compared with the "reactive" part (by capacitance and inductance also) of the circuit.

This individual impedance can be compared with the nature of dielectric behaviour and polycrystalline solid in which each crystal can be considered as an individual component. This includes the grain as well as

the grain boundaries. The impedance of polycrystalline samples may be measured at varying frequencies and similar equations can be derived for the spectra. Figure 2.3.3. shows a typical impedance plot. For such equations, equivalent circuits can be drawn with the possible components. This helps in understanding the microstructure of the packing of polycrystalline solids.

This technique has been proved to be an effective tool to follow up the solid state chemical reactions and phase transformations inside the solid samples during heat treatments²⁵. Sintering is another process, which can be monitored by AC Impedance spectroscopy²⁶. Initially it was planned to understand the microstructural changes that occur during the heat treatments of these zeolite-based precursors. However, it was not possible to get a resolved spectral arc for these sintered materials, using RT measurements. This is an indicative phenomenon that shows the materials have highly resistivity²⁷. So, the impedance spectra were taken in elevated temperatures viz., above 300 °C. It was for our curiosity, the spectra were taken in various temperatures to study the effect of measuring temperature. This was expected to result in a good realization to forgo with the study of sintering by impedance. It is important to note that this study itself is a novel one for this kind of materials. However, due to lack of time and machine availability, the current investigation is limited to only on the study of the influence of measurement temperature on the impedance of sintered samples and not on the changes during the process of sintering. This work was planned though there were no such reports available in literature for these materials

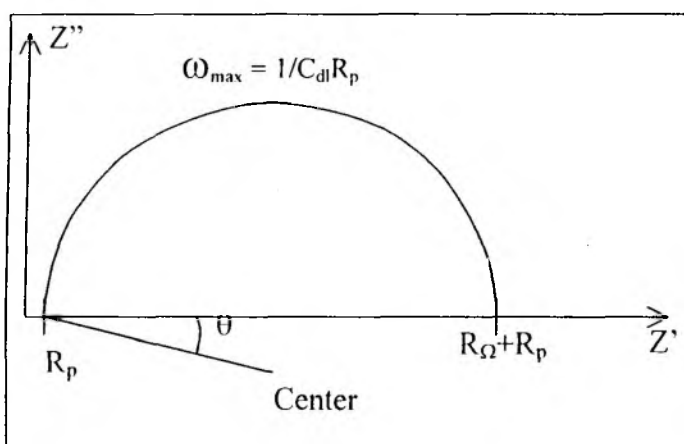


Figure 2.3.4. A typical Nyquist plot of AC Impedance plot of a simple circuit interpreting the bulk (grain) impedance.

prepared by this method. Also this was a preliminary work and has revealed considerable information about the nature of the materials at different temperatures. Other calculations using these impedance data have been prescribed in the later part of the thesis, wherever required.

2.3.8.c. Experimental

The sintered pellets were metallised and cured as described in the earlier section (2.3.7). The AC impedance of the sintered samples was measured using a SOLATRAN SI 1260 AC IMPEDANCE ANALYSER/

GAIN PHASE ANALYSER controlled by an IBM computer. The measurements were done in the frequency range of 1 Hz to 13 MHz. The instrument is equipped with a furnace attachment controlled by the computer interface. The sample pellets were electroded with silver paint with platinum wires and connected to the electrode leads. The measurements conditions are as given below. The impedance measurements were done at various temperatures and the effect of temperature and the electrical transport properties were studied.

The data collected from the AC Impedance unit was then processed by the software, *EQUIVALENT CIRCUIT*²⁸, and the plots were made at different modes with the different components of the equation as will be discussed in the later parts of the thesis. Figure 2.3.4. shows a simplified typical NIQUIST PLOT (also known as *Cole-Cole* plot) of impedance spectrum illustrating the various data which can be obtained on the basis of the simple

Randell's model of equivalent circuits. X and Y axes are the real and imaginary coordinates of the impedance experienced by the flow of current by the sample. R_p is the Polarization resistance generally originated by the electrode contact or the grain boundaries, R_Ω is the ohmic resistance mostly by the bulk of grains (in a polycrystalline solid matrix). The ω_{max} is maximum angular frequency ($=2\pi f$, where f is the frequency). It is equivalent to the inverse of the product of double layer capacitance and the polarization resistance generated mostly at the electrode junctions. θ is the depression angle.

2. 3. 9. THERMAL SHRINKAGE AND EXPANSION STUDIES BY TMA

The sintered pellets were lapped in carborundum powder of particle size of around 38 microns (400 U.S. mesh), for getting uniform thickness all over the disc. The disc dimensions were measured using a screw gauge and then used for shrinkage as well as the expansion measurements.

2. 3. 9. a. Thermal shrinkage studies

These studies were carried out on the green samples of the precursors to understand the extent of shrinkage on sintering or on any phase transitions. As described earlier, the zeolite samples were expected to collapse from their crystalline structure and become amorphous powder. There are possibilities for new phases to get crystallized from this amorphous matter. Under high temperature conditions the phases getting evolved are usually stable dense phases. When the dense phases are formed the volume of the same reduces to a considerable extent. This shrinkage is very characteristic for samples and the purity of phase. A maximum shrinkage yields a high-density material. Generally, the shrinkage at relatively lower temperature is very attractive. However, this is a significant criterion for this special case of application.

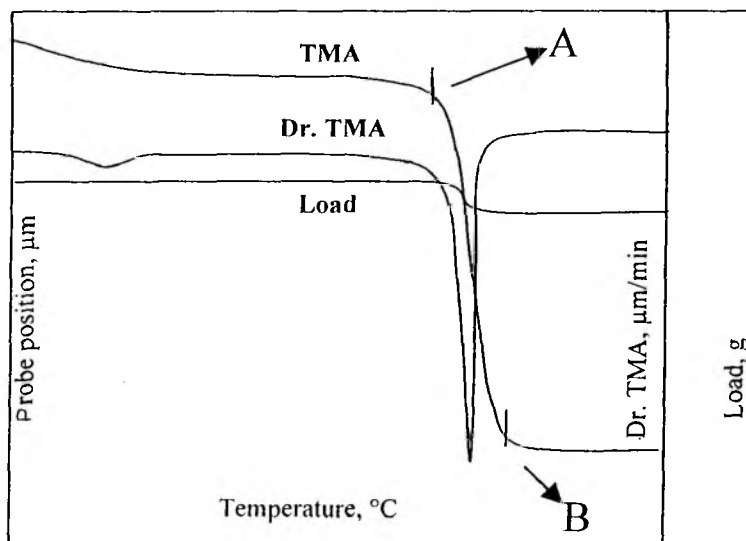


Figure 2.3.5. A typical shrinkage plot by TMA. Point A and B indicate the start and end of shrinking process.

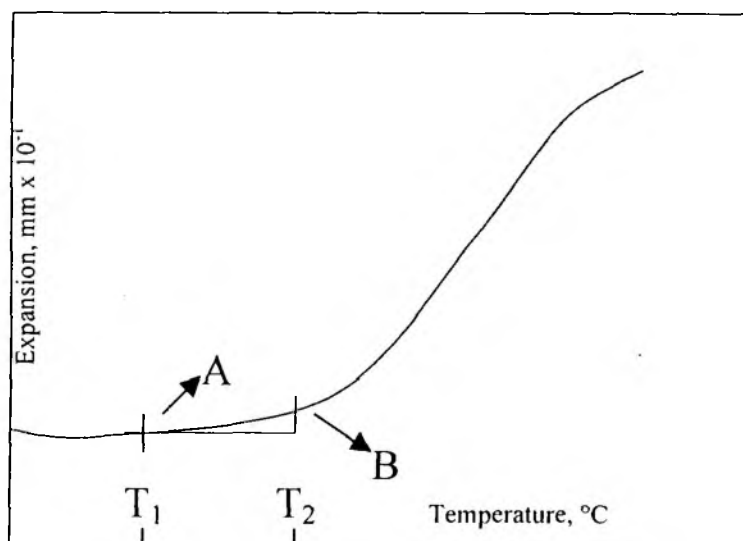


Figure 2.3.6. A Typical Expansion Plot by TMA. Points A and B are the expansion limits and T1 and T2 are the minimum and maximum temperatures within which the TEC is calculated.

The thermal shrinkage studies were carried out in SHIMATZU – 50H TMA dilatometer. The TMA was equipped with a high sensitive, 'Linearly Variable Differential Transducer' (LVDT) along with a high precision quartz probe. The probe was attached with a dilatometer rod head and a planar sample stub. At high temperatures, the furnace block heating was effectively controlled by a turbulent chamber facility connected to a cold water circulation loop. Rods of 4mm thickness and 16mm length were made out of samples and were lapped for uniform top and bottom surfaces. The green samples were analysed for the possible shrinkage during the course of sintering in between the temperature range of 25 °C to 1200 °C in reducing N₂ atmosphere. A static load of 10mg (dynamic load = 0) was given on the top of the sample during the course of measurement to ensure the precise measuring of shrinkage of the sample. The heating was controlled with a rate of 10 °C/min. The derivatives of the shrinkage curves were also plotted. A typical shrinkage TMA curve along with the Derivative and Load curves are given in Figure 2.3.5. A and B are the points between which the shrinkage occurs. The corresponding temperatures can be considered as the densification range. The derivative TMA shows a sharp peak pointing out the temperature at which the densification is at maximum rate. The load curve is to support with additional information like the shrinkage based on a mere solid state phase transformation or any liquid phase or melting processes. But unfortunately this measurement was not possible for all the samples. Hence, the shrinkage of other samples was measured using conventional method by measuring the change in the dimensions of sintered pellets manually with the help of screw gauge. The volumetric and linear variations were calculated and compared.

2. 3. 9. b. Thermal expansion studies

The thermal expansion coefficients (TEC) of sintered ceramic samples were measured in PERKIN ELMER TMA-7 in force free condition (i.e., at zero static and dynamic forces). The thermal expansion coefficient [$\alpha = (dv/v)dT$] is the one of the important property requirement for MEP technique. Expansion measurements were done in a relatively low temperature range (below 500 °C) due to the instrumental limitation. The LVDT was connected to copper alloy probe. The measurement was carried out in disc expansion mode in the temperature range of 25 °C to 450 °C with a heating rate of 20 °C/ min. The data were processed for calculating the linear thermal expansion coefficient (TEC) within the specified range of temperature. Figure 2.3.6. shows a typical shrinkage trend when

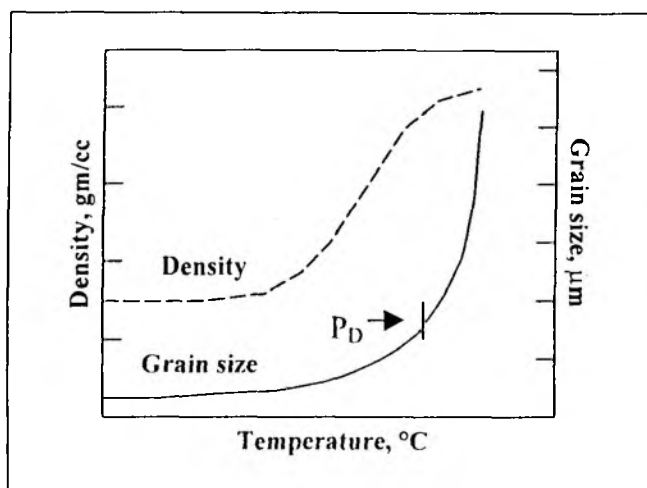


Figure 2.3.7. Typical Density plots. Density and Grain size vs. temperature have been shown.

the expansion is plotted against temperature. T1 and T2 are the two different temperatures between which the TEC was calculated. A and B are the expansion limits of the probe position. More details about the theory and the instrumental details are explained elsewhere²⁹.

2. 3. 10. APPARENT DENSITY AND LINEAR AND VOLUMETRIC SHRINKAGE OF CERAMICS

2. 3. 10. a. Apparent density measurements

To find out the density of both the green and samples sintered at different temperatures, the well-established conventional method of apparent

density calculations was followed for the samples. The average thickness (t) and the average diameter ($d/2 = r$) of the lapped, uniform sized sintered discs were measured and then the "apparent volume" (V_{app}) was calculated considering the sample disc as a cylinder using the equation,

$$V_{app} = \pi r^2 t$$

The apparent density of the samples was then calculated using the relationship,

$$\text{Apparent Density } (\rho_{app}) = \text{Apparent Volume } (V_{app}) / \text{Mass } (w)$$

The density changes during the different stages of sintering were followed and plotted against temperature. This plot gives an idea about the extent of densification and the temperature range at which the densification occurs. A typical density plot looks as illustrated in Figure 2.3.7. As the temperature increases the grain size and density also increase. After a point 'P_D', when the Density reaches a maximum but Grain size keeps increasing is the indication of 'coarsening'. The state of process up to this point is nothing but the 'densification'³⁰.

2. 3. 10. b. Linear and Volumetric Shrinkage measurements

The diameter (L_1) of the sintered disc was taken as the unidirectional length of the shrinking sample and then variation in length with respect to the original sample length (L_0) at room temperature was followed for various sample discs sintered at different temperatures. The linear shrinkage was calculated for a given disc using the following equation.

$$\% \text{ Linear shrinkage} = [(L_0 - L_1) / L_0] \times 100$$

The apparent volume (V_{app})₁ of the sintered sample disc and that of the green sample disc (V_{app})₀ were calculated as explained in section 2. 3. 9. a. The % volumetric shrinkage was calculated using the following equation,

$$\% \text{ Volumetric Shrinkage} = \{[(V_{app})_0 - (V_{app})_1] / (V_{app})_0\} \times 100$$

"... Those who think all scientific ideas are merely temporary explanations to be replaced later should reflect on his theory, which will be right for ever"

- 'His' being of course, Archimedes

REFERENCES

1. Demirgian, J.; Kishk, F.; Yang, R.; Marinsky, J. A.; *J. Phys. Chem.*, 83, 21, 2743 (1979)
2. Breck, D. W.; *Zeolite Molecular Sieves*, John Wiley & sons, NY 493 (1974)
3. Jandera, Z.; Tulloch, G.; *Proc. - Aust. Ceram. Conf.*, 9, 189 (1980)
4. Onoda, G. Y. Jr.; *Ceramic Processing Before Firing*, (Onoda, G.Y; Jr. Hench, L.L. Eds.) Wiley, New York, pp. 235 (1978)
5. Prochazka, S.; Johnson, C. A.; Giddings, R. A.; *Proc. Ing. Symp.*, Factors Densification Sintering Oxide Non-Oxide Ceram., Meeting Date 1978, 366, (Somiya, S.; Saito Eds.) *Shinroku. Gakujutsu Bunken Fukyukai*: Tokyo, Japan, (1979)
6. Otsuka, K.; Usami, T.; Sekibata, M.; *Yogyo Kyokaishi*, 89, 6, 309 (1981)
7. Endl, H.; Hausner, H.; *Ber. Dtsch. Keram. Ges*, 57, 6-8, 121 (1980)
8. Taylor, Jenifer. A. T., *Am. Ceram. Soc. Bull*, 74(6), 81 (1995).
9. Yu, J.; Fuzhou, D. X.; *Ziran Kexueban*, 22(5), 118 (1994)
10. Tomlin, D. W.; Sullenger, D. B.; Cantrell, J. S.; *Powder Diffr*, 8(1), 29 (1993)
11. Freiburg, C.; Reichert, W.; Melchers, M.; *Ber. Forschungszent. Juelich*, JUEL-2867, 99 (1994)
12. Fraser, Bruce.; *Chem. N. Z.*, 56(5), 76 (1992)
13. Meublat, L.; Le. P.; *Calorim. Anal. Therm*, 22, 127 (1991)
14. Isa, K.; Hasegawa, H.; Aarii, T.; *Netsu Sokutei*, 22(3), 160 (1995)
15. Williams, D. A.; Pettersen, E. K.; Paul, D. J.; Ahmed, H.; *Inst. Phys. Conf. Ser*, 134 *Microscopy of Semiconducting Materials*, 249 (1993)
16. Asai, T.; Kawai, S.; *Seramikkusu*, 20(7), 610 (1985)
17. Connor, C.; *Int. SAMPE Symp. Exhib*, 37(Mater. Work. You 21st Century), 955 (1992)
18. Hayashi, S.; *Annu. Rep. NMR Spectrosc*, 28, 29 (1994)
19. Yue, Y.; *Bopuxue Zazhi*, 12(5), 473 (1995)
20. MacKenzie, K. J. D.; Meinhold, R. H.; *Int. Ceram. Monogr.*, 1 (2, PROCEEDINGS OF THE INTERNATIONAL CERAMICS CONFERENCE, 1994), 1019 (1994)
21. MacKenzie, Kenneth J. D.; Meinhold, R. H.; *J. Mater. Chem.*, 6(5), 821 (1996)
22. MacKenzie, Kenneth J. D.; Meinhold, R. H.; Chakravorty, A. K.; Dafadar, M. H.; *J. Mater. Chem.*, 6(5), 833 (1996)
23. Colyer, L. M.; Greaves, G. N.; Carr, S. W.; Fox, K. K.; *J. Phys. Chem. B.*, 101, 10105 (1997)
24. Matsumoto, T.; *Kenkyu H- Tochigi-ken Ken'nan Kogyo Shidosho*, 11, 43 (1998)
25. Muccillo, E. N. S.; Kleitz, M.; *J. Eur. Ceram. Soc.*, 16(4), 453 (1996)
26. Kirkpatrick, K. S.; Mason, T.O.; Balachandran, U.; Poeppel, R. B.; *J. Am. Ceram. Soc.*, 77(6), 1493 (1994)
27. Barranco, A. P.; Pinar, F. C.; Martinez, O. P.; Tera, A. H.; *J. Mater. Sci. Lett.*, 16(7), 534 (1997)
28. Equivalent Circuit, (Version 3.97, May 1989), *AC Immittance Analysis system*, (Bernard A. B. Univ. of Twente, Ed.) The Netherlands © B.A. Boukamp/ UT' 85-89.
29. Touloukian. Y. S.; Kirby. R. K.; Taylor. R. E.; Desai. P.D.; *Thermal expansion properties - metallic Elemental and Alloys*, Vol 12, The TPRC Data Series, PLENUM PUBLISHING CORPORATION, NY, USA (1975)
30. Yan M. F.; *Mater.Sci. Eng.*, 48 (1981)

THE β - SPODUMENE (LAS systems)

Chapter



PART A. GENERAL STUDIES

3.1. CERAMIC PREPARATION AND CHARACTERISATION

3.1.1. INTRODUCTION

This chapter discusses a known silicate system namely **Lithium Aluminosilicates**, $\text{Li}_2\text{O}-\text{Al}_2\text{O}_3-\text{SiO}_2$ (LASs). However, the preparation of LAS ceramics using zeolites is a new area of research. The discussion in this chapter includes the preparation of LAS precursor powder samples and sintering at high temperatures and characterisation of both the precursor and then ceramic product to understand different aspects of sintering and their influences on the properties of the ceramic products. The later part of this chapter describes the characterisation with special techniques like shrinkage and expansion studies. Except the thermal expansion coefficient (TEC) and nuclear magnetic resonance (NMR) studies data and the discussions presented in this chapter have been published during the tenure of the Ph.D work¹⁻³.

3.1.1.a. *The importance of $\text{Li}_2\text{O}-\text{Al}_2\text{O}_3-\text{SiO}_2$ (LAS) systems*

The LAS system is by far the most important commercial system. It is mostly used for glass-ceramic materials having very low TECs and hence very high resistance to thermal shock. Among the trade names for materials in this system are Corning's *Corning Ware*, Owens-Illinois' *Cer-Vit* and PPG's *Hercuvit*. The very low TEC in this system, which in some cases are appreciably lower than that of fused silica are associated with the presence in the crystallised materials of crystalline β -spodumene ($\text{Li}_2\text{O} \cdot \text{Al}_2\text{O}_3 \cdot 4\text{SiO}_2$), which has a low TEC or β -eucryptite ($\text{Li}_2\text{O} \cdot \text{Al}_2\text{O}_3 \cdot 2\text{SiO}_2$), which has a TEC that is larger in number and negative. Commercial compositions are found in several ranges in this system. Different phase assemblages, characterised by different sets of properties, can result from using TiO_2 and ZrO_2 in varying proportions as the nucleating agents. Usually high temperature polymorphs of SiO_2 and Al_2O_3 are in association with these phases.

β -Spodumene is formed during the synthesis of LAS based ceramics at high temperatures (>1000 °C) usually as the major phase along with other phases. However, β -spodumene is of high interest for the application of electronic packaging in many aspects. The recent trend in ceramics packaging research shows that the composites or the solid solutions of various phases of LAS systems are challenging⁴. The current work also involves different phases of LAS along with β -spodumene, in some cases as solid solutions. Before going to the discussions on them, it would be more appropriate to have a mineralogical preview of the spodumene system along with the general material properties of this particular β -phase, because, this information would help in the

later discussions. A general overview of the other possible phases that are usually formed during the LAS based ceramics preparation is also given.

3.1.1.b. The ore spodumene and its β phase – a mineralogical background

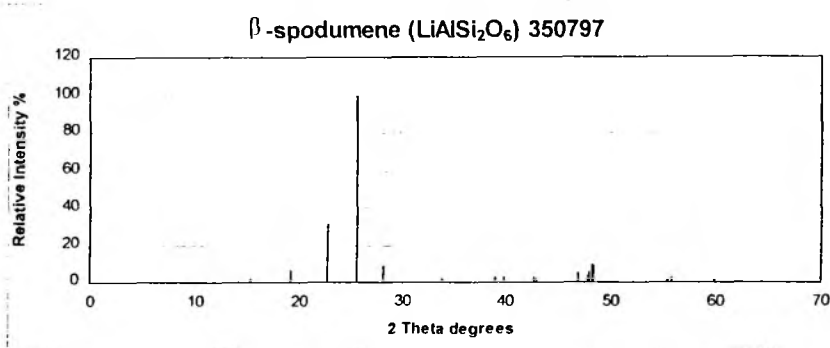


Figure 3.1.1. The powder XRD profile generated from standard JCPDS data (JCPDS file name is given above)

Spodumene is a brittle, crystalline mineral of the pyroxene group, varying in colour from transparent white to yellow, grey, green, and purple depending on the origin of its occurrence. It has a lithium aluminium silicate of formula $\text{LiAlSi}_2\text{O}_6$, with a hardness of

6.5 to 7 mohs and a relative

density of 3.13 to 3.20 g/cc. It occurs in massive form in large crystals, usually as a constituent in granitic pegmatites. Spodumene is an important lithium ore and is also used in the production of ceramics, enamel, and glass. Two transparent and highly coloured varieties of spodumene are used as gemstones: hiddenite, a yellow to emerald-green stone, and kunzite, which occurs as a pinkish-lilac crystal. β -Spodumene is the high temperature phase of spodumene, which is more stable. Figure 3.1.1 shows the XRD profile of β -spodumene from standard JCPDS data. It is formed usually at the temperature of around 1200 °C on heating the pure spodumene ore or any similar LAS oxide systems with comparable stoichiometry.

The typical formula of β -spodumene is $\text{LiAlSi}_2\text{O}_6$. However, this falls into the general formula as $\text{Li}_x\text{Al}_x\text{Si}_{3-x}\text{O}_6$ ($x=1$) of 'Virgilite' category. Virgilite is usually a solid solution formed during the phase evolution of β -spodumene in which the x varies from 0 to 1. The details of this concept are discussed in the later part of this chapter.

3.2. EXPERIMENTAL

3.2.1. PLAN OF WORK

Due to the obvious advantages of the zeolite based preparation route as explained in the first chapter, the preparation of the β -spodumene, by itself, is very interesting to study. It is also important to study the various factors influencing the preparation route as they control the properties of the ceramic products. The present study includes the preparation of powder precursors using ion exchange technique on zeolite powder and the physicochemical characterisation of the powder using various techniques. As discussed in the first chapter, in many ways this process is anticipated to be different from the conventional oxide based preparation. Hence, it was aimed to understand the course of high temperature solid state reactions and the phase transformations by following the changes in the sample's nature during the course of heating.

3.2.2. PREPARATION OF β -SPODUMENE

3.2.2.a. The LAS precursor powder preparation

Nearly 100 g of zeolite Y was exchanged three times ($N_x = 3$) with 1 M solution of ammonium nitrate salt to get the ammonium form of zeolite Y which was again exchanged three times with 1 M solution of lithium nitrate salt. The exchanges were carried out as per the procedure given in chapter 2, section 2.1.2.a. Finally, the dry powder labeled as LAS_{Y3} (meaning Lithium Aluminosilicate - Y zeolite, exchanged 3 times with 1 M Li salt solution) was used for consolidation and other studies.

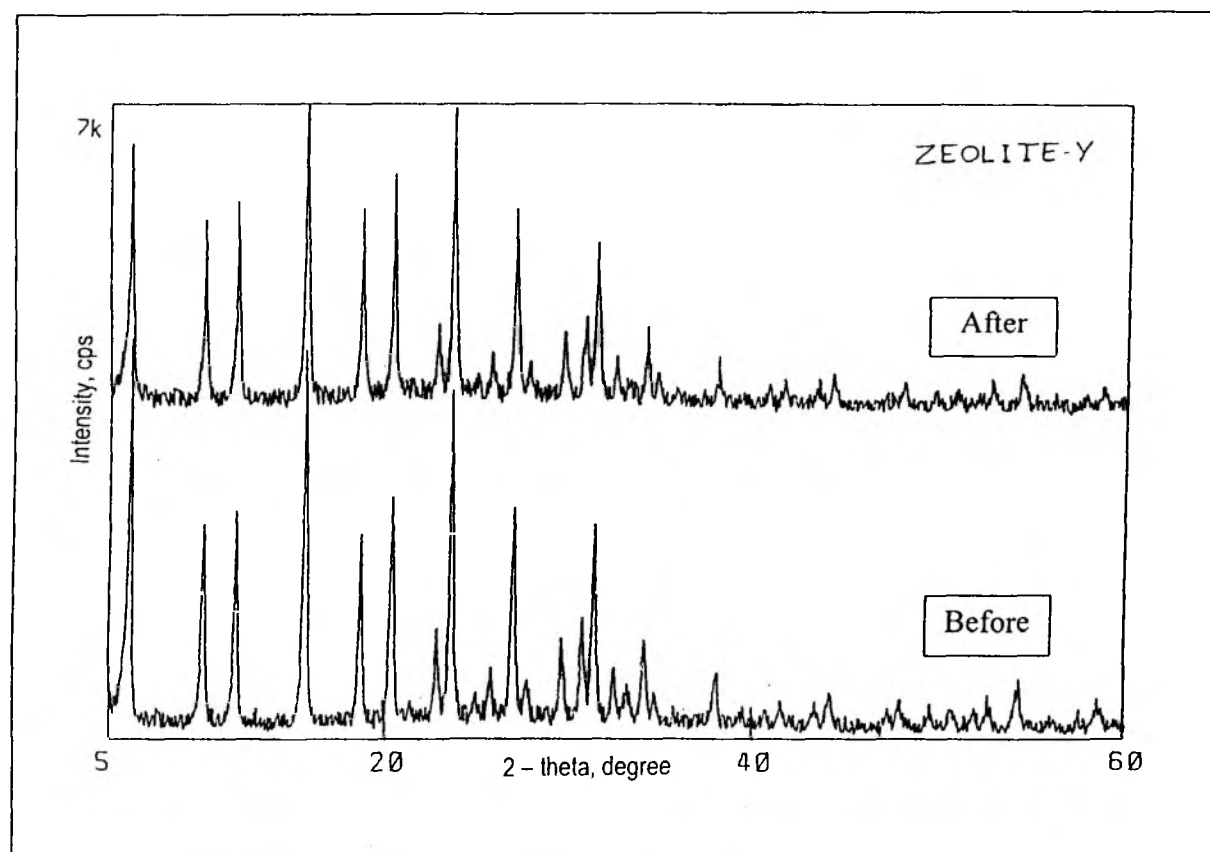


Figure 3.2.1. The XRD patterns of the sample LAS_{Y3} before and after ion exchange

3.2.2.b. Powder characterisation

The powder was characterised using TG/DTA and XRD techniques for its thermal and structural properties respectively. The chemical composition was found out from the atomic emission spectrum of Li. Nearly 30 mg of the LAS_{Y3} powder was taken for a TG/DTA analysis in N₂ atmosphere in the temperature range of 25 °C (RT) to 1000 °C with a heating rate of 10 °C/min.

The powder-XRD patterns of the fine dry zeolite powder before and after the exchanges were recorded (Figure 3.2.1.) and the crystallinity changes were checked. The chemical analysis of the exchanged sample was found

out using atomic absorption spectroscopy (AAS) as mentioned in the earlier chapter and the analysis shows the elemental ratios as listed in Table 3.2.1.

Table 3.2.1. Elemental analysis of the LASY3 by AAS

Zeolite	Conc. of LiNO ₃ soln.	N _x	Elemental ratios %			Residual Na wt. %	Label
			Si/Al	Li/Al	Na/Al		
Y	1 M	3	2.64	0.1285	0.0139	0.082	LASY3

3.2.3. SINTERING AT VARIOUS TEMPERATURES

The powder was bound with polyvinyl alcohol (PVA) and consolidated into pellets, each weighing roughly around 0.7 g as explained in chapter 2 - section 2.1.3.b. The pellets were fired at different temperatures viz., (T₂ =) 480, 600, 700, 800, 900, 1000, 1100, 1200 ° C in a programmed fashion at a heating rate of 4 °C/ min. The heating had a holding at 580 °C (T₁) for 180 min. (t₂) for binder removal. The samples were heated at higher temperature (T₂) isothermally for 360 min. (t₄) and cooled naturally (refer Figure 2.1.3., chapter 2, for more details about the parameters that are fixed during the programmed heating of the samples).

3.2.4. CHARACTERISATION OF CERAMICS

The heated pellets were crushed into fine powder and the XRD profiles were recorded for all the samples in the 2-theta range of 5 to 40 degrees with a scanning speed of 4 degree/min. The XRD data were processed and plotted in series to have a comparative view. Figure 3.3.1 shows the multiple plots of the XRD patterns that reflect the phase changes which are discussed later. Selected samples in the course of sintering were checked for the major changes in morphology and the particle size by SEM. The scanning electron micrograms are given in Figure 3.3.2. The chemical composition, thermal expansion, shrinkage, density and dielectric properties of the ceramic product were studied using various techniques.

3.3. RESULTS AND DISCUSSION

3.3.1. THERMAL PROPERTIES

Figure 3.3.1 shows the TG/DTA plot of LASY3 sample in the temperature region from 25 to 1000 °C. The TG of the powder LASY3 shows a total weight loss of around 23.8 % during the heat treatment up to 1000 °C. Except the initial weight loss (up to 260 °C), predominantly due to the loss of adsorbed water and organic matters, there is almost no loss after 400 °C. The DTA

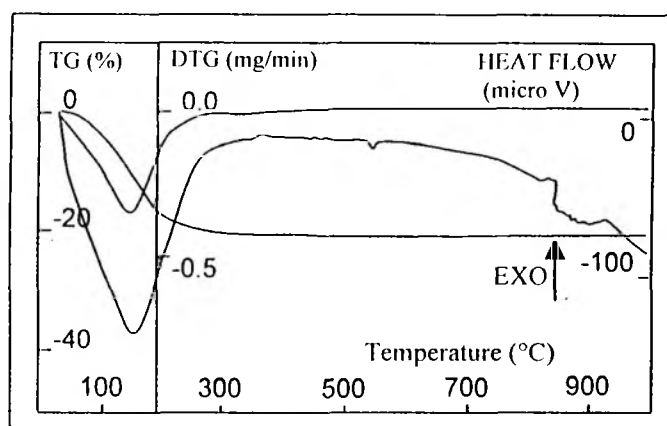


Figure 3.3.1. TG/DTA plot of LASY3

shows an endothermic decay after 740 °C. The exothermic shoulder at 812 °C does not correspond to any weight loss in TG. This is attributed to the zeolite structure collapse. Zeolite Y being a faujasite has a higher Si/Al ratio and is usually thermally stable upto a temperature greater than 900 °C. Li⁺ is well known for being a good alkali flux agent at high temperatures in many cases. Also, when compared to other cation exchanged Y zeolites, the thermal stability of Li-Y is relatively less. This depression in thermal stability may vary with the loading of Li into the zeolite. The effect of cation concentration in zeolite precursors has been discussed in the next part of this chapter. The next exothermic shoulder around 920 °C is assigned to the initiation of the crystallisation of LAS, β -spodumene. This is confirmed by the structure collapse and phase transformations in this region by XRD (Refer Figure 3.3.2).

3.3.2. PHASE TRANSFORMATIONS BY X-RAY DIFFRACTION

XRD patterns of the sample before and after ion exchanges show a crystallinity loss of around 3.5 % that is usually because of the multiple ion exchanges and intermittent heat treatments during the process. But the reduction in the width of the diffraction peaks of the sample after ion exchange indicates that the heat treatment at 480 °C reduces the strain due to crystal-defects and that the crystallites have become well defined and have grown bigger. Figure 3.3.2 shows the multiple plot of the powder XRD profiles of the sample heated at different temperatures ranging from 480 °C to 1200 °C. There is a trend of the crystalline phase changes. The crystalline zeolite phase collapses at a temperature above 700 °C and becomes completely amorphous. The temperature, at which the amorphisation occurs, depends on the thermal stability of the zeolite precursors.

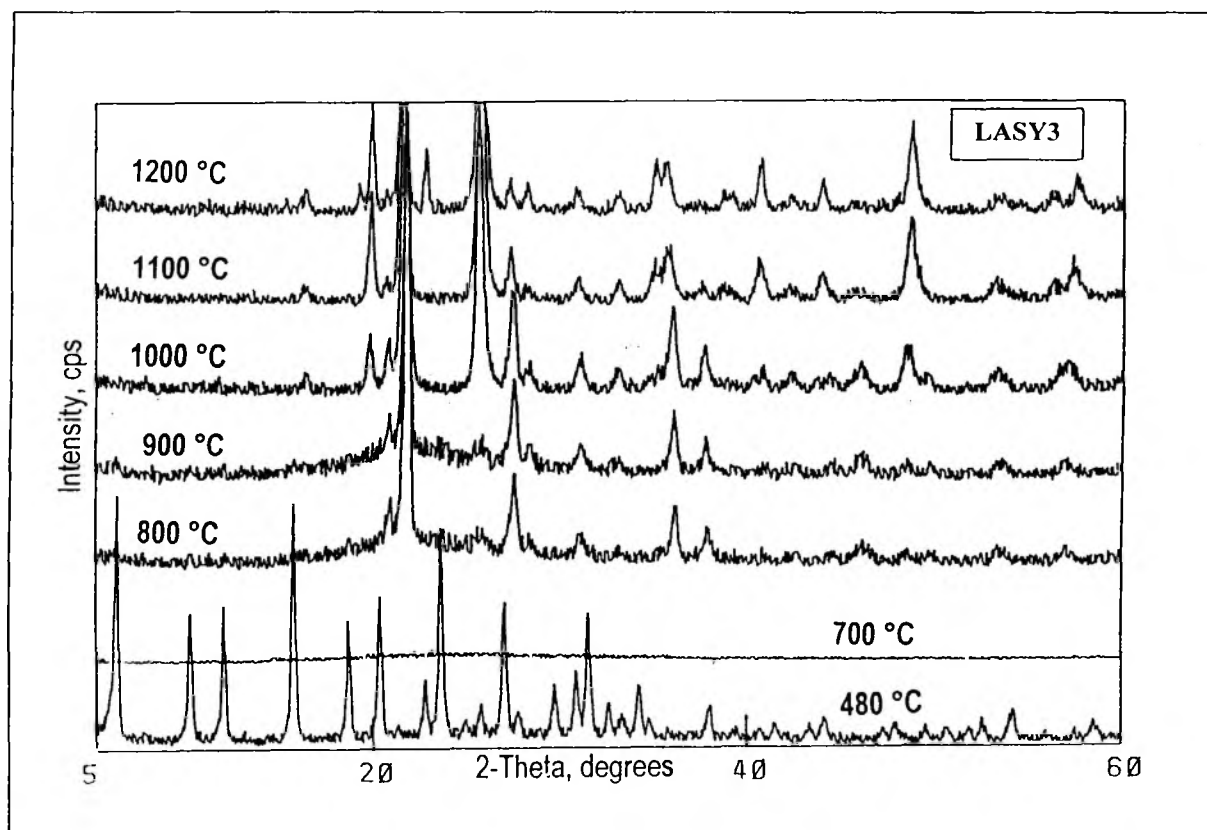


Figure 3.3.2. Powder XRD plots of LAS Y3 samples heated at different temperatures from 480 °C to 1200 °C

The thermal stability of zeolites exchanged with different cations has been studied well⁵. Above 900 °C, the amorphous matter crystallises into a highly crystalline LAS phases. The crystallisation follows with many intermediate phases.

Though there are a few earlier works^{5a} reporting the dense LAS phase formation at high temperatures using this route, there is no report on the mechanistic pathway of this transformation. In fact it is very interesting and important to understand this mechanism as it has a strong influence on the product formation and properties. The present work is not only to identify the final phases but also to make an attempt to understand the mechanism of the phase transformation. The major and explicit key intermediate phase during the transformation has been identified as virgilite solid solution (SS), one of the LAS dense phase group, which is very close to β -spodumene by structure. Section 3.3.4. of this chapter discusses more about this issue. The structure collapse and formation of dense phase have been compared with the TG/DTA data in the earlier part of the discussion and it is found to be in good agreement. Using the 'search-match' package available with the JCPDS file library, the phases formed during the process of phase transformations and densification are analysed. Table 3.3.1 lists the phases identified.

Table 3.3.1. Phases identified at different temperatures of sintering of LAS_{Y3}

Sample	Temperature, °C					
	480	800	900	1000	1100	1200
LAS _{Y3}	Zeolite Y	Zeolite Y Silica(C) Silica(HQ) Alumina AMORPH*	Zeolite Y Silica(C) Silica(HQ-K) Alumina Virgilite SS AMORPH*	Silica(C) Silica(K) Virgilite SS Mullite <i>β-spodumene</i>	Silica(C) Silica(K) Virgilite SS Mullite <i>β-spodumene</i>	Silica(C) Virgilite SS <i>β-spodumene</i> Mullite

C – cristobalite type; HQ – High-quartz type; K – Keatite type; SS – solid solution; AMORPH* - Amorphous phases

Phase	Formula	JCPDS file	Phase	Formula	JCPDS file
Silica (C)	SiO ₂	270605	Virgilite SS	Li _x Al _x Si _{3-x} O ₆	310707
Silica (HQ)	SiO ₂	120708	Mullite	Al ₆ Si ₂ O ₁₃	150776
Alumina	Al ₂ O ₃	100173	<i>β-spodumene</i>	LiAlSi ₂ O ₆	350797

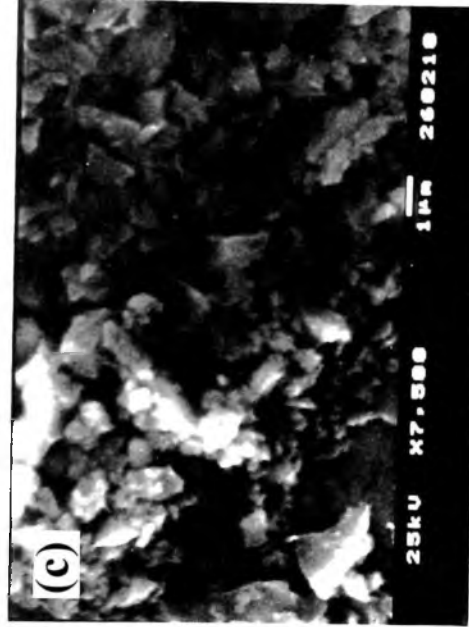
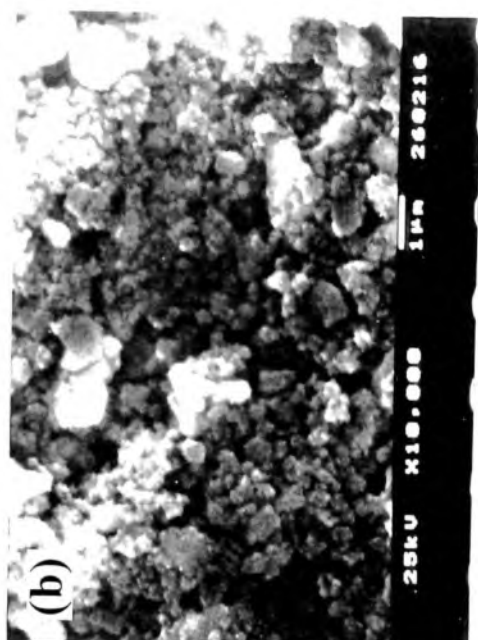
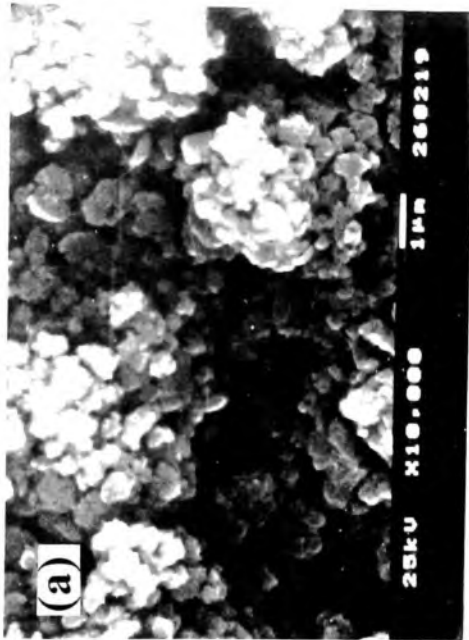


Figure 3.3.3. SEM photographs of LAS/3 samples heated at different temperatures from room temperature to 1200 °C.

3.3.3. SCANNING ELECTRON MICROSCOPY

The scanning electron micrographs of the samples fired at selected temperatures are given in Figure 3.3.3(a-e). The Figure 3.3.3(a) shows the microstructure of the sample LASY3 just dried after Li exchange and it shows a very crystalline nature of the sample with a regular uniform crystallite size corresponding to around 0.5 μm .

Figure 3.3.3(b) is for the sample heated

at 800 °C and shows an amorphous and agglomerated nature of the sample. It may be noted that the XRD multiple plots also show similar result at this range of temperature. The SEM of the sample fired at 900 °C is given in Figure 3.3.3(c) that shows the crystallisation of dense phases from the amorphous state. Figure 3.3.3(d) shows an ungoverned, irregular morphology of the crystallizing dense ceramic phase at 1000 °C. Finally, Figure 3.3.3(e) shows the sample sintered at 1200 °C which is almost regular with uniform sized particles of the crystals. Table 3.3.2 shows the change in the particle size observed by SEM for the samples heated at various temperatures.

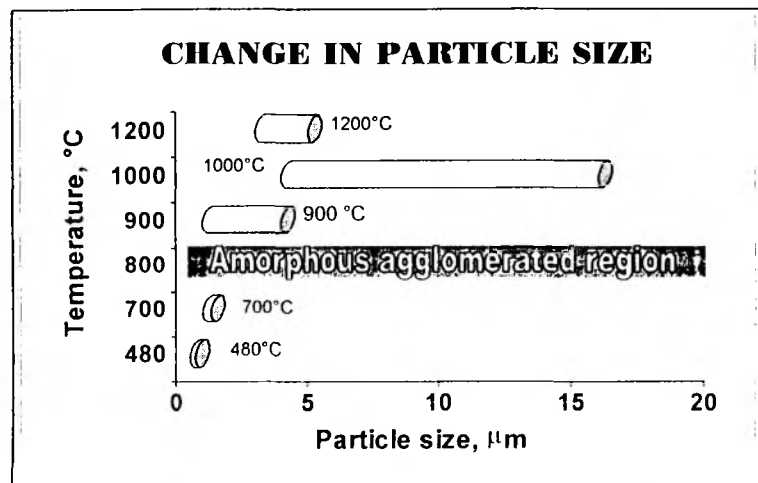


Figure 3.3.4. Magnitude of particle size changes during the course of sintering of LASY3

Table 3.3.2. Particle size variations by SEM

Sample name	Firing temperature, °C	Particle size range, μm
LASY3-480	480	0.5 - 1.0
LASY3-700	700	0.5 - 2.0
LASY3-800	800	(agglomerate flakes)
LASY3-900	900	1 - 4
LASY3-1000	1000	4 - 16
LASY3-1200	1200	3 - 5

The trend in the change of particle size variation at various temperatures reveals that the uniform particles of zeolite precursors further reduces due to structure collapse around 700 °C and above. At this temperature, grains do not have definite boundaries and are more or less like agglomerated flakes of solid mass. This is due to the formation of amorphous phase at this temperature. On further heating, the formation of intermediate starts and further the crystals of the dense ceramic phase start growing. Though the growth is ungoverned at the outset leading to the formation of asymmetric crystals with a large distribution of particle size, at high temperature the particles are found to have almost uniform particle sizes. It is known that mullite crystals develop faster. This is the reason for the formation of large particles. However, the distribution of particle size narrows down later at

higher temperatures, may be due to the mullite getting transformed into the virgilite and then to crystalline β -spodumene phases. At 1200 °C the particle size distribution becomes greatly narrow indicating the completion of the densification. Figure 3.3.4 illustrates the relative magnitude of distributions of the particle sizes of samples fired at various temperatures. The central region of the plot is the region where the sample is not having particles with well-defined boundaries but agglomerated mass.

3.3.4. POWDER X-RAY DIFFRACTION STUDIES

The observed interplanar 'd' spacings from the XRD pattern of sample LASY3 sintered at 1200 °C were corrected with respect to internal standard silicon. The tetragonal unit cell parameters for β -spodumene were refined using two different least square fitting programs. The refined unit cell parameters are compared with that of the literature values in Table 3.3.3. The unit cell parameters calculated for β -spodumene on the basis of XRD data of the sample sintered at 1200 °C are in good agreement with the literature values with minimum standard deviation as given in the Table 3.3.3. The occupancy of the cation Li^+ into the lattice sites was determined by simulating the XRD pattern. The fundamental transformation of the zeolite precursor to the ceramic dense phase can be represented as follows.

Table 3.3.3. Lattice parameters calculated from the powder XRD data

Precursor symmetry	Densified symmetry	Lattice parameters		
		Literature (Å)	Observed (Å)	Standard deviation
Cubic (LAS Y3)	Tetragonal (β -spodumene)	$a = 7.510$	$a = 7.5066$	± 0.0103
		$c = 9.208$	$c = 9.2021$	± 0.0165
	Cell volume, Å ³	$v = 1552.92$	$v = 1550.15$	± 5.3

Table 3.3.4. The overall compositional transformation of the precursor to ceramic

Zeolite	Formula	M ⁺	Composition	
			Precursor (RT)	Ceramic LAS (HT)
LASY3	$\text{Na}_{56}\text{Al}_{56}\text{Si}_{136}\text{O}_{384} \cdot \text{H}_2\text{O}$	Li^+	$\text{Li}_{56}\text{Al}_{56}\text{Si}_{136}\text{O}_{384}$	$\text{Li}_x\text{Al}_x\text{Si}_{3-x}\text{O}_6$ ($0 < x < 1$)

If one assumes that all the Na^+ ions in the zeolite precursor get exchanged with the Li^+ ions in solution (1:1 ratio), then the precursor composition at room temperature (RT) will be as given in Table 3.3.4. The ceramic LAS phase has been represented with a variable formula in which the factor 'x' varies from 0 to 1. This is because of the fact that the LAS system has several dense phases with varying Li content and number of moles of SiO_2 . However, there is no report on the possible intermediate LAS phases that are formed during the formation of the desired β -spodumene phase (refer section 3.3.2.). It would be more useful to make an attempt to understand the

mechanism by which the phase transformation occurs. Before going into the details, it would be appropriate to have an idea about the metastable phases of SiO_2 at high temperatures (in the range 800-1200 °C).

As a single component system, silica (SiO_2) has many polymorphs like α -(low-)quartz, β -(high-)quartz, tridymite, and cristobalite stable upto various temperatures viz., 573, 870, 1470 and 1713 °C at 1 atm pressure. At high pressures (>40 kbars) few more phases like coesite and stishovite are formed. Nevertheless, the pressure changes affect the formation temperature of these phases to some extent. High-pressure conditions bring down the temperature of formation of different phases drastically by several 100 °C.

However, the present case is not a single component system rather a ternary system of $\text{LiO}_2\text{-Al}_2\text{O}_3\text{-SiO}_2$. In presence of any other cation like Al and Li, the high quartz phase is more likely to form a separate family of aluminosilicate polymorph called keatite. Keatite structure is usually a solid solution in which atoms of Al and any other cation like Li could be diffused inside. Keatite has a structural formula as MAiSi_2O_6 ; where M is any metal like Li. This is formed by the gradual change of the SiO_2 structure by accommodating Al and Li ions into the lattice positions of Si.

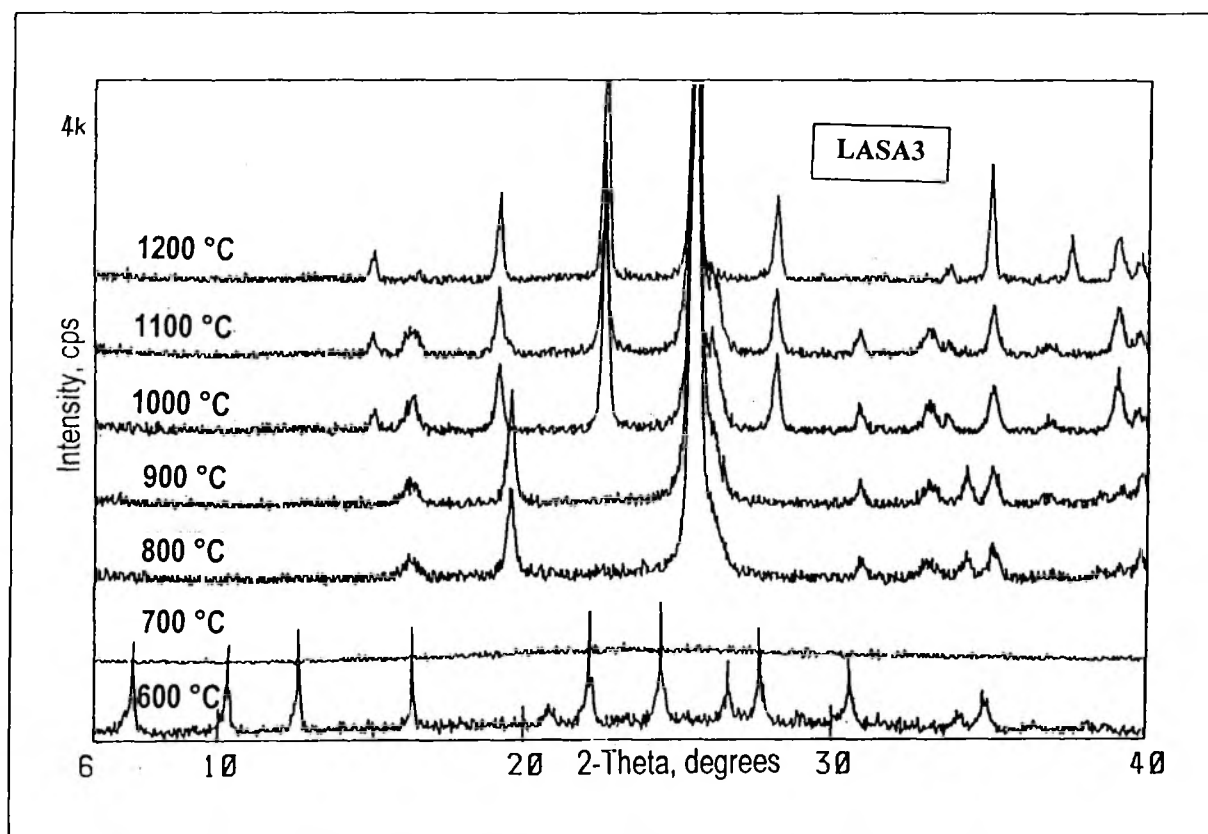


Figure 3.3.5. XRD multiple plots of LASA3 samples heated at different temperatures from 480-1200 °C

The XRD patterns obtained for the samples LASA3 show traces of this phase formation at temperatures above 800 °C. However, this is not observed very distinctly here. In order to assure this mechanistic pathway, it was planned to study the sintering of some other LAS sample prepared from some other zeolite.

Using similar ion exchange procedure as followed for the preparation of LAS3 sample (refer Section 2.1.2.a of chapter 2), around 40 g of zeolite A was exchanged 3 times with 1 M LiNO_3 solution and the exchanged dry powder was labeled as LASA3. The powder was bound using PVA and made into pellets and fired at different temperatures in the range of 480-1200 °C. The XRD patterns of the crushed fine powder of the pellets heated at different temperatures were recorded. Figure 3.3.5. shows the multiple plot of the XRD plots of LASA3 samples heated at different temperatures.

The structure changes are almost similar to the trend observed for LAS3. Zeolite precursor collapses at 700 °C and the metastable silica phases are formed above 800 °C. However, new peaks around 2θ (in degrees) = 25.56 in patterns for samples heated at 900 °C and above are to be noticed. Figure 3.3.6. gives the narrow range of XRD pattern from $2\theta = 15$ to 35 degrees of the samples heated in the range from 800 to 1200 °C.

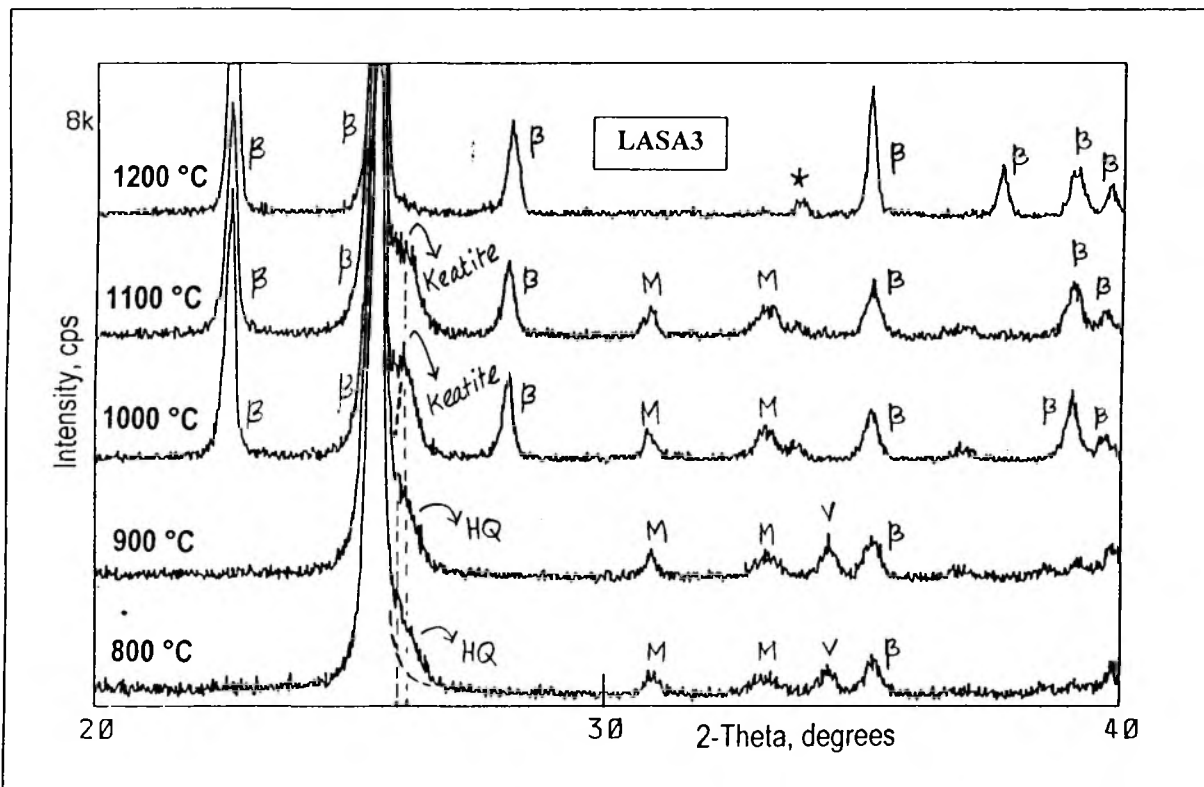


Figure 3.3.6. Close view of the expanded XRD profiles of LASA3 samples heated at 800-1200 °C

The phase changes of SiO_2 with or without the presence of other oxides were unknown till recent past. Evans reported a very preliminary study on the mechanism^{5b}. Later, Li reported a deeper insight about the mechanism and according to Li^{5c}, the high quartz phase of $\text{LiAlSi}_2\text{O}_6$ ($\text{Li}_2\text{O} \cdot \text{Al}_2\text{O}_3 \cdot 4\text{SiO}_2$) composition reconstructively transforms into the keatite phase at elevated temperature. According to this report the structure does not undergo major changes but most atoms in the structure undergo very meager positional changes during the phase transformation and hence, even DTA analysis usually does not show any significant peak for this process.

Though the intensities of XRD reflections observed for these phases are usually weak in presence of any other prominent phase formation, the three reflection of these phases (Table 3.3.5.) are usually the major ones.

Table 3.3.5. A match of three pairs of powder XRD reflections between high-quartz and keatite phases of $\text{LiAlSi}_2\text{O}_6$ composition. (Cu $K\alpha$ - radiation used)

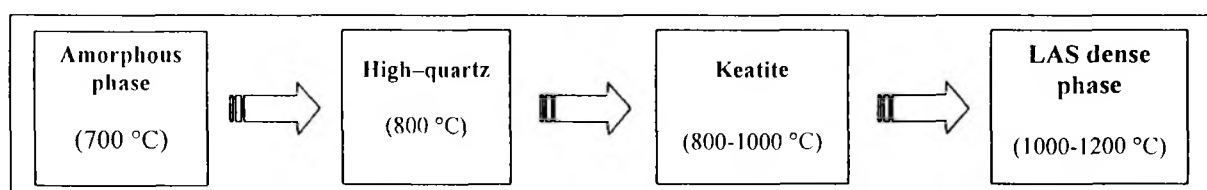
High-quartz (HQ) phase				Keatite (K) phase			
<i>hkl</i>	$2\theta, ^\circ$	<i>d</i> , Å	I_i/I_0	<i>Hkl</i>	$2\theta, ^\circ$	<i>d</i> , Å	I_i/I_0
100	19.65	4.518	11.7	111	19.26	4.608	8.3
101	25.58	3.482	100.0	201	25.55	3.486	100.0
112	48.24	1.887	19.1	400	48.27	1.885	10.0

The powder XRD reflections of LASA3 samples heated at this temperature range (800-1200 °C) were analysed for the possible matching with these data. It was found that the samples heated in the temperature range 800-1000 °C contain three major reflections corresponding to the phase transformation, 'High-quartz to Keatite'.

Table 3.3.6. A match of LASA3 reflections with the HQ and K phases at various temperatures

Peak	Details	High Quartz (HQ)	Keatite (K)	$2\theta, ^\circ$ of LASA3 samples at temperatures, °C					Remarks (temperature)
				800	900	1000	1100	1200	
Peak 1	$2\theta, ^\circ$	19.65	19.26	19.59 ^{HQ}	19.58 ^{HQ}	19.56 ^{HQ}	22.60 ^β	22.59 ^β	HQ → K (800 – 100Q)
	I_i/I_0	11.7	8.3	13.0	12.0	12.0	22.0	25.0	
Peak 2	$2\theta, ^\circ$	25.58	25.55	25.56 ^{HQ}	25.56 ^{HQ}	25.55 ^K	25.52 ^β	25.50 ^β	HQ ↔ K (800 – 1000)
	I_i/I_0	100.0	100.0	100.0	100.0	100.0	100.0	100.0	
Peak 3	$2\theta, ^\circ$	48.24	48.27	48.25 ^{HQ}	48.27 ^K	48.27 ^K	48.31	48.28 ^β	K → LAS (1000 - 1200)
	I_i/I_0	19.1	10.0	15.0	15.0	15.0	11.0	12.0	

The 2θ (in degrees) of reflections observed for the LASA3 samples at high temperatures are marked with superscript with the matching phases (Table 3.3.6.). The superscript mark 'HQ' stands for high-quartz, 'K' stands for keatite and 'β' stands for virgilite SS and β-spodumene (dense LAS) mixture. These assignments were cross-checked with the JCPDS standard data. The last column of Table 3.3.6. shows the over all phase transformation of the process at this range of temperature. The overall changes clearly show that the mechanistic pathway for the transformation of amorphous silica to β-spodumene is as follows.



The second part of the phase transformation is from Virgilite to β -spodumene. At higher temperature keatite transforms into virgilite SS (LAS solid solution) phase having a general formula $\text{Li}_x\text{Al}_x\text{Si}_{3-x}\text{O}_6$ ⁶. This phase is earlier to the intermediate phase. It has been already reported that in presence of any alkali element like Na at various concentrations, the high temperature treatment of similar system leads to the formation of disordered cristobalite. It is important to know that usually keatite coexists with either quartz or cristobalite or both⁷.

The quantification of keatite phase formed using the Li ions in its lattice would forecast the formation of the β -spodumene from the former. The XRD pattern recorded for the sample LASY3 fired at 900 °C can be used to calculate the amount of Li^+ cations present in the lattice sites of keatite⁸⁻¹⁰. The crystal details of keatite were used for the above purpose. In other words the occupancy of Li^+ , on the basis of the XRD data, was calculated and found comparable with the reported value in the literature⁸⁻¹⁰. According to the results shown in Table 3.3.7, the value of x is 0.31 in the equation $\text{Li}_x\text{Al}_x\text{Si}_{3-x}\text{O}_2$. The 'x' value for the minimum and maximum possibility of Li^+ occupancy (0.0 and 0.33) along with the lattice parameters that were reported by others have also been given for comparison.

Table 3.3.7. The occupancy and the unit cell values calculated and the literature values

x	a (Å)	c (Å)	Reference
0.00	7.459	8.604	8
0.20	7.496	9.038	9
0.29	7.510	9.208	10
0.31	7.521	9.210	This work
0.33	7.538	9.156	9

This calculation was thus significant to obtain a measure on the utilisation of Li for the phase transformation. As Li is volatile at high temperatures a reduction in the Li concentration is expected depending on the nature of binding of Li with the system. This loss of Li leads to non-stoichiometry in the sample. This is one of the main reasons why the thermodynamics of a solid state reaction changes and leads to unwanted side products in many of the Li based high temperature systems. This result shows that the Li uptake into keatite intermediate phase by the system is satisfactory.

3.3.5. STOICHIOMETRY - BULK COMPOSITIONAL ANALYSIS BY EDX

To confirm this and to check the overall stoichiometric balance throughout the course of reaction, a series of chemical analyses were carried out at different stages of heating during sintering. However, lithium, due to its low atomic number is difficult to analyse by the conventional solid (powder state) elemental analysis techniques like XRF and EDX. A quantitative analysis of Li was tried using ⁷Li NMR studies of the samples fired at higher

temperatures. This part of quantitative NMR work will be discussed in the later part of this chapter. The other elemental compositions have been shown in Table 3.3.8 for the samples fired at different temperatures.

Table 3.3.8. Elemental compositions and Si/Al ratio by EDX analysis

Sample name (temperature, in °C)	Elemental compositions and ratios in wt % (excluding Li)			
	Al	Si	Na	Si/Al
LASY3(480)	24.59	72.07	4.34	3.340
LASY3(900)	23.49	71.80	4.71	3.057
LASY3(1200)	23.92	72.01	4.08	3.101

Although, as expected, there is a minor dealumination with the increase in temperature, according to the values obtained, there is no significant change in the stoichiometry of other elements in the samples heated at different temperatures.

3.3.6. DIELECTRIC CONSTANT

The pellet of LASY3 sintered at 1200 °C was lapped for uniform thickness. It was electroded with silver paint and cured using the procedure as given in the chapter 2, section 2.3.7. The diameter of the electrode was measured using a vernier caliper and the area of the electrode was calculated. The thickness was measured using a screw gauge. The pellet was mounted on the sample holder as explained in the same section in chapter 2. Under the given conditions the capacitance values of the pellet were measured at different frequencies from 20 Hz to 1 MHz. α -Alumina was used as reference for measuring the capacitance in the LCR unit. The dielectric constant (DEC) of alumina was calculated as 9.526 at 1 MHz, which is comparable with the DEC, reported in literature. The dielectric constant of the sample was calculated as described earlier. The values are given in Table 3.3.9.

Table 3.3.9. The dielectric and other properties of LASY3 heated at 1200 °C

Sample dielectric Dimensions of LASY3	ν , Hz	C, pF	Q	ϵ_T (DEC)
Thickness, 't' = 0.097 cm Radius, 'r' = 0.530 cm Area, 'a' = 0.8825 cm ²	1,000,000	6.5710	136.7	8.1
	100,000	6.6165	79.9	8.2
	10,000	6.7510	51.5	8.4
	1,000	7.0050	26.5	8.7
	1,00	7.7650	13.2	9.6
	20	8.8250	11.1	11.0

where, ' ν ' is the frequency in Hz, 'C' is the capacitance in pF generated between the electrodes, 'Q' is a factor (where $Q = R\omega C$, where ' ω ' is the angular frequency applied across the electrodes, $2\pi\nu$) and ' ϵ_r ' is the DEC of the pellet.

The DEC of LASY3 was compared with that of β -spodumene reported in literature and found to be matching well. The DEC values (at 1 MHz) of other materials commonly used in packaging technology are given in Table 3.3.10. for comparison.

Table 3.3.10. The DEC of β -spodumene from LASY3 and other materials commonly used in MEP

Sl. No	Material	Formula	DEC @ 1 MHz
1	α -Alumina	Al_2O_3	9.6
2	Beryllium oxide	BeO	6.5
3	Alumina-96%	Al_2O_3 - 96%	9.3
4	Alumina-92%	Al_2O_3 - 92%	8.5
5	β -spodumene from LASY3	$LiAlSi_2O_6$	8.1

As discussed in chapter 1, low DEC materials are the most operative candidates for MEP technology. Though BeO has a very low DEC (= 6.5), it is highly toxic in the powder form, which is one of the major disadvantages of the conventional materials and hence unpopular. So, the β -spodumene prepared from LASY3 is apparently a better candidate for MEP having the lowest DEC (= 8.1) among the listed conventional materials.

3.3.7. DENSITY CALCULATIONS

The densities were calculated for the green and the sample sintered at 1200 °C using the procedure given in chapter 2. Table 3.3.11 shows the calculated densities of the samples.

Table 3.3.11. Density of the green and sintered LASY3

No.	Samples(temp. in °C)	Volume(cc)	Wt.(g)	Density (g/cc)
1	LASY3(RT)	1.32367	1.35625	1.0246
2	LASY3(1200)	0.45307	0.97710	2.1566

These densities were compared with the X – ray density of the β -spodumene phase and the relative density was calculated and the results are listed in Table 3.3.12, below. The achieved **relative density of above 90 % is an encouraging result for knowing the extent of sintering**. On further fine-tuning of chemical composition improved relative densities were achieved. They are discussed in the later part of this chapter.

Table 3.3.12. Density changes on sintering and the relative density

Sample name	Density in g/cc			Relative density, %
	Green state	Sintered	X-Ray	
LASY3	1.0246	2.1566	2.3790	90.6515

3.3.8. SHRINKAGE STUDIES ON GREEN SAMPLES

Figure 3.3.7. shows the thermomechanical analysis (TMA) plot of the green sample LASY3 in the temperature range from RT to 1200 °C. The TMA curve shows an usual and plain trend in which the sample is stable up to higher temperature (800 °C) and suddenly condenses to a dense phase. There

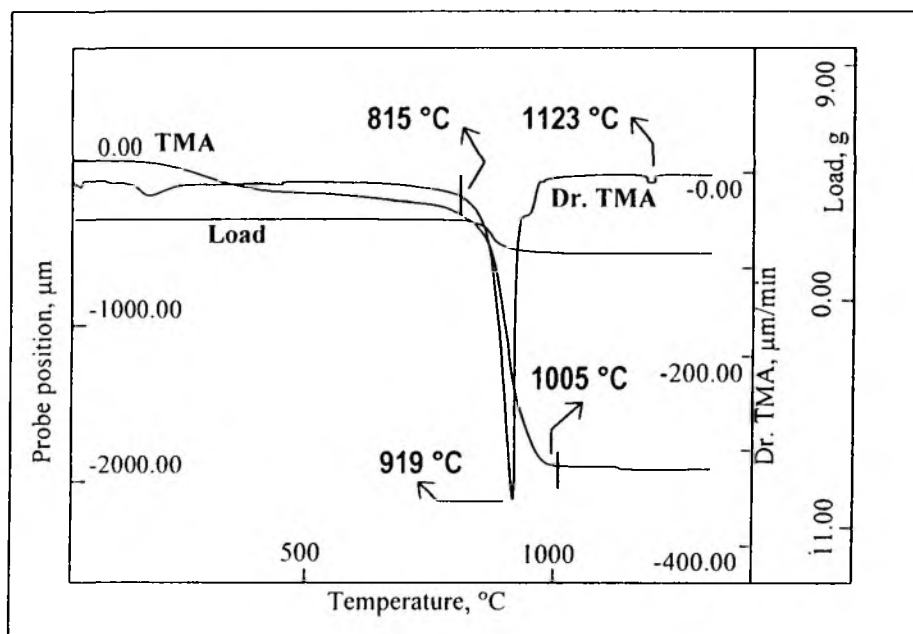


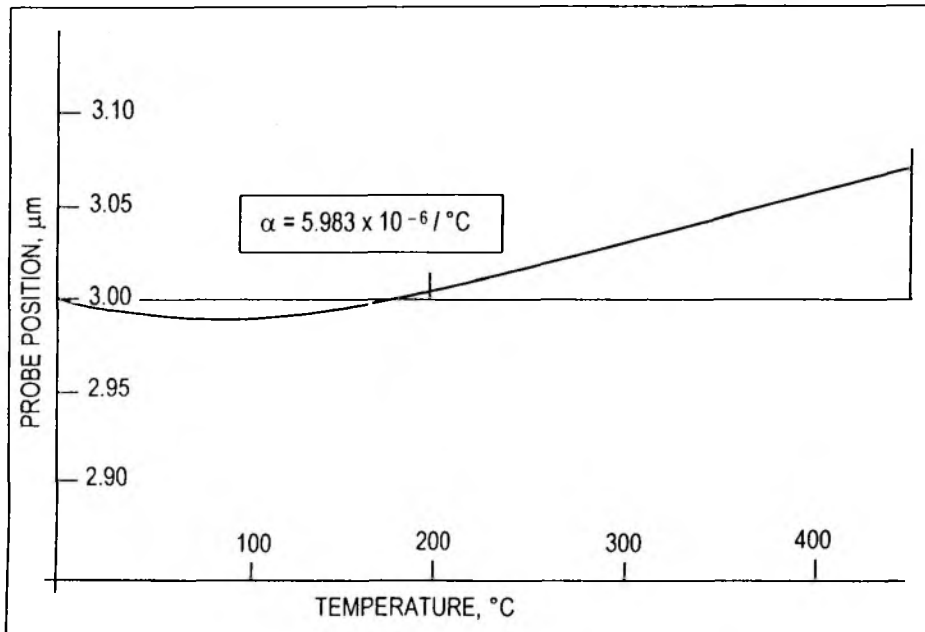
Figure 3.3.7. The shrinkage TMA plot of the green sample LASY3 in the temperature range from RT to 1200 °C

is an initial shrinkage of ~20% of the total shrinkage up to 800 °C which may be due to the expulsion of the adsorbed matter and the strain from the lattice. There is a strong densification after 813 °C up to 1005 °C indicating the structure collapse of the sample and then sintering of the sample. The XRD pattern of the sample sintered at 800 °C shows that the zeolite precursor has collapsed into an amorphous material. The highest densification rate was observed around 920 °C. This temperature is called as temperature at maximum densification (T_{Dmax}). The value of T_{Dmax} for LASY3 is relatively much less than that of MASY3 (Magnesium Aluminosilicate precursor from Y zeolite after 3 exchanges of 1 M Mg salt solution). A comparison of the two results is given in chapter 5. This comparison offers a good realization about the effect of cation on sintering of zeolite precursors for ceramic preparations. The over all shrinkage is estimated to be around 33.34 %. The derivative of TMA shows a sharp peak indicating that the shrinkage is a one step process. However, there is a shoulder around 990 °C indicating the possible chemical reaction extended even after the completion of densification. This is a typical case where the sintering is getting over before the high temperature solid state reactions. Usually, this kind of situation does not allow the phase transformation to complete which leads to unwanted side products (other impurity phases). But this can be controlled to some extent by the optimization of heating program. However such studies are beyond the scope of this thesis.

3.3.9. THERMAL EXPANSION STUDIES ON SINTERED SAMPLES BY DILATOMETRY

Measuring system	: Dilatometer	TMA – Perkin Elmer
Diameter	: 15.195 mm	
Height	: 3.009 mm	
Probe position (mm)	: Step:1	
Filename	: LIY3	
Temperature (rate)	: 20 to 450 °C (20 °C/min)	

Figure 3.3.8. Thermal expansion plot of sample LASY3 (sintered at 1200 °C) in the temperature range of 20 to 400 °C (TEC plot)



The disc of sample LASY3 heated at 1200 °C is used for the expansion analysis. However, the measurement beyond 450 °C was not possible because of the instrumental limitations. Figure 3.3.8 shows the thermal expansion curve measured in force free conditions, in the temperature range, 25 to 400 °C. The curve shows a typical 'lower bend' in the region of temperature range up to around 175 °C. The thermal expansion coefficient measured at a range of 20 to 200 °C is $5.983 \times 10^{-6} / ^\circ\text{C}$ and it agrees with the reported TEC value for β -spodumene ($\text{TEC} = \sim 5 \times 10^{-6} / ^\circ\text{C}$)¹¹. However the increase in the TEC may be attributed to two factors namely (i) the symmetry nature of β -spodumene phase and (ii) the impurity phases present, particularly the oxides of alkali elements viz., Na, Li. The first factor, the anisometric nature of phase present in the sample makes the expansion anisotropic. Table 3.3.13 collects the individual contribution from each coordinate of the particular crystal symmetry to describe the effective thermal expansion coefficient ' α'_{eff} '. The principal coefficients α_1 , α_2 , α_3 are symmetry dependant whereas the secondary coefficients α_4 , α_5 , and α_6 are dependant on the crystal shape. On the basis of symmetry of the crystalline ceramic phase, the prediction of their contribution to the effective TEC is easier. β -Spodumene has tetragonal symmetry and hence does not have dependence of secondary coefficients but α'_{eff} is dependent strongly on α_1 and α_3 . If α_3 is relatively higher (usually is the case) and the crystals are oriented along c-axis, such increments are observed. The second reason is due to the impurity phases present viz., mullite and virgilitite. Mullite is a well-known material often added to alter the TEC of a material¹³. Park has demonstrated that the TEC increases drastically on addition of 4 – 8 wt.% of alkali and boron mixed oxide as a fluxing agent, which also enhances the extent sintering¹⁴.

The measurement done in a different temperature range between 20 to 450 °C has resulted in an increase in the TEC to $51.759 \times 10^{-6} / ^\circ\text{C}$. The increment in the TEC is attributed to the characteristic feature of the temperature range in which it was measured. The temperature dependence on TEC has been well studied in many oxide solids. Kingery remarks in his book¹⁵, a typical case in which the values for oxide structures with dense packing of oxygen ions are in the range of $6 - 8 \times 10^{-6} / ^\circ\text{C}$ at room temperature and increases to $15 \times 10^{-6} / ^\circ\text{C}$ near the Debye characteristic temperature, θ_D . The temperature dependence of the TEC has been studied on variety of materials¹⁶⁻¹⁹. In our investigation on LASY3, when the TEC of the sample measured at different temperature ranges are plotted versus temperature up to where the TEC is measured, as shown in Figure 3.3.9, a curve appears to have a dual slope above and below the zero expansion level. This is a typical advantageous feature of many LAS systems having negative TECs. This property makes the material suitable for microelectronic applications.

Table 3.3.13. The effective thermal expansion coefficients for various crystal symmetries

Symmetry	Principal coefficients			Secondary coefficients		
Cubic	α_1	α_1	α_1	0	0	0
Hexagonal	α_1	α_1	α_3	0	0	0
Tetragonal	α_1	α_1	α_3	0	0	0
Trigonal	α_1	α_1	α_3	0	0	0
Orthorhombic	α_1	α_2	α_3	0	0	0
Monoclinic	α_1	α_2	α_3	0	α_5	0
Triclinic	α_1	α_2	α_3	α_4	α_5	α_6

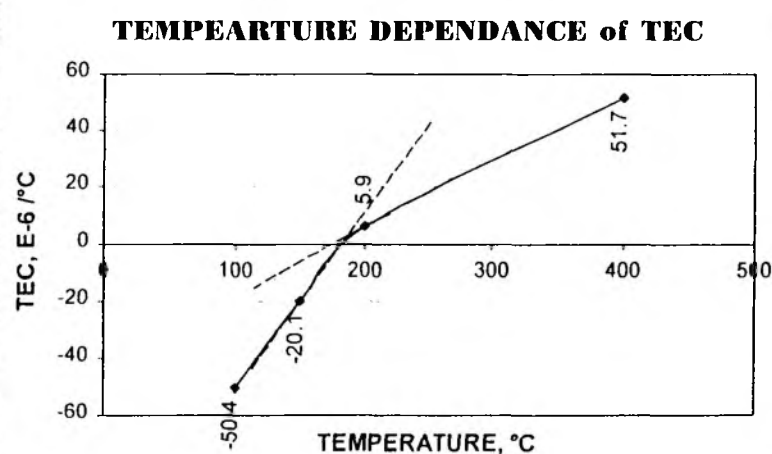


Figure 3.3.9. The temperature dependence of the TEC on LASY3 – β -spodumene synthesised by zeolite route. Temperatures plotted are the upper limits of the TEC measurements.

According to the literature available, this kind of phenomena is also observed in sintering of metals and metallic alloys. If the kinetics of this process is studied, more understanding can be acquired on the mobility of the defect sites during the thermal vibrations at high temperatures. A similar work has been reported earlier on Zn and Cd elements in terms of mobility of vacancies during inter-metallic diffusion processes²⁰.

3.3.10. NMR STUDIES ON LASY3 SYSTEM

In early 80's, Asai, Fyfe and Klinowski were few of the earlier groups initially tried to exploit solid state NMR for silicate and silicate based ceramic materials^{21,22}. Oldfield and Engelhardt developed many new experiments in the area of solid state NMR for the characterisation of ceramic materials^{23,24}. The next two decades have witnessed the capability of solid state NMR on ceramic characterisation. There are general NMR reports on the ceramics synthesised by conventional routes like spodumene or cordierite, which are widespread in MEP technology. Jancke has reported a study of NMR characterisation using ²⁹Si NMR of cordierite synthesised by sol-gel route²⁵. However, there are not many reports on the sintering of zeolite based ceramics²⁵. The present NMR based investigation is somewhat unique, as there is no documentation of a multinuclear approach to study the sintering phenomenon of the zeolite-based ceramic precursor, LASY3 by solid state NMR to find out the phase changes as a function of temperature. This includes the NMR studies on nuclei namely, ²⁹Si, ²⁷Al and ⁷Li.

This particular route follows amorphization of the crystalline raw material (zeolite) as a first step and consecutively the crystallization of new ceramic phases from the amorphous matter. This gives an opportunity for one or more amorphous phases to co-exist at a given temperature and this is clearly observed and evidenced by the raise in the baseline in the XRD pattern taken for sample heated at 800 °C. It is obvious, that the characterisation of this state of matter just by XRD is extremely difficult. Though XRD is useful for the phase identification, the inherent disadvantage of XRD is the inability to detect materials having small crystallite size (below 0.1 micron). So, XRD becomes ineffective in the case of samples having both crystalline and glassy phases together. Here the support of NMR is very effective to study even the so-called amorphous 'crystals'. NMR provides information at local molecular level and principally does not depend on the crystallinity. The present study involves the NMR spectral characterisation of the samples that are sintered at various temperatures in the range from 480 °C to 1200 °C, through the nuclei ²⁹Si and ²⁷Al. The ⁷Li NMR has been studied using the quadrupolar echo (QUADECHO) pulse sequence. General experimental conditions are described in chapter 2, section 2.3.6.b. Table 3.3.14 lists the different types of silicates and their notations along with the ²⁹Si NMR chemical shifts. It is important to note that the chemical shift moves to low field as the ordering of Si-O-Si increases. The present study involves various silicates viz., soro- and ino- silicates which have chemical shifts in the range of -68 to -96 ppm. Various such silicates that are encountered in this investigation are listed in the Table 3.3.15.

Table 3.3.14. Types of silicates and their NMR chemical shift ranges (δ , ppm)

Sr. no.	Types of silicates	Order	Notation	δ , ppm
1.	Neso-silicates	Mono-	Q ⁰	-60.0 to -83.0
2.	Soro-silicates	Di-	Q ¹	-68.4 to -95.3
3.	Ino- and cyclo-silicates	Chain- and Ring-	Q ²	-80.0 to -96.0
4.	Phyllo-silicates	Layer-	Q ³	-91.5 to -101.5
5.	Tecto-silicates	3D cross linked-	Q ⁴	-107.0 to 121.0

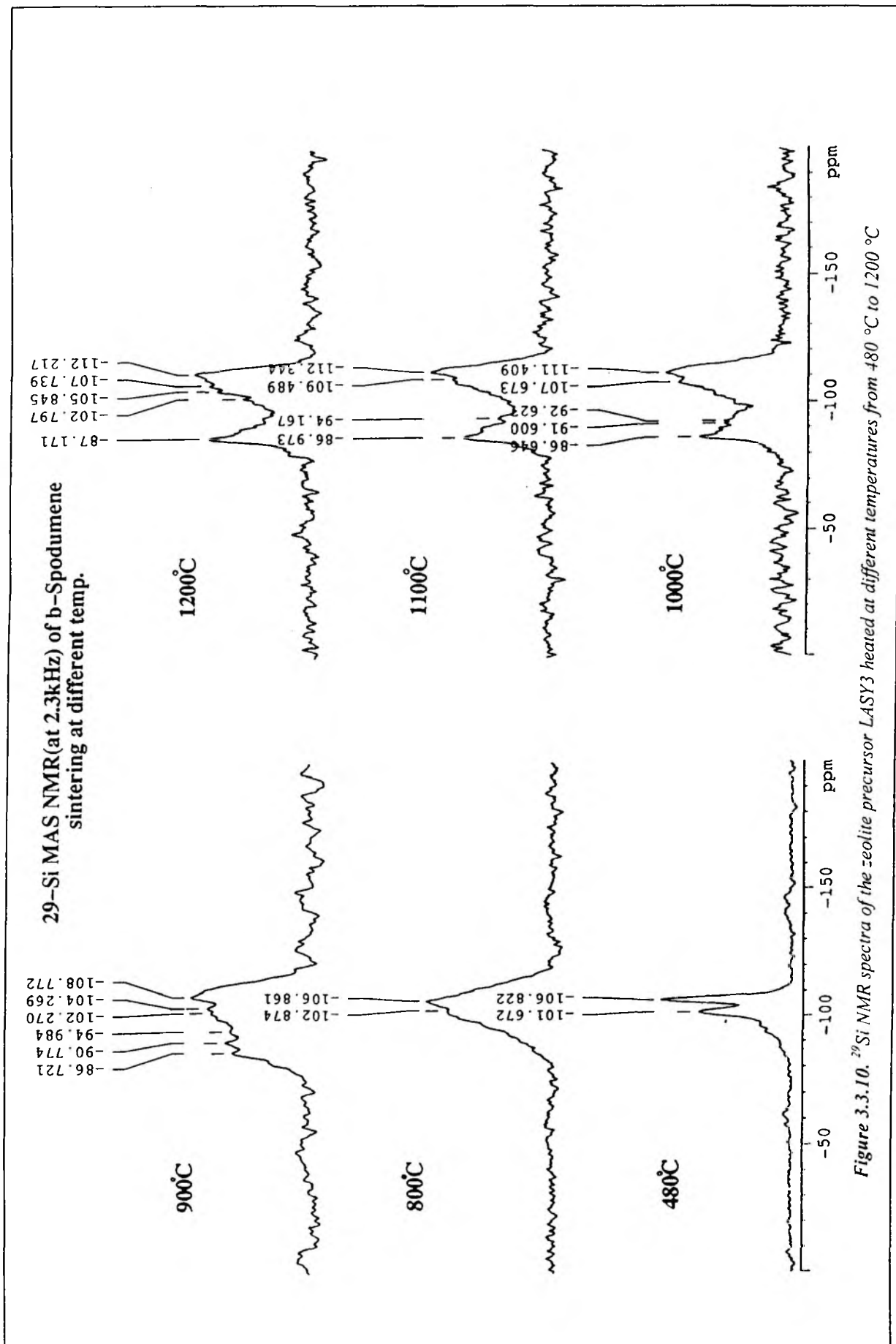


Figure 3.3.10. ²⁹Si NMR spectra of the zeolite precursor LASY3 heated at different temperatures from 480 °C to 1200 °C

Table 3.3.15. Chemical shifts of silicate phases identified.

Sl. no	Name of the phase	Formula	²⁹ Si Chemical shift, ppm		Ref.
			Observed	Reported	
1.	Cristobalite	SiO ₂	-108.7	-108.5	27
2.	Sodium disilicate	Na ₂ Si ₂ O ₅	- 94.9	- 94.4	26
3.	β-spodumene	LiAl[Si ₂ O ₆]	- 91.6	- 91.6	28
4.	Lithium sorosilicate	Li ₂ Si ₂ O ₅	- 92.6	- 92.7	26
5.	Sillimanite	Al ₂ SiO ₅	- 87.1	- 87.1	28
6.	α-quartz	SiO ₂	-107.6	-107.4	26
7.	Mullite	Al ₆ Si ₂ O ₁₃	- 87.1	- 87.0	29

3.3.10.a. ²⁹Si Nuclear magnetic resonance studies

Figure 3.3.10. shows the ²⁹Si MAS NMR spectra recorded at a spinning speed of 2.3 kHz of LASY3 samples heated at different temperatures ranging from 480 to 1200 °C. All these NMR studies in the present investigation are related to only one sample namely LASY3. The spectrum recorded for the sample heated at 480 °C is typical of that of a zeolite with medium Si/Al ratio where the Q⁴ (4Si-0Al) and Q⁴(3Si-1Al) environments are clearly distinguished by peaks at -106.9 and -101.3 ppm respectively. The peak positions match with the literature values of these environments. The shoulders at higher field next to the Q⁴ (3Si-1Al) indicate the presence of very low level populations of (2Si-2Al) and (1Si-3Al) environments.

The NMR spectrum of sample heated at 800 °C is broad due to the structure collapse. The amorphous environment is also reflected by XRD of the same sample. Better resolution begins from the samples heated over 900 °C onwards into two distinct symmetric bands. One moves upfield in the range of around -87 ppm indicating the formation of Q¹ (3Al) type of sorosilicate species and another to a downfield range of around -110 ppm indicating the crystallisation of Q⁴ (0Al) type of tectosilicates and exclusively the polymorphs of SiO₂.

From the crystallization point of view, NMR spectrum of sample heated at 900 °C is a combination of the two broad bands, probably including many other phases which are amorphous after the structure collapse of zeolite metaphase. The actual crystallisation seems to start above 900 °C and end at 1100 °C with a clear distinction of two separate bands.

At 900 °C, the major peak (belongs to the right band) at -108.77 ppm corresponds to the SiO₂ polymorph, cristobalite (reported $\delta = -108.5$ ppm)²⁷. The powder XRD profile of this sample shows the presence of two different SiO₂ phases (JCPDS files 270606 and 120708). The second SiO₂ may be related to the high quartz structure, which is usually expected in this range of temperature. However, XRD results show that the zeolite structure has not completely collapsed and partly remains with a heavy loss of crystallinity. Hence, the NMR spectrum for sample heated at 900 °C shows the co-existence of both LAS based HT product and the polymorphs of SiO₂. The formation of two major bands along with the broad component in between them proves this. The broad component is due to the existence of the zeolite environment still at this temperature.

The NMR spectra of samples heated in the range, 900 °C to 1200 °C includes the movement of the peak at $\delta = -86.72$ ppm to a symmetric peak at $\delta = -87.17$ ppm. The peak at -86.72 ppm (of the left band) shows an environment of Q³ type of silicate that corresponds to sillimanite, observed at $\delta = -86.9$ ppm, which later turns to Al₂SiO₅, (reported $\delta = -87.1$ ppm³⁰) type of species at high temperature. The amorphous broad component in between the two bands disappears as the temperature increases indicating the segregation of crystallized products into two major categories from the amorphous matter.

At 1000 °C the formation of lithium aluminosilicate species starts as indicated by the peak at $\delta = -91.6$ ppm. The reported value is $\delta = -91.6$ ppm²⁷. Virgilite (Li_xAl_xSi_{3-x}O₆) is the previous phase to crystalline β -spodumene. At high temperatures, the fraction x becomes an integer x = 1 to form β -spodumene (LiAlSi₂O₅). This observation is supported from the XRD characterisation described earlier. As the Si/Al ratio is considerably high in ceramic phases, it is not possible to have Si-Al ordering like low Si/Al ratio zeolites have. Also it is very well known that the Si signal shifts upfield as the Si/Al ratio increases during sintering.

Oldfield reports the same kind of spectrum for a mixture of mullite and SiO₂. Figure 3.3.11 shows the spectrum observed by Oldfield and coworkers for the mixture of mullite and SiO₂, spun at a speed of 2.5 kHz (MAS) and almost similar experimental conditions. The spectrum consists of relatively narrow peak at -87.0 ppm, due to crystalline mullite and a broader peak at -108.3 ppm due to a nearly pure SiO₂ glass (pure SiO₂ glass is at approximately -111 ppm). In the present study, the XRD profile for the particular sample heated upto 1100 °C shows the presence of

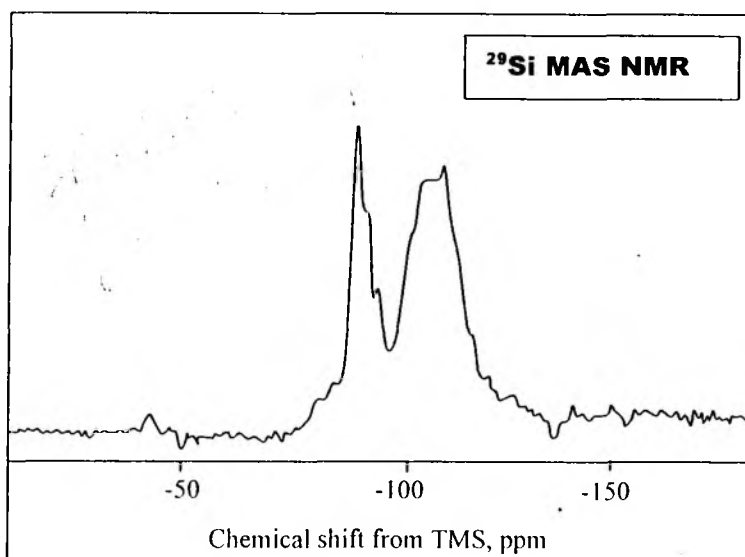


Figure 3.3.11. Mullite-SiO₂ mixture, 2.5 kHz, ²⁹Si MAS NMR, {ref. Oldfield et al, *Am. Ceram. Soc. Bull.*, 66(4) 656-63 (1987) }

mullite and SiO₂. From the temperature 1100 °C to 1200 °C, the spectral lines are sharper indicating that the crystallization is getting over with two major components. One includes the glassy and crystalline SiO₂ phases and the other includes the LAS phase, β-spodumene and mixture of mullite and glassy silica (Al₆Si₂O₁₃, observed $\delta = -87.17$ ppm and reported $\delta = -87.1$ ppm³⁰) as major crystalline impurities. These results are in good agreement with the XRD characterisation of the same. The results are in accordance with the reported literature³¹.

3.3.10.b. ²⁷Al Nuclear magnetic resonance studies

²⁷Al being a quadrupolar nucleus the typical quadrupolar features are seen. Unlike ²⁹Si, it becomes difficult to quantify ²⁷Al spectrum as the complication arises, because of its quadrupolar nature. However, the narrow and sharp peak at 59.03 ppm indicates the presence of typical tetrahedrally coordinated Al atoms in zeolite environment. The LASY3 sample heated upto 800 °C shows a considerable amount of octahedral occupation close to 0 ppm. This is due to the collapse of the zeolite structure at that temperature. Klinowski and his coworkers³² have studied the dealumination and the thermal destruction of zeolite framework using NMR. Figure 3.3.12 shows the ²⁷Al NMR of the samples heated at various temperatures.

LASY3 sample heated at 900 °C shows a reduction of intensity and another broad peak starts growing near 0 ppm (4.31 ppm at 900 °C) indicating the formation of the amorphous matter in which the Al atoms are moving to the octahedral positions. Assignments are based on the fact that Al atoms, when tetrahedrally coordinated by oxygen atoms resonate at 50 ± 20 ppm and when octahedrally coordinated, resonate at 0 ± 10 ppm³³⁻³⁴.

The slight shifting of the main tetrahedral peak from 59.03 ppm to 57.87 ppm and to 58.66 ppm at 480, 800 and 900 °C respectively shows the gradual collapse of zeolite structure. On the other hand, the formation of the sharp peak at 13.6 ppm (at 900 °C) shows a well ordered octahedral coordination of Al atoms as the same in alumina. The detection of the presence of alumina phase (JCPDS 100173) at 900 °C by XRD is confirmed by NMR. The alumina again transforms into other products at high temperatures.

It is clearly understood from the XRD results that the β-spodumene is formed through the key intermediate phase virgilite. The slow conversion of virgilite to β-spodumene is in fact a conversion from octahedral to tetrahedral again. The Al atoms are tetrahedrally coordinated in β-spodumene. The formation of β-spodumene is observed by XRD in the range of 900°C to 1000 °C. This is reflected by the movement of the tetrahedral peak at 58.67 ppm (of 900 °C) to 55.80 ppm (1000 °C) at the expense of the octahedral peak (4.31 ppm). It continues to remain at 55.11 ppm at the temperature range of 1200 °C indicating the completion of crystallisation of β-spodumene around 1200 °C.

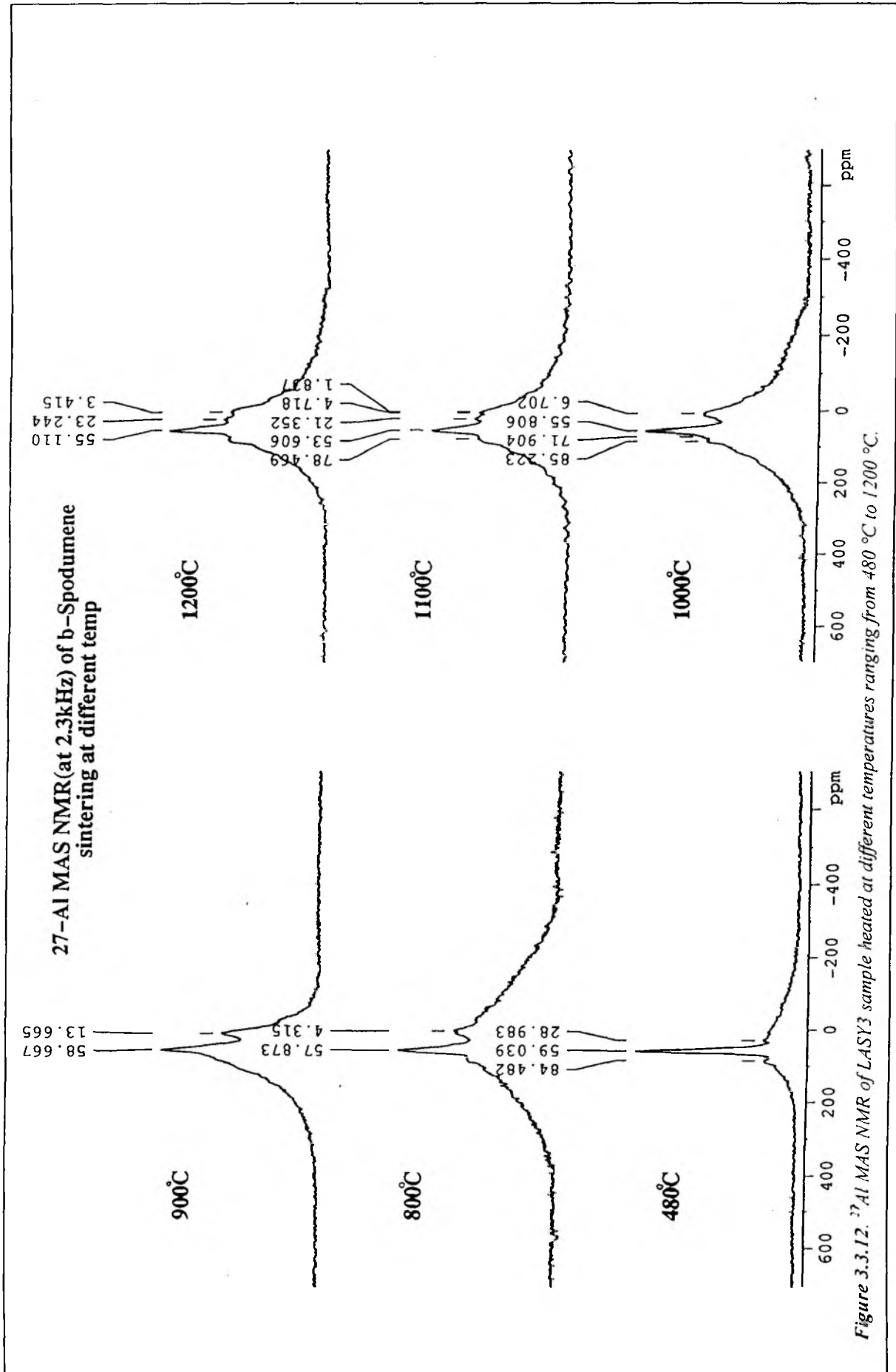


Figure 3.3.12. ²⁷Al MAS NMR of LASY3 sample heated at different temperatures ranging from 480 °C to 1200 °C.

The new peak around 21 ppm to 23 ppm in the spectra of samples heated from 1100 to 1200 °C is the range where the Al is in five coordination and will be in distorted octahedral structure. This is due to the presence of mullite that is according to the XRD results, another major intermediate in LAS sintering. This is in accordance with the result of Merwin³⁵. He has proved that the ²⁷Al MAS NMR spectra of sintered- and fused-mullite measured at different Larmor frequencies revealed clearly the presence of 3 distinct Al sites, i.e., of octahedral (M1), tetrahedral (M2), and distorted tetrahedral (A1*) sites. Due to this reason, there are satellite side bands around the tetrahedral peak at 53.60 ppm of sample heated at 1100 °C (possibly distorted).

The spectrum recorded for the sample heated at 1200 °C looks more simple and the tetrahedral main peak due to the LAS ceramic phase β -spodumene remains intact with the distorted environment at 55.11 ppm. The distorted tetrahedral of mullite Al atoms show a peak around 23.24 ppm and the octahedral mullite at 3.42 ppm. Hence for sample heated at 1200 °C, the NMR shows peaks for two major phases mullite and β -spodumene. The main peak moves towards high field to 53.6 ppm to 55.1 ppm indicating the mullite phase with a distorted octahedral coordination of Al.

3.3.10.c. ⁷Li nuclear magnetic resonance studies

The ⁷Li QUADRECHO NMR results are shown in the Figure 3.3.13. At the very outset, it is important to note that the position of ⁷Li nuclei is very distinct from that of the other nuclei like ²⁹Si and ²⁷Al. In fact the Li ions are highly mobile in the zeolite environment, as they do not sit in the lattice positions. However in dense ceramic phases, the lithium mobility is highly restricted and is fixed with the lattice positions (only lattice vibrations).

The narrow Li signal at 0 ppm in the beginning of sintering (for the sample calcined at 480 °C) indicates its mobile nature and thus averaging out the quadrupolar interactions isotropically. The quadecho conditions preclude the possibility of missing out if any possible appearance of broad feature at this temperature. The onset of the phase transformation of LAS zeolite precursor into a condensed LAS phase is clearly seen by the appearance of the broad component for the sample heated at 900 °C. The broad component is definitely due to the satellite transitions that are normally observed for ⁷Li in many simple Li compounds and for immobile Li oxide materials viz., lithium acetate, lithium carbonate, layered oxides of Li, which are diamagnetic. However, the loss of so-called 'powder pattern' features of the satellite transitions is due to the lack of very high crystallinity for the β -spodumene. This is also due to the fact that there is a distribution of chemical environment of Li as it remains in more than one phase viz., virgilite, β -spodumene and other amorphous (glassy) Li oxides, during the process of crystallisation. These are commonly noticed in many Li glasses.

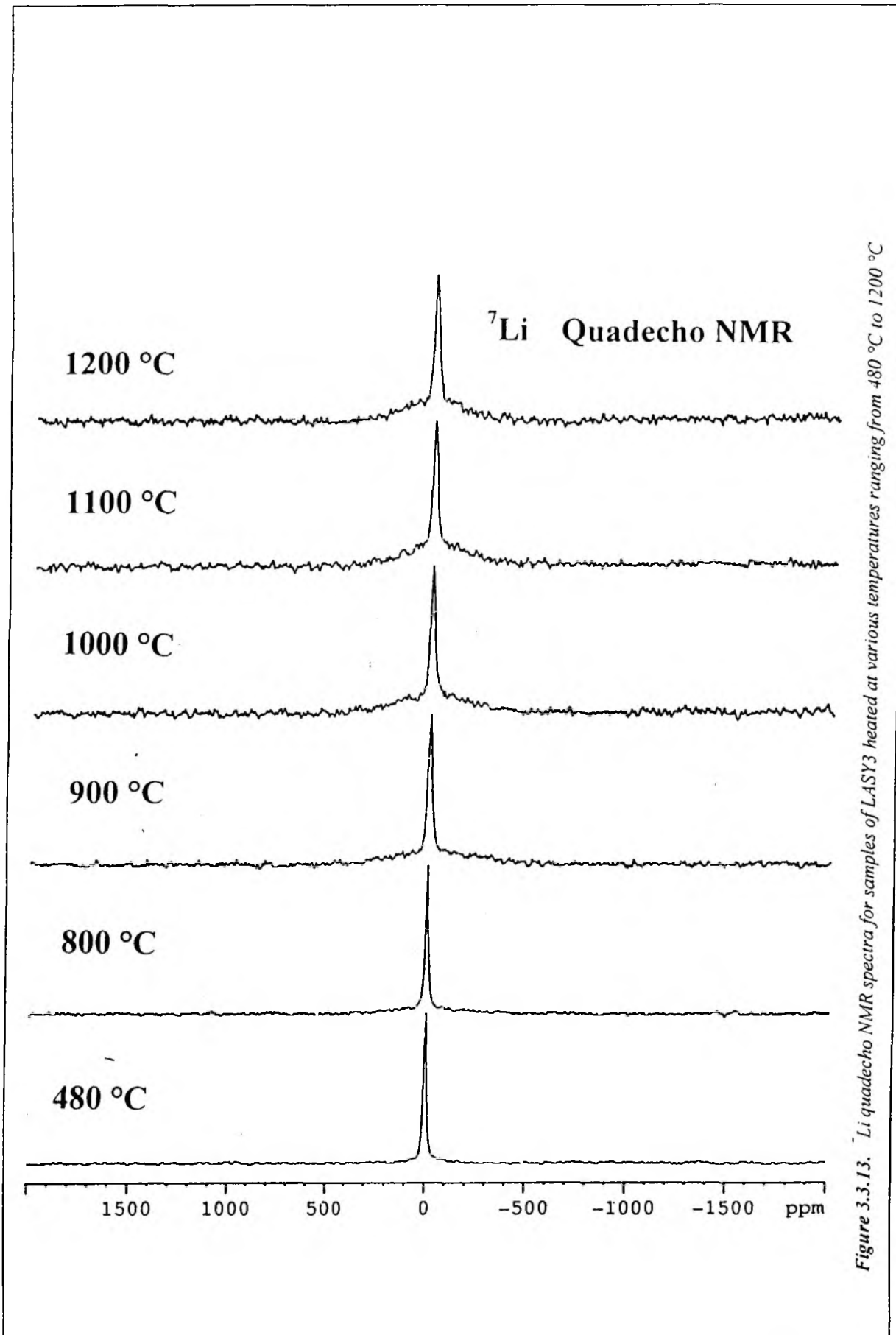


Figure 3.3.13. ⁷Li quadecho NMR spectra for samples of LASY3 heated at various temperatures ranging from 480 °C to 1200 °C

Another possible reason may be due to the dipolar interaction of Li with Al. Engelhardt reports these types of dipolar interactions in his book for Li exchanged Na-A zeolites²⁶. In the present study in the LAS systems, $\text{Li}_x\text{Al}_x\text{Si}_{3-x}\text{O}_6$ (virgillite) and also $\text{LiAlSi}_2\text{O}_6$ (β -spodumene) there is a 1:1 site population for Li:Al. It is possible that Al broadens the satellite features and makes it not prominent. Figure 3.3.14 shows the ^7Li NMR spectrum recorded for various conditions. It shows that the quadrupolar features are enhanced using a quadecho pulse sequence instead of the single pulse and also that the Al:Li dipolar interaction suppresses the enhancement.

3.3.10.d. Quantitative NMR study on Li content

Evaporation of Li is a common problem in many Li based HT ceramic preparations. Li being a volatile element, the stoichiometry of the ceramic phase at high temperatures will not be the same as that of the starting precursor. Hence it is important to monitor the Li content through out the sintering process. The analysis of Li content by atomic absorption spectroscopy (AAS) was somewhat difficult, as the high temperature dense phase (especially the silica-rich) LAS ceramics are rather difficult to be digested into aqueous solution for AAS. So, the AAS based analysis may not be reliable and an additional technique is needed to support the results. The quantitative solid state NMR study can be employed for this purpose as it uses the solid mass itself for the analysis. There are many such studies reported in literature³⁶.

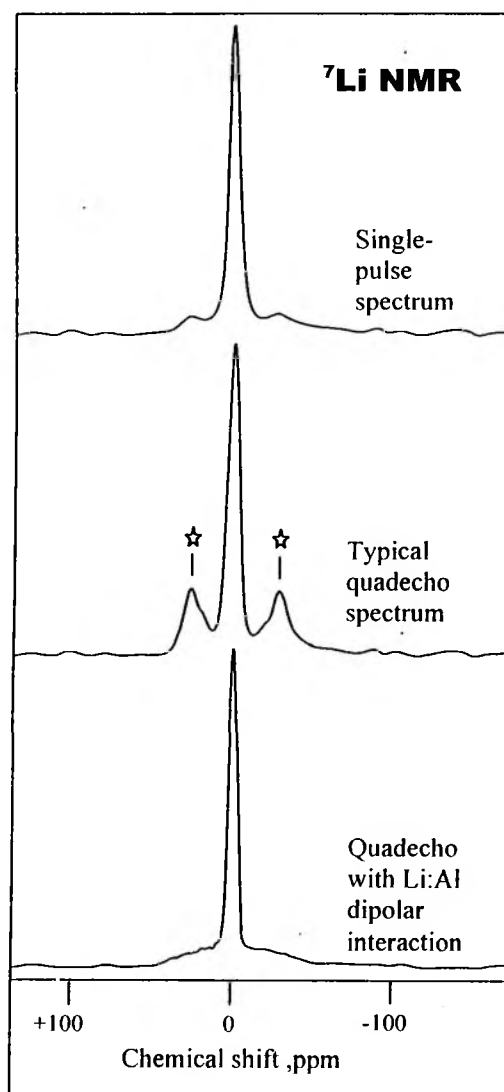


Figure 3.3.14. ^7Li NMR spectrum of single pulse quadecho and quadecho with Li:Al interaction. * shows the enhanced quadrupolar features in typical quadecho conditions.

The LASY3 samples heated isothermally at different temperatures viz., 800, 1000 and 1200 °C for 6 h, were crushed into fine powder and used for NMR study. Samples weighing exactly 0.18735 g each were loaded in the NMR sample tubes with uniform packing. Using the similar probe used for the quadecho ^7Li spectroscopy, the ^7Li single pulse static signals were collected using experimental conditions mentioned in chapter 2. The FIDs were Fourier transformed with a line broadening of 40 Hz for minimum signal/noise ratio. Phase and base line corrections were done and integration was performed over the main central transition signal. Figure 3.3.15 shows the ^7Li static NMR spectra recorded for samples heated at different temperatures. The integrated area values are plotted in Figure 3.3.16. Generally the spectra look very narrow for samples heated at low temperatures and

become broad for samples heated at high temperatures. The broadening is due to the fact that the Li ions get into lattice positions at high temperature that restricts the mobility of them. However the reduction in the intensity along with broadening keeps the integrated value the same indicating that the lithium loss is negligible during high temperature treatments. The Li content in terms of the integrated values plotted in Figure 3.3.16. The value varies marginally from 1985.9 (800 °C) to 1920.1 (1200 °C) which is commonly observed marginal loss in Li based high temperature material synthesis³⁷.

3.3.10.e. Summary of multinuclear NMR studies on sintering of LASY

Multinuclear NMR studies on the sintering process of LASY has given a better understanding of the entire process in terms of the nuclear environment of the elements irrespective of crystalline and amorphous nature of the state at a given temperature. The NMR results are quite supportive and appropriate to the results obtained by XRD at similar temperatures. Few aspects like the presence of alumina only in the range of 900 °C by XRD is confirmed by the ^{27}Al NMR results. ^{27}Al being a quadrupolar nucleus, is relatively difficult for interpretations. However, the literature sources suggest that the high speed spinning at higher

field will increase the resolution of the spectrum that would help in distinguishing the overlapping peaks. Special NMR experiments which would decrease the quadrupolar interactions like multiquantum (MQ) might help to understand the spectrum better.

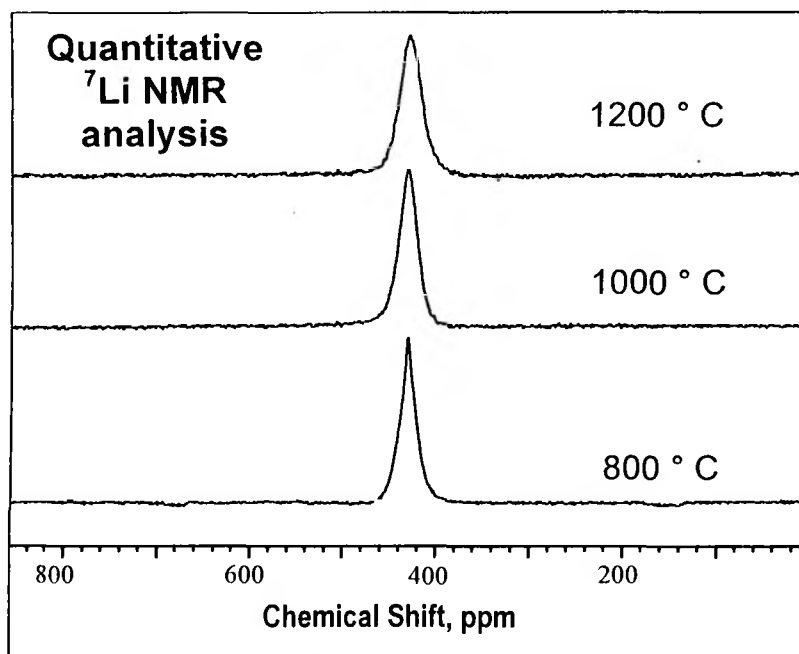


Figure 3.3.15. Quantitative ^7Li NMR study on LASY3 sample sintered at various temperatures (800, 1000 and 1200°C)

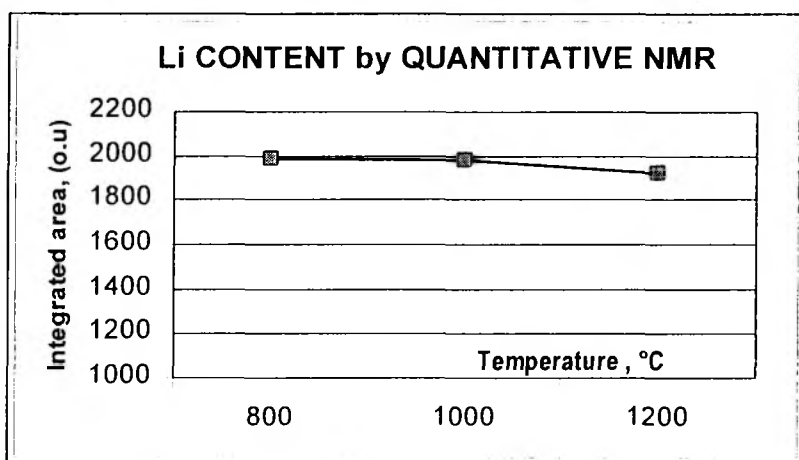


Figure 3.3.16. Quantitative ^7Li NMR studies on sintered samples of LASY3 sample. The integrated area over the central transition signal is given in text.

CHAPTER 3

PART B. INFLUENCE OF PRECURSOR STOICHIOMETRY ON LAS SYSTEM

3.4. INTRODUCTION

The second part of this chapter deals with the studies carried out to find out the influence of variation of different parameters on the sintering of LAS systems. It is well known that in solid state HT reactions, the difference in chemical compositions of the precursor materials drastically affects the purity of the phases formed at high temperatures. In solid state HT reactions unlike the liquid state reactions, generally there is not much control on the thermodynamics of the reactions. Hence it is very important to know the way in which the sintering process and the phases formed get affected when the composition of the precursor is changed. Consequently, one can achieve a reliable control over the quality of the final product.

Practically, all Na⁺ ions in the zeolite lattice can not be exchanged and hence there would be always a fraction of residual Na in the precursor composition. It is very important to note that this influences the purity of the final phase and the sintering process as well. This will, however be discussed in the later sections of this chapter. In this view, in the sintered ceramic product, all expected lattice sites for Li⁺ in the lattice of β -spodumene need not be occupied by the Li⁺ cations. Also, the occupancy of the Li⁺ ion in the entire unit cell may vary with the defect structure and the phase purity. This influences however, the purity of the final phase, as well the sintering process due to the fact that the presence of trace amount of Na in the precursor acts as a flux during the solid state high temperature phase transformations. In general, alkali oxides and fluorides are known as fluxing agents. This aspect has been well discussed by many workers and reported³⁸⁻⁴⁰. One of the major elements present in the system, viz., Li⁺, itself is known to behave as a 'self-flux' at high temperature⁴¹. It is usually added in some systems as an external fluxing reagent.

In oxide based conventional preparations, meeting the stoichiometric requirement is rather unrestrained as the components (in the case LAS, the components could be SiO₂, Al₂O₃, and LiO₂) are mixed apparently. However, in zeolite based route, the case is different. Firstly, for a given zeolite precursor the SiO₂/Al₂O₃ is fixed. However one can choose or synthesize the zeolite with desired Si/Al ratio.

Secondly, cation concentration can be altered by the magnitude of cation exchange. However, the number of cations that can be exchanged is directly proportional to the number of Al atoms present in an unit cell, depending on the valency of the cation (in Li exchanged zeolite, the cation is Li⁺ and the valency is 1; So, the ratio Al:Li would be 1:1). In this aspect, the compositional variations in zeolites are easily possible with respect to the concentration of cations and Si/Al ratio. As mentioned in chapter 1, in today's ceramics market composites are

much attractive materials than single-phase ceramics. In that view, better fine-tuning of the chemical composition of the precursor is required to make composites and solid solutions with improved properties. It has been often reported that in oxide systems the presence of excess SiO_2 in the precursor powder also affects the reactions at HT. Takeo Iga has reported that the presence of excess SiO_2 in sintering of alumina inhibits both densification and grain growth⁴². It is also proved that this does not affect the material transport during the sintering but the grain growth. Yong Bai Son and coworkers have studied the crystallisation behavior of similar systems in Al_2O_3 rich and SiO_2 rich conditions to understand their individual effects⁴³. However the influence of excess SiO_2 is different with different systems and hence, it would be an interesting study. The studies on the influence of cation concentration and the Si/Al ratio (in the precursor powder) on the sintering behaviors have been discussed in this part of the chapter.

3.4.1. EFFECT OF CATION CONCENTRATION AND Si/Al RATIO IN PRECURSOR

3.4.1.a. Plan of work

It was planned to prepare samples with varied cation concentration. The differences in the sintering behavior with respect to different concentrations of Li in the precursor samples were followed by various techniques. XRD was the main tool used by which the phase changes were followed.

3.4.1.b. Experimental

3.4.1.b.1. Sample preparation

The Li content in the zeolite precursor was modified by changing the concentration of the cation solution and the number of exchanges. Zeolite Y was first exchanged three times with 1 M solution of NH_4NO_3 to get the NH_4 form of Y and then with the different molar solutions of LiNO_3 . Solutions were prepared with different molar concentration from 0.01 M to 1 M as listed in the Table 3.4.1. The number of repeated exchanges were changed with sample to sample as listed in the table. The elemental compositions analysed by AAS are also given.

Table 3.4.1. Sample details for cation concentration variation.

Sample name	Conc. of Li soln.	No. of exchanges	Elemental ratios, wt. %		
			Li	Na	Si/Al
LASY1	1 M	1	0.53	0.076	3.392
LASY2	1 M	2	0.76	0.082	3.417
LASY3	1 M	3	1.31	0.075	3.401

Nearly 10 g of three zeolites namely zeolite A, zeolite P and zeolite Y with a Si/Al ratio 1.12, 1.8 and 2.51 respectively were exchanged with each 300 ml of 1 M LiNO₃ solution for three times. Li⁺ using the similar procedure prescribed in chapter 2 – Section 2.1.2.a. for ion exchange. The powders designated as LIA3, LIP3 and LIY3 respectively as per given in Table 3.4.2.

Table 3.4.2. Sample details for Si/Al variation

Sample	Source	Conc. of Li solution	No. of exchanges	Si/Al
LIA3	Zeolite A	1 M	3	1.12
LIP3	Zeolite P	1 M	3	1.80
LIY3	Zeolite Y	1 M	3	2.51

3.4.1.b.2. Consolidation and sintering

The powders of all three samples were mixed with appropriate amount of binder PVA and dried. They were pressed into pellets and then sintered at various temperatures from 480 °C to 1200 °C as per the procedure given in chapter 2. The pellets were fired at different temperatures viz., (T2 =) 480, 600, 700, 800, 900, 1000, 1100, 1200 °C in programmed fashion with a heating rate of 4 °C/ min. The heating had a holding at 580 °C (T1) for 180 min. (t2) for binder removal. The samples were heated at higher temperature (T2) isothermally for 360 min. (t4) and cooled naturally (see in chapter 2 for more details about the temperature and time parameters).

3.4.1.b.3. Characterisation

The powder XRD patterns of samples sintered at different temperatures were recorded. The phases were identified and matched with the JCPDS available with the Rigaku XRD instrument. A semi-quantitative analysis of the various phases present in the samples heated at 1200 °C was carried out. The results are discussed in the following sections. Densities of all the LASy samples heated up to 1200 °C were measured and the general trend of density changes with respect to the cation concentrations were analysed, as the density variations at various temperatures are hints of the extent of densification. The shrinkage of the samples due to densification was measured and analysed.

3.4.1.c. X-ray based phase study

3.4.1.c.1. Effect of cation concentration on phase transformation

Figure 3.4.1 shows the multiple plot of the XRD profiles obtained for the samples heated at 750 °C of the 'LASy_n' (zeolite) precursors (LASy1, LASy2 and LASy3) having different cation concentrations. 'n' in the sample label

indicates the number of times of exchanges carried out with the cation Li^+ . Table 3.4.3 shows the Li loading and the residual Na present in each sample.

The phase estimations of the XRD profiles have been carried out. The simplified results of the phase identifications are given in Table 3.4.3 along with the matching JCPDS files. As per the results, it seems the overall behavior of the phase transformation is similar in all the samples. However, the major transformations occur at different temperatures for different samples. At 800 °C all the samples form amorphous matter along with silica polymorphs and alumina. One of the silica polymorphs represented here as 'silica (a)' is found to be structurally closer to keatite (SiO_2) [JCPDS-270605] and the other is a silica polymorph (represented here as) 'silica (b)' is found to be structurally closer to cristobalite (SiO_2) [JCPDS-120708]. Keatite type of SiO_2 continues to remain till the end of crystallisation where as cristobalite type of SiO_2 disappears at high temperatures.

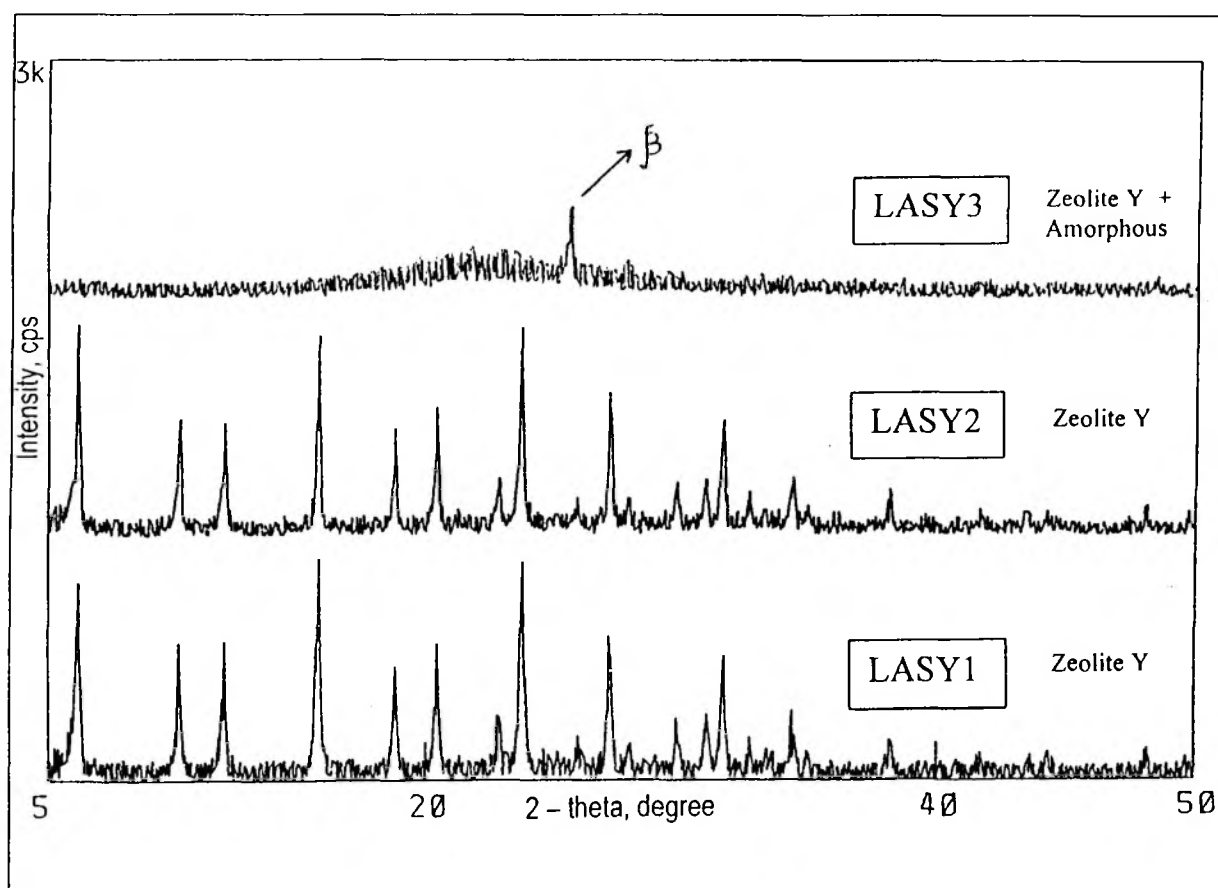


Figure 3.4.1. The XRD profiles of LAS samples with different Li^+ concentration heated at 750 °C

Table 3.4.3. Various phases identified during the sintering of the sample with different Li concentrations (JCPDS files with which the recorded XRD profile was compared, are given below)

Sample	Temperature (°C) and the phases formed					
	480	800	900	1000	1100	1200
LASY1	Zeolite Y	Zeolite Y Silica(a) Silica(b) Alumina AMORPH*	Zeolite Y Silica(a) Silica(b) Alumina Virgilite SS AMORPH*	Silica(a) Silica(b) Alumina Virgilite SS Mullite AMORPH*	Silica(a) Silica(b) Virgilite Mullite <i>β-spodumene</i>	Silica(a) Silica(b) Mullite Virgilite SS <i>β-spodumene</i>
LASY2	Zeolite Y	Zeolite Y Silica(a) Silica(b) Alumina AMORPH*	Zeolite Y Silica(a) Silica(b) Alumina Virgilite SS AMORPH*	Silica(a) Silica(b) Alumina Virgilite SS Mullite AMORPH*	Silica(a) Silica(b) Virgilite SS Mullite <i>β-spodumene</i>	Silica(a) Mullite Virgilite SS <i>β-spodumene</i>
LASY3	Zeolite Y	Zeolite Y Silica(a) Silica(b) Alumina AMORPH*	Zeolite Y Silica(a) Silica(b) Alumina Virgilite SS AMORPH*	Silica(a) Silica(b) Virgilite SS Mullite <i>β-spodumene</i>	Silica(a) Virgilite SS Mullite <i>β-spodumene</i>	Silica(a) Virgilite SS <i>β-spodumene</i> Mullite

AMORPH* - Amorphous phases

Phase	Formula	JCPDS file	Phase	Formula	JCPDS file
Silica (a)	SiO ₂	270605	Virgilite SS	Li _x Al _x Si _{3-x} O ₆	310707
Silica (b)	SiO ₂	120708	Mullite	Al ₆ Si ₂ O ₁₃	150776
Alumina	Al ₂ O ₃	100173	β -spodumene	LiAlSi ₂ O ₆	350797

In LASY1 and LASY2 the amorphous phase extends up to 1000 °C where as in LASY3, major part of it crystallises into other crystalline forms. On the other hand, the β -spodumene phase starts crystallising early, at relatively lower temperature in LASY3 (1000 °C) compared to LASY1 and LASY2. This is due to the fact that when the precursor has composition closer to the stoichiometric requirement, the phase transformation is easier and in many cases, simpler without any side products. In LASY3 the lithium content is relatively very high (1.31 wt.%), nearly more than 2.5 times than that in LASY1 (0.53 wt.%). Also, in LASY1 the trace of cristobalite (polymorph of SiO₂) is found even after 1100 °C as an impurity phase.

3.4.1.d. Density based study

3.4.1.d.1. Effect of cation concentration on density

The magnitude of densification can be realised by comparing the values of density of the green sample at room temperature and that of the sintered product at high temperature. It is known that the green density is always lower than that of the sintered density. However, the difference between the

two densities is an important factor in density based ceramic applications. In the case of pure single phase, the density is dependent only on the synthesis procedure. In contrast, for composite materials with more than one phase, the density is dependent on many variables. In the case of the present material of interest, the cation concentration in the zeolite precursor is one such variable, which directly influences both the number and amount of side products formed during the HT treatment. This is evidenced by the discussion in the earlier section. However, it is important to study the change in density as a function of cation concentration. This is due to the fact that the apparent density of the final product is the effective value of the characteristic densities of individual phases.

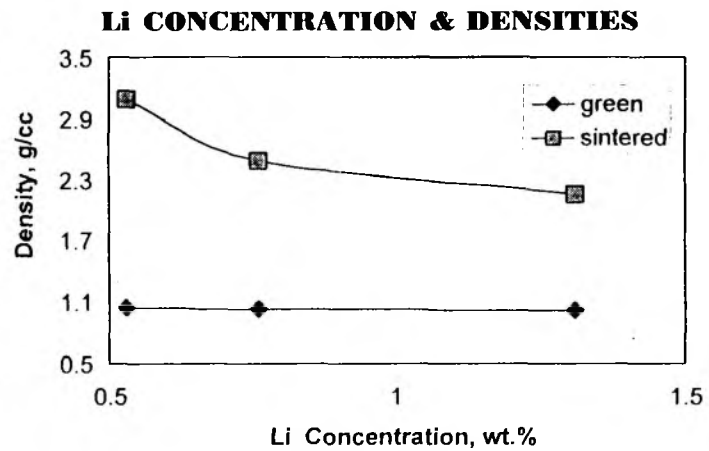


Figure 3.4.2. Influence of cation concentration on ceramic density.

Table 3.4.4. Green and sintered densities of LASY samples

Sl. no.	Sample	Li conc. wt. %	Density, g/cc	
			Green	Sintered
1	LASY1	0.53	1.0530	3.0889
2	LASY2	0.76	1.0391	2.4873
3	LASY3	1.31	1.0246	2.1566

The green and sintered densities (ρ_{app}) of the three samples LASY1, LASY2 and LASY3 (as shown in Table 3.4.4.) were measured using the procedure prescribed in chapter 2. The Figure 3.4.2 shows the graph of the densities (both green and sintered) plotted against the cation concentrations. As the precursors are from the same source, even after chemical modifications there is no significant change in green densities of the samples. The sintered density decreases from 3.0889 to 2.1566 (in gm/cc) with increasing lithium concentrations from 0.53 to 1.31 wt.%. Table 3.4.5 shows the respective HT phases formed at 1200 °C when the three different LASY samples were heated. The observed apparent density and the X-ray density of the individual phases are given.

Table 3.4.5. Phases formed and their individual densities

Sample	Phases (at 1200 °C)	Relative amounts*	ρ observed (g/cc)	Phases	ρ X-ray [#] (g/cc)
LASY1	Silica(a) Silica(b) Mullite Virgilite SS <i>β-spodumene</i>	Very low Very low Medium Low Low	3.0889	Silica(a) Silica(b) Keatite Mullite Virgilite SS	2.533 – 2.648 2.194 – 2.334 2.497 – 2.503 3.125 – 3.166 --
LASY2	Silica(a) Mullite Virgilite SS <i>β-spodumene</i>	Very low Medium Low Medium	2.4873	<i>β-spodumene</i>	2.379
LASY3	Silica(a) Virgilite SS <i>β-spodumene</i> Mullite	Very low Very low High Low	2.1566	* Very low = < 20% Low = 20-30% High = 60-80% Medium = 30-60 % Very high = > 80%	

* - relative amounts are based on the semi-quantitative estimations

- according to CRC hand book of materials, (CRC -1985)

At 1200 °C, though all the three samples yield the same phases, the relative weight fractions of the existing individual phases are very important which govern the observed apparent density of the material. The phase transformation, above 1000 °C follows through the crystallisation of β -spodumene at the expense of virgilite and mullite intermediate phases. Mullite, being the densest phase among those formed during the heating of LASY

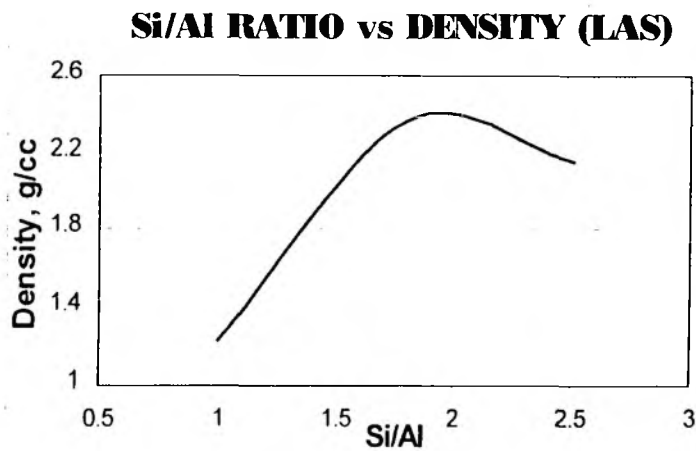


Figure 3.4.3. Influence of Si/Al ratio on density of LASY samples.

samples and having a highest X-ray density of 3.1 g/cc, the relative quantity of its presence becomes the major factor that decides the observed density of the ceramic product. At higher lithium concentrations, mullite finds relatively more Li to react with and forms β -spodumene reducing its own concentration. Hence the effective density is less. However, at low Li concentrations the mullite to β -spodumene transformation is relatively less and hence the excess mullite increases the density.

3.4.1.d.2. Effect of Si/Al ratio on density

Figure 3.4.3 shows the densities of all the three samples that are sintered under similar conditions at 1200 °C. The curve shows a maximum near Si/Al = 2 indicating that the density dependence on the Si/Al ratio is nonlinear. The highest density (2.36 g/cc) is observed around Si/Al ratio 1.80.

Table 3.4.6. Densities of LASY samples with different Si/Al ratio

Sample	Si/Al	Density, g/cc
LIA3	1.12	1.225
LIP3	1.80	2.360
LIY3	2.51	2.151

The following may be a possible reason. The major side product in this process is mullite ($Al_6Si_2O_{13}$), which has a Si/Al ratio of 0.33. The formation of this phase is dependent on the availability of Al and the excess SiO_2 available at high temperatures in the amorphous solid mixture apart from the amount of SiO_2 consumed for the LAS (virgilite or β -spodumene) phase formation. Table 3.4.6 shows the apparent densities of the samples with

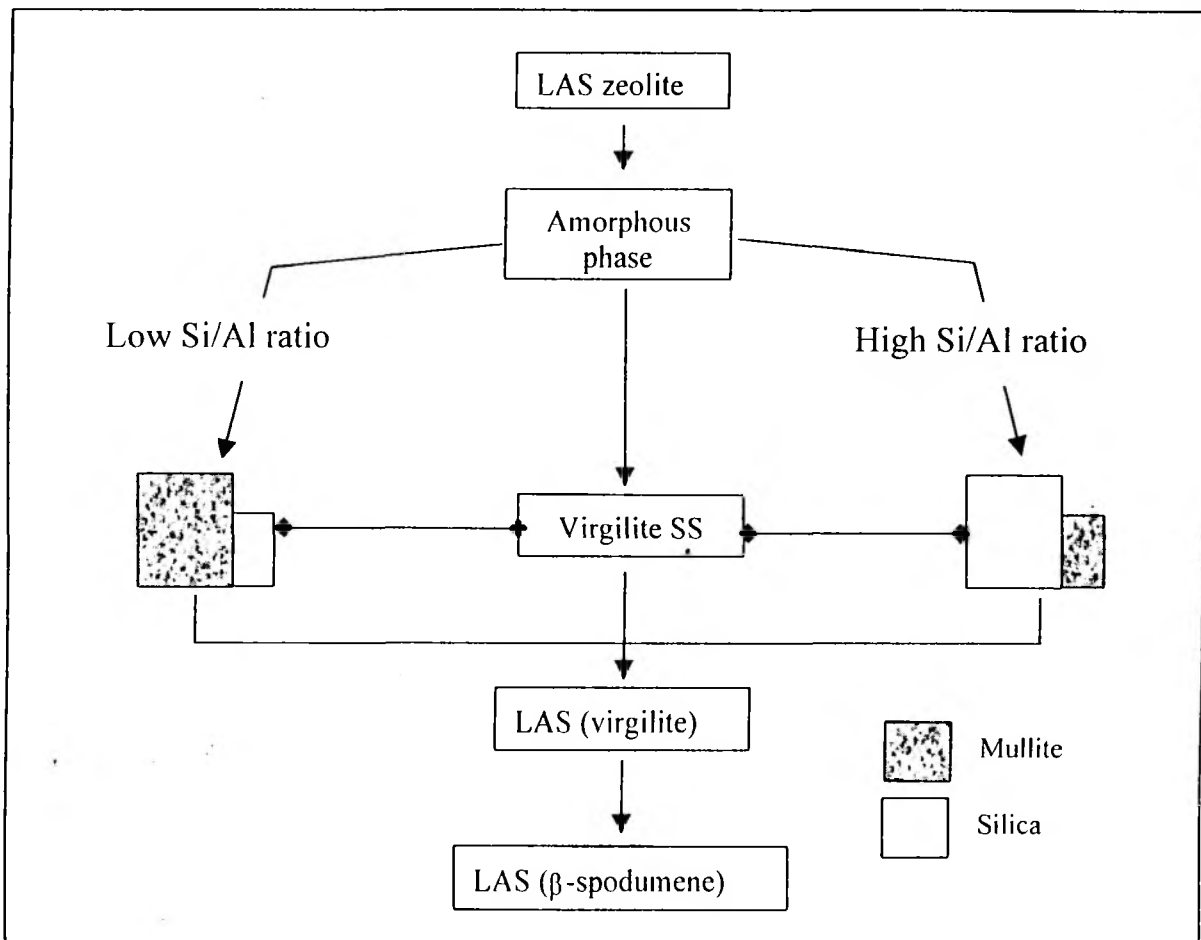


Figure 3.4.4. Schematic representation of the possible mechanistic pathways of the crystallisation of LAS ceramic phases at different Si/Al ratios. The relative magnitude of mullite and excess SiO_2 has been schematically represented.

different Si/Al ratio. Beyond 1000 °C, the sample with low Si/Al ratio (LASA3) level in precursor, has a low excess of SiO₂ compared to that of high Si/Al. This low content of excess SiO₂ reacts with the available Al₂O₃ and forms mullite. When the Si/Al ratio increases, the formation of mullite also proceeds. Hence, the overall density of the system increases as well. When the Si/Al ratio of the amorphous matter apart from the LAS phase crosses beyond 0.33, the formation of mullite stops due to the unavailability of Al₂O₃ leaving excess of relatively low density SiO₂ in the system. Hence the silica, which has a lower density, starts crystallising into its respective polymorph thermodynamically possible at that temperature. This leads to the termination of increase in density and the consecutive decrease. On the basis of the phases identified and estimated semi-quantitatively, the pathway of the phase transformation at different situations of varying Si/Al ratios may be proposed as given in the schematic diagram. Figure 3.4.4 shows the most possible mechanistic pathway.

3.4.1.e. Shrinkage based study

Kodama of Hitachi Ltd., has exclusively studied the impact of unidirectional shrinkage during sintering to fabricate ceramic packaging substrates which meet requirements of very low dimensional tolerances (high dimensional accuracy)⁴⁴. As present LAS material has a potential scope in the same application, it would be more important to have coverage on this aspect. Unidirectional (or linear) shrinkage is unique in those systems where in there is an orientation of crystal growth during the process of crystallisation. Unlike volumetric (three-dimensional) shrinkage, unidirectional changes may be measured to understand the influence of orientation effects due to their nature including the particle size of the precursor powder, their crystal structure and the sintering history.

Bruneton has studied the influence of heterogeneity that comes firstly from the use of different reagents as gel formers (Si and Al alkoxides) or of a mixed nature (Si-Al ester) and secondly from the hydrolysis-polycondensation route on the shrinkage and expansion of sol-gel based ceramic production⁴⁵. However, the present study on the shrinkage of zeolite based precursors for the ceramic sintering has been attempted for the first time. Particularly, in zeolite based ceramic preparation, where densification process includes a phase transformation or/and crystallisation from an amorphous intermediate phase, the study on unidirectional shrinkage is very important as the anisotropic shrinkage can be well influenced by typical stoichiometric conditions. The current investigation is to study the change in unidirectional shrinkage as a function of the precursor chemical composition. The study has been carried out with different Li concentrations and different Si/Al ratios as described below.

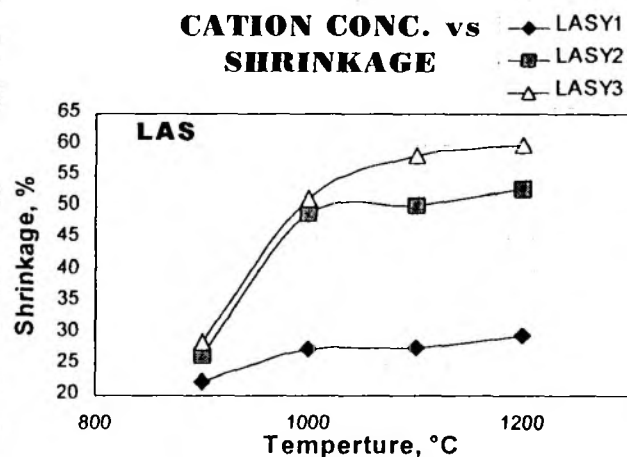


Figure 3.4.5. The influence of cation concentration on Shrinkage of LAS samples.

3.4.1.e.1. Influence of cation concentration on shrinkage

Figure 3.4.5. shows the shrinkage observed for the samples LASY1, LASY2 and LASY3. The cation concentration has a tremendous influence on the shrinkage of the LAS materials. The three samples have a similar shrinkage without significant changes at lower temperature 900 °C. At 1200 °C LASY1 reaches a minimum shrinkage of 29.58 %, where as LASY3 exhibits a shrinkage of 60.07%. This is due to the fact that at high Li concentrations the formation of β -spodumene is enhanced as explained earlier, which forms a major single phase (by estimation, more than 70 %). When less quantity of impurity phases are present, it is always expected that bulk homogeneity in crystal packing and in lattice ordering of atoms is better. Thus the pores and defects are usually reduced leading to a high shrinkage. As per the application point of view in MEP technology, minimum shrinkage is usually desirable. Hence, one must think about reduction of excess shrinkage without

losing the high phase purity and apparent density. Recent report from NASA suggests that the change in atmospheres at which the sintering occurs effectively influence the shrinkage strains⁴⁶.

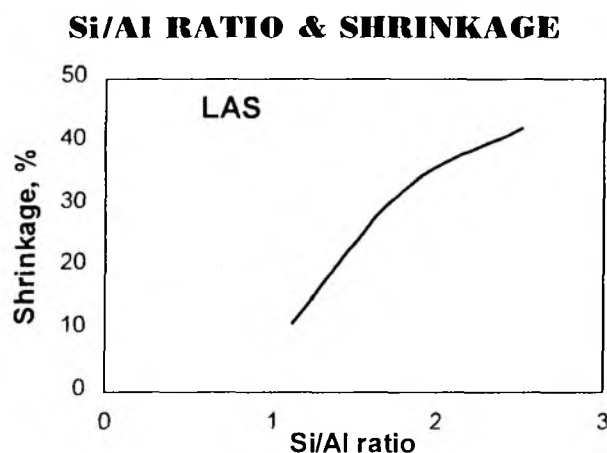


Figure 3.4.6. Influence of Si/Al ratio on the shrinkage of LAS samples

3.4.1.e.2. Influence of Si/Al ratio on shrinkage

Figure 3.4.6. shows the shrinkage observed for the samples LASY1, LASY2 and LASY3. The cation concentration has a strong influence on the shrinkage of the LAS materials. The shrinkage increases as the Si/Al ratio increases from 1.12 to

2.51. Table 3.4.7. shows the % shrinkage observed for the three different LAS samples with different Si/Al ratios. LASA3, LASP3 and LASY3 are the samples prepared by the Li exchange (3 times) of Na in A, P and Y zeolites respectively having different Si/Al ratios (refer Table 3.4.7.). LASY3 has the highest shrinkage of 42.01 %. This may be due to the fact that the sintering is enhanced by the presence of excess SiO₂ as it converts itself into denser SiO₂ polymorph cristobalite compared to other polymorphs of SiO₂ possible at that temperature.

Table 3.4.7. Influence of Si/Al ratio on shrinkage

Sample	Si/Al	Shrinkage %
LASA3	1.12	10.922
LASP3	1.80	32.138
LASY3	2.51	42.014

3.4.2. EFFECT OF SINTERING ATMOSPHERE

3.4.2.a. Plan of work

It was planned to change the sintering atmosphere of LAS samples to study the effect of atmosphere during sintering. The major possible changes are the availability of atmospheric oxygen during oxidative air atmosphere and the oxygen deficient argon atmosphere. This is basically to study by XRD whether the atmospheric oxygen involves in the phase transformation or not and if so how much.

3.4.2.b. Experimental

As described in chapter 2 the HT solid state phase transformation reactions were performed in programmable furnace. The reactor setup has been described with schematic figure in chapter 2. Pellets of LASA3, LASP3 and LASY3 were sintered both in oxidative air atmosphere and in reducing argon (INOX) atmosphere. The gas flow was controlled by a mass flow controller with a flow rate of 40 ml per minute. A detailed procedure is given in chapter 2. The pellets were heated with a heating rate of 4 °C/min and sintered at 1200 °C for 6 h. followed by a natural cooling to RT. They were crushed into powders and were characterised by XRD and the phases formed were identified.

3.4.2.c. Results and discussion

Figure 3.4.7. shows the multiple plots of the XRD profiles obtained for the samples LASA3 (a) and LASY3 (b) heated in both air and argon atmospheres. The various phases formed along with their semi-quantitative estimations during the course of sintering of different LAS samples at 1200 °C both in oxidative air and reductive argon atmosphere are given in Table 3.4.8. In oxidative atmosphere, generally, from the observations it is clear that the oxygen uptake at high temperatures leads to various oxides of Si and Al individually or together, which hinders the formation of β -spodumene. In case of low Si/Al ratio zeolite sources like LASA3 and LASP3, due to presence of relatively higher aluminum content, there is formation of alumina (JCPDS 100173) phases at 1200 °C. However, there is a distinct increase in the formation of β -spodumene phase, which is very attractive as per the phase purity, is concerned. However, as discussed earlier the density of these materials are relatively low. In reductive argon atmosphere, the general observation is that the number and quantity of the side products formed are less. For instance, the formation of multiple polymorphs of silica is restricted and only one polymorph of SiO_2 (JCPDS 270605) is formed. It is very interesting to see at low Si/Al ratio samples like LASA3 and LASP3, there is no silica formation. They have only mullite and β -spodumene* phase (JCPDS 350794). This is close to the composition of the phase, $\text{LiAlSi}_3\text{O}_8$. Also the main and very interesting result is that the precursor LASY3 has formed a single phase, β -spodumene* (refer Figure 3.4.8.). This proves that with proper fine-tuning of the chemical composition of the zeolite precursor and with an optimised heating conditions, high purity single-phase ceramics can be prepared using zeolite as precursors without undesired side products.

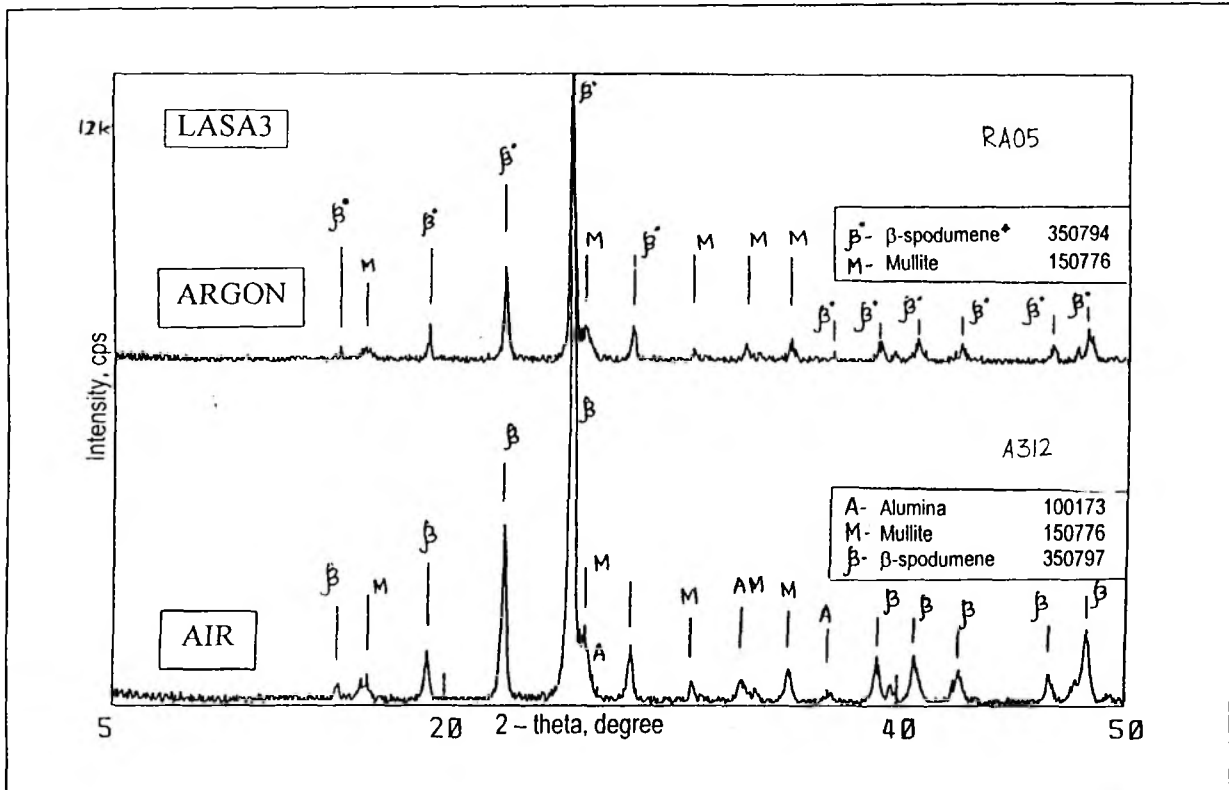


Figure 3.4.7.a. XRD patterns obtained for the LASA3 samples sintered in argon atmosphere.

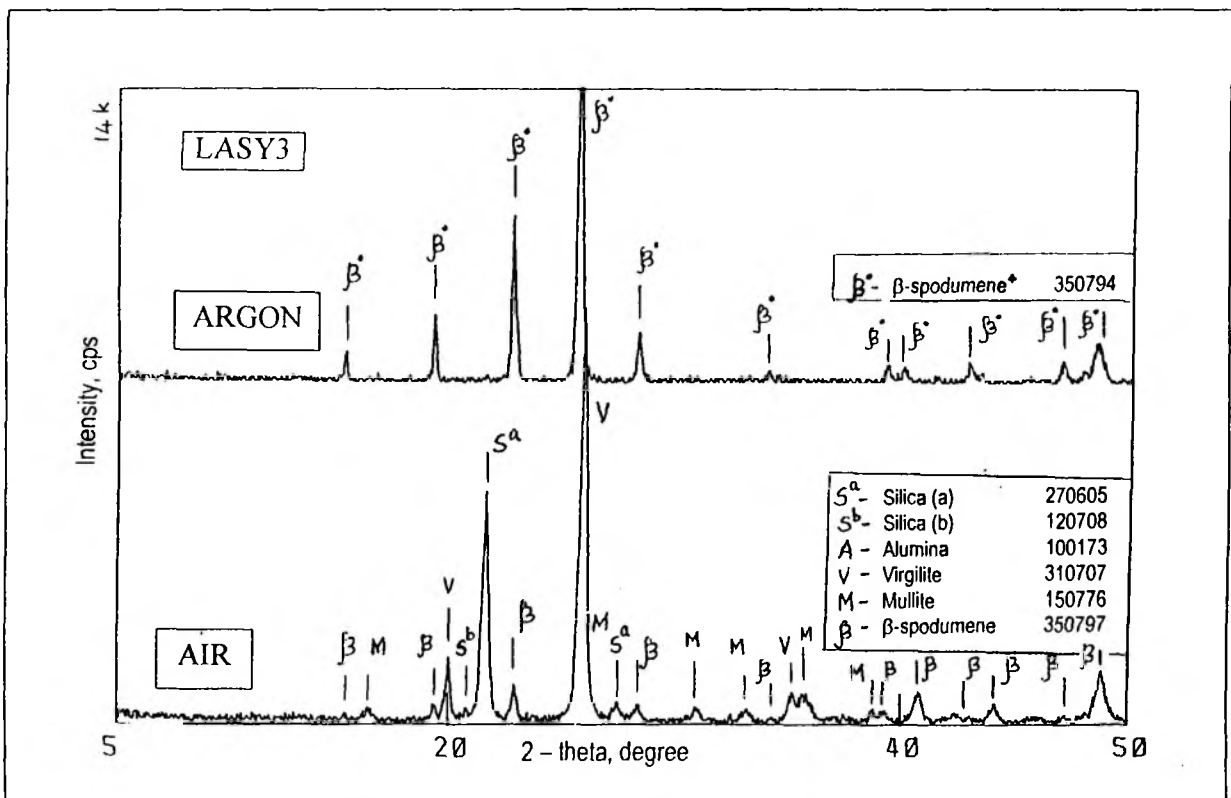


Figure 3.4.7.b. XRD patterns obtained for the LASY3 samples sintered in argon atmosphere.

Table 3.4.8. The semi-quantitative analysis of various phases formed during the different sintering of LAS samples in different atmospheres.

Sample	Zeolite source	In air (oxidative)		In argon (reductive)	
		Phase	Estimation, %	Phase	Estimation, %
LASY3	Y	Silica (a)	01.1	β -spodumene ⁺ (single phase)	100.00
		Mullite	21.2		
		Virgilite SS	07.4		
		β -spodumene	70.3		
LASY2	Y	Silica(a)	03.8	Silica (a)	01.8
		Mullite	31.0	Mullite	05.2
		Virgilite SS	21.4	Virgilite SS	93.0
		β -spodumene	43.8		
LASY1	Y	Silica (a)	04.2	Silica (a)	04.3
		Silica(b)	01.7	Mullite	03.3
		Mullite	34.7	Virgilite SS	92.4
		Virgilite SS	29.4		
		β -spodumene	30.0		
LIP3	P	Silica (a)	01.1	β -spodumene ⁺	96.2
		Mullite	03.6	Mullite	03.8
		β -spodumene	95.3		
LIA3	A	Alumina	01.9	β -spodumene ⁺	98.1
		Mullite	04.3	Mullite	01.9
		β -spodumene	93.8		

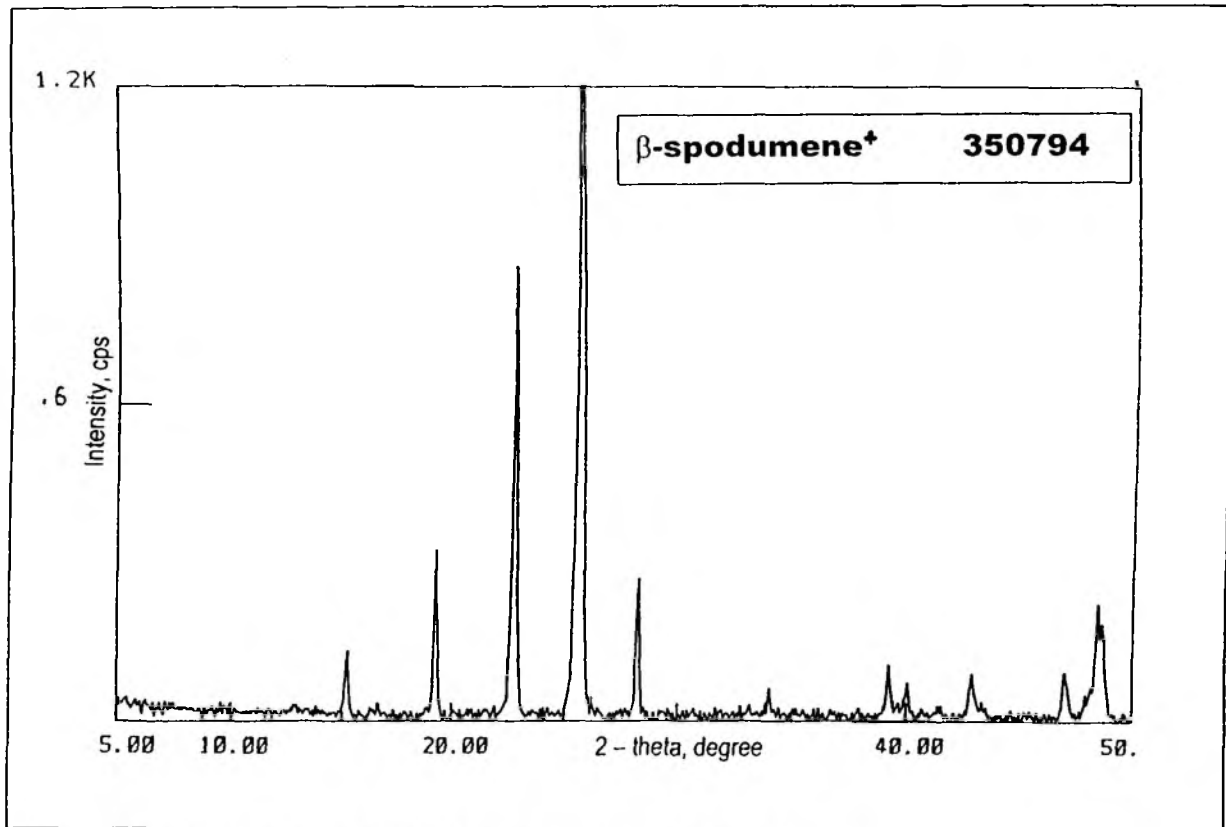


Figure 3.4.8. The XRD pattern of LASY3 with β -spodumene as single phase

3.4.3. PROBABLE PHASE TRANSFORMATION MECHANISM

The chemical compositional variation studies in the zeolite based LAS precursors which are discussed in the later part of this chapter prove that with fine tuned chemical composition and an optimised heat treatment it is possible to produce highly pure lithium aluminosilicate ceramics without impurity phases. However, the understanding of an overall pathway of the phase transformation seems to be somewhat tougher as there are many crystalline and amorphous phases involved in the entire transformation process.

According to available literatures, the oxide based or alkoxide based LAS precursors usually transform into a high-quartz (HQ) structure, which then transforms to β -spodumene or β -spodumene⁺ (refer appendix) through keatite phase that is structurally close to β -spodumene^{47,48}. Astrid proposes the pathway of β -quartz to β -spodumene in the presence of N₂, which stabilises the quartz phase up to 1200 °C⁴⁹. On the basis of this literature information and also according to the present observations by XRD and multinuclear MAS NMR studies, it is viable to propose a most possible phase transformation pathway of the zeolite based ceramic preparation as given below.

In present zeolite based ceramic preparations, it is observed that the crystalline zeolite precursor collapses at moderately high temperatures (in the range of 800 to 900 °C) and forms an amorphous phase. Figure 3.4.9.

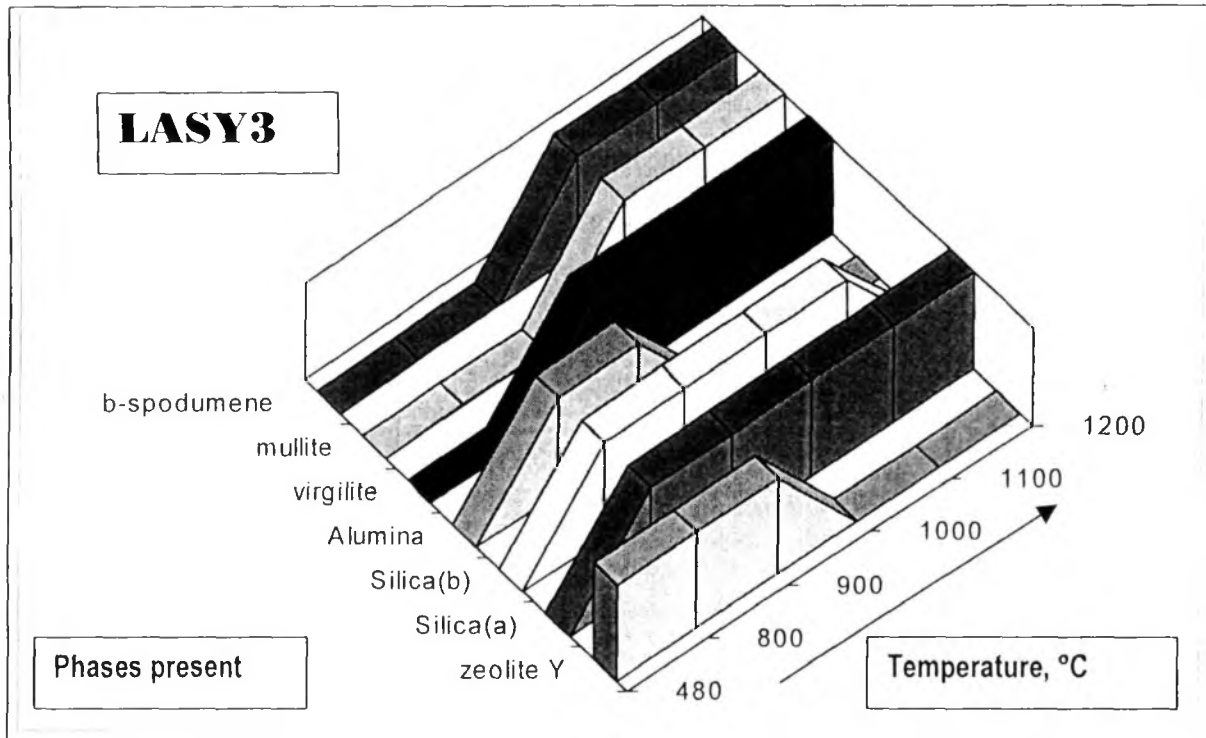


Figure 3.4.9. Existences of various crystalline phases present at different temperatures from 480 to 1200 °C.

shows the existences of various crystalline phases during the heat treatment of the sample LASY3 (excluding the amorphous glassy phase). This contains partially or fully crystallised silica polymorphs (JCPDS 270605 and 120708). Consequently, the polymorphs of SiO₂ like meta-stable high quartz (HQ) and cristobalite are formed. Above 900 °C, depending on the Al content in the precursor, these polymorphs along with Al, form mullite (JCPDS 150776). If the Al content is considerably high, in oxidising atmosphere, alumina (JCPDS 100173) is also formed along with mullite.

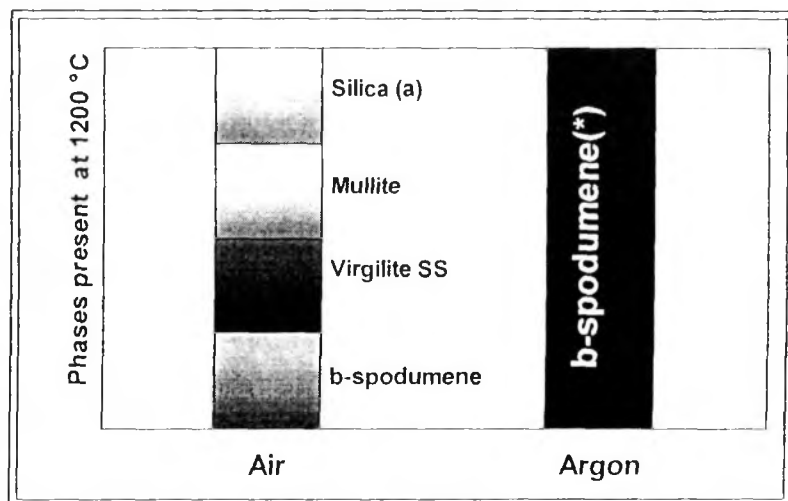


Figure 3.4.10. Single phase production at reductive atmosphere ('β' has been represented as 'b')

Above 1000 °C, during the second part of the transformation from HQ to LAS ceramics (β-spodumene or β-spodumene*), there is an intermediate phase namely virgilite SS (JCPDS 310707). This is a solid solution and is observed in between HQ and β-

spodumene (JCPDS 350797) or β -spodumene* (JCPDS 350794). This intermediate phase has a chemical composition of $\text{Li}_x\text{Al}_x\text{Si}_{3-x}\text{O}_6$, (where x takes wide range of values from 0 to 1). As the temperature increases, the Li and Al atoms move into the interstices positions of the SiO_2 based keatite framework and hence the x increases from zero to one ($x = 0 \rightarrow 1$). When ' x ' tends to become 1, the stoichiometrically balanced β -spodumene ($\text{LiAlSi}_2\text{O}_6$, $x=1$) (JCPDS 350797) is formed. The advantage of reducing atmospheric change has been depicted schematically in Figure 3.4.10. The phase or β -spodumene* (JCPDS 350794) has been represented as b-spodumene*).

3.5. CONCLUSIONS

The widely used electronic LAS ceramic phase, β -spodumene has been successfully prepared using zeolite as a precursor and both the precursor and the ceramic have been characterised using various physico-chemical techniques. Techniques like multinuclear MAS NMR and approaches like density and shrinkage based composition variation studies are novel to the zeolite based LAS ceramic systems and have revealed interesting results. They have given better understanding about the phase transformation phenomena at higher temperatures in the ceramic preparation using zeolites as precursors. The results from TG and XRD studies together show that the structure collapse and the recrystallisation of the dense ceramic phases occur at the temperatures less than 950 °C, giving a straight proof for better chances of low temperature processability through this novel ceramic preparation route. The SEM studies show that the ceramic particle size growth though is uncontrolled primarily, a narrow particle size distribution with a range as small as of 3-5 μm is observed at higher temperatures of 1200 °C. The crystal symmetry and lattice parameters of the dense ceramic phase, β -spodumene were determined and were found to be matching with that of the literature values.

XRD studies on the phase formation of the ceramic dense phase shows that the phase formation from the amorphous state is through a meta-phasic silica polymorph namely keatite. On further heating, Al substitutions in the Si positions of keatite, changes this to virgilite, a LAS pro-phase to β -spodumene. Stoichiometry of the system through out the thermal treatment shows that it is intact till final temperature at 1200 °C though there is a minute loss of volatile lithium after 1000 °C.

Dielectric constants of LAS ceramic compositions prepared using zeolites as precursors are relatively lower than that of the materials that are being widely used for the MEP applications and hence these are suited better. This material shows a relative density of above 90%, which is an encouraging result to understand the extent of sintering. A single step shrinkage by TMA measurements with a maximum densification temperature (T_{Dmax}) around 919 °C shows a linear shrinkage around 35 %. Thermal expansion studies show that these ceramic materials are low expansion materials, which have a wide scope and demand in the high temperature ceramic application. The TEC of the ceramic is found to be matching with that of silicon, which is one of the important prerequisites for MEP applications. The thermal dependence of the TEC of these materials gives new directions on further studies.

Multinuclear NMR studies on different stages of the formation of β -spodumene ceramic phase from zeolite precursors have given a better understanding of the process. The appearance of the bands corresponding to the tectosilicate ranges (from -107 to -112 ppm) in ^{29}Si NMR spectra shows the phase predomination of several silica polymorphs at the temperature range of 900 - 1000 °C. One of the observations by XRD, the co-existence of glassy silica and crystalline mullite mixture has been supported by the results of ^{29}Si NMR studies. The changes in the environment of Al during the course of phase formation has been understood by sorting out the broad band in ^{27}Al NMR spectra, as a distribution of tetrahedral (M1), octahedral (M2) and distorted tetrahedral (A1*) environments. The loss of powder pattern features, which are normally observed at these temperatures in ^7Li quadrupole NMR studies, shows the possible lack of crystallinity and phase purity and the dipolar interaction between the Li and Al atoms due to the 1:1 population of Li:Al in the ceramic phases. However, it is understood that better resolved NMR patterns with high spinning speeds may provide more information.

Series of variation studies were effectively carried out to study the effect of variations in the precursor stoichiometry on the sintering processes, the phases, density and the shrinkage of the ceramic formed. Effect of cation concentration has proved that Li concentration is indirectly proportional to the temperature at which the dense phase is formed. The density of the ceramic material increases with the Si/Al ratio to certain extent and reduces on further increase in Si/Al ratio. This is due to control on the formation of mullite, which is the major factor that decides the apparent density of the ceramic composite.

Shrinkage is higher for the sample having high Li concentration. Though this difference is less pronounced in lower temperatures viz., 900 °C, at higher temperature, viz., 1200 °C, shrinkage difference is observed to be as large as 30%. High Si/Al ratio leads to high shrinkage because of the higher formation of dense silica and mullite phases.

A study on the effect of sintering atmosphere has proved that in reductive atmosphere the number and quantity of side products are effectively reduced. LASY3 has crystallised into a single LAS ceramic phase. This shows that single phases can be aimed by fine-tuning the stoichiometry and sintering conditions. Usually undesired side products have been frequent problems in many such preparations. After a rational watch on the phases formed for various samples of different chemical compositions, a most probable phase transfer mechanism has been proposed.

"... The scientist does not study nature because it is useful to do so. He studies it because he takes pleasure in it, and he takes pleasure in it because it is beautiful"

- Poincaré

REFERENCES

1. Selvaraj, K.; Ramaswamy, V.; Ramaswamy, A. V.; *Asian J. Phys.*, 6, 132 (1997)
2. Selvaraj, K.; Ramaswamy, V.; Ramaswamy, A. V.; "Preparation of...characterization", *paper presented in National symposium on electroceramics*, 13th – 15th March 1996, Rajkot, INDIA
3. Selvaraj, K.; Ramaswamy, V.; Ramaswamy, A. V.; *Materials Research Society*, Proc. 12th Int. Zeolite Conf., 3, 2033 (1999)
4. Casey, J. A.; DeCarr, S. M.; *U.S. patent*, 4, US 5264399 A 23 (1993)
5. Yu, B. L.; Dyer, A.; Enamy, H.; *Thermochim. Acta*, 200, 299 (1992)
- 5a. Ruedinger, B.; Fischer, R. X.; *Stud. Surf. Sci. Catal.*, 98 (Zeolite Science 1994: Recent Progress and Discussions), 283 (1995)
- 5b. Evans, D. L.; *Acta Cryst.*, A25, S 234 (1969)
- 5c. Li, C. T.; *Acta Cryst.*, B27, 1132 (1971)
6. Parise, J. B.; Carbin, D. R.; Subramanian, M.A.; *Mat. Res. Bull.*, 24, 303 (1989)
7. Martin, B.; *Eur. J. Min.*, 7(6), 1389 (1995)
8. Shropshire, J.; Keat, P. P., Vaughan, P. A.; *Z Kristallogr.*, 112, 409 (1959)
9. Osterag, W.; Fischer G. R.; Williams J. P.; *J. Am. Ceram. Soc.*, 51, 651 (1968)
10. Parise, J. B.; Corbin, D. R.; Subramanian, M. A.; *Mat. Res. Bull.*, 24, 303 (1989)
11. Li, T.; *Taoci Zazhi*, 6, 17, (1993)
12. Touloukian, Y.S.; Kirby R. K.; Taylor, R. E.; Desai, P. D.; *Thermal expansion properties - metallic Elemental and Alloys*, 12, The TPRC Data Series, Plenum publishing corporation, NY, USA (1975)
13. Choi, D. M.; You, J. K.; Lee, E. S.; *Yoop Hakhoechi*, 30(5), 381 (1993)
14. Park, J. H.; Kim, H. M.; Lee, H. S.; *Yoop Hakhoechi*, 29(7), 533 (1992)
15. Kingery, W. D.; *Introduction to Ceramics*, 1st edition, pp 591, John Wiley, NY, USA, (1976)
16. Srivastava, S. P.; *J. Phys. Chem. Solids*, 39(10), 1143 (1978)
17. Shcherban, N. I.; *Elektron. Stroenie i Fiz.-khim. Svoistva Splavov i Soedinenii na Osnove Perekhodn. Met.*, 99-103 From: Ref. Zh., Metall. 1977, Abstr. No. 51307(1976)
18. Remenyuk, P. I.; Rarenko, I. M.; Polyak, M. I.; *Ukr. Fiz. Zh.*, 25(8), 1389 (1980)
19. Pozdeeva, E. V.; Avericheva, V. E.; Guzeev, M. N.; Deposited Doc., VINITI 1564-75, 8 pp. Avail. BLLD (1975)
20. Varotsos, P.; Alexopoulos, K.; *Phys. Rev. B: Condens. Matter.*, 21(8), 3379 (1980)
21. Asai, T.; Kawai, S.; *Seramikkusu*, 20(7), 610 (1985)
22. Klinowski, J.; Thomas, J. M.; Thompson, D. P.; Korgul, P.; Jack, K. H.; Fyfe, C. A.; Gobbi, G. C.; *Polyhedron*, 3(11), 1267 (1984)
23. Timken, Hye Kyung. C.; Oldfield, E.; *J. Am. Chem. Soc.*, 109(25), 7669 (1987)
24. Engelhardt, G.; *Trends Anal. Chem.*, (Pers. Ed.), 8(9), 343 (1989)
25. Jancke, H.; Unger, B.; Muller, R.; *Fresenius' J. Anal. Chem.*, 357(5), 514, (1997)
26. Engelhardt, G.; Michel, D.; *High-Resolution solid state NMR of silicates and zeolites*, Wiley & Sons, Norwich (1987)
27. Janes, N.; Oldfield, E.; *J. Am. Chem. Soc.*, 107, 6769 (1985)
28. Magi, M.; Lippma, A.; Samoson, G.; Engelhardt, G.; Grimmer, A. R.; *J. Phys. Chem.*, 88, 1518 (1984)
29. Turner, G.L.; Kirkpatrick, R. J.; Risbud, S. H.; Oldfield, E.; *Am. Ceram. Soc. Bull.*, 66 (4) 656 (1987)
30. Turner, G. L.; Kirkpatrick, R. J.; Risbud, S. H.; Oldfield, E.; *Am. Ceram. Soc. Bull.*, 66(4), 656 (1987)
31. Subramanian, M. A.; Corbin, D. R.; Farlee, R. D.; *Mater. Res. Bull.*, 21(12), 1525 (1986)
32. Klinowski, J.; Thomas, J. M.; Fyfe, C. A.; Gobbi G.C.; *Nature*, 8, 296, (1982)
33. Muller, W.G.; Behrens, J.S.; Scheler, G.; *Chem. Phys. Lett.*, 79(1) 59 (1981)
34. Fyfe, C.A.; Thomas, J.M.; Klinowski, J.; and Gobbi, G.C.; *Angew. Chem Int. Ed Engl.*, 22(4) 259 (1983)
35. Merwin, L. H.; Sebald, A.; Rager, H.; Schneider, H.; *Phys. Chem. Miner.*, 18(1), 47 (1991)
36. Ramanathan, C; Ackerman, J. L.; *Magn. Reson. Med.*, 41(6), 1214 (1999)
37. Gunay, E.; Redington, M.; Hampshire, S.; *Key Eng. Mater.*, 89-91(Silicon Nitride 93), 387 (1994)
38. Hsu, Jen Yan.; Wu, Nan Chung.; Yu, Shu Cheng.; *J. Am. Ceram. Soc.*, 72(10), 1861-7 (1989)
39. Vasil'ev, G. S.; Sulimenko, E. I.; *Metall. Koksochim.*, 95, 8 (1988)
40. Sakir, N. F.; Yusfin, Yu. S.; Chernousov, P. I.; Galkin, V. I.; Urbanovich, G. I.; *Stal.*, (10), 11 (1987)
41. Yoon, Ki Hyun.; Shin, Hyun Min.; Kang, Dong Hean.; *Mater. Sci. Monogr.*, 66C, 2029 (1991)
42. Iga, Takeo.; *Nagoya Kogyo Gijutsu Kenkyusho Hokoku*, 43(1), 69, (1994)

43. Son, Y B.; Kim, C H.; Jang, S. D.; Liu, J.; Sarikaya, M.; Aksay, I. A.; *Jpn. J. Appl. Phys., Part 1*, 33(2), 1101 (1994)
44. Kodama, Hironori.; *Mater. Res. Soc. Symp. Proc.*, 264(Electronic Packaging Materials Science VI), 117 (1992)
45. Bruneton, E.; Bigarre, J.; Michel, D.; Colombari, Ph.; *J. Mater. Sci.*, 32(13), 3541 (1997)
46. Zhu, Dongming.; Miller, Robert A.; *Surf. Coat. Technol.*, 108-109 (1-3), 114 (1998)
47. Yang J.S.; Sakka S.; Yoko T.; Kozuka H.; *J. Mater. Sci.*, 26 [7] 1827 (1991)
48. Shyu J.J.; Lee H.H.; *J. Am. Ceram. Soc.*, 58 [5-6] 163 (1975)
49. Astrid N.; Yi-Bing C.; *J. Am. Ceram. Soc.*, 80 [12] 3045 (1997)

THE CORDIERITE (MAS systems)

Chapter

4

PART A. GENERAL STUDIES

4.1. CERAMIC PREPARATION AND CHARACTERISATION

4.1.1. INTRODUCTION

This chapter will discuss another important system viz., **Magnesium Aluminosilicates**, $\text{MgO-Al}_2\text{O}_3\text{-SiO}_2$ systems (MASs). This includes the preparation of MAS phases and in specific, the cordierite ($2\text{MgO}\cdot 2\text{Al}_2\text{O}_3\cdot 5\text{SiO}_2$) phase from zeolite precursors by heat treatment at various temperatures ranging from 480 °C to 1350 °C. The process of sintering was studied using various characterisation techniques. Thermal expansion and shrinkage studies, density measurements were carried out to understand the properties of material. This part of the work has recently been published¹. In addition, AC impedance spectroscopy has been used as a special technique to study the dependence of impedance on working temperature of cordierite ceramics. AC impedance spectroscopy has emerged as an efficient tool to study the microstructure of ceramics. AC impedance study on the sintered cordierite (magnesium aluminosilicate) ceramic phase prepared using zeolite precursors is a novel study, which is of great interest and scope. The electronic properties of the ceramic products are basically dependent on their microstructure. The effect of cation concentration and Si/Al ratio on the sintering behaviour, shrinkage and sintered density were studied and reported for the first time on cordierite ceramics prepared using zeolites as precursors. The major intermediate phases and byproducts that are formed during the heat treatments have also been discussed.

4.1.1.a. The importance of $\text{MgO-Al}_2\text{O}_3\text{-SiO}_2$ (MAS) systems

This ternary system is important in understanding the behaviour of a number of ceramic compositions that falls into this class. This system is composed of several binary compounds individually together with two ternary compounds, cordierite, $2\text{MgO}\cdot 2\text{Al}_2\text{O}_3\cdot 5\text{SiO}_2$ and sapphirine, $4\text{MgO}\cdot 5\text{Al}_2\text{O}_3\cdot 2\text{SiO}_2$, both of which melt congruently. Figure 4.1.1 shows the common compositions in the ternary system $\text{MgO-Al}_2\text{O}_3\text{-SiO}_2$. Ceramic compositions that in large part appear on this diagram include magnesite refractories, forsterite ceramics, steatite ceramics, and cordierite ceramics. $\text{MgO-Al}_2\text{O}_3\text{-SiO}_2$ system forms glass-ceramic materials having high electrical resistivity and high mechanical strength. The high strength has been associated with the presence of crystalline β -cordierite. The compositions of some useful glass-ceramic materials in this system cover a range of MgO, Al_2O_3 , SiO_2 and TiO_2 . TiO_2 is added mostly during the crystallisation of these systems as an efficient nucleating agent (sometimes ZrO_2 also).



Cordierite ceramics are particularly useful since they have a very low coefficient of thermal expansion (TEC) and a good resistance to thermal shock. Cordierite, unlike β -spodumene, has been studied extensively due to its application in many different areas from structural to electronic application. Usually these ceramics are formed around 1350 °C. Amongst the available synthesis routes for cordierite ceramic, sol-gel has been unique in its exceptional advantages by means of the phase purity and improved material properties^{2,3}. However, due to its

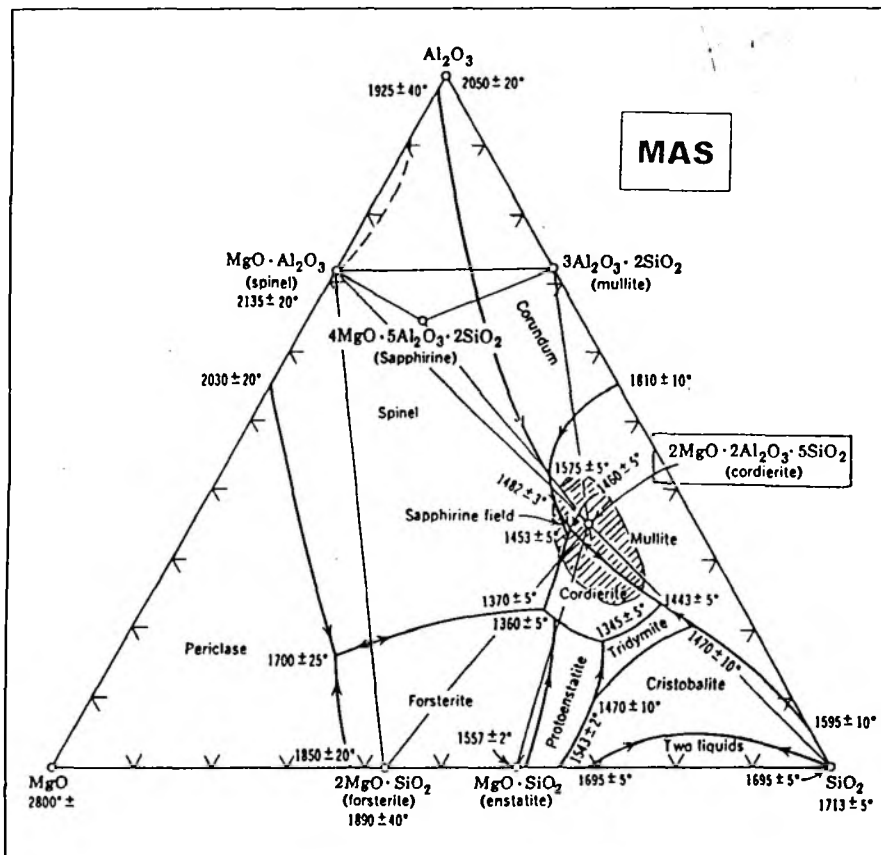


Figure 4.1.1. Phase diagram - Common compositions in MAS ternary system $MgO-Al_2O_3-SiO_2$. (from Kingery, W. D., Introduction to ceramics, Wiley Publications 1976, p 308)

failure in cost effectiveness, there has been a need for an alternative route. A serious problem in many routes for cordierite preparation is the low bulk density of the sintered bodies. There are many recent reports on this aspect of improving the bulk density of cordierite ceramic materials^{4,5}.

High-density cordierite honeycombs with high thermal shock resistance are the promising candidates in the replacement of conventional catalyst supports for catalytic converter applications.

These ceramics are in high demand to meet the environmental problems today. Business Communications Co Inc (BCC) notes that ceramics used in chemical processing and environmental-related applications represent a strong market. This sector constituted a value of \$1.26 bn in 1996 and is projected to increase to \$1.65 bn in 2001, reflecting an average annual growth rate (AAGR) of 5.6%. Growth will be anchored by heavy demand for ceramic catalysts and catalyst support in the chemical industry and automobiles⁶.

4.1.1.b. The cordierite and its other phases – A mineralogical background

The name 'Cordierite' is originally used after the French mineralogist, P.L.A. Cordier (1777-1861) for a magnesium aluminosilicate mineral called iolite or dichroite. Different cordierite phases exist at various temperature ranges depending on their thermodynamic stability. Few of them that are often encountered in many

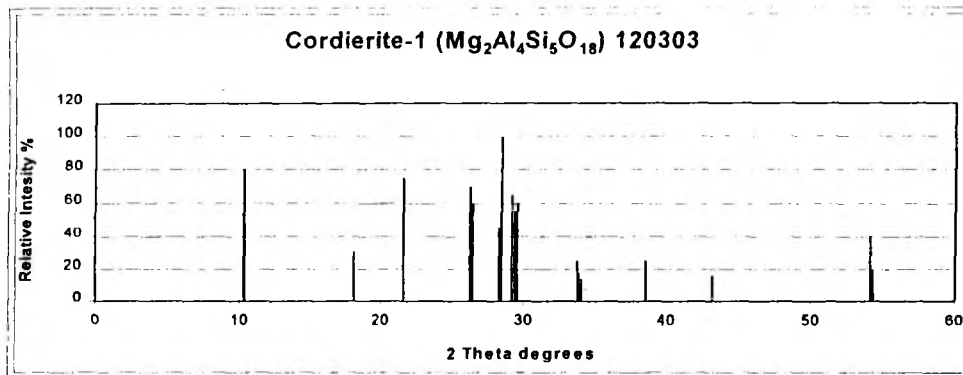


Figure 4.1.2. XRD profile of cordierite from standard JCPDS data.

cordierite synthesis processes are μ -cordierite, β -cordierite and α -cordierite. β to α Conversion occurs at high temperatures near to incongruent melting (>1350 °C).

μ -cordierite forms in some cases during the devitrification of cordierite type glass below 1000 °C. However, the β -form is generally referred to as 'cordierite' and hereafter it will be followed in the same way in this thesis. This phase is formed usually above 1300 °C on heating magnesium aluminosilicate (MAS) precursor of comparable stoichiometry. Figure 4.1.2. shows the computer generated XRD profile of cordierite with in the 2-theta range of 0 – 60 degrees.

The typical formula of this phase is Mg₂Al₄Si₅O₁₈. Conventionally cordierite is prepared by heating the stoichiometrically mixed oxides of Si, Al and Mg at high temperatures. Though cordierite was identified later to have potential scope for technical ceramic applications, still there are technical constraints for such preparations. However, the present investigation deals with the recent novel route namely zeolites to ceramics.

4.2. EXPERIMENTAL

4.2.1. PLAN OF WORK

Similar to β -spodumene, cordierite ceramics are also attractive for their various material properties, which can be altered by the preparation routes and the sintering conditions. The present study includes the preparation of cordierite ceramic phases using ion exchanged zeolite precursors and the characterisation of both precursor powder and the ceramic product after high temperature treatment using various techniques.

4.2.2. PREPARATION OF CORDIERITE

4.2.2.a. The MAS precursor powder preparation

Zeolite (Na-)Y is used for the preparation of precursor for general studies. Around 100 g of zeolite Y was exchanged three times ($N_x = 3$) with 1 M solution of ammonium nitrate salt to get the ammonium form of zeolite Y which was again exchanged three times with 1 M solution of magnesium nitrate salt. The ion exchanges were carried out as per the procedure given in chapter 2, section 2.1.2.a. Finally, the dry fine powder was labeled as MASY3 (meaning Magnesium AluminoSilicate prepared from Y zeolite by 3 exchanges of 1 M Mg nitrate solution) and was used for consolidation and for the further studies.

4.2.2.b. Powder characterisation

MASY3 powder was characterised using TG/DTA and XRD techniques for its thermal and structural properties respectively. Nearly 30 mg of the sample was taken for TG/DTA analysis in N_2 atmosphere in the temperature range of RT to 1000 ° C with a heating rate of 10 °C/min. The powder-XRD patterns of the fine dry zeolite

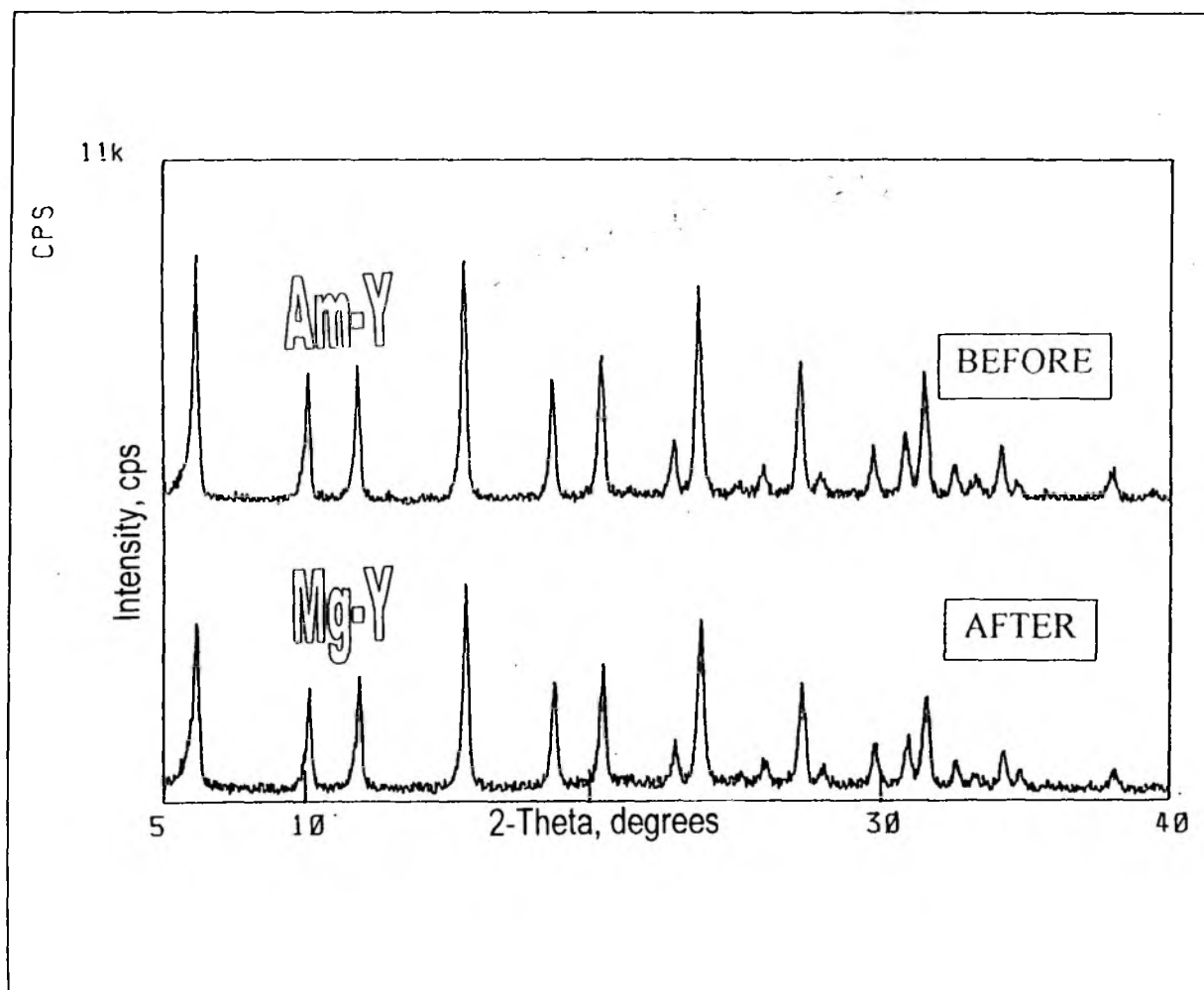


Figure 4.2.1. XRD profiles of zeolite samples before and after three Mg exchanges.

powders before and after the exchanges were recorded and the crystallinity changes were checked (shown in Figure 4.2.1.) The chemical analysis of the exchanged sample was found out using AAS as mentioned in the earlier chapter and the analysis shows the elemental ratios as listed in Table 4.2.1.

Table no. 4.2.1. Elemental analysis of MAS Y3

Zeolite	Conc. of Mg(NO ₃) ₂ soln.	N _x	Elemental ratios %			Residual Na wt. %	Label
			Si/Al	Mg/Al	Na/Al		
Y	1 M	3	3.4198	0.1072	0.00837	0.0837	MASY3

4.2.3. CONSOLIDATION AND SINTERING

Using PVA the powder was bound and consolidated into pellets as explained in chapter 2 - section 2.1.3.b., each pellet weighing roughly around 0.7 g. The pellets were fired at different temperatures viz., (T₂ =) 480, 700, 800, 900, 1000, 1100, 1200 ° C in a programmed fashion with a heating rate of 4 °C/ min. with the program parameters as T₁ = 580 °C ; t₂ = 180 min. The samples were heated at higher temperature at different T₂s (as given above) with t₄ = 360 min. isothermally and later cooled naturally (refer Figure 2.1.3., chapter 2, for more details about the parameters that are fixed during the programmed heating of the samples).

4.2.3.a. Nomenclature of samples

Table 4. 2. 2. shows the nomenclature of samples prepared and used for various studies in this work. MAS Y3 is the source prepared with three times Mg exchange with NH₄ form of Y zeolite. These designations will be used for the ensuing discussion.

Table No. 4.2.2. Nomenclature of samples prepared and their details

Sl. No	Sample Name	Precursor source	Heated at T, °C	Rate of heating, °C min ⁻¹	Holding time at T, hr.	Atmosphere
1	MASY3-480	MASY3	480	4	6	Air
2	MASY3-800	MASY3	800	4	6	Air
3	MASY3-900	MASY3	900	4	6	Air
4	MASY3-1000	MASY3	1000	4	6	Air
5	MASY3-1100	MASY3	1100	4	6	Air
6	MASY3-1200	MASY3	1200	4	6	Air
7	MASY3-1300	MASY3	1300	4	6	Air
8	MASY3-1350	MASY3	1350	4	6	Air

4.2.4. CERAMIC CHARACTERISATION

The heated pellets were crushed into fine powder in an agate mortar and the powder XRD profiles were recorded for all the samples in the 2-theta range of 5 to 40 degrees with a scanning speed of 4 degree/min. The XRD data were processed and plotted in series to have a comprehensive view of the phase changes. The changes in the phases were discussed in the following section. Selected samples in the course of sintering were checked for the major changes in morphology and the particle size by SEM for size variations. The chemical composition, thermal expansion, shrinkage, density and dielectric properties of the ceramic product were studied using various techniques.

4.3. RESULTS AND DISCUSSION

4.3.1. THERMAL PROPERTIES

Figure 4.3.1 shows the TG/DTA plot of MASY3 sample in the temperature region from 25 to 1000 °C. The TG of the powder MASY3 shows a total weight loss of around 22.8 % during the heat treatment up to 1000 °C. Major

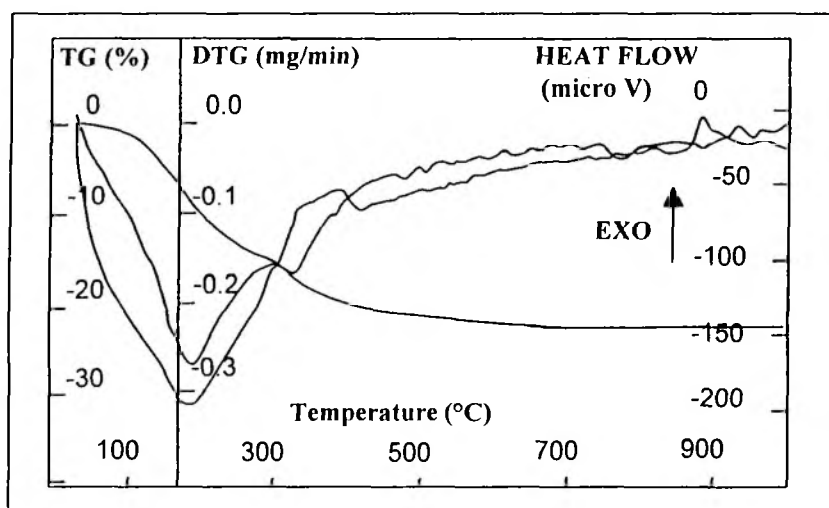


Figure 4.3.1. TG/DTA plot of MASY3

weight loss is observed before 450 °C, in two steps; one is up to 280 °C (peak max at 185 °C) and the other is up to 410 °C (peak-max at 320 °C). However, this is usually observed for faujasite type zeolites and predominantly due to the loss of adsorbed water and organic and other matter. There is an exothermic peak around 865 °C accompanied by no weight loss.

This may be attributed to the zeolite structure collapse followed by transformation of phase, which is observed distinctly in powder XRD profiles obtained at these temperature ranges. This is due to the fact that at this temperature, usually glass silica gets converted into its crystalline polymorph cristobalite. At this temperature the TMA based shrinkage studies show significant changes. This aspect is discussed in the later part of the chapter. Firstly, like Li^+ , the cation Mg^{2+} is also known for being an alkali flux agent at high temperatures. The formation of cordierite phase is exclusively beyond 1250 °C, as the phase changes observed by XRD patterns. Hence the TG should be done at higher temperature range to understand the recrystallisation process of the cordierite dense phase. Due to the non-availability of such high temperature instruments, this was not possible. However, the collapse of the zeolite structure is relatively at higher temperature than that for LAS samples (refer chapter 2).

4.3.2. PHASE TRANSFORMATIONS BY X-RAY DIFFRACTION

Figure 4.3.2. shows the multiple plot of the powder XRD patterns of MASY3 sintered at various temperature ranging from RT to 1350 °C. The changes in the powder patterns shows the typical trend of zeolite based ceramic preparation. Similar to the LAS systems, here also the amorphisation is followed by the crystallisation of

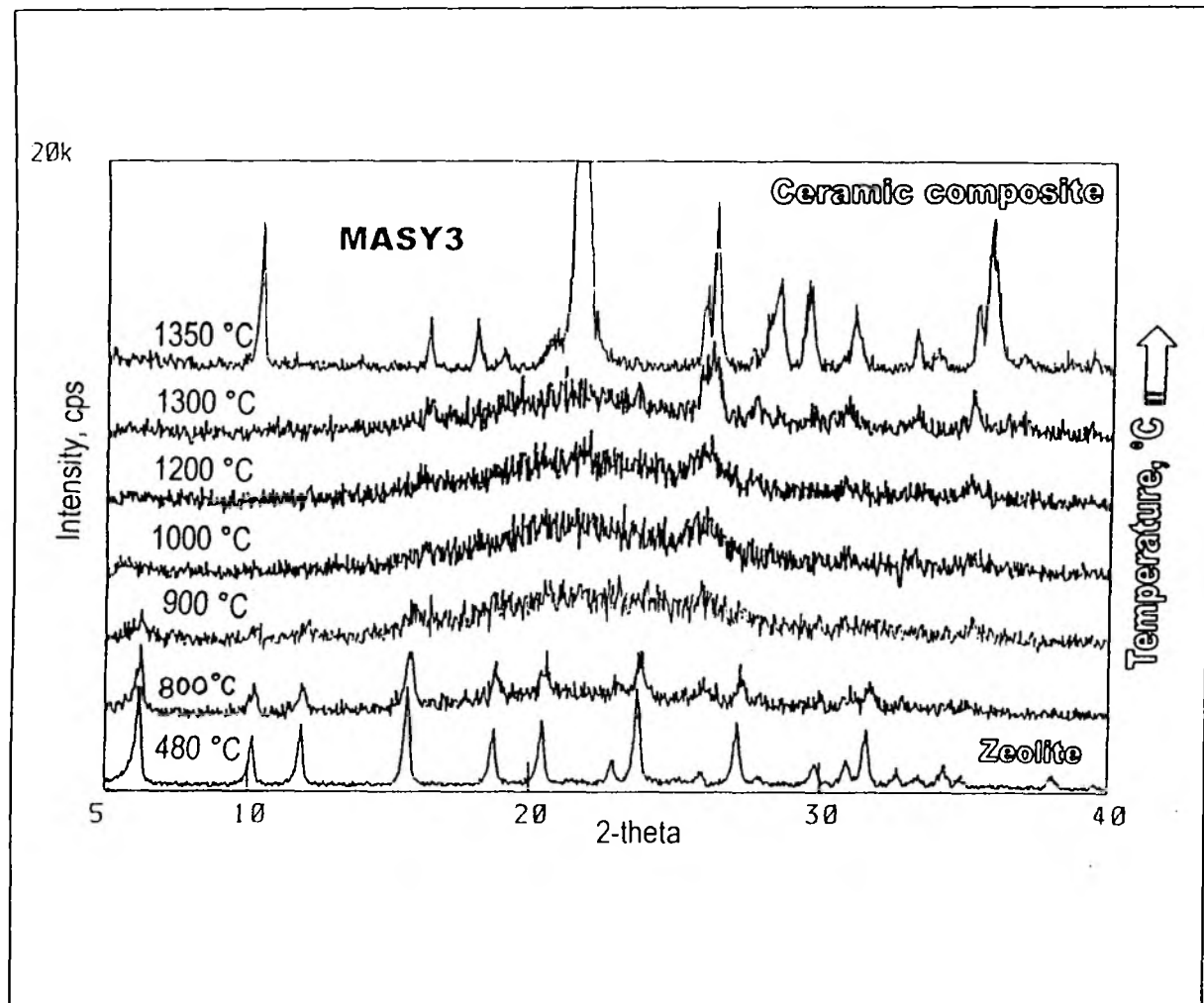


Figure 4.3.2. Multiple plot of XRD profiles of MASY3 samples fired at different temperatures ranging from 480 °C to 1350 C.

dense phases. The third pattern from the bottom in Figure 4.3.2, corresponds to the sample MASY3-900, and shows the initiation of the crystallisation of the dense phases from the amorphous bulk. This reveals the formation of peaks corresponding to mullite (JCPDS 150790) phase. As the temperature increases further, the mullite phase grows further and above 1100 °C, the formation of cordierite phase (JCPDS 130293) starts along with a silica polymorph, (cristobalite type) (JCPDS 270605). At a temperature of 1350 °C (sample MASY3-1350) the formation of cordierite is the maximum though other phases also crystallise as well. The product formed by sintering the sample MASY3, thus yielded a ceramic that contains cordierite. The temperature ranges of the processes, structure collapse and formation of dense phase, have been compared with the TG/DTA data in the earlier part of the discussion and it is found to be in good agreement. Using the 'search-match' package available with the JCPDS file library, the phases formed during the process were identified and estimated semi-

quantitatively and are listed in Table 4.3.1. The ceramic phase was found to possess cordierite (major), mullite (minor) and silica (very low). Unlike, high temperature MAS systems, which contain β -spodumene phase, the ratio of major phase (cordierite) to the side products, is rather low in MAS systems.

Table 4.3.1. Phases identified at different temperatures on sintering MASY3

Sample	Phases and temperature, °C						
	480	900	1000	1100	1200	1300	1350
MASY3	Zeolite Y	Mullite AMORPH*	Mullite AMORPH*	Mullite Cordierite	Mullite Cordierite Silica	Mullite Cordierite Silica	Mullite Cordierite Silica

AMORPH* - Amorphous phases

Phase	Formula	JCPDS file	Phase	Formula	JCPDS file
Mullite	$Al_6Si_2O_{13}$	150776	Cordierite	$Mg_2Al_4Si_5O_{18}$	130293
Silica	SiO_2	270605			

4.3.3. SCANNING ELECTRON MICROSCOPY

Table 4.3.2 shows the change in the particle size observed by SEM. The average size distribution out of 10 measurements of different particles of each sample is listed in Table 4.2.2. In the temperature range from 700 °C to 1000 °C, the measurement was not possible due to agglomeration.

Table 4.3.2 Particle size variations by SEM

Sample name	Firing temperature, °C	Particle size range, μm
MASY3-480	480	1 - 1.5
MASY3-700	700	1 - 1.0
MASY3-800	800	(agglomerate flakes)
MASY3-900	900	(agglomerate flakes)
MASY3-1000	1000	4 - 11
MASY3-1200	1200	7 - 14
MASY3-1300	1300	12 - 16
MASY3-1350	1350	13 - 16

The trend in the change of particle size variation at various temperatures seems to be similar to that of the LAS systems. However, there is an effective reduction in size as well as the distribution of size for the final ceramic product, MAS3-1350 at 1350 °C. Figure 4.3.3. illustrates schematically, the relative magnitude of particles size

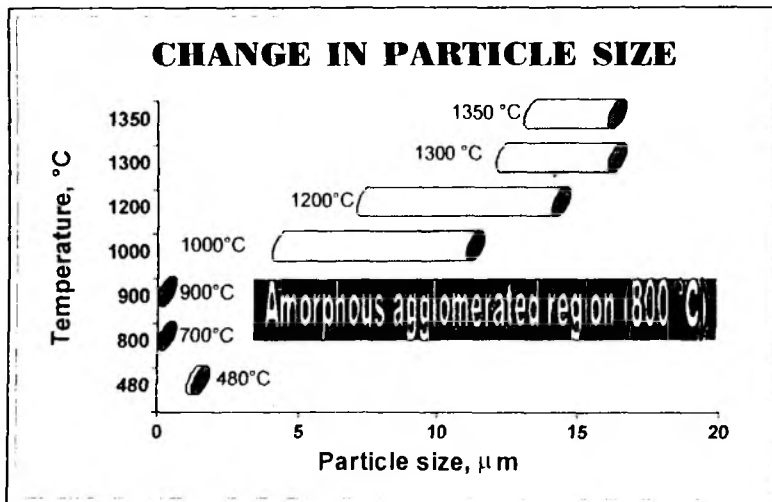


Figure 4.3.3. Magnitude of particle size changes during the course of sintering of MAS3

distribution in the respective range of temperatures.

The zeolite precursor has a very narrow particle size distribution around 1 μm. As the structure starts collapsing around 700 °C and above, the particles look more like agglomerated flakes and the particle size measurement became difficult, as there is no definite boundary for the flakes. Unlike LAS3, for MAS3 sample, this amorphous

agglomerated region persists up to 1000 °C. At this temperature, grains do not have definite boundaries and are like agglomerated flakes of solid mass. The amorphous phase is expected to contain amorphous silica and other oxides. On further heating, the formation of intermediate starts and the crystals of the dense ceramic phase start growing as seen in the XRD patterns. Similar to the LAS3 sintering, though the growth is uncontrolled at the outset, leading to the formation of asymmetric crystals with a large distribution of particle size, at higher temperatures, the particles are found to have substantially uniform particle sizes. From many reports, it is usually observed that mullite crystallises faster from the amorphous mass^{7,8}. The multiple plot of powder XRD patterns of the fired MAS3 sample (Figure 4.3.2) shows that the formation of mullite though may start around 900 °C, a notable trend of gradual growth is observed till 1200 °C for a long temperature window of about 300 °C. As per the report⁸, the thermodynamically stable mullite phase can exist with a particle size as small as 0.017 to 0.15 μm. In this system, the mullite crystal growth may have a low rate till 1200 °C beyond which other major phases start crystallising. However, the distribution of crystal size narrows down at higher temperatures, due to the formation cordierite at the partial expense of mullite formed. Above 1300 °C, the major crystalline cordierite phase seems to have a relatively narrow particle size distribution. Figure 3.3.3 illustrates the relative magnitude of distributions of the particle sizes of samples fired at various temperatures. The central region of the plot indicates the region where the sample is not having particles with well-defined boundaries but amorphous mass.

4.3.4. XRD BASED CRYSTAL STUDIES

The XRD data obtained for the sample MASY3-1350 were indexed using PDP11 software and the 'h' 'k' and 'l' values were calculated. The unit cell parameters were calculated and compared with that of the literature values. Table 4.3.3. shows the lattice cell parameters along with the corresponding literature values.

Table 4.3.3. Lattice parameters calculated from the powder XRD data

Precursor symmetry	Densified symmetry	Lattice parameters		
		Literature (Å)	Observed (Å)	Standard deviation
Cubic (Mg-Y) (MASY3)	Orthorhombic (Cordierite) (MASY3-1350)	a = 17.083	a = 17.0149	± 0.0190
		b = 9.7380	b = 9.7633	± 0.0128
		c = 9.3350	c = 9.3314	± 0.0092
	Cell volume, Å ³	v = 519.33	v = 518.53	± 2.3

The unit cell parameters calculated for cordierite (JCPDS 130293) on the basis of XRD data of the sample MASY3-1350 are in good agreement with the literature values with minimum standard deviation as given in Table 4.3.3.

Table 4.3.4. The overall compositional transformation of the precursor to ceramic phase

Zeolite	Formula	M ⁺	Composition	
			Precursor (RT)	Ceramic LAS (HT)
MASY3	Na ₅₆ Al ₅₆ Si ₁₃₆ O ₃₈₄ . H ₂ O	Mg ²⁺	Mg ₂₈ Al ₅₆ Si ₁₃₆ O ₃₈₄	14Mg ₂ Al ₄ Si ₅ O ₁₈ (+ 66SiO ₂)

Table 4.3.4. shows the overall composition of the precursor and the product after the reaction. The stoichiometric possibility of the consumption of precursor shows that considerable amount of SiO₂ would be formed in excess along with the main phase. This shows that for a pure single-phase cordierite production, the precursor composition should be altered to get a lower Si/Al ratio (in this specific case, the ideal ratio of Si/Al of precursor is = 1.25) in such a way to meet the required stoichiometry. However, this example of making cordierite from zeolite Y was chosen to demonstrate the relative ease of preparation of ceramic phases, β-spodumene and cordierite from the same zeolite precursor. The effect of variations in Mg concentration and Si/Al ratio of MASY samples on the sintering and the phase formations have also been studied and discussed in the later part of this chapter.

4.3.5. DIELECTRIC CHARACTERISATION

Table 4.3.5. The dielectric and other properties of MASY3 pellet sintered at 1350 °C

Sample dielectric Dimensions of pellet *	ν , Hz	C, pF	Q	ϵ_T (DEC)
Thickness, 't' = 0.100 cm Radius, 'r' = 0.55 cm Area, 'a' = 0.9503 cm ²	1,000,000	6.313	29.7	7.5
	100,000	6.641	21.8	7.9
	10,000	7.130	15.8	8.5
	1,000	7.995	8.13	9.5
	1,00	10.405	3.46	12.4
	20	17.165	2.65	20.4

* 'v' is the frequency in Hz, 'C' is the capacitance in pF generated between the electrodes, 'Q' is the Q factor (where $Q = R\omega C$, where ' ω ' is the angular frequency applied across the electrodes, $2\pi\nu$) and ' ϵ_T ' is the DEC of the pellet.

A pellet of MASY3-1350 was lapped with fine carborundum for uniform thickness. It was electroded with silver paint and cured using the procedure as given in the chapter 2, Section 2.3.7. The diameter of the electrode was measured using a Vernier caliper and the area of the electrode was calculated. The thickness was measured using a screw gauge. The pellet was mounted on the sample holder as explained in the same section in chapter 2. Under the given conditions the capacitance values of the pellet were measured at different frequencies from 20 Hz to 1 MHz. α -Alumina was used as reference for measuring the capacitance in the LCR unit. The dielectric constant (DEC) of alumina was calculated as 9.526 at 1 MHz, which is comparable with the DEC, reported in literature. Table 4.3.5 shows the dielectric constant (DEC) values calculated for the sample. The DEC of MASY3 is found to match with that of cordierite reported in literature⁹. The increment in the DEC for this particular case is due to the presence of silica and mullite, which have higher DEC. The DEC values (at 1 MHz) of other materials commonly used in packaging technology are given in the Table 4.3.6. for comparison.

Table 4.3.6. The DEC of cordierite from MASY3 and other materials commonly used in MEP

Sl. No	Material	Formula	DEC @ 1 MHz
1	α -Alumina	Al ₂ O ₃	9.6
2	Beryllium Oxide	BeO	6.5
3	Alumina-96%	Al ₂ O ₃ - 96%	9.3
4	Alumina-92%	Al ₂ O ₃ - 92%	8.5
5	β -Spodumene	LiAlSi ₂ O ₆	8.1
6.	Cordierite	Mg ₂ Al ₄ Si ₅ O ₁₈	7.5

It is known that the most operative candidates for MEP (Microelectronic Packaging) technology are low DEC materials. As it is known that due to its toxicity in the powder form, BeO is not popular though it has a very low DEC (= 6.5). From this point of view, the cordierite seems to be a better candidate for MEP having the lowest DEC (=7.5 for cordierite prepared from MASY3) among the listed conventional materials.

4.3.6. DENSITY CALCULATION

The densities were calculated for the green and the sample MASY3-1350 using the procedure given in the chapter 2. Table 4.3.7. shows the calculated densities of the samples.

Table 4.3.7. Density of the green and sintered MASY3

No.	Samples	Volume(cc)	Wt.(g)	Density (g/cc)
1	MASY3 (green)	0.64388	0.71040	1.0624
2	MASY3-1350 (sintered)	4.15801	1.02250	2.4541

These densities were compared with the X – ray density of the phase cordierite and the relative density was calculated although the MASY3-1350 is not a pure single phase of cordierite, to have a comparative idea of density and the results are listed in Table 4.3.8. The **relative density of above 98 % is a remarkable sintering result**. On further fine-tuning of chemical composition improved relative densities were achieved, which are discussed in the later part of this chapter.

Table 4.3.8. Density changes on sintering and the relative density

Sample name	Density in g/cc			Relative density, %
	Green state	Sintered	X – ray*	
MASY3-1350	1.0246	2.4591	2.508	98.0502

* ref:- X-ray crystal structure –Minerals, CRC Hand book of Physics and Chemistry (1974)

4.3.7. SHRINKAGE STUDIES ON GREEN SAMPLES BY TMA

Figure 4.3.4. shows the shrinkage TMA plot of the green sample MASY3 in the temperature range from RT to 1200 °C. The TMA curve shows an usual and plain trend in which the sample is stable up to higher temperature and then suddenly condenses to a dense phase. However, there is a gradual initial shrinkage of ~20% of the total shrinkage up to 880 °C. There is a strong densification since 889 °C up to 1011 °C indicating the structure collapse of the sample followed by sintering of the sample. The XRD pattern of the sample sintered at 800 °C shows that the zeolite precursor has collapsed into an amorphous material. The highest densification rate was observed around 920 °C. The temperature of maximum densification rate (T_{Dmax}) is observed at 979 °C. The

value of T_{Dmax} for LASY3 is relatively lower (920 °C) than that of MASY3. This comparison offers a good realization about the effect of cation on sintering of zeolite precursors for ceramic preparations. The over all

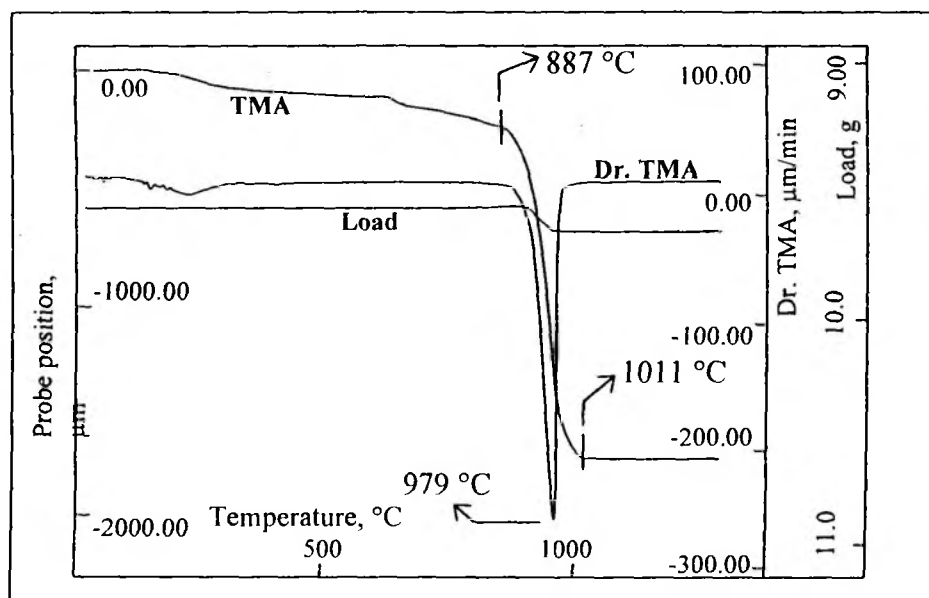


Figure 4.3.4. The Shrinkage TMA plot of the green sample MASY3 in the temperature range from RT to 1200 °C

shrinkage is estimated to be around 32.86 %.

The derivative of TMA shows a sharp peak indicating the shrinkage is a one step process. However, the XRD patterns show that the crystallisation starts at much higher temperatures (~ 1250 °C) after the completion of densification. In other words, the sintering is getting over before the

high temperature solid-state reactions. Particularly, for MAS system, the temperature of crystallisation of cordierite is much delayed than the formation of β -spodumene in LAS system. Usually, this kind of situation does not allow the phase transformation to complete which leads to unwanted side products (other impurity phases). That is the exact reason why cordierite formation in MASY3 sample was accompanied by considerable amount of mullite and silica phases.

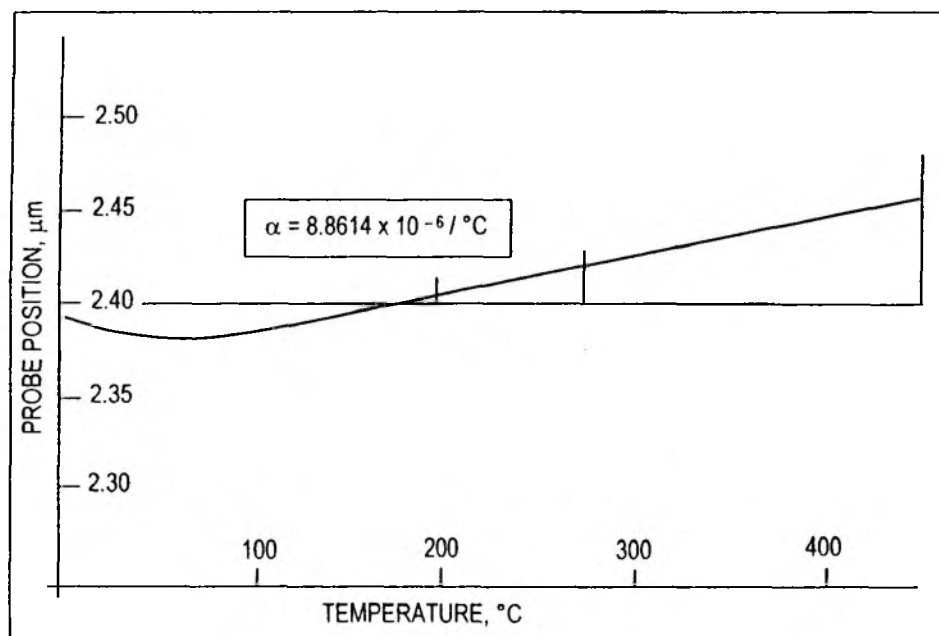
4.3.8. THERMAL EXPANSION STUDIES ON SINTERED SAMPLES BY DILATOMETRY

The sample of MASY3-1350 is used for the expansion analysis. The measurement was taken from RT to 450 °C (higher temperature measurement was not possible because of the instrumental limitations). Figure 4.3.5 shows the thermal expansion curve measured in force free conditions, in a temperature range of 25 to 450 °C. The curve shows a typical 'lower bend' in the region of temperature range up to around 180 °C. The thermal expansion coefficient measured at a range of 20 to 200 °C is $8.8614 \times 10^{-6} / ^\circ\text{C}$ and it falls close to the reported value TEC value of cordierite. According to literature the high purity cordierite has a TEC around $2.06 \times 10^{-6} / ^\circ\text{C}$ ¹⁰. However, Ikeda reports a range of TEC values around 4.2 or $5.8 \times 10^{-6} / ^\circ\text{C}$ for Invar-cordierite cermet-type sintered compact, where the metal alloy, Invar has a TEC around 7.4 or $9.7 \times 10^{-6} / ^\circ\text{C}$ ¹¹. It is known thus that the pure cordierite has a low TEC and it increases when mixed with higher TEC materials. The literature reports that mullite has a higher TEC than cordierite and that the mullite has been added to cordierite phase to alter the TEC of cordierite¹². Thus the presence of mullite in the ceramic cordierite which is prepared from MASY3 increases the

TEC considerably. In addition to that the increment in the TEC may be attributed to two common factors namely (i) the symmetry nature of cordierite phase and (ii) the impurity phases present, particularly the oxides of alkali elements viz., Na, Li. The first factor, the anisometric nature of phase present in the sample makes the expansion anisotropic. Table 3.3.11 in chapter 2 collects the individual contribution from each coordinate of the particular crystal symmetry to describe the effective thermal expansion coefficient ' α' '_{eff}. Cordierite, having an orthorhombic structure, does depend on the principal coefficients α_1 , α_2 , α_3 like the β -spodumene and not on the secondary coefficients α_4 , α_5 , and α_6 which are dependant on the crystal shape. Phase studies by XRD shows the presence of significant amounts of mullite (in the MAS product at 1350 °C) and it is also known from literature that mullite is often added to alter the TEC of a material¹³.

Measuring system	: Dilatometer	TMA – Perkin Elmer
Diameter	: 13.670 mm	
Height	: 2.355 mm	
Probe position (mm)	: Step: 1	Atmosphere (rate): Argon(2ml/min)
Filename	: MAS3	
Temperature (rate)	: 20 to 450 °C (20 °C/min)	

Figure 4.3.5. Thermal expansion plot of sample MAS3 (sintered at 1350 °C) in the temperature range of 20 to 400 °C (TEC plot)



4.3.9. AC IMPEDANCE SPECTROSCOPY STUDIES ON MAS CERAMICS

4.3.9.a. Introduction

Conventional electrical measurements of dielectric properties and resistance studies for the characterisation of materials used for electrical applications were limited to fixed frequencies. However, the development of impedance spectroscopy (IS) has made it possible to cover a broad range of frequencies. The technical development of the instrumentation now allows a fast tuning to higher frequencies with shorter intervals of frequencies with high precision and measuring of gain and phase angle over a wide range. Also the microprocessor-controlled units provide a precise and fast data recording along with various data processing facility according to the recent developments of the impedance spectroscopic theory.

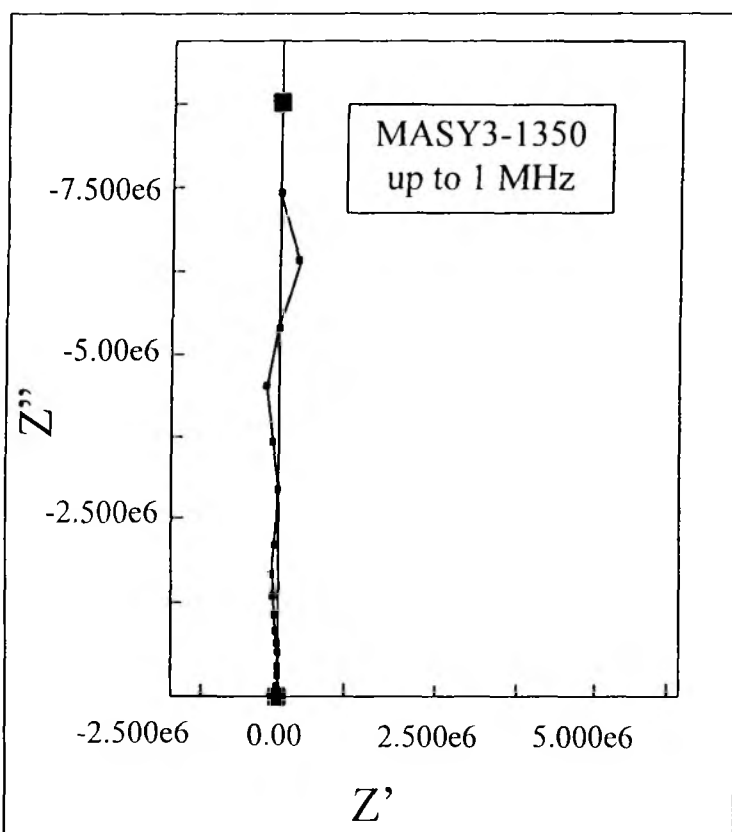


Figure 4.3.6. AC Impedance spectrum of sample MASY3-135 recorded in RT from 1 Hz to 1 MHz. Z' and Z'' are the real and imaginary components (Ohms) of total impedance Z .

The plots of real versus imaginary components can be used to analyse the systems in terms of simple equivalent circuit parameters¹⁴. The individual contribution of the grains and the grain boundaries towards the total impedance of the system can be estimated and thus it gives a measure of the existence of large number of grain boundaries if the grains are very small or vice versa. The basic theory of AC circuits and the IS have been given in chapter 2.

Doped and undoped zinc oxide varistors are few of the typical materials, which are successfully characterised by IS¹⁵. Doped varistor shows reactive contribution to the total impedance whereas the undoped zinc oxide shows only the resistive contribution from the bulk of the grain interior. The hydration of cement and the

phase formation of high T_c superconductors are some of the typical dynamic processes studied by this technique^{16,17}.

4.3.9.b. Plan of work

It was aimed to understand the change in microstructure during the course of phase transformation of ceramic phase from zeolite using impedance spectroscopy. The spectral output was very bad due to heavy resistive effect of the sample, when the sample was done initially. However, the result could indicate that the measuring temperature had to be raised to get a reasonable output gain. Figure 4.3.6 shows the impedance spectrum recorded in room temperature for sample MASY3-1350. The linear trend along the Y-axis direction shows the material is highly resistive and the grain boundary effects can be visualised only either at very high working frequencies or at elevated measuring temperatures where the major contribution of ohmic resistance for the total impedance becomes negligible. The impedance recorded at high frequencies (up to 32 MHz) also showed a low-resolution spectrum. However, frequency generator in the instrument has a upper frequency limitation at 32 MHz. So, there was a need for optimisation of measuring temperature.

Moreover, it would be interesting to know the effect of operational temperature on its electronic properties of the ceramic materials as substrates due to the fact that the substrate in electronic circuits get heated up during operation. Hence it was planned to carry out the spectroscopic measurements on MASY3-1350 sample at various temperatures ranging from 100 °C to 600 °C. Though the operational temperature of circuits will not go up to such a high temperature as 600 °C, it was expected that the resolution of the spectrum will increase at high temperatures and would help in understanding the effect of temperature on the total impedance.

The current study includes the impedance spectral studies on MASY3-1350 sample at a working frequency range of 1 Hz to 32 MHz. The resistance (R) and capacitance (C) values at various temperatures have been estimated from the spectra. The variation in R and C as a function of temperature has been studied. The nature of conductivity in the sample has been discussed by considering the change in the activation energy of the charge flow at various temperatures. The influence of frequency on the activation energies has been studied. The results are discussed with reference to the various reasons for the changes encountered as a function of temperature.

4.3.9.c Effect of temperature on AC Impedance

As per the procedure given in the chapter 2, the impedance spectra of MASY3-1350 were recorded at various temperatures viz., 300, 400, 500, 550, 600 °C. Figure 4.3.7.a shows the spectra recorded in between the temperature range of 300 to 400 °C for the complete range of frequency from 1 Hz to 1 MHz. Figure 4.3.7.b shows the expanded version of the marked region given in Figure 4.3.7.a., which covers the total impedance response of the sample at 400 °C in the sample frequency range. The semicircle shows the typical model of combination of an R and C circuit. The reduction in the diameter of the semi circle of the spectrum at 300 °C to that of 400 °C is the direct indication of the reduction in the total impedance (nearly 10 fold) as the temperature increases.

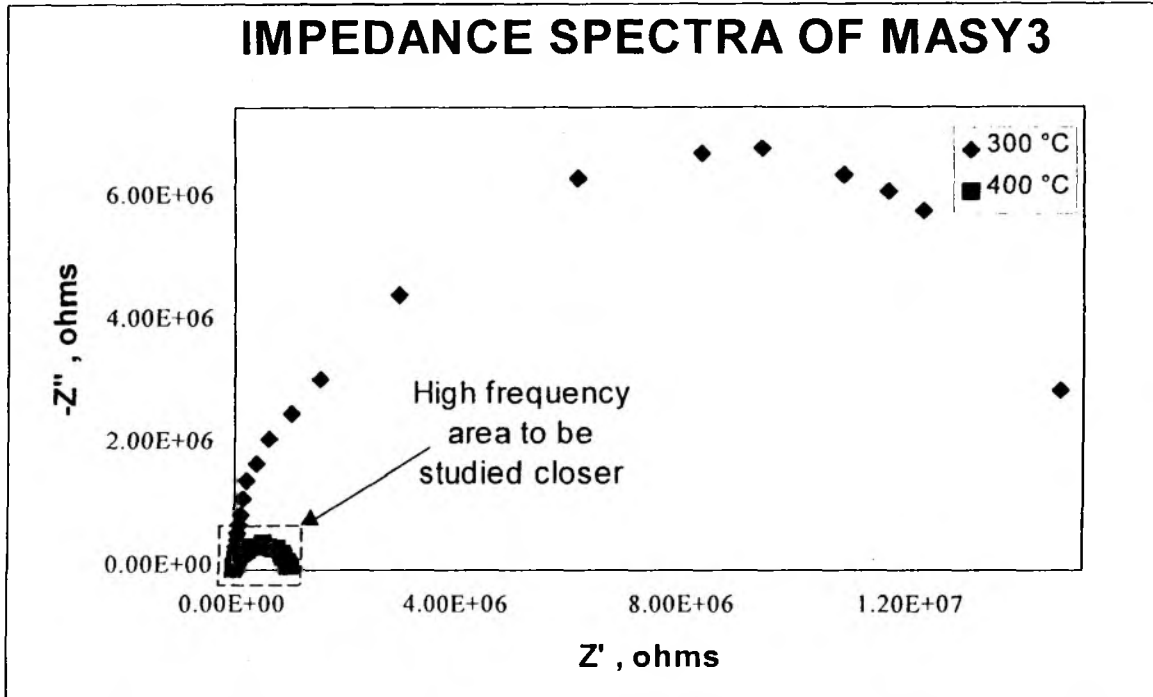


Figure 4.3.7.a. The AC Impedance spectra measured in full range of frequency from 1 Hz to 1 MHz at 300 °C and 400 °C of MASY3 sintered at 1350 °C

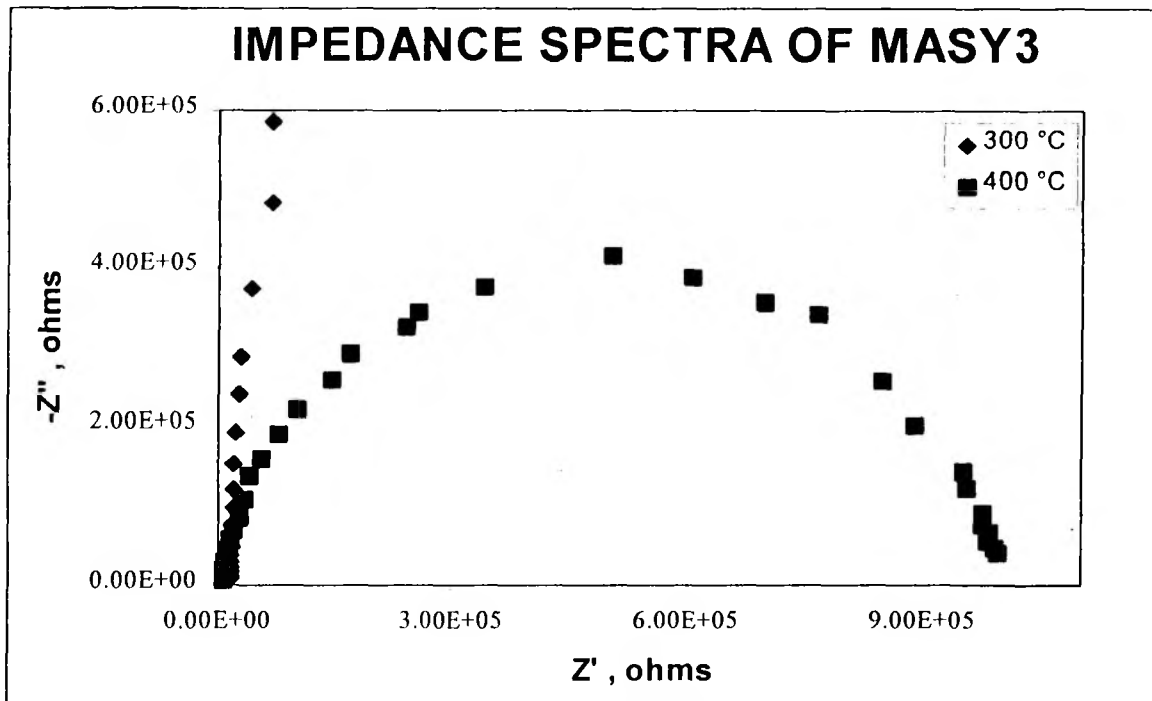


Figure 4.3.7.b. The AC Impedance spectra measured higher frequency range at 300 °C and 400 °C of MASY3 sintered at 1350 °C. The expanded version of the part marked with dotted line in the earlier figure 4.3.7.a.

As given in Figure 2.3.4, chapter 2, the change in the individual contribution of the ohmic and polarisation impedances towards the total impedance can be realised by the change in the spectra at increasing temperatures.

Figure 4.3.8 shows the AC impedance spectra recorded for the sample MASY3-1350 at 500, 550 and 600 °C in the frequency range of 1 Hz to 32 MHz. This shows that as the temperature increases the total impedance decreases. However, compared to the ohmic bulk resistance (R_{Ω}), the polarisation resistance (R_p) has a negligible contribution for the change in the total impedance as a function of temperature.

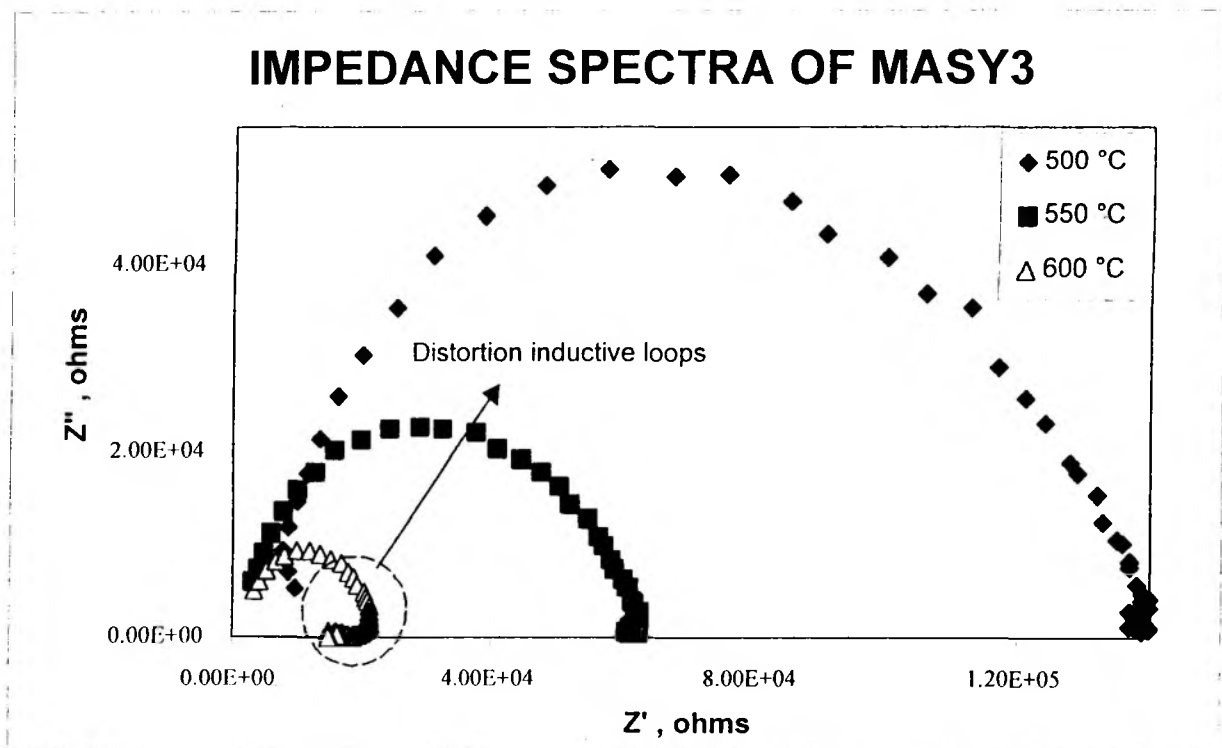


Figure 4.3.8. The AC Impedance spectra measured at 500, 550 and 600 °C in full frequency range of 1 Hz to 1 MHz of MASY3 sintered at 1350 °C.

Table 4.3.9. shows the various parameters calculated from the AC Impedance results. 'T' is the temperature at which the impedance spectrum was recorded, 'Centre_r' is the real centre, 'Centre_i' is the imaginary centre, 'D' is the diameter of the estimated semicircle (R_{Ω}). 'Low C' and 'High C' are the lower and upper limits of the intersection on x-axis by the semicircle. The 'Angle_d' is the angle of depression, θ in degrees, ' ω_{max} ' is the maximum angular frequency ($= 1/C_d R_p$), and 'R' and 'C' are the estimated resistance and then capacitance in ohms and farads respectively.

Table 4. 3.9. Various parameters estimated from the AC Impedance results.

T (°C)	Centre _r (Ohms)	Centre _i (Ohms)	D	Low C	High C	Angle _d (degree)	ω_{max}	R (Ohms)	C (Farads)
300	8.06E+06	1.46E+06	1.64E+06	-6395.5	1.61E+07	10.2802	1.65E+03	1.61E+07	3.68E-11
400	5.00E+05	1.04E+05	1.02E+06	368.88	9.99E+05	11.8091	3.18E+04	9.99E+05	3.08E-11
500	7.04E+04	2.03E+04	1.40E+05	3340.21	1.38E+05	16.8137	2.28E+05	1.34E+05	3.12E-11
550	3.10E+04	1.13E+04	6.76E+04	-88014	6.29E+04	19.4388	5.65E+05	6.38E+04	2.62E-11
600	1.15E+04	1161.63	2.08E+04	1152.48	2.18E+04	6.4201	1.63E+06	2.06E+04	2.96E-11

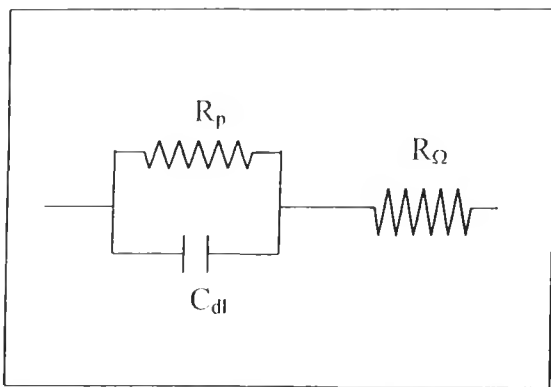


Figure 4.3.9. Randles equivalent circuit model

The values of real and imaginary centres are lowering indicating the decrease in the total impedance of the system as the temperature increases. This reflects in the change of diameter of the spectral semicircle, in the low and high intersection on the x-axis (R_p and $R_\Omega + R_p$ respectively). This can be easily visualised by using the Randles model of equivalent circuits. Figure 4.3.9. shows a model equivalent circuit for the polycrystalline solid phase similar to that of the present case where the bulk resistance, and polarisation resistance along with the double layer capacitance can be indicated as R_Ω , R_p and

C_{dl} respectively. However, the rate of decrement of R and C are different. In other words, while the resistance of the system decreases drastically as a function of increasing temperature, the capacitance does not show any significant change. This indicates that the contribution of the double layer capacitance (C_{dl}) that is usually expected at the electrode-electrolyte junction, towards the total impedance is negligible when compared with that of the ohmic resistance due to the bulk.

4.3.9.d. Studies on the electrical conductivity mechanism

An expanded part of the plot of C and R estimated by the spectral results versus temperature is shown in Figure 4.3.10. The inset shows the full plot with range of temperature. It would be interesting to understand the reason for such partial influence of temperature on the R and C of the system. However, it needs more understanding about the nature of available infrastructure in the microstructure and the crystal structure of the ceramic phases.

Table 4.3.10 gives the R and C values calculated by the AC impedance measurements. It is well known that the conduction in solid electrolytes is either through electron or by ion.

Table 4.3.10. R and C calculated for MAS Y3-1350

T, °C	R, ohms	C, farads
300	1.61e+07	3.68e-11
400	9.99e+05	3.08e-11
500	1.34e+05	3.12e-11
550	6.38e+04	2.62e-11
600	2.06e+04	2.96e-11

In either case, the diffusion coefficient of the carrier, 'D' and the electrical conductivity, 'σ' are closely related. The famous Nernst-Einstein's equation states the relation as,

$$\frac{\sigma}{D} = \frac{n q^2}{k T}$$

where, 'q' is the charge of the carrier particle and 'n' is the concentration per unit volume which make a contribution 'σ' to the conductivity, 'T' is the absolute temperature and 'k' is the Boltzmann's constant. It is more appropriate to remember here that the simultaneous measurement of D and σ can disclose important information about the mechanism of the conduction and diffusion¹⁸.

However, one of the characteristic features of the ionic conductivity of a solid electrolyte is its variation with temperature¹⁹. This fact is the main impetus for the present investigation to understand the mechanism of the conductivity in this solid material. According to the report, two facts stand out plainly;

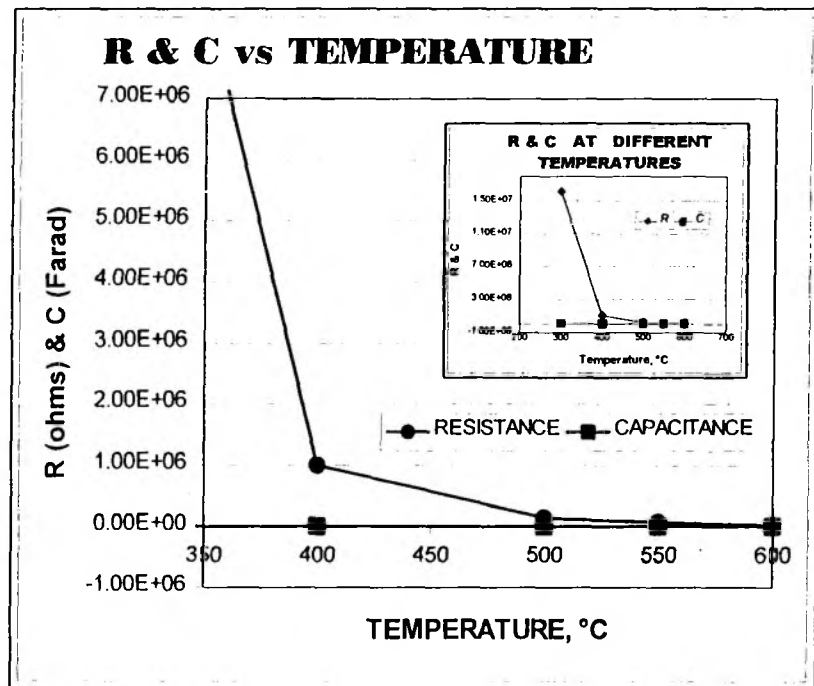


Figure 4.3.10. The resistance and capacitance for MAS Y3-1350 as a function of measuring temperature

1. The existence of two main regions in the conductivity curve
2. In both these regions, the logarithm of conductivity is roughly a linear function of T⁻¹

It is also known that the diffusion coefficient, D is inversely proportional to the activation energy, E_a of the current flow also, reflects this trend when it is plotted versus the inverse of T. Hence, it was planned to calculate the activation energy of the solid samples MAS Y3-1350 at various temperatures and to check for the dual trend of the activation energy as a function of temperature, which would give an idea about the possibility of the ionic conduction.

4.3.9.e. Studies on activation energies

According to Arrhenius theory, the rate of diffusion of the charge carriers, k can be written as,

$$k = A e^{-E_a/RT}$$

where A is the pre-exponential factor, E_a is the activation energy, R is the universal gas constant ($R = 8.314$ J/K/mol) and T is the temperature in K. This equation can be modified as,

$$\log k = -E_a/(2.303 RT) + \log A$$

which is equivalent to the equation of a straight line, $y = mx + c$, where,

$$y = \log k \quad ; \quad x = 1/T \quad ; \quad \text{and} \quad m = -E_a/(2.303 R)$$

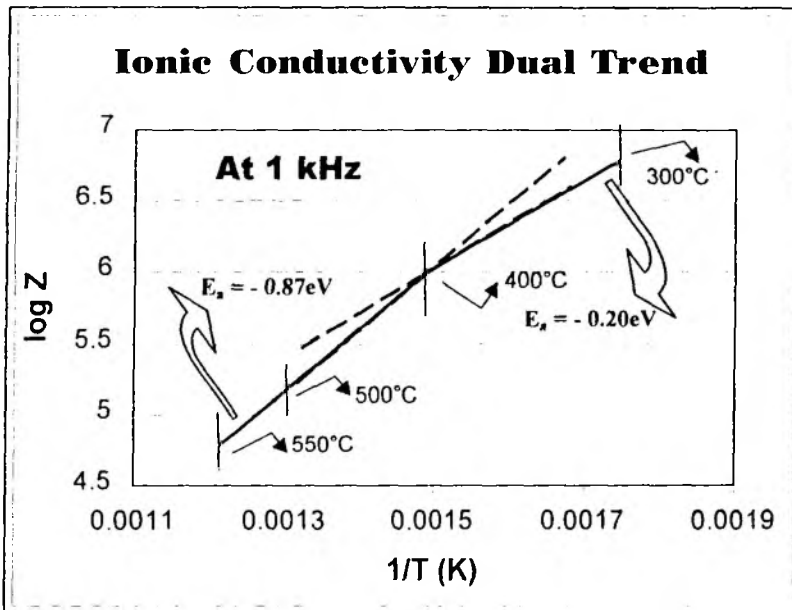


Figure 4.3.11. Dual conductivity trend observed at 1000 Hz for different temperatures ranging from 300 to 550 °C for the sample MASY3-1350 (from impedance spectroscopy results)

Similarly, replacing the k with the impedance (Z) of the system, a plot of log Z versus inverse of T will give a straight line corresponding to the slope from which the activation energy can be calculated. Similar to the reported work in the literature, the existence of dual trend in the change of impedance with temperature is a characteristic feature of the ionic conductivity¹⁹. It was hence planned to calculate the activation energy of the electrical conductivity at various temperatures to verify this.

Figure 4.3.11. shows the Arrhenius plot of log Z versus 1/T in K. There are two distinct trends of the change of impedance as a function of temperature. The main two regions, having a "knee" at 400 °C, one from 300 °C to 400 °C and the other from 400 °C to 550 °C, are individually linear and have distinct slopes. The activation energy calculated for the low temperature range 300 °C to 400 °C is higher ($E_a = -0.20$ eV) than that of the high temperature region ($E_a = -0.87$ eV). As this is a characteristic feature of ionic conductivity, the mechanism in cordierite ceramic prepared from MASY3 is more likely to be 'ionic'. The aliovalent (any impurity ion with a valency differing from that of the corresponding ion of the host lattice) nature of the cations present in the system are usually expected to respond to the electrical field applied as the charge carrier.

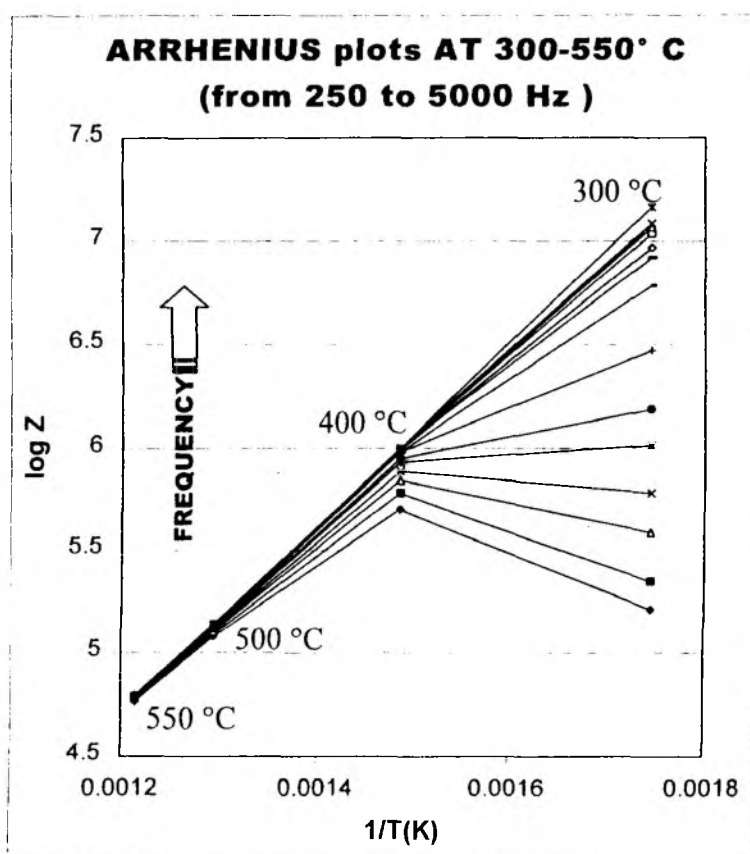


Figure 4.3.12. Arrhenius plots for the temperature range 300 to 550 °C in the low frequency range from 250 to 5000 Hz

Arrhenius plot (Figure 4.3.11) is though according to the result obtained at 1 kHz, the slopes of this dual trends seem to have a strong influence on the frequency of the applied voltage. Figure 4.3.12 shows such Arrhenius plots of $1/T$ versus $\log Z$ recorded at various temperatures in different applied frequencies. Table 4.3.11 shows the $\log Z$ values obtained for the impedance response at various frequencies in the temperature range of 300 °C to 550 °C. Though the dual slope trend having a "knee" at 400 °C remains in all these frequencies, the slope of the low temperature range (300 °C to 400 °C) changes significantly as a function of frequency. This may be explained by the concept of Frenkel and Schottky models of defects for the solid crystal structure. It

is clear from the literature that the two different regions of the dual ionic conductivity have distinct properties¹⁹.

The high temperature section of the curve below the transition region or "knee", in general is an intrinsic property of the substance, and measurements in this region are quite reproducible. On the other hand, the low temperature conductivity not only displays a smaller slope but also depends in magnitude on the particular specimen employed and to some extent on its thermal history. This can be realised by the variation shown by the measurements as seen in Figure 4.3.12. However, this fact has been proved already for few simple electrolyte systems like KCl¹⁸.

Table 4.3.11. Impedance results – log Z values at various frequencies from 251 to 5010 Hz in the temperature range of 300 °C to 550 °C.

Frequency (Hz)	log Z at different temperatures (°C)			
	300	400	500	550
1/T →	0.001745	0.001486	0.001294	0.001215
5010	5.212188	5.702431	5.082785	4.768638
3980	5.350248	5.783189	5.093422	4.777427
3160	5.589950	5.845098	5.107210	4.782473
2510	5.778151	5.885361	5.110590	4.783904
2000	6.008600	5.928396	5.120574	4.788168
1580	6.181844	5.949390	5.123852	4.790285
1260	6.465383	5.978181	5.130334	4.796574
1000	6.785330	5.980458	5.133539	4.793092
794	6.918030	5.989005	5.136721	4.795185
631	6.970812	5.989450	5.136721	4.795880
501	7.033424	5.992995	5.139879	4.792392
398	7.064458	5.992111	5.143015	4.791691
316	7.086360	5.995635	5.143015	4.790285
251	7.164353	5.997386	5.146128	4.789581

To have a close look into the intrinsic property that is usually expected at high temperature region, the dual trend line may be considered as the superimposition of two straight lines obtained from the two different temperature regions which are having different slopes. Then these lines can be represented as $A_1 \exp(-E_{a1}/RT)$ for the low temperature region and $A_2 \exp(-E_{a2}/RT)$.

The Frenkel model of crystal structure can be used for further understanding of this. Figure 4.3.13. shows a typical cubic structure where an interstitial position has been marked with a bigger sphere at $\frac{1}{2}, \frac{1}{2}, \frac{1}{2}$.

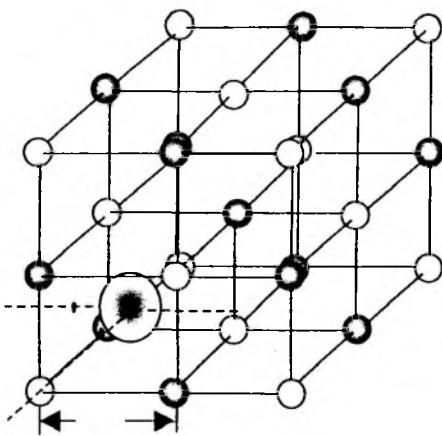


Figure 4.3.13. Frenkel model of a cubic crystal and the interlattice position at $(\frac{1}{2}, \frac{1}{2}, \frac{1}{2})$

Frenkel supposed that under the influence of thermal fluctuations, atoms will from time to time undergo such large displacements that they become detached from normal lattice positions and find themselves in interlattice (interstitial) positions. An ion in the interstitial position will vibrate about this point in the normal way, until there is again a large fluctuation in energy when it will be pushed through a gap in the surrounding atoms to the next interstitial position (e.g., from $\frac{1}{2}, \frac{1}{2}, \frac{1}{2}$ to $\frac{3}{2}, \frac{1}{2}, \frac{1}{2}$). The vacancies created by this jumping will be replaced by the neighboring ions. Thus both vacancies (also called as Frenkel defects) and interstitial are mobile as pairs. The formation and recombination of vacancies occurs until a dynamic equilibrium is setup depending on the temperature and pressure. The occurrence of this dynamic equilibrium decides the position of "knee" in the

Arrhenius plot. Also the activation energy, E_a of the process, thus varies before and after the attainment of equilibrium. However, it is obvious that the concentration of defects will depend on temperature through a Boltzmann factor involving their energy of formation.

However, as expected, the energy of activation has a strong dependence of the temperature. Figure 4.3.14. shows the E_a calculated at two different temperature range (from 300-500 °C and 500-600 °C). Usually the E_a at the high temperature region is lower than that at low temperature region. The trend of the current investigation holds good for the same and thus additionally supports the possibility of ionic conductivity. It is also noticed that at low temperature the variation of E_a with respect to frequency is larger than that of high temperature.

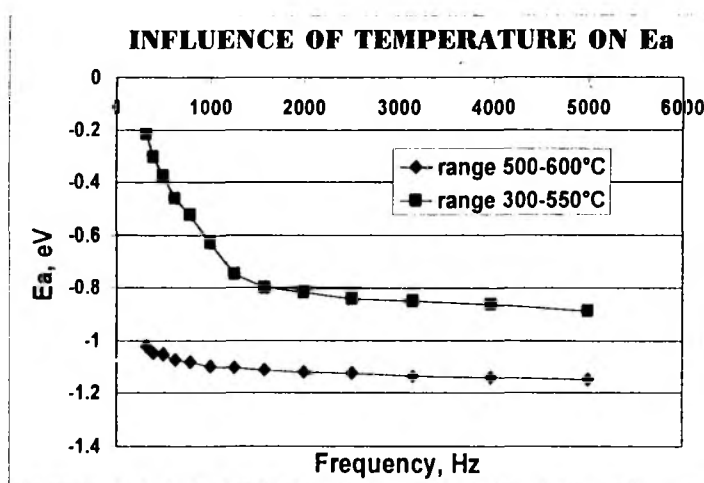


Figure 4.3.14. The activation energies (E_a) calculated for MAS_{Y3-1350} at low temperature range (300-550 °C) and high temperature range (500-600 °C) for the frequency range 300 to 5000 Hz

4.3.9.f. Conclusions

The AC impedance studies on the cordierite-mullite composite prepared using zeolite precursors have shown that the ohmic resistance is the most dominating component to the total impedance compared to the double layer capacitance. The dual nature in energy of activation for the electrical conductivity as a function of temperature indicates the possible ionic conduction.

CHAPTER 4

PART B. INFLUENCE OF PRECURSOR STOICHIOMETRY ON MAS SYSTEM

4.4. INTRODUCTION

This part of the chapter will discuss other important aspects namely the influence of various parameters that affect the sintering process and property of the sintered products. This includes the preparation of MAS precursors with various chemical compositions and sintering of the precursors at different atmospheric conditions to study the influence of the effect of the atmosphere on the sintering and then phase purity. Though the major phase is cordierite ($2\text{MgO}\cdot 2\text{Al}_2\text{O}_3\cdot 5\text{SiO}_2$) the sintering atmosphere changes the dense product phases.

Unlike LAS systems, in MAS systems we have a very basic difference in the nature of chemical modifications. Li^+ is a univalent cation whereas Mg^{2+} is a divalent ion. Hence, there is a reduction in the number of cations per unit cell in MAS and it would be just $\frac{1}{2}$ that of LAS. Thus, each Mg^{2+} cation would be supporting two neighboring Al^{3+} atoms through oxygen atoms for the total charge balance. It is observed from the ion exchange results that the loading of M^+ per exchange (in wt. %) is lesser for MAS system than LAS. Also, as explained in the first part of this chapter, the thermal stability is higher for MAS than LAS and hence the structure collapse and shrinkage are at much higher temperature for MAS systems. However, the amorphous window (the range of temperatures in which the system prefers to be amorphous i.e., the temperature range from the structure collapse and recrystallisation of dense phase.) is longer for MAS than LAS. Mullite is the key intermediate phase for MAS systems. However, the study on the sintering behaviors of MAS precursors in the cases of higher and lower Mg content and higher and lower Si/Al ratio is very interesting and important. Son Yong studied the effect of higher silica and alumina content in the precursors on the glass ceramic product. He has reported that both the conditions affect the crystallisation and the microstructure of MAS glass²⁰. However, it is a non-zeolitic route.

Ruedinger and coworkers have studied the phase formation of MAS ceramics on Mg exchanged P zeolite²¹. However, the phase formation may be influenced by various possible factors and it is really meaningful to study them as this novel route of precursor powder synthesis and the product ceramics have got an immense potential in microelectronic applications. However, there are no reports on the various factors and their influences on the cordierite phase formation from Y zeolite especially on the properties of the ceramic products like density and shrinkage. As these properties are vital, which make these products to be better candidates in the ceramic market for special applications like MEP, they are, thus important to study.

4.4.1. EFFECT OF CATION CONCENTRATION AND SI/Al RATIO

4.4.1.a. Plan of work

Similar to the variation studies described in chapter 3 - part B, samples with varied chemical compositions were prepared and differences in the sintering behaviors with respect to the different concentrations of Mg and Si/Al

ratio in the precursor samples were studied by various techniques. The influence of chemical composition changes on phase formation, density and shrinkage of the ceramic product were studied.

4.4.1.b. Experimental

4.4.1.b.1. Sample preparation

The Mg^{2+} content in the zeolite precursor was modified by changing the concentration of the cation solution and the number of exchanges similar to the procedure followed as described in chapter 2 section 2.1.2.a. Zeolite Y was first exchanged three times with 1 M solution of NH_4NO_3 to get the NH_4 form of Y and then with different molar solutions of $Mg(NO_3)_2$ to obtain MASY precursors with different Mg loading.

Table 4.4.1. Sample details for cation concentration variation and the elemental compositions

Sample name	Conc. of Mg soln.	No. of Exchanges	Elemental ratios, wt. %			Residual Na wt. %
			Si/Al	Mg/Al	Na/Al	
MASY01	0.1 M	1	3.4206	0.0790	0.00756	0.081
MASY05	0.5 M	1	3.3539	0.0814	0.00932	0.101
MASY1	1.0 M	1	3.3921	0.0940	0.01035	0.111
MASY2	1.0 M	2	3.4061	0.1069	0.00966	0.103
MASY3	1.0 M	3	3.4198	0.1072	0.00837	0.089

Solutions were prepared with different molar concentration from 0.01 M to 1 M as listed in the Table 4.4.1. The number of repeated exchanges were changed with sample to sample as listed in the table. The elemental ratios were calculated for the X-ray fluorescence analysis.

10 g of three zeolites namely zeolite A, zeolite P and zeolite Y with a Si/Al ratio 1.12, 1.80 and 2.51 respectively were exchanged with each 300 ml of 1 M $Mg(NO_3)_2$ solution for three times using the similar procedure described in chapter 2 for ion exchange. The Si/Al ratio of the samples as obtained by XRF analysis for the powders designated as MASA3, MASP3 and MASY3 respectively are given in Table 4.4.2.

Table 4.4.2. Sample nomenclature and details for Si/Al variation

Sample name	Source	Si/Al (before exchange)	Conc. of Mg solution	No. of exchanges
MASA3	Zeolite A	1.12	1 M	3
MASP3	Zeolite P	1.80	1 M	3
MASY3	Zeolite Y	2.51	1 M	3

4.4.1.b.2. Consolidation and sintering

The powders of all samples were mixed with appropriate amount of binder PVA and dried. They were pressed into pellets and then sintered at various temperatures from 480 °C to 1350 °C as per the procedure given in chapter 2 section 2.1.4.

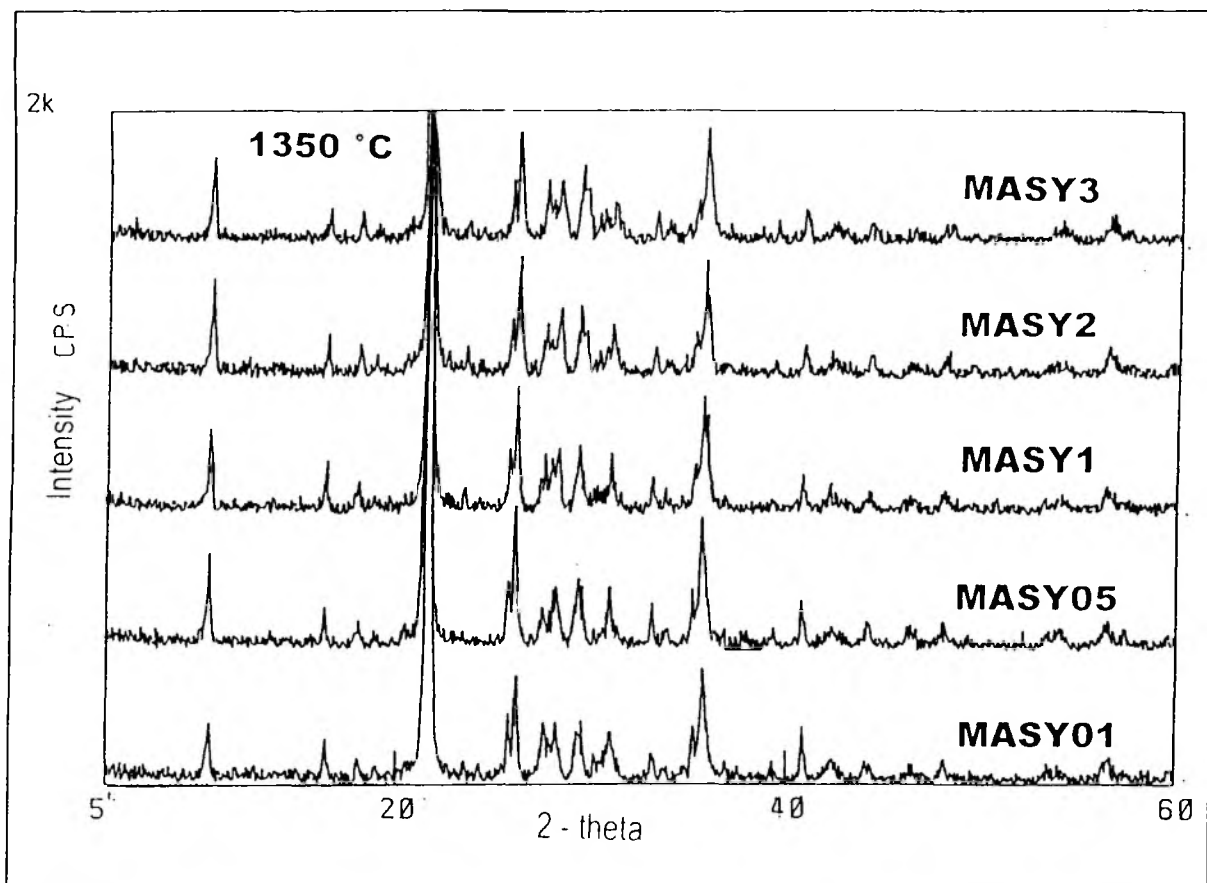


Figure 4.4.1. Multiple XRD plots of all the MAS samples heated at 1350 °C for 6 h.

The pellets were fired at different temperatures viz., (T2 =) 480, 700, 800, 900, 1000, 1100, 1200, 1300, 1350 °C in a programmable furnace at a heating rate of 4 °C/ min. The samples were heated at 580 °C (T1) for 180 min. (t2) to remove the binder. The samples were heated at higher temperature (T2) isothermally for 360 min. (t4) and cooled naturally (refer chapter 2, section 2.1.4. for more details).

4.4.1.b.3. Characterisation

The powder XRD patterns of the samples sintered at different temperatures were recorded. The phases were identified and matched with the JCPDS files. The semi-quantitative analysis of the various phases present in the samples heated at 1350 °C was carried out. The results are discussed in the following sections.

Densities of all the MASY samples heated up to 1350 °C were measured and the general trend of density changes with respect to the cation concentrations and Si/Al ratios were analysed. The density variation at various temperatures indicates the extent of densification. The shrinkage of the samples due to densification were measured and analysed.

4.4.1.c. X-ray based phase study

4.4.1.c.1. Effect of cation concentration on phase transformation

Figure 3.4.1 shows the multiple plot of XRD profiles for samples heated at 1350 °C of the precursors MASY01, MASY05, MASY1, MASY2 and MASY3. Table 4.4.1. shows the elemental ratios of each element present in the systems and the residual Na present in each sample. The phase estimations of the XRD profiles have been carried out.

Table 4.4.3. Various phases identified during the sintering of the sample with different Mg concentrations (JCPDS files with which the recorded XRD profile was compared, are given below)

Sample	Temperature (°C) and the phases formed							
	480	800	900	1000	1100	1200	1300	1350
MASY01	Zeolite Y	Zeolite Y	Zeolite Y AMORPH*	Mullite AMORPH* Silica	Mullite AMORPH* Silica	Mullite AMORPH* Silica	Mullite AMORPH* Cordierite Silica	Mullite AMORPH* Cordierite Silica
MASY05	Zeolite Y	Zeolite Y	AMORPH* Mullite	Mullite AMORPH* Silica	Mullite AMORPH* Silica	Mullite AMORPH* Silica	Mullite AMORPH* Cordierite Silica	Mullite Cordierite Silica
MASY1	Zeolite Y	Zeolite Y	AMORPH* Mullite	Mullite AMORPH*	Mullite AMORPH* Silica	Mullite AMORPH* Silica	Mullite Cordierite Silica	Mullite Cordierite Silica
MASY2	Zeolite Y	Zeolite Y	AMORPH* Mullite	Mullite AMORPH*	Mullite AMORPH* Silica	Mullite AMORPH* Cordierite Silica	Mullite Cordierite Silica	Mullite Cordierite Silica
MASY3	Zeolite Y	Zeolite Y	AMORPH* Mullite	Mullite AMORPH*	Mullite AMORPH* Silica	Mullite AMORPH* Cordierite Silica	Mullite Cordierite Silica	Mullite Cordierite Silica

AMORPH* - Amorphous phases

Phase	Formula	JCPDS file	Phase	Formula	JCPDS file
Mullite	$Al_6Si_2O_{13}$	150776	Cordierite	$Mg_2Al_4Si_5O_{18}$	130294
Silica	SiO_2	270605			

Table 4.4.3 shows the simplified and comprehensive results of the phase identifications along with the matching JCPDS files. As per the results, the overall phase transformation of MASY sample of different chemical compositions with respect to the cation concentration seems to be simple and the number of phases involved are less compared to that of LASY samples. It has been found from the semiquantitative estimation that silica (JCPDS 270605) is in low amounts (5 to 8 wt. %) and is almost same in all the samples

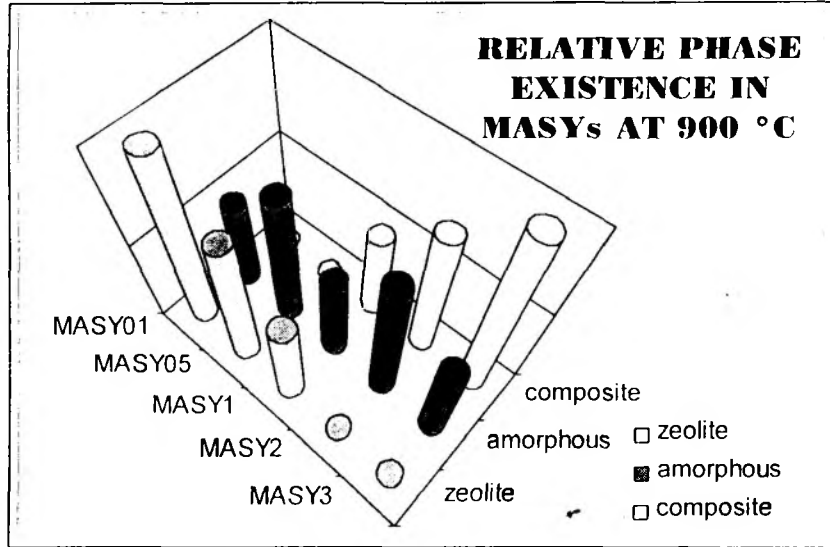


Figure 4.4.3. The schematic representation of the relative existences of the phases in various MASY samples at 900 degrees

heated at 1350 °C and this shows that the silica formation is not significantly influenced by Mg loading. Hence, it will be convenient to exclude the amount of silica for the further discussions. Apart from this, the key intermediate, mullite (JCPDS 150776) seems to be the only satellite phase and seems to be dominating in all these samples above 1000 °C.

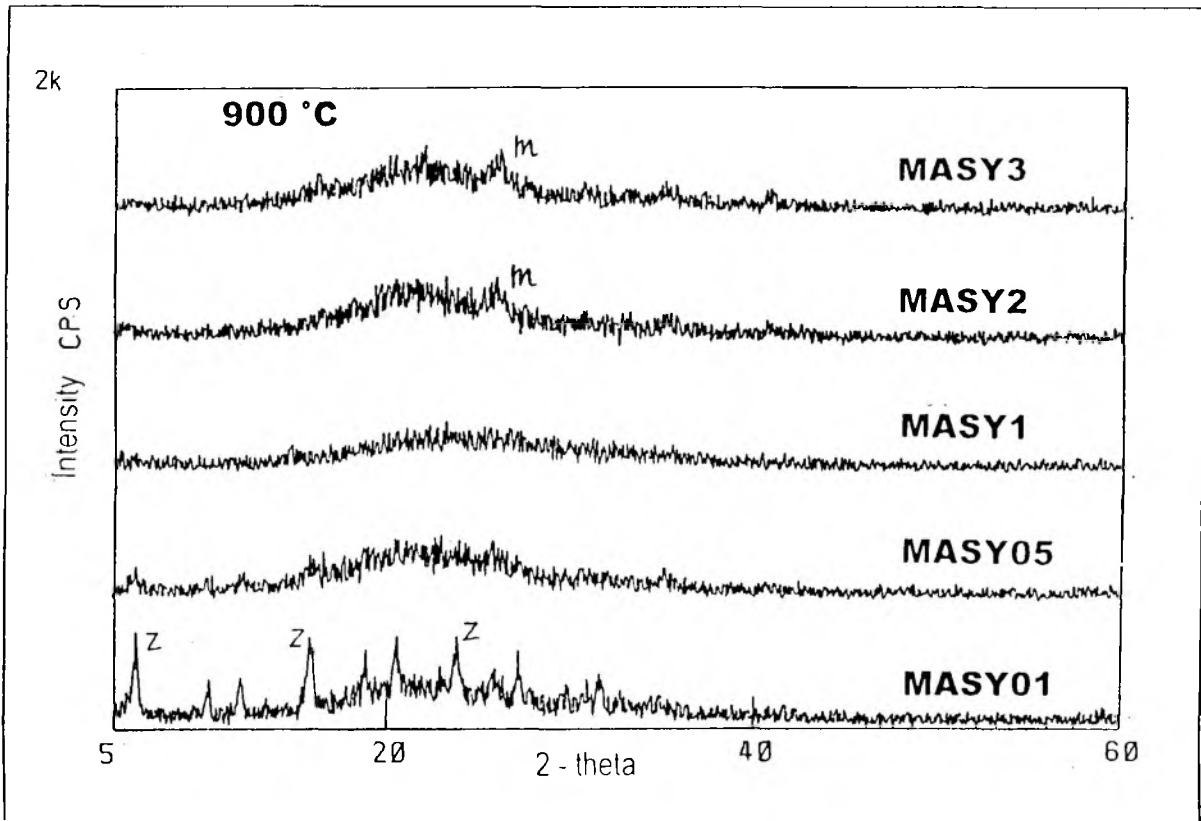


Figure 4.4.2. Multiple plot of different MASY samples at 900 °C. (z - zeolite ; m - mullite)

However, one can see the distinct change in the existence of the phases as the effect of cation concentrations. The starting material (zeolite Y) and the final products (mullite and cordierite – JCPDS 150776 and 130294 respectively along with low quantity of silica) are highlighted. It shows that at low cation concentrations (MASY01 and MASY05) the zeolite precursor's thermal stability is higher and so the structure collapse occurs at higher temperatures (900 °C) whereas the other three high Mg content samples start collapsing around 800 °C itself.

Similar results are seen at higher temperatures too. The final composite material (mullite and cordierite) is formed at relatively higher temperatures (1350 °C) for samples with low Mg content whereas the high Mg samples crystallise into the product at a lower temperature (1300 °C). However, as the amorphous window is observed as relatively longer for MAS system, two stages of temperature were selected to monitor the effect of cation. One is the collapse of the zeolite structure at 900 °C and the second temperature is 1100 where the recrystallisation occurs. Figure 4.4.2. shows the multiple plot of all MASY samples heated at 900 °C for 6 h.

At 900 °C, MASY01 shows the collapse of zeolite phase whereas MASY3 shows the formation of cordierite-mullite composite. This is a clear evidence that cation concentration has a strong effect on the ease of high temperature phase transformation of zeolite MAS precursors. The schematic illustration (Figure 4.4.3) shows the relative existence of different phases, which indicates the proportionate change of phases at 900 °C. This shows that the Mg cation concentration is directly proportional to the relative ease of the phase transformation in MAS

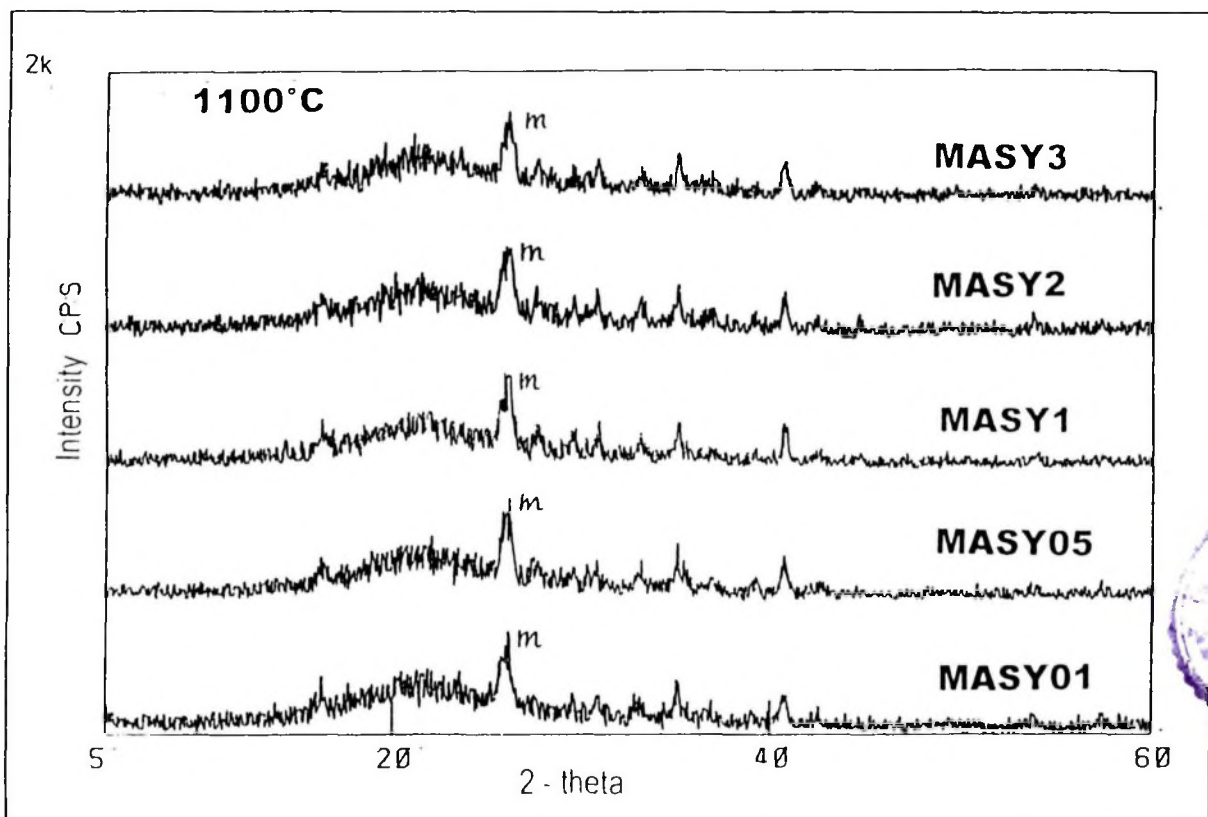
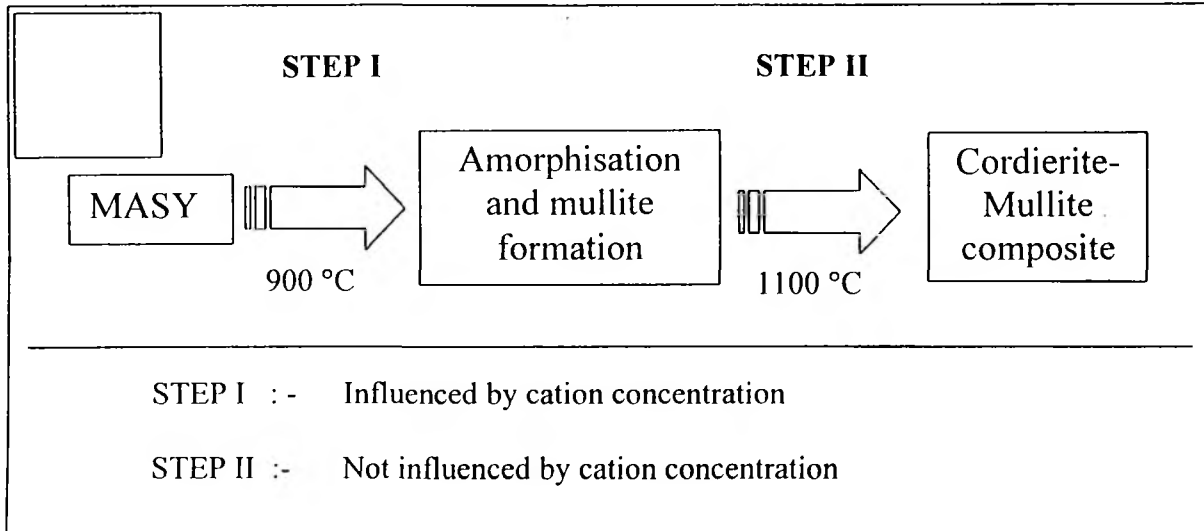


Figure 4.4.4. XRD multiple profiles of various MASY samples heated at 1100 °C. (m – mullite)

zeolite precursors, which is similar to that observed for LAS systems. However, this does not seem to have similar influence on the formation of the cordierite-mullite composite product at higher temperatures. Figure 4.4.4 shows the XRD multiple plots of all MASY samples, which are heated at 1100 °C for 6 h.



At 1100 °C the XRD of all MASY samples show the formation of the cordierite-mullite composite starts from the amorphous matter. This state of phase transformation is not showing any significant difference as a function of Mg concentration. It is clear from this that though there is a distinction in the phase status and the mullite formation which starts selectively in the higher Mg loaded sample MASY3 at a temperature of 900 °C. The formation of cordierite-mullite composite is not affected by the cation concentration variation. This is a typical example where the thermodynamics takes over the formation of the reaction products irrespective of the chemical stoichiometry. However, the semi-quantitative estimations show a trend as function of Mg concentration. Using the in-built Rigaku search-match facility, the semi-quantitative individual phase estimations were carried out on the XRD output of all MASY samples sintered at 1350 °C for 6 h. The results are as given in Table 4.4.4.

Table 4.4.4. The phase estimations of all MASY samples sintered at 1350 °C for 6 h. (excluding silica)

Sample Name	Heated up to, °C	Matching phases	Estimation, %
MASY01-1350	1350	Cordierite	71.0
		Mullite	29.0
MASY05-1350	1350	Cordierite	73.6
		Mullite	26.4
MASY1-1350	1350	Cordierite	73.4
		Mullite	26.6
MASY2-1350	1350	Cordierite	75.4
		Mullite	23.6
MASY3-1350	1350	Cordierite	76.6
		Mullite	23.4

Figure 4.4.5. shows a typical plot of the phase estimations (excluding silica) with respect to the MASY samples heated up to 1350 °C for 6 h. The cordierite formation is naturally enhanced by the increase in the Mg content where as the relative existence of mullite is decreasing. This result supports the discussion given in the earlier section 4.4.1.c.1. on influence of cation concentration on phase transformation. This study is relatively simple, due to the fact that the number of phases involved in MASY system are only two (excluding the low quantity of silica), unlike LASY (lithium aluminosilicates from Y zeolite precursors) systems.

4.4.1.c.2. Effect of Si/Al ratio

In section 4.4.1.b.1., Table 4.4.3. show the details of MAS samples prepared for the study of effect of Si/Al ratio on the sintering of the MAS systems and their phase transformations. The Si/Al ratios of these

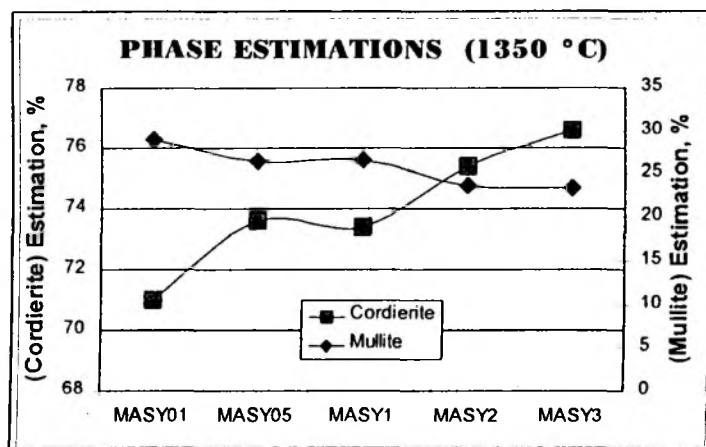


Figure 4.4.5. The relative existence of the phases in cordierite-mullite composite estimated by 'search-match'.

samples were analysed by XRF and are reported in the Table. The samples were heated at 1350 ° for 6 h and their XRD were recorded. Figure 4.4.7. shows the multiple plot of the XRD patterns recorded for the cordierite-mullite composites prepared by heating the zeolite precursors at 1350 °C. This shows almost similar patterns for all three samples. Table 4.4.5 shows the semi-quantitative estimations of the phases formed during the heating of MAS samples with different Si/Al ratios at 1350 °C for 6 h. The phases were identified and matched with the JCPDS files using the search-match facility of the Rigaku XRD software.

Table 4.4.5. MAS samples prepared with different Si/Al ratios

Sample	Source	Si/Al	Phases formed at 1350 °C	Estimations, %
MASA3	Zeolite A	1.12	Cordierite	79.1
			Mullite	20.9
MASP3	Zeolite P	1.80	Cordierite	78.5
			Mullite	21.5
MASY3	Zeolite Y	2.51	Cordierite	76.6
			Mullite	23.4

On heating the precursor at 1350 °C for 6 h. all the three samples form the mullite-cordierite composite. Though change in the estimated phase fractions of mullite and cordierite is not much significant, it is clear that as the Si/Al ratio increases the mullite formation is more pronounced. In other words, at low Si/Al ratio the cordierite formation is higher. The over all finding is that lower Si content with maximum Mg content enhances the formation of cordierite in the composite. The overall result of this study has been depicted schematically in Figure 4.4.6.

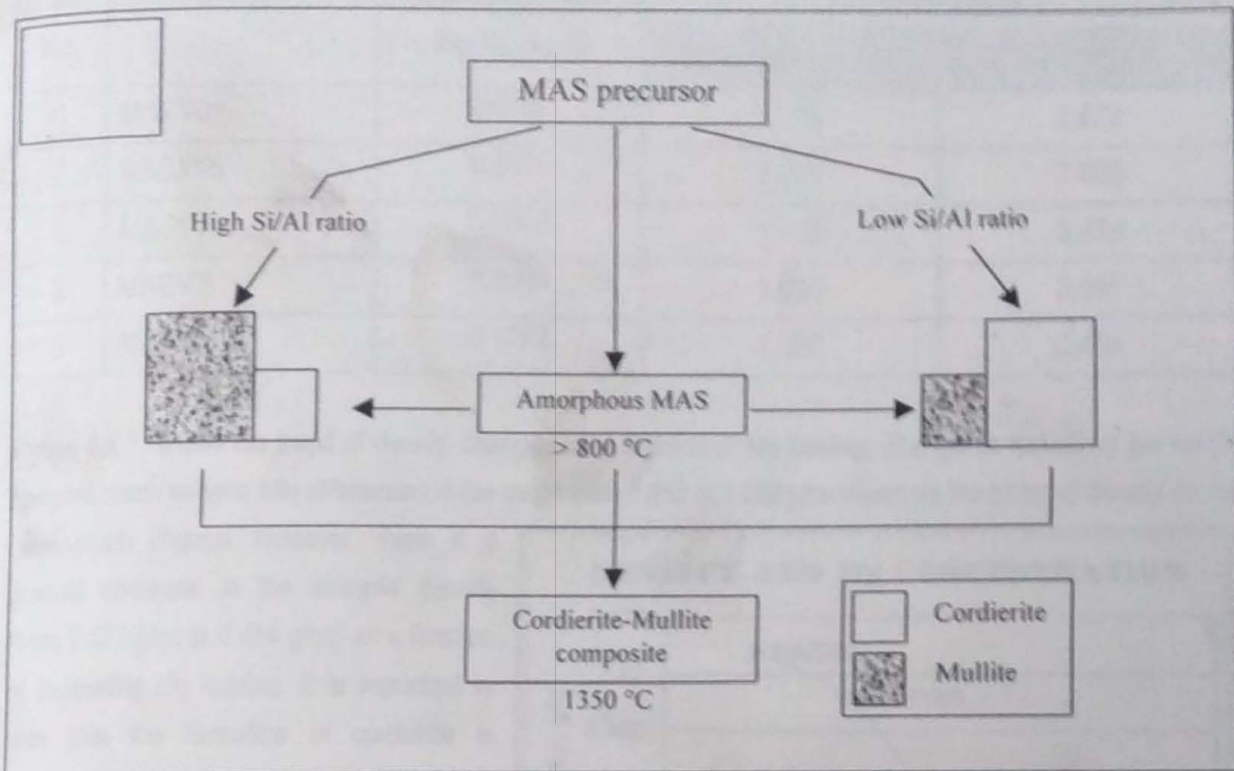


Figure 4.4.6. Influence of Si/Al ratio on the formation of cordierite-mullite composite

4.4.1.d. Density based study

4.4.1.d.1. Effect of cation concentration on density

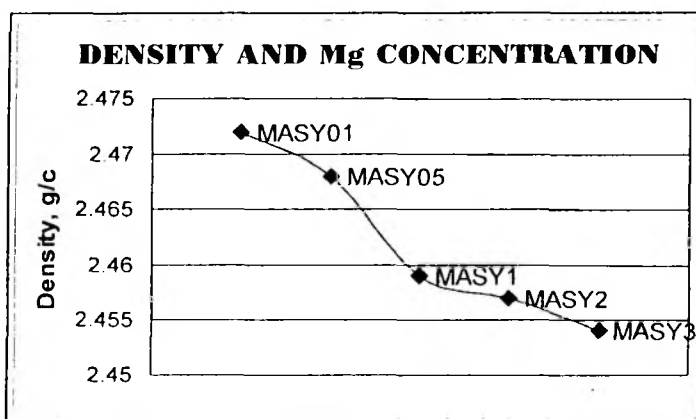
The difference between the green and sintered densities is an ideal index by which the sintering process can be judged. This part of the study is very important for all those applications that involve apparent density of the ceramic materials. Cordierite is a widely used material for structural application like catalyst support in catalytic converters²²⁻²⁴. Cordierite is a better alternative for the recent MEP industry as a substrate material²⁵⁻²⁶. These two are the current area of advanced application of cordierite where the density is a very vital selection parameter.

It is known that in the case of pure single phase, the density is dependent only on the synthesis procedure. However, for composite materials with more than one phase, the density is dependent on many variables. In the present system, MAS, though the cation concentration does not have strong influence on the temperature at which the cordierite-mullite composite forms it would be interesting to see whether the density of the composite have any dependence on the cation concentration. As it is known that the apparent density (ρ_{app}) of the final composite material is the effective value of the characteristic densities of individual phases, MAS system will not have many variables as it is observed that mullite is the only satellite phase along with the main phase cordierite. Table 4.4.6. shows the green and sintered densities (ρ_{app}) of the MAS samples with different Mg loading.

Table 4.4.6. Green and Sintered densities of LASY samples

Sl. No.	Sample	Elemental ratio Mg/Al, wt. %	Density, g/cc	
			Green	Sintered
1	MASY01	0.0790	1.238	2.472
2	MASY05	0.0814	1.201	2.468
3	MASY1	0.0940	1.119	2.459
4	MASY2	0.1069	1.020	2.457
5	MASY3	0.1072	1.062	2.454

Figure 4.4.7. shows the trend of density changes as a function of Mg loading. The green density of the MAS Y samples seem to have little differences in the range from 1.062 to 1.238 g/cc where as the sintered density do not have much change. However, there is a gradual decrease in the sintered density (from 2.472 g/cc to 2.454 g/cc) as a function of increasing Mg loading. It is important to note that the formation of cordierite is enhanced by the increase in Mg loading. The X-ray densities (from CRC Handbook of materials, 1985) of the individual phases present in the composites are given in the Table 4.4.7.

**Figure 4.4.7.** Influence of cation concentration on sintered ceramic density.**Table 4.4.7.** Individual phases formed on sintering of MAS Y samples and their x-ray densities

SJ. No	Name	Formula	Corresponding JCPDS file	Density _{x-ray} , g/cc
1	Mullite	Al ₆ Si ₂ O ₁₃	150776	3.166
2	Cordierite	Mg ₂ Al ₄ Si ₅ O ₁₈	130294	2.508

Since mullite has a higher X-ray density (3.166 g/cc) the reduction in mullite content as a function of increasing Mg content reduces the apparent density of the composite. Also the increase in the presence of the relatively lower density phase, cordierite (2.508 g/cc) as a function of Mg loading also accounts for the gradual decrease in the apparent density of the composite from 2.472 g/cc to 2.454 g/cc.

4.4.1.d.2. Effect of Si/Al ratio on density

Table 4.4.8. shows the sintered density of the cordierite-mullite composite formed at 1350 °C on heating the MAS samples varying with the Si/Al ratio. Comparing the X-ray densities of cordierite and mullite, mullite is a dense

phase, which is, formed more in the composite prepared by using the precursor with high Si/Al ratio. MASY3 has a high Si/Al ratio and hence the presence of mullite is more. This raises the apparent density of the composite to 2.454 g/cc. On the other hand, the low Si/Al ratio precursor forms a composite in which the cordierite phase is leading to a lowering in the density (2.151 g/cc)

Table 4.4.8. MAS sample with different Si/Al ratios and their ceramic densities

Sample	Si/Al	Phases present	X-ray density g/cc	Estimation	Sintered density, g/cc
MASA3	1.12	Cordierite	2.508	79.1 %	2.151
		Mullite	3.166	20.9 %	
MASP3	1.80	Cordierite	2.508	78.5 %	2.237
		Mullite	3.166	21.5 %	
MASY3	2.51	Cordierite	2.508	76.6 %	2.454
		Mullite	3.166	23.4 %	

4.4.1.e. Shrinkage based study

4.4.1.e.1. Effect of cation concentration on shrinkage

The percentage shrinkages of the MASY samples with different Mg concentrations, which are heated at various temperatures, have been calculated and listed in Table 4.4.9.

Table 4.4.9. Shrinkages measured for different MASY samples heated at different temperatures

Temperature, ° C	Samples & Shrinkages, %				
	MASY01	MASY05	MASY1	MASY2	MASY3
1000	13.6	14.46	15.01	15.12	15.63
1200	33.02	33.04	32.94	32.71	31.95
1300	33.07	32.94	32.56	32.38	30.42
1350	33.19	33.24	33.07	32.91	32.86

Figure 4.4.8.a shows the shrinkages of these samples plotted against the various temperatures. Though till 1200 °C all the samples show similar shrinkage patterns, above 1250 °C the shrinkage trend changes from sample to sample. To have a close view of these values the high temperature part of the plot has been given in Figure 4.4.8.b. Around 1300 °C the sample MASY3 (high Mg concentration) shows a coarsening phenomenon that is usually expected to be accompanied by a rapid phase transformation process. Also XRD patterns shows that though the mullite starts forming above 1000 °C, the cordierite formation occurs only around 1300 °C (reported temperature of phase transformation to cordierite is 1345 $\{\pm 5\}$ °C)²⁷.

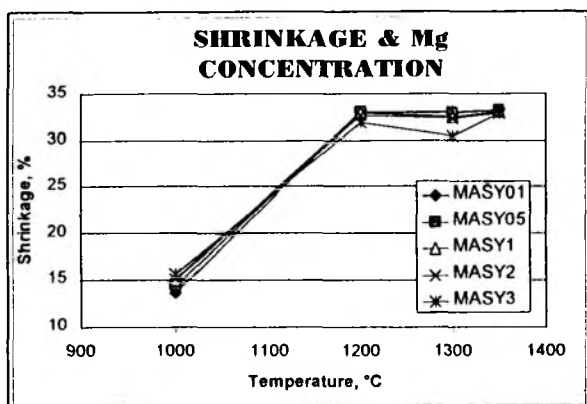


Figure 4.4.8.a. Shrinkage of MAS samples with different Mg concentrations at various temperatures

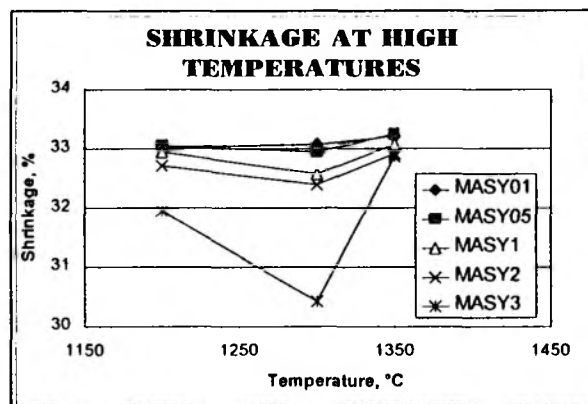


Figure 4.4.8.b. Shrinkage of MAS samples with different Mg concentrations at high temperatures (1200-1350)

As the Mg concentration increases the coarsening is an indication of the rapid formation of more cordierite. This is another clear indication for the influence of cation concentration on the phase formation. However, around 1350 °C the systems again shrink back to original trend line as the formed cordierite phase sinters to dense phase.

4.4.1.e.2. Effect of Si/Al ratio on Shrinkage

It is known that for any composite material, for instance the present system of interest, viz., cordierite-mullite composite, the shrinkage is based on the relative quantities of the phases formed and their individual shrinking as a result of high temperature treatment. The increase in the Si/Al ratio has resulted in the increment of mullite formation in this system as discussed in section 4.4.2.b. As mullite is relatively denser (3.11 g/cc) compared to cordierite a dense composite is formed with maximum shrinkage of 32.86 % (refer Table 4.4.10). Figure 4.4.9 shows the trend of shrinkage as a function of Si/Al ratio. Though high shrinkage is not a very attractive factor for the MEP application, a dense and highly shrunk composite is highly hermetic and hence is very ideal for the application in this view.

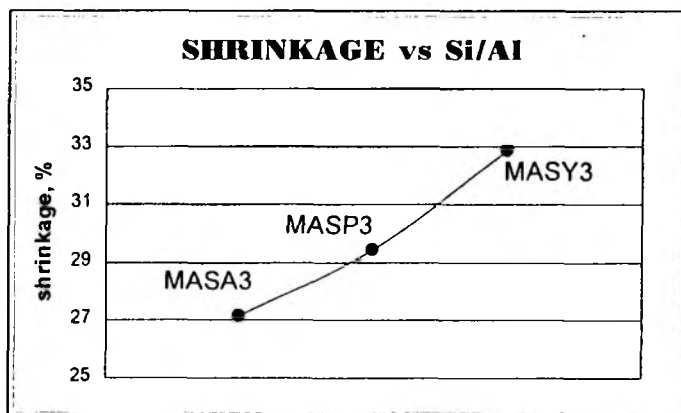


Figure 4.4.9. Effect of Si/Al ratio on shrinkage of MAS samples after heating upto 1350 °C for 6 h

Table 4.4.10. Shrinkage of MAS samples with different Si/Al ratio on heating upto 1350 °C

Sample	Si/Al	Shrinkage
MASA3	1.12	27.14
MASP3	1.80	29.44
MASY3	2.51	32.86

4.4.2. EFFECT OF SINTERING ATMOSPHERE

4.4.2.a. Plan of work

The section 3.4.2. of chapter 3 has described the various results of similar studies on LAS systems. The important finding is that in reduced atmosphere the number and quantity of side products are less and also in few cases there are possibilities for a single-phase formation. With that background information similar studies were tried on MAS systems. It was planned to study the sintering of MAS samples at different atmosphere. It was planned to carry out the sintering of three different MAS samples namely MASY3, MASA3 and MASY01. The results of MASY3 (high Si/Al ratio), MASA3 (low Si/Al ratio) were supposed to be compared to understand the variation of Si/Al ratio. The results of MASY3 (high Mg content) and MASY01 (low Mg content) were supposed to be compared to understand the effect of Mg loading.

4.4.2.b. Experimental

The samples MASY3, MASA3 and MASY01 (Table 4.4.1. and 4.4.2.) were sintered using the same heating program as followed for other samples but at different atmospheres. As per the reaction setup described in chapter 2, the sintering was carried out either in air and argon atmospheres. The flow rate was adjusted to 40 mL min⁻¹. The heating rate was fixed to 4 °C min⁻¹. The pellets of the samples were heated upto 1350 °C with a holding at 550 °C for binder removal and with a holding at 1350 °C for 6 h. The pellets were cooled naturally inside the furnace in respective atmospheres and crushed into fine powder using agate mortar and pestle. The powder XRD profiles were obtained for all these ceramic products and the phases were identified. The semi-quantitative phase estimations were carried out using the Rigaku search-match facility and the results were compared.

4.4.2.c. Results and discussion

Figure 4.4.10, Figure 4.4.11. and Figure 4.4.12 show the multiple plot of XRD profiles of the sample MASY3, MASA3 and MASY01 heated upto 1350 °C for 6 h. respectively.

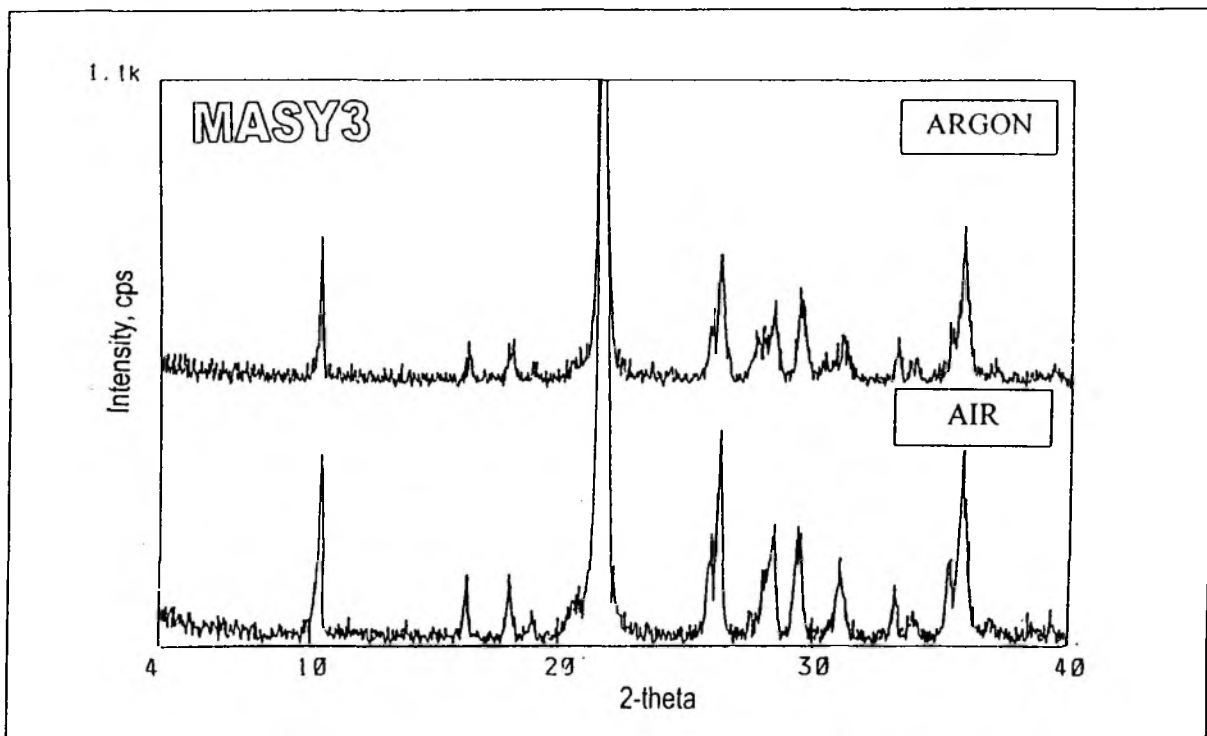


Figure 4.4.10. XRD multiple profile of MASY3 heated in air and argon atmosphere

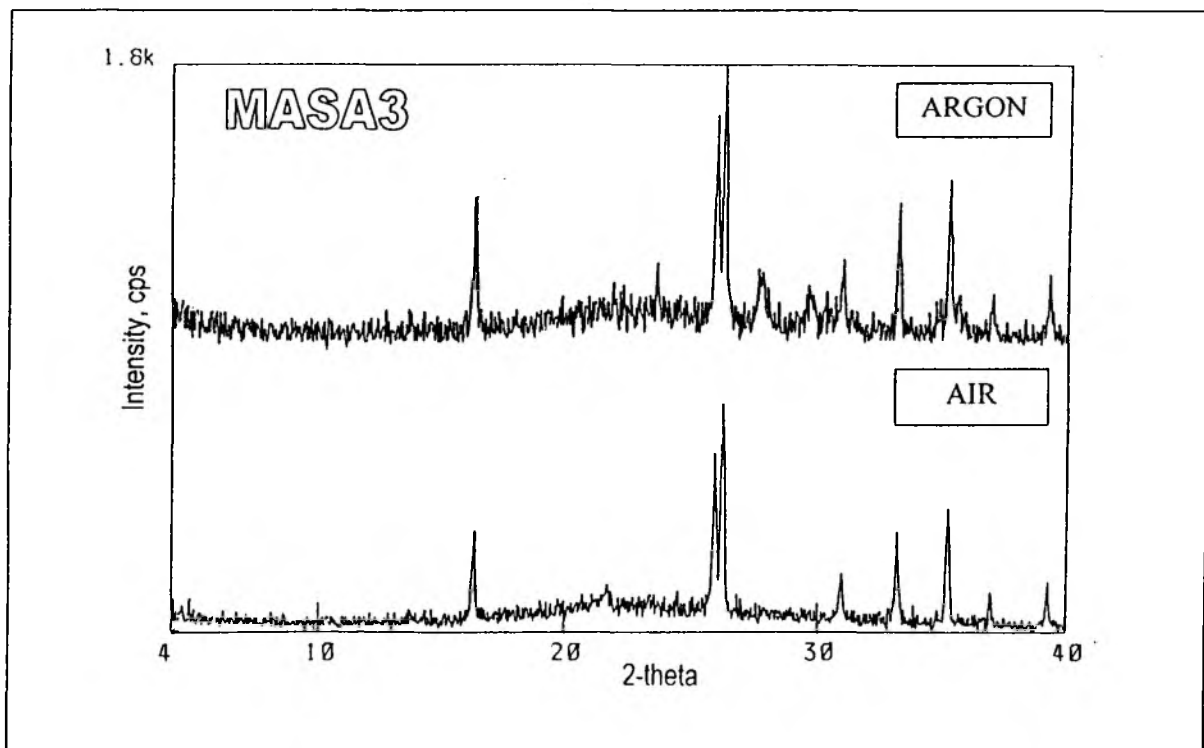


Figure 4.4.11. XRD multiple profile of MASA3 heated in air and argon atmosphere

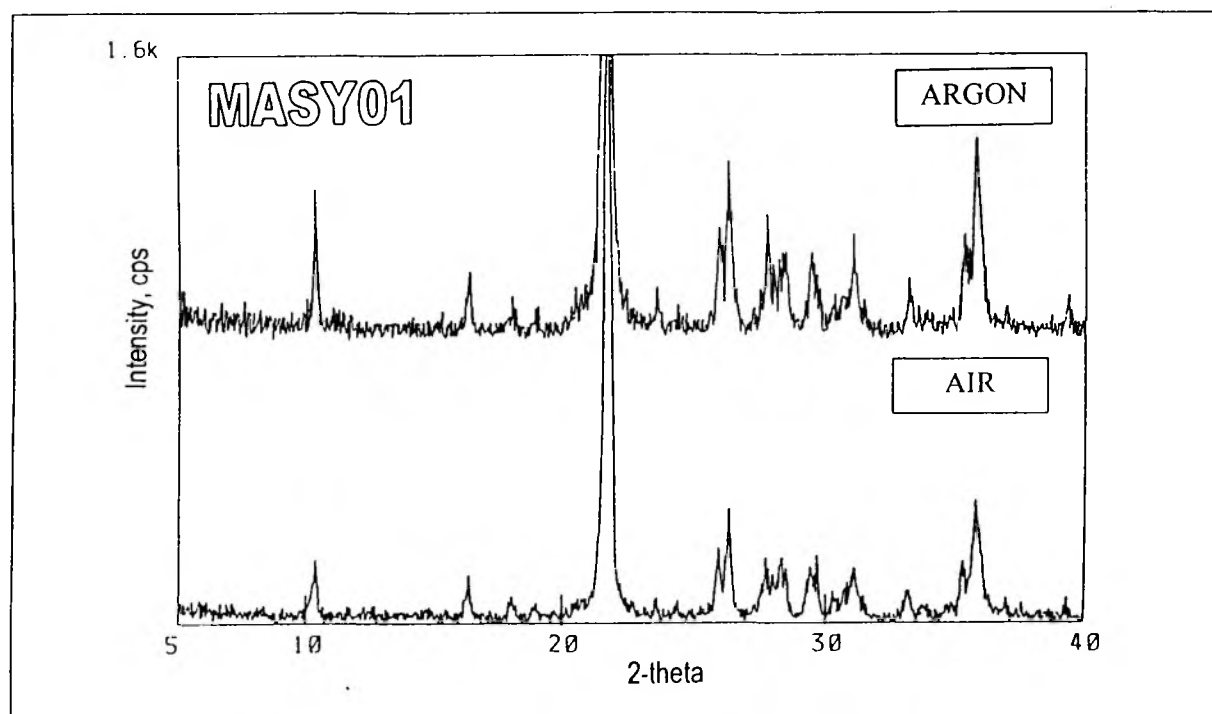


Figure 4.4.12. XRD multiple profile of MASY01 heated in air and argon atmosphere

The Figures include the XRD multiple profiles of samples heated both at air and argon atmospheres. The semi-quantitative phase analyses of all these XRD profiles were estimated and are given in Table 4.4.11.

Table 4.4.11. The semi-quantitative analyses of various phases formed during the different sintering of MAS samples in different atmosphere.

Sample	Zeolite source	In air (oxidative)		In argon (reductive)	
		Phase	Estimation, %	Phase	Estimation, %
MASY3	Y	Cordierite	76.6	Cordierite	73.8
		Mullite	23.4	Mullite	26.2
MASY01	Y	Cordierite	71.0	Cordierite	78.0
		Mullite	29.0	Mullite	22.0
MASA3	A	Mullite	100	Mullite	100

The effect of cation concentration on the different sintering studies at various atmospheres shows an unusual trend. While the oxygen-free argon atmosphere reduces the cordierite formation in the high Mg content sample (MASY3), it facilitates the formation of cordierite in low Mg content sample, MASY01. This indicates that the Mg content governs the cordierite formation whereas the available oxygen governs the mullite formation. Also to

some extent the Mg concentration does not influence the formation of mullite as mullite does not include any Mg in its structure.

Another interesting observation is that at low Si/Al ratio (sample MASA) in both oxidative and reductive atmospheres, only mullite (100 %) is crystallised at 1350 °C. As compared to the other samples and their phases, cordierite phase may form above 1350 °C which has not been checked during the current investigation. This suggests that high Si/Al ratio is needed for the formation of cordierite phases. As the results shows that the change in atmosphere does not have a same trend for samples with different Mg ratios (MASY3 and MASY01) further studies on few more samples with different Mg concentration may help in understanding the effect of atmosphere on this system.

4.5. CONCLUSIONS

One of the popular commercial magnesium aluminosilicate (MAS) materials is cordierite (– mullite composite) that could be prepared successfully through the zeolite precursor method during the present investigation. AC impedance spectroscopy is one of the advanced solid state analytical tools and has been tried for the characterisation of the MAS ceramic products and their electronic behaviour at various temperatures. Other techniques like TG/DTA, SEM, XRD have been used for the routine characterisation. The lattice parameters for the crystal structure of cordierite phase have been determined and found matching with the reported. The XRD results show that the phase transformation includes an amorphous phase around 900 °C. However, the phase remains amorphous upto 1200 °C followed by a slow formation of mullite. Supporting inferences were observed by the change in particle sizes using SEM. The shrinkage studies on MASY3 sample shows a single step shrinkage at high temperature around 890 °C with an over all shrinkage of about 32 %. This material has a relative density of 98 % that is very attractive for MEP applications along with this minimum shrinkage. The expansion study proves that this material can be exploited as a low expansion material in special applications like MEP and the TEC is matching the reported values for the similar material prepared by other routes. The low dielectric constant (7.5 at 1 MHz) observed for this material shows its immense scope in electronic industries.

The effect of measuring temperature on the electric conductivity of the cordierite-mullite ceramic composite (prepared from MASY3 after heating at 1350 °C) has been studied in the temperature range of 300-600 °C. The AC impedance spectra results show that as the temperature increases the total impedance reduces to nearly 10 fold. However, polarisation resistance has a negligible contribution to the total impedance as a function of temperature. This indicates that the contribution of electrical double layer capacitance to the total impedance of the system is negligible. The microstructure of the material has been visualised using a simple Randles model of equivalent circuits. The rate of decrement of the resistance and capacitance has been analysed.

An attempt has been made to understand the electrical conductivity in the material. With the fact that one of the characteristic features of the ionic conductivity of a solid electrolyte is its variation with temperature, the

conductivity changes of this material as a function of temperature were studied. The results show that the energy of activation (E_a) changes with the temperature. The energy values ($\{E_a (300 - 400 \text{ }^\circ\text{C}) = - 0.20 \text{ eV}\}$ and $\{E_a (400- 600 \text{ }^\circ\text{C}) = - 0.87 \text{ eV}\}$) calculated, have a significant difference for two different temperature ranges to prove that this characteristic dual trend is an indication of a possible ionic conductivity in the material. The reason for the dual trend in activation energy as a function of temperature has been explained using the Frenkel crystal model with interlattice positions and the dynamic equilibrium between the creation and recombination of Frenkel defects (vaccancies).

The second part of the chapter discusses the influences of different changes in the chemical composition of the precursor on the phase transformation processes at high temperatures and on density and shrinkage of the final phase assemblages. It is observed that the cation concentration influences the amorphisation of zeolite precursor around $900 \text{ }^\circ\text{C}$ where as the formation of cordierite-mullite composite is not influenced. Increase in the Mg loading increases the formation of cordierite and decreases the mullite formation. For precursor with low Si/Al ratio more cordierite is formed where as more mullite is formed for the one with high Si/Al ratio. The density measurement shows that the Mg loading facilitates a good sintering as it increases the density of the composite and the Si/Al ratio also increases the density. Shrinkage generally decreases with an increase in Mg loading where as increases with Si/Al ratio.

Sintering atmosphere has a peculiar effect on sintering of MAS samples. With low cation loaded sample, reduction atmosphere increases the formation of cordierite where as, with high Mg loaded sample the reduction atmosphere reduces the cordierite formation. Moreover with low Si/Al ratio sample like MASA3, mullite is formed as a single phase in both reductive as well as oxidative atmospheres.

“...Science seldom proceeds in the straightforward logical manner imagined by outsiders. Instead its steps forward (and backward) are often very human events in which personalities and cultural traditions play major roles”

- James Watson

REFERENCES

1. Selvaraj. K.; Ramaswamy. V.; Ramaswamy. A.V.; *Stud. in Surf. Sci. & Catal.*, 623, Vol. 113, (1998)
2. Pal, D.; Chakraborty, A. K.; Suchitra S; Sen, S. K.; *J. Mater. Sci.*, 31(15), 3995 (1996)
3. Sales, M.; Alarcon, J.; *J. Mater. Sci.*, 30(9), 2341 (1995)
4. Alvarez-E.; Fernandez, C.; *Span. ES 2034882 A1* 1 Apr (1993)
5. Naga, S. H.; Sallam, E. H.; Ibrahim, D. M.; *Interceram*, 43(4), 243 (1994)
6. *Advanced ceramics opportunities (RGB-208)*, Business Communications Co Inc, Norwalk, CT 06855, USA, Jul 1997
7. Nakagawa, Y.; Sawabe, Y.; Hamano, K.; *Taikabutsu*, 42(11), 678 (1990)
8. Sen, S.; Thiagarajan, S.; *Ceram. Int.*, 14(2), 77 (1988)
9. Risbud, S H.; Allen, G. D.; Poetzingler, J. E.; *Mater. Sci. Res.*, 21(Ceram. Microstruct. '86), 359 (1987)
10. Sano, S.; Koyama, T.; *Jpn. Kokai Tokkyo Koho*, JP 62078149 A2 10 Apr (1987)
11. Ikeda, N.; Emura, K.; Itabashi, M.; Hayashi, K.; *Nippon Kinzoku Gakkaishi*, 54(10), 1136 (1990)
12. Iwai, S.; Muramatsu, S.; Harayama, Y.; Gomyo, T.; *Jpn. Kokai Tokkyo Koho*, JP 01087555 A2 Heisei, 3 pp. 31 Mar (1989)
13. Choi, D. M.; You, J. K.; Lee, E. S.; *Yoop Hakhoechi*, 30(5), 381 (1993)
14. Macdonald, J. R. (ed.) *'Impedance spectroscopy emphasizing solid materials and systems'*, Wiley, NY, (1987)
15. Smith, A.; Baurndard, J.F.; Abelard, P.; *J. Appl. Phys.*, 65, 5119 (1989)
16. Christensen, B.J.; Coverdale, R.T.; Olson, R.A.; Ford, S.J.; Garbozi, E.J.; Jennings H.M.; Mason. T.O.; *J. Am. Ceram. Soc.*, 77, 2789 (1994)
17. Copper, E.A.; Meson. T.O.; *J. Am. Ceram. Soc.*, 78, 857 (1995)
18. Lidiard, A. B.; *'Ionic conductivity' in Handbuch der Physik*, Vol 20, S. Fligge (Ed.) Pringer Verlag, Berlin, (1957)
19. Lehfeldt, W. Z.; *Physik*, 85, 717 (1933)
20. Son, Y. B; Kim, C. H.; Jang, S D; Liu, J.; Sarikaya, M.; Aksay, I. A.; *Jpn. J. Appl. Phys., Part 1*, 33(2), 1101 (1994)
21. Ruedinger, B.; Fischer, R. X.; *Eur. J. Mineral.*, 9(6), 1257 (1997)
22. Hosonoya, M.; Kobayashi, N.; *Jpn. Kokai Tokkyo Koho*, JP 10244154 A2 14 Sep 1998 Heisei, 5 pp. (1998)
23. Fordham, R. J.; Oliveira, F. A.; Costa N. J. F.; Quadackers, W. J.; *Microsc. Oxid. 3, Proc. Int. Conf., 3rd Meeting Date 1996, 671*. Edited by: Newcomb, S. B.; Little, J. A. Institute of Materials: London, UK. (1997)
24. Suzuki, M.; *JETI*, 46(5), 56 (1998)
25. Wingefeld, G.; Aldinger, F.; *Ger. Offen*. DE 3923491 A1 24 Jan 1991, 7 pp. (1991)
26. Chance, D. A.; Goland, D. B.; Tong, H M.; U.S. US 5194196 A 16 Mar 1993, 12 pp. (1993)
27. CRC Handbook of materials, CRC Publishers, (1985)

COMPREHENSIVE SUMMARY AND FUTURE SCOPE

Chapter

5

5.1. INTRODUCTION

The preparation of electronic ceramic materials using zeolites as precursors is a novel approach by itself and in fact it is an incipient area of research. This method has been claimed for its wide range of advantages over the conventional way of ceramic preparations. However, the curiosity to understand the extent of these advantages and limitations if any, was the basic objective of the investigation. The commercial importance of the two dense phase systems, viz., LAS and MAS ceramics has given an extra-stimulus to select these two systems for the investigation. Exposing this field of research to the modern spectroscopic techniques and understanding the nature of the materials as well as the techniques are the two prime advantages gained by this research work. The present chapter presents a comprehensive summary of this dissertation and future scope of the research problem.

5.2. THE DISSERTATION WORK

In view of the idea that it would help in understanding the uniqueness of the present novel route from the conventional ceramic preparation routes, a basic introduction about the various processes that are involved in the preparation of precursor powder and ceramic fabrication has been given in the first chapter. The first chapter provides an overview of the global ceramic market and demands. It also describes the advantages of zeolite precursor over the conventional routes along with an introduction about MEP technology and zeolites. It briefs the present research problem along with the plan of work of the thesis.

The second chapter describes the methodology adopted for the preparation of precursor powder and the ceramic preparations. It gives the details of the materials that are used for the sample preparations. The last part of this chapter describes the principle and instrumental details about various characterisation techniques and the experimental conditions that are followed during the measurements. A theoretical introduction and details of instrumentation have been given for few of the new techniques such as AC impedance spectroscopy.

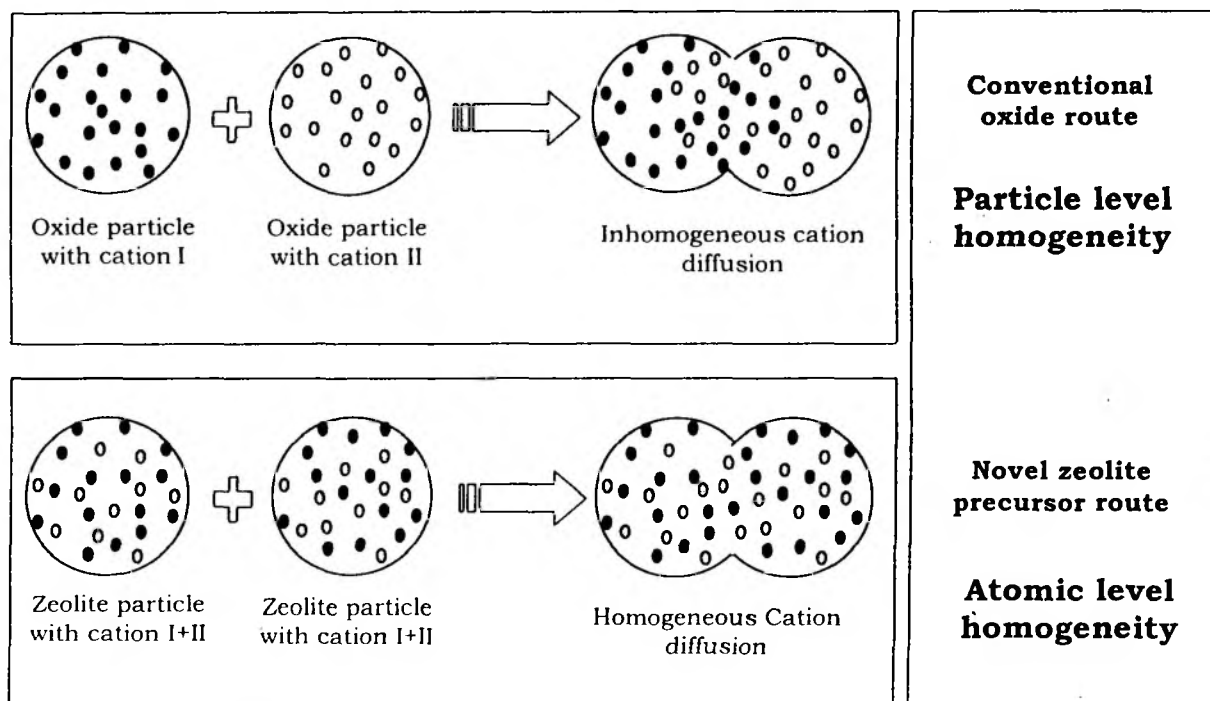
The third chapter of the thesis deals with lithium aluminosilicate (LAS) system. β -Spodumene ceramic samples were prepared using the powder of zeolite Na-Y that was exchanged with lithium after three ammonium exchanges (LASY3). Thermal stability and other transformations that are involved on heating were analysed by

TG/DTA experiments. The pellets of the PVA bound powder were heated to high temperature upto 1200 °C. The change in the nature of the sample at different temperatures was analysed using XRD and SEM. The particle size variations during the course of heating and lattice constants of the ceramic phase β -spodumene were determined and analysed. The dielectric constant, TEC, shrinkage and density of the final ceramic product prepared from powder sample LASY3 were determined. A multinuclear solid state NMR study, including for ^{27}Al , ^{29}Si and ^7Li nuclei on LASY3 samples heated at various temperatures was tried. The effect of cation concentration and Si/Al ratio of the precursor powders on phase transformations from zeolite to ceramic phase and on the density and % shrinkage of the final products were studied. A possible phase transformation mechanism and other findings are given in the end of the chapter.

Magnesium aluminosilicate (MAS) dense system has been studied in fourth chapter. Similar to LAS preparation, the Na-Y zeolite was exchanged with Mg nitrate solution to prepare MAS powder and other studies were carried out. Apart from the common characterisation techniques used, AC impedance spectroscopy, an advanced tool was employed to study the properties of the cordierite ceramic samples. The contributions by the possible individual components for the total impedance of the system were analysed. The most feasible nature of electrical conduction in the sample was predicted and the influence of temperature on the energy of (activation of) electrical conduction was also studied. The findings are summarised at the end of the chapter.

5.3. REALISATION

After a series of detailed studies as described in the previous chapters, few substantial concepts were realised. The process of ceramic preparation using zeolite as precursor is not only novel but also a competent route by which a variety of phase assemblages with different phase compositions could be prepared. The characterisation of the powder precursor shows that the powder has a small particle size with a narrow distribution, which is usually considered as one of the very important criteria for better ceramic fabrication. The premier ion exchange capacities of these zeolite powders offer an excellent way to alter the chemical composition of the precursor effectively. Compared to the literature reported, this route is found to have a facile phase transformation with relatively lesser impurity phases. This is due to the better chemical homogeneity of the precursor powder. The following scheme illustrates the concept of various levels of homogeneity that can be achieved by different ways of precursor preparation procedures.



This zeolite route gives an atomic level homogeneity, which reduces the transformation temperature to considerable extent. Hence, it is possible to think about the usage of inexpensive metals for making conducting patterns on MEP substrates, which is one of the today's most wanted demands and which is expected to bring down the cost of such products drastically. However, more systematic optimisations are needed to practically reach such levels of low temperature processability.

One of the distinct features of this route is the collapse of crystalline phase to an amorphous phase during the heat treatment of these precursors. It is interesting to observe that the formation and existence of this amorphous phase is dependent on the chemical nature of the precursor. For instance, LAS samples had a narrow amorphous region between 700 °C to 800 °C whereas MAS samples had a broad window from 800 °C to 1100 °C. This is due the nature and relative amount of the cation. Li is a highly mobile cation and fluxing action at high temperature reactions to minimise the sintering temperature. Mg, in that way is not a very mobile cation. One point is very clear that due to the valency difference of Li (1+) and Mg (2+), the ratio of the number of cations exchanged into zeolite Y will be 2:1 with respect to the cations Li and Mg respectively. As the relative amount of the cations available during the recrystallisation of dense phases from amorphous state is more for LAS than for MAS, LAS facilitates the solid state reaction at relatively low temperatures.

However, the crystallisation of the dense phases from the amorphous mixture does not appear to be simple. At this stage, if one considers the amorphous powder as a mixture of (three) individual oxides of Si, Al and Li or Mg as the case may be, all the metastases of the respective ternary phase formations are possible. Also, the individual single component systems as SiO_2 , Al_2O_3 and Li_2O or MgO , as the case may be, can have its own internal transformations. For e.g., SiO_2 usually has many such processes namely quartz inversion, inversion of

cristobalite, inversion of tridymite and conversion of quartz at different temperatures. Consequently, these kind of processes increase the complexity in understanding the simultaneous transformation mechanisms of the systems like the ones, which are presently studied during this investigation. However, it was attempted to understand the phase transfer mechanism of LAS high temperature reactions. The high-quartz to keatite conversion has been identified by the XRD reflections as a most possible mechanism, which in turn goes to virgilite and finally to β -spodumene phase. This result indicates that many such studies could yield more information to understand the mechanism.

The understanding about the mechanistic pathway helps to predict the properties of the final ceramic product. To cite an instance, the intermediate phase formed during a heat treatment has a direct impact on the particle shape and the formation of porosity, which eventually decides the density of the product (for e.g., density varies with the different amounts of mullite phase formed in various MASY samples. Refer Table 4.4.4. and Figure 4.4.7. in chapter 4). The pores and grain boundaries are responsible for their characteristic reflections on the property of the material as they form the so-called 'microstructure'. Its strong influence on the electrical conductivity and the dielectric constants (DEC) is well known. However, the DEC values of the ceramic materials prepared using this method are found to be lower and hence these materials are useful in MEP applications. Another conspicuous point is that the ceramic materials formed were having a very high relative density (as good as 98 %). Because, achieving high bulk density has been one of the major problems^{1,2} usually faced during many ceramic preparations (for e.g., using clay precursors like kaolin).

Enhancing the qualification of these materials for MEP application, the TEC studies show that these ceramic materials prepared using zeolite precursors have a relatively lower thermal expansion, which is matching with that of silicon. However, the TEC measurements at higher measuring temperature range (above 400 °C) would give more details about it which was not possible during the course of the present study due to instrumental limitations.

The ability of NMR spectroscopy has been well realised by the multinuclear NMR studies carried out on the LAS samples. The NMR results support the other observations like the ones from powder XRD. The shift of the ²⁹Si bands from -106 ppm towards the upfield in the range of - 87 ppm clearly indicates that the Si environment is changing from the typical Q⁴ (zeolite) to Q¹ and Q² (chain and ring) type which is typical for dense phase systems like mullite and quartz. There is a distinct band split at high temperatures (>1000 °C) for the LAS dense phases along with cristobalite type of environment. The ²⁷Al spectra shows a third band around 23 ppm indicating a distorted tetrahedral environment (A1*) apart from the regular octahedral (M1) and tetrahedral (M2) environments. The regular quadrupolar features were suppressed and not seen in ⁷Li quadrupole spectra indicating the nullifying dipolar interactions between Li and Al quadrupolar nuclei. However, the resolution of the spectra could be further improved by increasing the spinning speed of the sample rotor (e.g., above 10 kHz or more) to distinguish the individual bands clearly so that the overlapping peaks can be identified and correlated well.

Many reports are found in literature about the novel materials for the applications in gas and temperature sensors. Even zeolites being porous materials have been tried for this application³. However, mechanically strong and thermally stable porous as well as dense ceramics are preferred for many reasons⁴⁻⁵. As one of the preliminary screening tests, usually the nature of electrical conductivity is checked for the material. The current investigation includes such an attempt on the cordierite ceramic sample prepared from MAS₃ powder. The result suggests that the conductivity of the material is ionic type. Further studies in this area may extend this concept of employing this type of stable ceramic materials in sensor applications. Literature shows that cordierite has been tried earlier for this kind of application⁶.

It is well known that mainly the number of phases and the quantity of each present in the sintered ceramic body decide many of these properties. The semi-quantitative phase estimations carried out on LAS and MAS materials reveal a strong and sharp influence of the chemical nature of the precursors. However, the overall observation leaves few points to our perception. The cation (Li^+ or Mg^{2+} as the case may be) concentration level in the precursor powder has a direct impact on the ease of phase transformation reactions. High cation concentration reduces the phase transformation temperature to considerable extent. High cation concentration increases the yield of the desired major ceramic phase (β -spodumene in the case of LAS and cordierite in case of MAS). However, the nature of the cation has a specific influence on the width of the temperature window at which the amorphous phase exists. Precursor composition with highly mobile cation (like Li^+) crystallises into dense phase at relatively lower temperatures.

It is observed in both the systems that the density of the ceramic product goes down with the increase in the cation concentration of the precursor and the reason is that in both the cases, the prominent side product is mullite. Mullite is denser than the desired LAS or MAS phases and it is formed more when the cation concentrations are low. Hence, the density of the total system is low at high cation concentration levels, as the extent of formation of relative lower density LAS or MAS phases increases. However, the shrinkage increases along with the cation concentration.

A swing in the relative formation of mullite and silica was observed when the Si/Al ratio of the precursor is changed. At a situation where the Si content in the precursor is high, silica is formed more than mullite and this increases the density and % shrinkage and vice versa. This kind of variations in relative existence of the phases helps to alter the properties of the ceramic materials for specific applications. This may reflect on the other properties also like thermal expansion coefficient and the thermal conductance.

5.4. LIMITATION

Though this novel ceramic route using zeolite precursors offers many advantages, there are few limitations too realised during the course of the work. The non-framework cation loading through ion exchange has a maximum limit for a given zeolite-cation pair. It is the limiting equilibrium that puts constraint to reach the proper stoichiometry in some cases. However, this can be encountered to some extent by choosing the ratio of the other two components viz., Si and Al. On academic interest, if one wants to study the phase formation at extreme (too low or too high) levels of individual components viz., SiO₂, Al₂O₃ and Li₂O or MgO, these precursors may not support. The modification of chemical composition of all three components becomes difficult if once the system is set or exchanged for ions. For instance, lowering the Si content of a given zeolite is not as easy as to lower the Li content. However, the zeolite source could be chosen with the desired Si/Al ratio.

Many zeolite preparations usually involves the usage of alkali hydroxides (like sodium hydroxide) to achieve and maintain high pH level (as high as pH =12) for zeolite crystallisation. This sodium is exchanged with the desired cation later as per the stoichiometric need. However, the zero Na level is not possible by ion exchanges in many cases. As the presence of Na, according to literature, disturbs the phase transformation by inducing pre-matured sintering before the completion of high temperature reaction or crystallisation of dense phase, Na removal becomes very important. According to the literature, the safe Na level may be less than 15 ppm. This leads to more number of ion exchanges on the precursor powder. However a possible alternative has been suggested in the following sections. Compared to the conventional oxide route, this route seems to be more time consuming as the preparation of the powder involves series of ion solution phase exchanges, handling of slurry and filtration.

5.5. UPDATE OF THE FIELD

Though the present work was started in the end of 1994 with availability of minimum references in literature, during the course of the present investigation, few reports appeared in the related area from other research groups.

Hoghooghi and coworkers worked on the development of near-net shape forming of celsian-ceramics using zeolite precursors⁷. A ceramic composite consisting of gahnite (ZnAl₂O₄) crystallites in an amorphous sodium aluminosilicate matrix from zinc exchanged zeolite-A precursor was reported by Coyler and coworkers⁸. He has reported ²⁷Al NMR characterisation of the materials. Later, he reported an in situ study of ceramic formation from Co²⁺ and Zn²⁺ exchanged zeolite-A using combined XRD/XAFS techniques⁹. However, the idea about large-scale preparation from natural resources was a constant drive for many researchers. In 1995, a spanish research group reported the possibilities of such exploitation from natural zeolite rocks. The sintering, electrical and mechanical properties of ceramic materials prepared from Cuban natural zeolite minerals were studied and reported¹⁰. The possibilities of using natural zeolite for synthesizing ceramic pigments were investigated by Pogrebenkov and coworkers¹¹.

It is very interesting to see the analogues of branches started in this area of research. Dondur and coworkers have reported the crystallisation kinetics of the dense phase, hexacelsian, from the amorphous phase prepared by heating the ion exchanged zeolite powders¹². The ceramic materials prepared by zeolite route have got applications in multiple directions. For instance, a process for manufacturing of the zeolite ceramics, useful for control of Escherichia coli (including enterohemorrhagic E. coli), soil microorganisms in water has been patented in Japan¹³. The possibility of obtaining ceramic facing tiles based on natural zeolite in combination with calcium-magnesium materials (diopside, wollastonite, tremolite) has been reported by Pogrebenkov and coworkers¹⁴. Si_3N_4 is another system, which has been at high demand in advanced ceramic industries. The synthesis of combination of this material along with celsian has been tried using zeolite route very recently and reported¹⁵.

5.6. FUTURE SCOPE

It has been really a problem to reduce the residual Na level in the precursors even by multiple ion exchanges. To overcome this problem, the idea of synthesizing the zeolite itself in sodium free conditions can be thought off. For instance synthesis of zeolite A in presence of cation like Li has been already reported. Perhaps, the ceramic produced from this powder could be expected to form highly pure single spodumene phase. Solid state ion exchange technique, which is believed to be a better process in some cases, may also be tried to increase the extent of cation exchange.

Many new combinations of zeolites and cations could be tried to produce different assemblages of phases with improved properties of ceramic products. The phase transformation discussion in the present work is all based on the XRD recorded for the samples that are heated at different temperatures, cooled to room temperature and then crushed into powder before the scanning. Hence the temperature we mention here are not the real temperature that was being felt by the sample during the course of XRD scanning. Hence, an in-situ high temperature XRD study will give a clear picture about the actual and accurate temperature at which the phase transformation and other changes occur. In addition this will reduce the time of phase transformation study to a large extent.

The AC impedance studies on these materials can be extended to follow up the sintering process and the results can be improved after further optimisation. The details about the gradual change in the microstructure of the precursor powder during the course of sintering and phase transformation processes could be acquired if the spectra are taken for samples heated at different temperatures which was in fact the original aim of the present work.

The new emerging field of microwave sintering can be tried on these precursor powders so that the energy or temperature required for sintering might be reduced and also, it may change the phase transformation mechanism. Shrinkage and dilatometric measurements can be carried out for samples with different cation

concentrations to study the influence of cation concentration on the sintering (by shrinkage) and TEC (by dilatometry). High-resolution solid state NMR with enhanced speed of sample spinning can be used for the characterisation of these materials to confirm the phase transformation mechanism. Many such studies in future may improve this special route of ceramic preparation and the quality of the products.

This area of research could be apprehended as an extra dimension of the versatility of zeolites by a zeolite chemist or as a search for new raw materials to prepare improved ceramics by a ceramist. However, one point is clear that this field of research will keep going ahead for several decades as we anticipate its potential scope.

May these materials be called in future as '**zeomics**' meaning ceramics from zeolites?

"...I do not know what I may appear to the world, but to myself I seem to have been only like a boy playing on the sea-shore, and diverting myself in now and then finding a smoother pebble or a prettier shell than ordinary, whilst the great ocean of truth lay all undiscovered before me"

- Newton

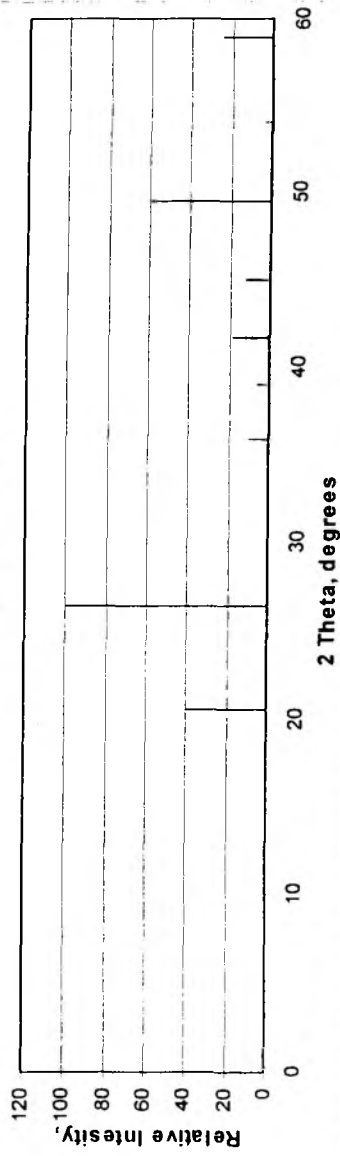
REFERENCES

1. Mortel, H.; Schwinka, V.; Cimmers, A.; Lindina, L.; Schwinka, R.; *Key Eng. Mater.*, 132(Pt. 3, Euro Ceramics V), 2139 (1997)
2. Rahaman, M. N.; Hu, C. L.; *Mater. Manuf. Processes*, 8(4-5), 475 (1993)
3. Osada, M; Sasaki, I; Nishioka, M; Sadakata, M; Okubo, T.; *Microporous Mesoporous Mater.*, 23(5-6), 287 (1998)
4. Lozinski, A; Wierzba, H.J.; *Proc. SPIE-Int. Soc. Opt. Eng.*, Volume Date 1995, 2634 59-62 (1995)
5. Iwahara, H.; Hibino, T.; *Proc. - Electrochem. Soc.*, 93-7(Proceedings of the Symposium on Chemical Sensors II, 1993), 464 (1993)
6. Yamada, K.; Asai, M.; Kamiya, N.; *Jpn. Kokai Tokkyo Koho*, JP 10030908 A2 3 Feb 1998 Heisei, 9 pp.
7. Hoghooghi, B.; Mckittrick, J.; Butler, C.; Helsel, E.; Lopez, O.; *Mater. Res. Soc. Symp. Proc.*, 346 (Better Ceramics through Chemistry VI), 493-8 (English) (1994)
8. Colyer, L, M.; Greaves, G. N.; Dent, A. J.; Carr, S. W.; Fox, K. K.; Jones, R. H.; *Stud. Surf. Sci. Catal.*, 84 (Zeolites and Related Microporous Materials, Pt. A), 387, (1994)
9. Colyer, L. M.; Greaves, G. N.; Dent, A.J.; Fox, K. K.; Carr, S. W.; Jones, R. H.; *Nucl. Instrum. Methods Phys. Res.*, Sect. B, 97(1-4), 107 (1995)
10. Hernandez V. M.; Raymond H. O.; Alvarado M. A.; Jacas R. A.; Roque M. R.; *J. Mater. Sci. Lett.*, 14(23), 1653 (1995)
11. Pogrebenkov, V. M.; Sedel'nikova, M. B.; Vereshchagin, V. I.; *Glass Ceram.*, 55(1-2), 55 (1998)
12. Dondur, V.; Tomasevic C. M.; Kremenovic, A. D. J.; Dimitrijevic, R.; *Phys. Chem. '98, Int. Conf. Fundam. Appl. Aspects Phys. Chem.*, 4th, 395-397. Eds., Ribnikar, S.; Anic, S.; Society of Physical Chemists of Serbia: Yugoslavia. (1998)
13. Mori, K.; Sato, K.; *Jpn. Kokai Tokkyo Koho* JP 11000387 A2 6 Jan 1999 Heisei, 4 pp.
14. Pogrebenkov, V. M.; Mel'nik, E. D.; Vereshchagin, V. I.; *Glass Ceram.*, 55(1-2), 19 (1998)
15. Boskovic, S.; Kosanovic, D.; Dondur, V.; Dimitrijevic, R.; *Ceram. Int.*, Volume Date 2000, 26(1), 33 (1999)

APPENDIX

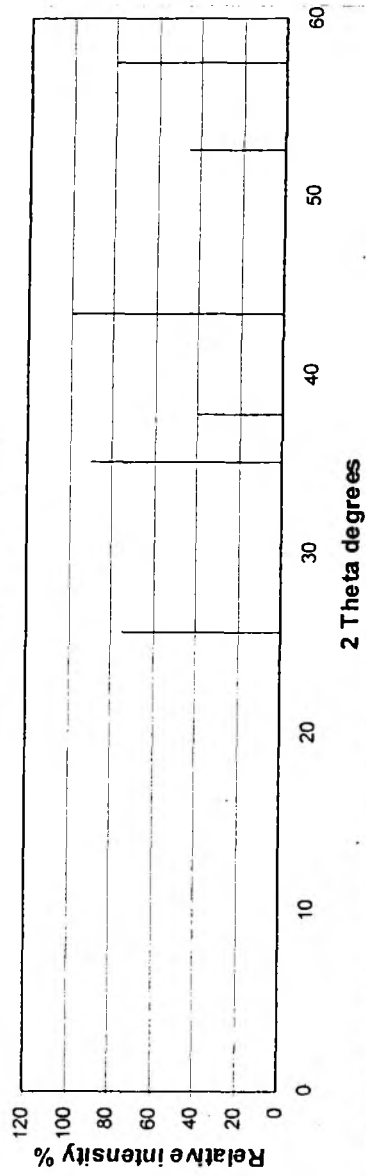
This appendix contains the JCPDS - XRD profile data of various phases observed both in LAS and MAS systems during the course of the present investigation. The titles are given according to the names of the phases used in the text. The JCPDS file names are given in parentheses next to the title along with the formula. The XRD reflections are given in the order of the decreasing relative intensities (I/I_0) with corresponding $2 - \theta$ in degrees.

Silica (HQ) (SiO₂) 120708



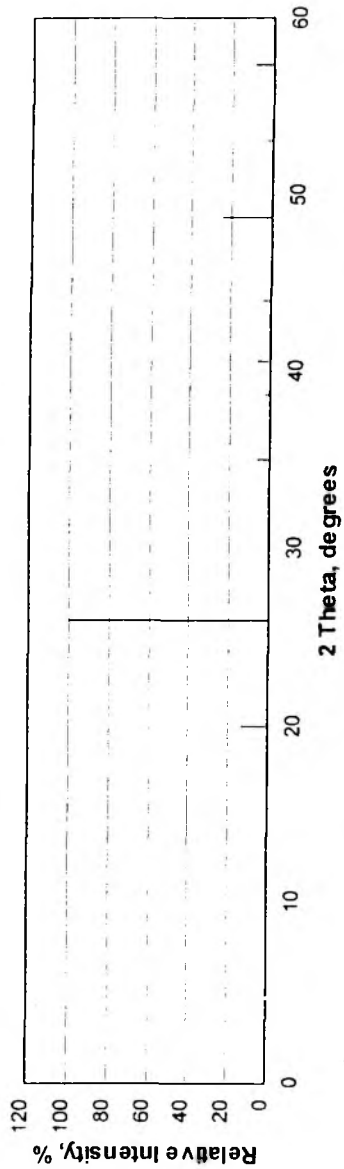
<u>2 Theta</u>	<u>I/I₀</u>
26.358	100
49.448	60
20.498	40
67.152	35
58.868	25
66.517	20
41.692	18
45.016	12
35.890	10
39.059	6

Alumina (Al₂O₃) 100173



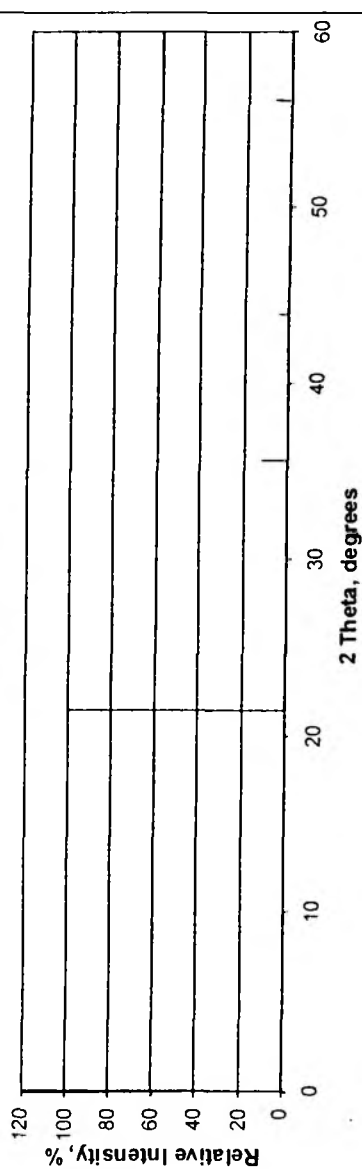
<u>2 Theta</u>	<u>I/I₀</u>
43.397	100
35.148	90
57.555	80
25.543	75
68.214	50
52.577	45
37.750	40
66.517	30
76.865	16
95.236	14

Virgilite-SS (Li_xAl_xSi_{13-x}O₆) 310707



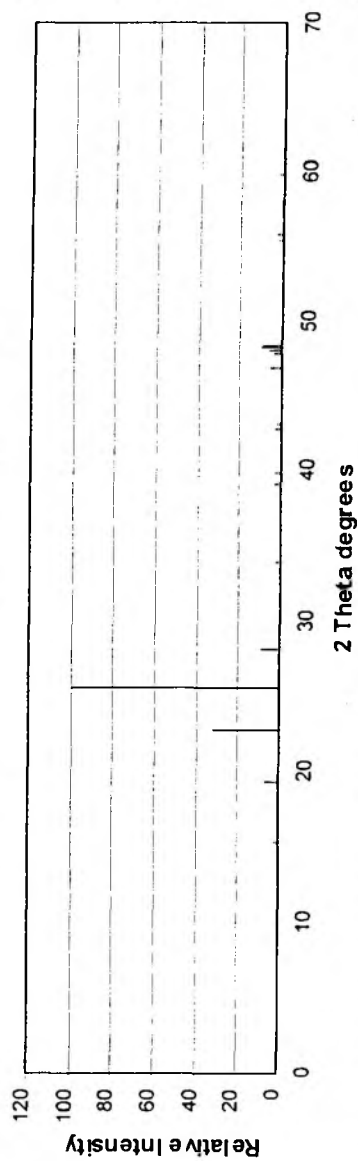
2 Theta	I/I ₀
25.905	100
48.672	25
19.960	13
57.353	9
66.306	9
34.963	6
40.561	6
65.255	6
79.595	6
43.967	4

Silica (C) (SiO₂) 270605



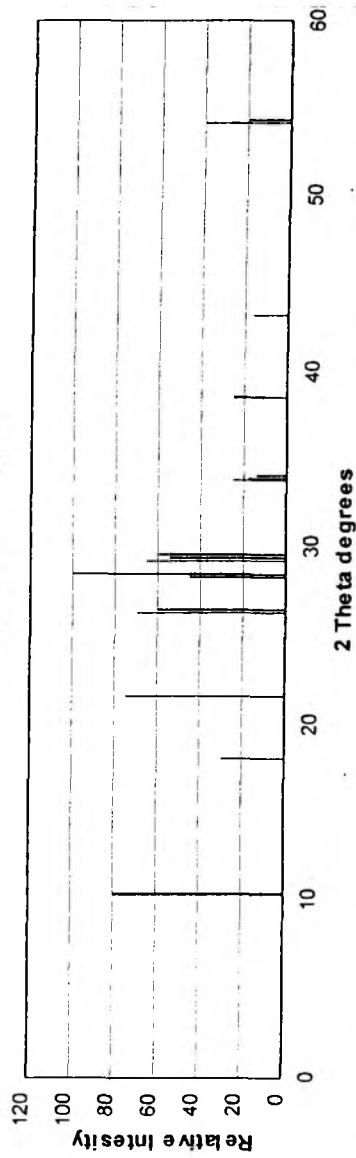
2 Theta	I/I ₀
21.575	100
35.611	12
56.149	7
63.898	5
43.967	4
79.595	3
68.321	2
75.296	2
86.190	2
41.975	1

β -spodumene (LiAlSi₂O₆) 350797



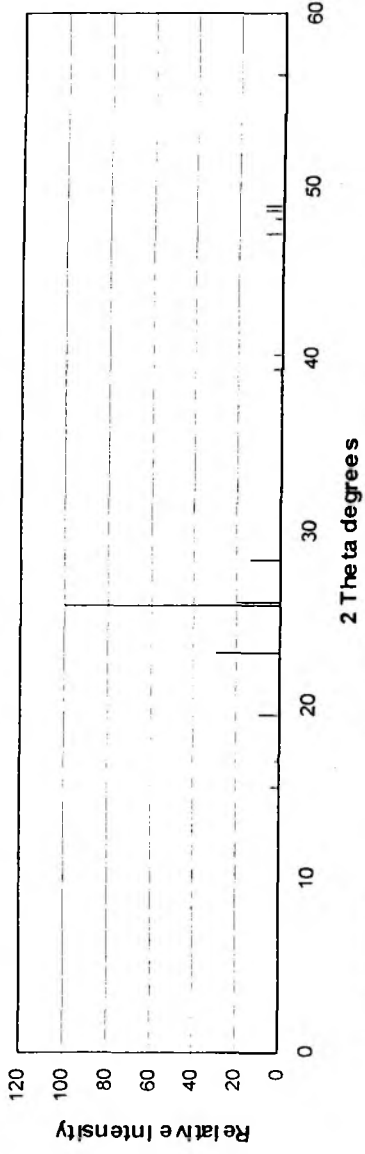
2 Theta	I/I ₀
25.543	100
22.745	32
48.284	10
28.174	9
48.381	9
19.244	7
47.994	6
46.838	5
47.801	4
39.059	3

Cordierite (Mg₂Al₄Si₅O₁₈) 120303



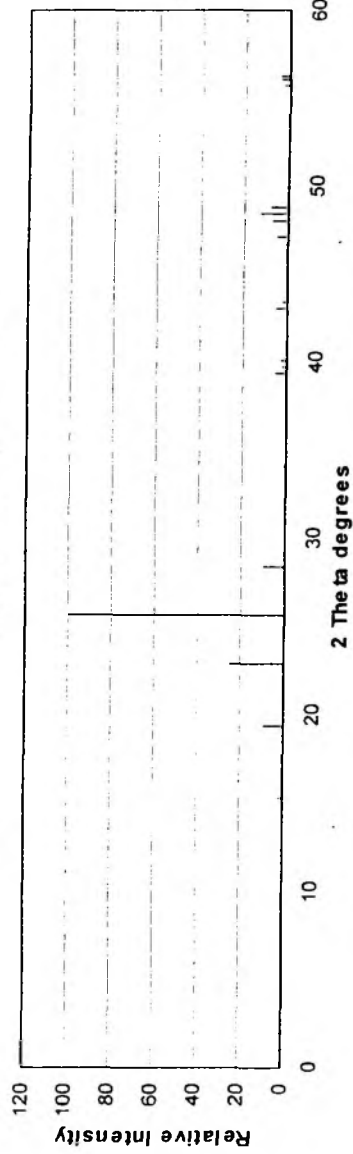
2 Theta	I/I ₀
28.448	100
10.341	80
10.430	80
21.665	75
26.267	70
29.268	65
26.449	60
29.633	60
29.450	55
28.265	45

Lithium Aluminosilicate (Li₆Al₆Si_{2.4}O₆) 210503



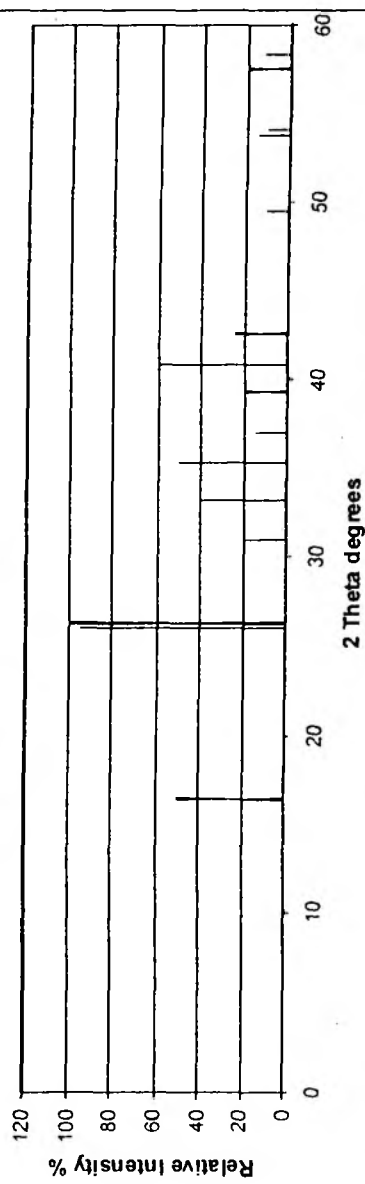
<u>2 Theta</u>	<u>I/I₀</u>
25.724	100
22.925	30
25.905	20
28.357	14
19.423	10
47.223	8
48.575	8
48.865	8
15.315	4
39.340	4

b-spodumene(*) (LiAlSi₃O₈) 350794



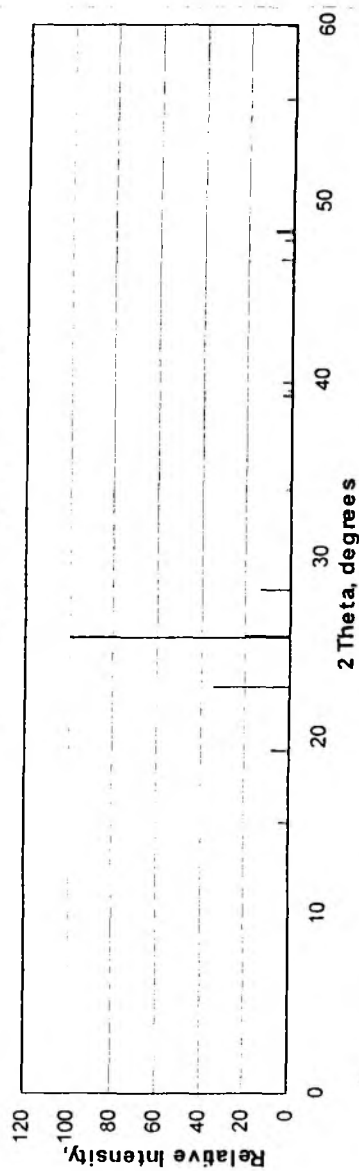
<u>2 Theta</u>	<u>I/I₀</u>
25.633	100
22.835	25
48.478	13
28.357	10
19.333	9
48.768	8
48.091	7
39.340	5
43.017	5
47.126	5

Mullite (Al₆Si₂O₁₃) 150776



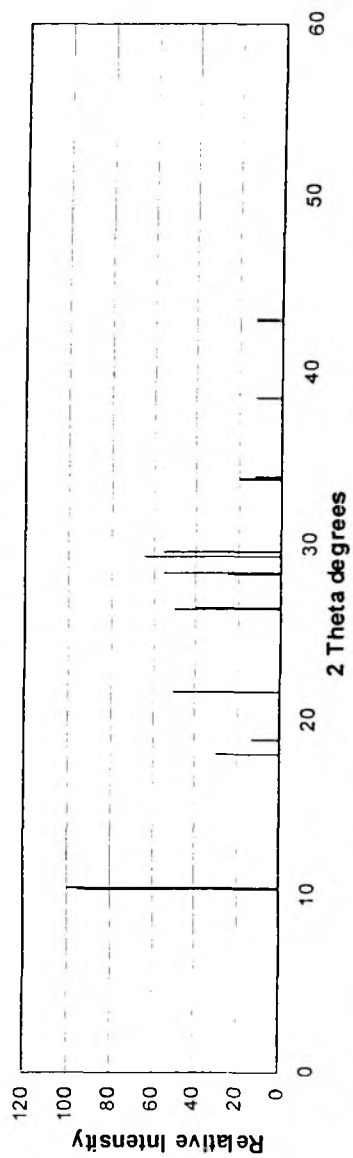
<u>2 Theta</u>	<u>I/I₀</u>
26.267	100
25.996	95
40.843	60
16.474	50
35.241	50
33.209	40
60.700	35
42.543	25
31.005	20
39.246	20

β -spodumene (LiAlSi₂O₆) 220408



<u>2 Theta</u>	<u>I/I₀</u>
25.543	100
22.745	35
25.633	20
28.174	14
19.244	8
48.284	8
48.381	8
46.741	6
15.226	4
39.059	4

Cordierite (Mg₂Al₄Si₅O₁₈) 130294



<u>2 Theta</u>	<u>I/I₀</u>
10.430	100
10.341	95
29.359	65
29.359	65
28.448	55
29.633	55
21.665	50
26.358	50
26.449	40
18.081	30

LIST OF PUBLICATIONS

1. A novel route, using zeolites as precursors for the preparation of microelectronic ceramics, β -spodumene and Cordierite and their characterizations. **K. Selvaraj, Veda Ramaswamy and A.V. Ramaswamy**, Stud. in Surf. Sci. & Catal., Vol 113, p 623, (1998)
2. Preparation of microelectronic packaging substrate ceramic β -spodumene using zeolite Na-Y as precursor and its characterization, **K. Selvaraj, Veda Ramaswamy and A.V. Ramaswamy**, Asian J. of Phys., 132, Vol 6, No. 1&2 (1997)
3. Better possibilities of compositional engineering in zeolite based novel precursors for electronic ceramics, **K. Selvaraj, Veda Ramaswamy, A. V. Ramaswamy**, Mater. Res. Soc. Proc., 2033, Vol. 3, (1999)
4. Mechanism of high temperature crystallisation of β -spodumene phases from amorphous phase of zeolite precursors. **K. Selvaraj, V. Ramaswamy and A.V. Ramaswamy**. (Submitted) *42 pages copy - to which journal*
5. Effect of temperature on the impedance of the cordierite-mullite ceramics prepared using ion exchanged zeolite precursors. **K. Selvaraj, A. Narayanasamy, V. Ramaswamy and A.V. Ramaswamy**. (Submitted)
6. Multinuclear solid state NMR characterisation of preparation of β -spodumene ceramics using zeolite as precursor. **K. Selvaraj, K. Damodaran, S. Ganapathy, V. Ramaswamy and A.V. Ramaswamy**. (to be communicated)
7. Thermal expansion studies on β -spodumene ceramics prepared through zeolite route. **K. Selvaraj, M. Marimuthu, V. Ramaswamy and A.V. Ramaswamy**. (to be communicated)
8. High resolution scanning electron microscopic studies on the phase transformation of Li - Y zeolite to LAS dense phases. **K. Selvaraj, M. Marimuthu, V. Ramaswamy and A.V. Ramaswamy**. (to be communicated)
9. Effect of Mg concentration on the phase transformation of zeolite precursor to cordierite ceramics. **K. Selvaraj, V. Ramaswamy and A.V. Ramaswamy**. (to be communicated)
10. Preparation of high temperature LAS single-phase ceramic using Li exchanged zeolite precursor. **K. Selvaraj, V. Ramaswamy and A.V. Ramaswamy**. (to be communicated)

LIST OF PAPERS PRESENTED IN SYMPOSIA

1. Preparation of microelectronic packaging substrate ceramic β -spodumene using zeolite Na-Y as precursor and its characterization. **K. Selvaraj, Veda Ramaswamy and A.V. Ramaswamy**, paper presented in National Symposium on Electroceramics, 13th – 15th March 1996, Rajkot, INDIA
2. Preparation and characterization of aluminosilicate based ceramic substrates using zeolites as precursors. **Veda Ramaswamy and K. Selvaraj**, paper presented in VII All India Meeting of Women in Science, 5-7, Sept 1996, Univ. of Roorkee, Roorkee. INDIA.
3. A novel route, using zeolites as precursors for the preparation of microelectronic ceramics, β -spodumene and Cordierite and their characterizations. **K. Selvaraj, Veda Ramaswamy and A.V. Ramaswamy**, paper presented in 13th National symposium on Catalysis, 2nd - 4th April, 1997, IIP, Dehradun, INDIA
4. Better possibilities of compositional engineering in zeolite based novel precursors for electronic ceramics, **K. Selvaraj, Veda Ramaswamy, A. V. Ramaswamy**, paper presented in 12th International Zeolite Conference, Baltimore, 5-10, July, 1998 USA
5. Phase evolution studies of electronic ceramic β -spodumene through zeolite based unconventional preparation with reference to the lattice silicon, **K. Selvaraj, A. V. Ramaswamy and Veda Ramaswamy**, paper presented in 5th IUMRS International Conference in Asia, Bangalore, 13-15, Oct, 1998 INDIA

